Universitat de Girona

DIHYDROGEN BONDS: A STUDY

David HUGAS GERMÀ

ISBN: 978-84-694-2209-0
Dipòsit legal: GI-190-2011
http://hdl.handle.net/10803/7921

Universitat de Girona

Master of Science Thesis

Dihydrogen Bonds: A study

by

David Hugas Germà

Girona, summer 2010

Doctoral programme of "Química teòrica i computacional"

Supervisor: Dr. Sílvia Simon Rabasseda
Co-Supervisor: Prof. Dr. Miquel Duran Portas

Memòria presentada per optar al títol de Doctor per la Universitat de Girona

Departament de Química
Àrea de Química Física

Institut de
Química Computacional

La doctora Sílvia Simon i Rabasseda, professora d'Universitat a l'Àrea de Química Física de la Universitat de Girona i el professor doctor Miquel Duran i Portas, catedràtic d'Universitat a l'Àrea de Química Física de la Universitat de Girona CERTIFIQUEN QUE:

En David Hugas i Germà, llicenciat en Química per la Universitat de Girona, ha realitzat sota la seva direcció, a l'Institut de Química Computacional i al Departament de Química de la Facultat de Ciències de la Universitat de Girona el treball d'investigació que porta per nom:

"Dihydrogen Bonds: A Study"

que es presenta en aquesta memòria per optar al grau de Doctor per la Universitat de Girona.

I perquè consti a efectes legals, signen aquest certificat:

Dra. Sílvia Simon i Rabasseda

Prof. Dr. Miquel Duran i Portas

Girona, a 23 de juny de 2010

Als meus pares,
als meus avis,
al meu cosí i als meus oncles.

Agraïments

A les mires del cel,
ones ultraviolades, infraroges.
Entre el submarinista i el peix que no sap on va,
entre els ossos calcificats, cèl·lules.
Bullen partícules d'H_2O al sòtil despintat,
entre sistemes solars, entre l'espai perdut.
L'astronauta camina amb la seguretat de saber
que els ampers són el voltatge partit resistència.
Camina sense escrúpols per ser com és, i no
s'expressa
[obertament perquè no pot.
És així, l'astronauta,
i es mira el cel desconcertat:
ones alfa, ones gamma.

— Antònia Font
Càpsula d'emergència (2004)

Massa temps. Cada any que passa, miro enrera i veig que la llicenciatura queda més lluny i que encara no he acabat el doctorat. Però tot té coses bones i dolentes. Les dolentes les deixarem per un altre dia, que si estic escrivint aquest apartat és que la tesi està a punt de començar el llarg, tediós, feixuc i burocràtic procés que acabarà, en el menor temps possible—creuem els dits—en la seva defensa final. Llavors ja veurem què passa.

Amb una etapa tan llarga han passat moltes coses. I molta gent, moltíssima. De tot tipus, de molts llocs, per molts motius, de molts caràcters, de moltes relacions, coneguts per efecte directe de la recerca o coneguts pel simple fet de ser viu. Ara tots ells formen part de la meva vida, encara que sigui poquíssim. N'hi ha que no coneixia, n'hi ha que ja no hi son, n'hi ha que es

quedaran una estona i n'hi ha que hi seran sempre. I tots ells tenen alguna cosa a veure amb mi i amb aquest compendi, i per bé o per mal, amb major o menor mesura, m'han canviat. Me'n deixaré molts. No m'ho tingueu en compte.

Els primers de la llista són els meus pares. M'han animat a seguir endavant i a sortir dels sotracs amb paciència, afabilitat i amor. Són els millors del Món, encara que soni infantil. I no és perquè només en tingui uns! Els avis, els que hi són i els que no. Una em va cuidar de petit, em vestia i em feia els dinars. L'altra m'ha ensenyat a escoltar. Un em va despertar la curiositat per les coses i l'altre és el que em continua demostrant com ser tossut per seguir endavant.

Els segons de la llista són els directors de tesi i els caps visibles de l'Institut de Química Computacional. La Sílvia Simon, que aquesta serà, espero, la seva primera tesi dirigida i presentada. No deixa de ser un petit honor. Tot el que hi ha aquí dins i que sigui on sóc, ella també n'és culpable. En Miquel Duran, co-director de la tesi, per tenir idees màgiques de com orientar la recerca. En Miquel Solà, per haver confiat en mi a l'assignar-me la beca. I a la cap absoluta de l'IQC: La Carme López. Ja sabeu com n'és d'important una secretària competent en aquests llocs.

No tot han sigut DHBs durant aquest temps. Altres projectes d'altra gent que han tingut més o menys èxit. Un dels aspectes bons del doctorat és la possibilitat de col·laborar amb altres grups i veure altres maneres de fer. S'aprenen moltes coses, altres maneres d'organitzar-se, de treballar i de fer. La primera estada van ser tres mesos a la Università di Torino, amb el professor Piero Ugliengo. Quant de temps fa d'això! El temps vola. Com els articles. La segona estada va ser a Berlin, amb un tema que sóna fantàstic: "Wavepacket dynamics on conical intersections". Gràcies a en Lluís Blancafort que em va posar en contacte amb la Letícia Gonzàlez a la Freie Universität Berlin, llàstima que no en sortís res publicat, però tant l'experiència professional com personal va ser extraordinària. I la última estada a la Vrije Universiteit Amsterdam, amb el professor Matthias Bickelhaupt, que sap treure el suc com ningú de qualsevol tema.

Els soldats rasos que han passat pel meu costat (o jo he passat pel seu) durant tot aquest periple, que en definitiva són els que m'han hagut d'aguantar. Tots aquells que han passat per l'antic despatx 166 (abans una casa comunal, ara un parell de dúplex) o voltaven per l'IQC en algun moment o altre. A veure si me'n recordo de tots: la Montse Casas (trufes!), en Miquel Torrent (pobre de mi!), en Xavier Fradera (va marxar, va tornar i va tornar a marxar), en Josep Maria Luis (escolteu les seves teories sobre parelles), en Xavier Gironés

(encara no ho entenc), en Pedro Salvador (CHA-CHA-CHA i CP), en Jordi Poater (cal tenir paciència per aguantar-me al costat), l'Eduard Matito (lo cavaller), l'Albert Poater (parlant d'escoltar teories...), en Quim Chaves (Zipi) i en Juanma Barroso (Zape), la Mireia Güell (talons llunyans), en David Asturiol (no tothom pot ser campió d'Espanya d'slot), la Sílvia Osuna (divina), la Cristina Butchosa (friki fins i tot pels estàndards IQC), en Dani Masó (quan érem joves...), en Ferran Feixas (Frodo), l'Anna Dachs i l'Anna Diaz (com en Zipi i en Zape, però en femení), l'Eloy Ramos (aquest noi és alt), en Sergi Ruíz (Japó t'espera), la Laia Guillaumes (tu saps on et poses, piltrafilla?)... i hi han més noms, que ens hem fet més o menys. Hi ha tot el sector experimental, envoltats de fums tòxics i brutícies estranyes que s'entossudeixen a dir-nos "raros" mentre es dediquen a treballar amb materials perillosos i contaminants. Però què hi farem, tothom és feliç a la seva manera. També hi ha tota la gent que m'he anat trobant a les estades: la Marta Corno, la Inés Corral i en Willem-Jan van Zeist.

Finalment, un grapat de gent que es poden contar amb els dits d'una mà. No han desenvolupat res de la recerca, no han estat en cap article, no tenen cap índex d'impacte en cap revista (bé, alguns si) però tenen un gran pes en tot aquest espectacle, una importància fonamental per haver-me entès i haver-me donat ànims, girar-me els punts de vista i fer-me veure la part bona de les coses. El camí amb vosaltres és més fàcil i entretingut. Gràcies.

I ara què més?

List of Publications

- D. Hugas, S. Simon, and M. Duran. Counterpoise-corrected potential energy surfaces for dihydrogen bonded systems. *Chem. Phys. Lett.*, 386(4–6):373–376, 2004.
- D. Hugas, S. Simon, and M. Duran. $MH\cdots HX$ dihydrogen bond with $M = Li$, Na and $X = F, Cl, Br$: A CP-Corrected PES calculation and an AIM analysis. *Struct. Chem.*, 16(3):257–263, 2005.
- D. Hugas, S. Simon, and M. Duran. Electron density topological properties are useful to assess the difference between hydrogen and dihydrogen complexes. *J. Phys. Chem. A*, 111(20):4506–4512, 2007.
- D. Hugas, S. Simon, M. Duran, C. Fonseca Guerra, F.M. Bickelhaupt. Dihydrogen bonding: Donor-acceptor bonding ($AH\cdots HX$) versus the H_2 Molecule ($A-H_2-X$). *Chem. Eur. J.*, 15(23):5814–5822, 2009.

.

List of Symbols and Abbreviations

Abbreviation	Description	Definition
ADF	Amsterdam density functional	page 141
AIM	atoms in molecules theory	page 90
AO	atomic orbital	page 13
BCP	bond critical point	page 91
BSSE	basis set superposition error	page 82
CCP	cage critical point	page 91
CHA	chemical Hamiltonian approach	page 85
CDF	constrained dimer function	page 85
CP	counterpoise correction to BSSE	page 85
CSD	Cambridge structural database	page 31
DFT	density functional theory	page 63
DHB	dihydrogen bond	page 24
ELF	electron localization function	page 118
GGA	generalized gradient approximation	page 81
GTO	Gaussian-type orbital	page 82
HB	hydrogen bond	page 15
HF	Hartree-Fock method	page 71
HK	Hohenberg-Kohn	page 65
HOMO	highest occupied molecular orbital	page 142
IR	infrared	page 19
IRC	intrinsic reaction coordinate	page 105
LCAO	linear combination of atomic orbitals	page 13
LDA	local density approximation	page 81

Abbreviation	Description	Definition
LUMO	lowest unoccupied molecular orbital	page 142
LSDA	local spin density approximation	page 81
MO	molecular orbital	page 13
MP2	Møller-Plesset second-order correction	page 80
MPPT	Møller-Plesset perturbation theory	page 78
NMR	nuclear magnetic resonance	page 18
PES	potential energy surface	page 87
PW	plane wave	page 84
RCP	ring critical point	page 91
RHF	restricted Hartree-Fock	page 74
ROHF	restricted open-shell Hartree-Fock	page 76
RSPT	Rayleigh-Schrödinger perturbation theory	page 60
SCF	self-consistent field	page 73
SCF-MO	self-consistent field-molecular orbitals	page 23
STO	Slater-type orbital	page 82
VDD	Voronoi deformation density	page 143
VWN	Vosko-Wilk-Nusair (VWN) parameterization	page 141
XC	exchange correlation	page 80

List of Figures

List of Tables

Contents

Abstract

Català

Un *pont de dihidrogen* (dihydrogen bond, DHB) és un tipus de pont d'hidrogen atípic que s'estableix entre un hidrur metàl·lic i un donador de protons com un grup OH o NH. Es pot representar com a $\mathrm{A-H\cdots H-M}$, on A és un element electronegatiu que potencia l'acidesa del protó, com en el cas del pont d'hidrogen típic, i M és un metall menys electronegatiu que l'hidrogen i fa que el parell d'electrons σ de l'enllaç $\mathrm{H-M}$ actuin com un acceptor. Els ponts de dihidrogen són claus en les característiques geomètriques i altres propietats de compostos que en presenten. Poden ser els causants de l'estructura geomètrica específica tan de molècules petites com el dímer de NH_3BH_3, com d'estructures superiors més complicades com complexes metàl·lics o sòlids. Tenen la capacitat de canviar els punts d'ebullició i de fusió, propietats magnètiques i espectroscòpiques i altres característiques, tal com ho fan també els ponts d'hidrogen encara que els enllaços hidrogen-hidrogen no són tan forts com els anteriors. En aquest sentit els ponts de dihidrogen poden ser útils, fins a cert punt, quan es poden aplicar a certes molècules o en síntesis moleculars concretes per a obtenir nous materials amb propietats o característiques especials o fins i tot fetes a mida. El treball desenvolupat en aquesta tesi està orientat a millorar la comprensió dels ponts de dihidrogen, aprofundint en certs aspectes de la seva naturalesa atòmica/molecular utilitzant mètodes teòrics basats en la química física quàntica i treballant per a obtenir models fiables com a base d'investigacions futures.

En aquesta tesi s'investiguen els DHBs des de diferents punts de vista, començant per sistemes petits i incrementant la seva mida aplicant diferent

mètodes. S'utilitzen geometries, energies, densitats electròniques i interaccions orbitalàries per a descriure'ls. En un primer estadi, i com a exemple de sistemes senzills, s'estudien els sistemes $M-H\cdots H-X$ (M = Li, Na, $H-Be$, H_2-B i X = F, Cl, Br) que presenten DHBs a nivell HF, DFT/B3LYP i MP2. Alguns d'aquests complexes tenen punts estacionaris amb dues freqüències imaginàries degenerades, mentre que d'altres es consideren punts mínims en la superfície d'energia potencial (SEP o PES). La correcció de counterpoise (CP) s'ha aplicat a tota la PES per a obtenir punts estacionaris lliures de l'error de superposició de base (BSSE). Es demostra que l'ús de PES corregides per CP és necessari si es vol aconseguir una bona descripció d'aquests enllaços dèbils. Alguns dels complexes de liti i sodi presenten un punt mínim nou amb una topologia diferent, per exemple en el número de freqüències imaginàries. A més a més, el BSSE a nivell MP2 dels complexos $M-H\cdots H-X$ (M = $H-Be$, H_2-B i X = F, Cl, Br) és del mateix ordre que les energies d'interacció. Per tant, es poden obtenir conclusions errònies si només es té en compte la PES sense corregir.

Seguidament s'ha aplicat la teoria d'àtoms en molècules (atoms in molecules, AIM) a sèries de sistemes amb ponts d'hidrogen i de dihidrogen calculats a nivell B3LYP i MP2 utilitzant la base 6-31++G(d,p). S'ha analitzat la topologia de la densitat electònica i la densitat energètica als respectius punts crítics d'enllaç (bond critical points, BCP), optimitzats al seu mínim d'energia. Encara que no hi ha diferències importants quan aquestes propietats es representen com a funció de l'energia de dimerització, es poden separar en dos grups ben definits si aquestes propietats es relacionen amb distàncies intermoleculars. Quan s'analitza la dependència de diferents propietats amb les distàncies d'enllaç optimitzades, les tendències específiques dels sistemes amb pont de dihidrogen són per una banda una densitat electrònica més baixa al punt crític d'enllaç i per l'altra una concentració/exhauriment més baixa d'aquesta densitat que es pot traduir com a un comportament diferent pels components de la Laplaciana. A més, els conjunts de molècules creen dos gràfics diferents que permeten la seva classificació entre sistemes amb ponts d'hidrogen i de dihidrogen.

El següent objectiu de la investigació és determinar si un sistema amb una distància entre hidrògens $H\cdots H$ molt curta és un pont de dhidrogen o una molècula H_2. L'enllaç central $H-H$ en el complex lineal H_4 pot existir en dos tipus d'enllaç qualitativament diferents, corresponent a dos estats electrònics diferents, que són un DHB donador-acceptor i una molècula H_2 central amb un parell electrònic enllaçant. Aquest punt de vista es desenvolupa a partir d'un anàlisi utilitzant el funcional de Kohn-Sham i s'aplica en sistemes més

comuns per entendre'n l'enllaç. S'estudia l'enllaç central $H-H$ en els sistemes H_4 lineal, $Li-H\cdots H-X$, $BH_4\cdots H-X$ i $AlH_4\cdots H-X$, amb diferents X, utiltizant el model orbitalari molecular quantitatiu inclós en la teoria del funcional de densitat de Kohn-Sham al nivell de teoria BP86/TZ2P. Primer es resolen les qüestions de com es pot distingir teòricament entre un enllaç DHB $H\cdots H$ donador-acceptor o la formació d'un enllaç molecular H_2, utilitzant el sistema model de l'H_4. A partir dels resultats d'aquest anàlisi s'obté una comprensió dels enllaços en sistemes més reals (alguns dels quals s'han estudiat experimentalment), i com difereixen de l'enllaç del sistema H_4.

Finalment, es fa un estudi de les característiques geomètriques i energètiques del cristall molecular de BH_3NH_3 per estudiar el paper dels ponts de dihidrogen en un sistema cristal·lí. Les modelitzacions a nivells HF i DFT (B3LYP, PW91, PBE i PBE0) indiquen que les molècules de BH_3NH_3 es cohesionen dins del cristall mitjançant ponts de dihidrogen. Els hidròdgens en el cristall interaccionen amb un o dos dels seus hidròdgens veïnals. Les distàncies d'enllaç dels DHBs són més llargues per HF que pels mètodes DFT, variant entre 2.488 a 1.895 Å, una distància d'enllaç que cau dins dels estàndards dels DHB. La força d'aquestes interaccions és dèbil i depèn de la distància en la que interactuen els hidròdgens. Altres càlculs sobre una llosa del cristall de BH_3NH_3 indiquen una expansió del sistema en el seu punt mínim d'energia respecte el cristall, apuntant a un comportament diferent quan es modelitzin interaccions sobre la seva superfície. La comparació de les freqüències d'*stretching* anharmòniques dels grups $N-H$ i $B-H$ del cristall amb les de la molècula aïllada, presenten un desplaçament cap al vermell, reafirmant que hi ha ponts de dihidrogen al cristall.

English

A *dihydrogen bond* (or DHB) is a kind of unconventional hydrogen bond, established between a metal hydride bond and a proton donor like OH or NH. It can be represented as $A-H\cdots H-M$, where A is an electronegative element which enhances the proton acidity as in the typical hydrogen bond, and M is a metal less electronegative than H and makes the σ electron pair of the $H-M$ bond act as an acceptor. They are the key to important structure features and properties in compounds which have them. They can be responsible for the specific geometry not only of small molecules like the NH_3BH_3 dimer, but also of higher structures like metallic complexes or solids. They can also change the boiling and melting points, magnetic and spectroscopic properties and other characteristics like hydrogen bonds, although hydrogen-hydrogen bonds are not as strong as the former. It is in this fashion that dihydrogen bonds can be profitable, up to a plausible extent, when they can be used in certain molecules or certain syntheses to obtain a new material with particular or even tailored properties or geometries. The work developed in this thesis is aimed to have a deeper understanding of dihydorgen bonds, deepening on certain aspects using theoretical methods and working towards having reliable models to set a basis of further investigations.

In this thesis, the DHB are investigated from different points of view, starting from small systems and increasing its size through different methods. Geometries, energies, frequencies, electronic densities and orbital interactions have been used to characterize them. The first step, and as an example of simple systems, dihydrogen bonded systems $M-H\cdots H-X$ (M = Li, Na, $H-Be$, H_2-B and X = F, Cl, Br) are studied at the HF, DFT/B3LYP and MP2 levels of theory. Some of these complexes are found to be stationary points with two degenerated imaginary frequencies, while the others are considered as minima in the potential energy surface (PES). Counterpoise (CP) corrections are considered on the whole PES in order to get basis set superposition error (BSSE) free minima. It is shown that the use of CP-corrected PES is necessary in order to obtain a good description of these weak bonds. Some of the lithium and sodium complexes present a new minimum with different topology, i.e. number of imaginary frequencies. Furthermore, the BSSE at the MP2 level of $M-H\cdots H-X$ ($M = H-Be$, H_2-B and X = F, Cl, Br) and the interaction energy are about the same order. So, wrong conclusions may be obtained if only the uncorrected PES is considered.

The next step in the research is to apply the atoms in molecules theory

(AIM) to a series of hydrogen- and dihydrogen-bonded systems calculated at B3LYP and MP2 level, with a 6-31++G(d,p) basis set. The topology of the electron density and the energy densities at the respective energy-optimized bond critical points has been analysed. Even though there are no significant differences when these properties are represented as a function of the dimerization energy, they can be separated into two well-defined sets if those properties are correlated with intermolecular distances. When analyzing the dependence of various properties with equilibrium bond lengths, the specific trends of dihydrogen bond systems consist of lower electron density at the bond critical point and lower concentration/depletion of that density which can be translated in a different behavior for the Laplacian components. Furthermore, the sets of molecules form two different plots which allow for a valuable classification between hydrogen- and dihydrogen-bonded systems.

The following objective in this investigation is to determine if a close interacting $H \cdots H$ system is a dihydrogen bond or a H_2 molecule. The central $H-H$ bond in linear H_4 can exist in two qualitatively different bonding modes corresponding to two different electronic states, namely a donor-acceptor DHB and a central H_2 molecule with an electron-pair bond. This insight evolves from Kohn-Sham density functional analysis and it is further applied here to understand the bonding in more realistic model systems. The central $H-H$ bond in linear H_4, $Li-H \cdots H-X$, $BH_4 \cdots H-X$ and $AlH_4 \cdots H-X$ complexes with various X is studied by using the quantitative molecular orbital model contained in Kohn-Sham density functional theory at the BP86/TZ2P level of theory. First are addressed the questions of how one can distinguish, in principle, between a $H \cdots H$ donor-acceptor DHB and the formation of an H_2 molecule by using the simple H_4 model system. The results of these analyses have been used to obtain an understanding of the bonding in more realistic model systems (some of which have been studied experimentally), and how this differs from the bonding in H_4.

Finally, a study on the geometric and energetic characteristics of the ammino borane (BH_3NH_3) crystal has been carried out to investigate the role of dihydrogen bonds in a crystalline system. Modellizations at HF and DFT (B3LYP, PW91, PBE and PBE0) levels show that the BH_3NH_3 molecules hold together inside the crystal by means of dihydrogen bonds. Hydrogens in the crystal interact with one or two of its hydrogen neighbours. DHBs lengths are longer for HF than for DFT methods, ranging from 2.488 to 1.895 Å, a standard DHB length. The strength of these interactions is a weak interaction which depends on the length of the interacting hydrogens. Further calculations on the ammino borane crystal slab show an expansion of the system at

its minimum energy point with respect to the crystal, pointing to a different behavior when modelling surface interactions. Comparing the crystal $N-H$ and $B-H$ anharmonic stretching frequencies with those of the isolated molecule, a displacement to the red is shown, reaffirming that the DHB interactions are present.

Chapter 1

Introduction

The Force is what gives a Jedi his power. It's an energy field created by all living things. It surrounds us and penetrates us. It binds the galaxy together.

— Obi-Wan Kenobi
Star Wars: A new Hope (1977)

1.1 Types of interaction

When an interaction takes place between two or more particles, different *forces* appear where one acts upon the others. The resultant net force obtained from the sum of all force vectors involved is proportional to the mass of the body times the amount of acceleration. Following Newton's Second Law of Motion:

> The rate of change of momentum of a body is proportional to the resultant force acting on the body and is in the same direction.

Besides, for each set force an opposite one appears as a reaction to the first one. As stated in Newton's Third Law:

> All forces occur in pairs, and these two forces are equal in magnitude and opposite in direction.

If the net force resulting from the sum of all acting forces on a body is null, then there is no change in the body state of motion:

> Every body perseveres in its state of being at rest or of moving uniformly straight forward, except insofar as it is compelled to change its state by force impressed.

Those three laws were written down by Sir Isaac Newton (1643–1727) in his *Philosophiæ Naturalis Principia Mathematica* [188], setting the basis of classical mechanics. What Newton's laws don't explain is the inner nature of these forces and where do they come from.

More than 300 years after Newton's principles, Physics has a deeper insight on the nature and typology of forces. Nowadays it is widely assumed that there are four fundamental interactions: gravitational, strong, electromagnetic and weak. Each of them acts in a different scale, range and strength. In table 1.1 the fundamental interactions are listed with their strength magnitude:

Table 1.1: Comparison between the four fundamental forces. Relative strengths are approximate and depend on the particles and energies involved.

Interaction	Relative strength	Range (m)	Long-distance behaviour
Gravitation	1	∞	$G\frac{m_1 m_2}{r^2}$
Weak	10^{25}	10^{-18}	$\frac{e^{-m_{W,Z}r}}{r}$
Electromagnetic	10^{36}	∞	$\frac{1}{4\pi\varepsilon_0}\frac{q_1 q_2}{r^2}$
Strong	10^{38}	10^{-15}	*

All non-charged particles of any size and mass interact in an infinite range due to gravitation. Any body in the universe is attracted to the other bodies, as well as, in turn, it attracts them. Although it is the weakest of all four fundamental forces, it describes the movement of astronomic bodies, from orbits to the galactic dynamics.

In a shortest range there are the weak interactions which are set at an atomic scale and take part in α and β decays and other nucleus related reactions. These interactions are responsible for the energy liberated in fusion and fission reactions.

At really short distances (10^{-15} m) is where the strongest interaction of all four fundamental ones happens: the strong interaction. It is responsible for the tighten up of the positively charged protons and neutrons in a really compressed space, like the atomic nucleus, and not allowing them to scatter away.

The last fundamental interaction to consider is precisely the model which explains the chemical interactions between atoms and molecules. The electromagnetic interactions act between charged particles, attracting those with different sign and repelling those with the same one. The "magnetic" part of the term comes from the fact that when charged particles move, e.g. electrons orbiting around the nucleus, they create a magnetic field that induces movement in other charges at range. Electromagnetism is much more stronger than gravitation, and therefore can describe almost any natural phenomena: from the impenetrability of macroscopic bodies to light scattering. The different strength interactions which are showed in chemical bonding are an effect of electromagnetism acting in different ways, resulting in various balances of pull-push forces among electrons, their orbits, protons and neutrons. Thus, all the atomic interactions studied in this thesis are based on this interaction model.

1.1.1 Electrostatic interactions and chemical bonds

As it has been stated in the latter section 1.1, electromagnetism has a part in the explanation behind the electronic orbit around the nucleus. Nowadays, the most widely spread atomic model is based on the one proposed by Niels Bohr [35], where a positively charged nucleus is surrounded by orbiting electrons. These must observe three postulates, one of them being that the electron, due to its centripetal force induced by the positive charges at the

nucleus, spins around it in orbit-shaped paths without emitting or absorbing energy. This postulate is needed otherwise the electron should fall towards the nucleus as stated in the electromagnetic theory. The electron is a moving charge and it should radiate energy, which will lead to a decrease of its mechanical energy, reducing its speed and lowering its orbit; collapsing eventually into the nucleus. In section 2.1 a deepest mathematical insight of the atomic model will be given.

Atoms group themselves to form molecules, higher structures that usually have different properties than the atoms that compound them. These are hold together through the *chemical bond*, which is, again, an electromagnetic interaction amongst the nuclei and the electrons. Theoretically, all the atomic particles in an isolated molecule affect each other no matter how far apart they are, but usually there is an interaction between two atoms that is predominant over the rest. Moreover, this interactions are restrained to atoms separated in an approximate range of 3 Å, depending on a wide set of involved properties but being the electronic configuration of the participating atoms the most important of them. If the molecule is in the neighbourhood of other molecules—same, similar or different to itself—interactions between them are possible and usually they are less strong than the intramolecular ones.

In energetic terms, a chemical bond entails a lowering in the total energy of the compound. Thus, there is a liberation of energy and atoms achieve a stability which could not be obtained while they were set apart. The amount of energy liberated is related to the attraction and repulsion terms between the subatomic particles participating in the bond, which are in balance between them, but not always. Positively charged nuclei repel other nuclei and negatively charged electrons do the same between them, while nuclei attract electrons. These attraction forces make the atoms get close to one another up to a certain distance, known as *bond length*, where an energy minimum is achieved. Figure 1.1 depicts the total energy of a two atom interaction referred to the distance between these atoms:

At r_o falls in the length between the nuclei where the system's energy reaches a minimum and is below zero. At this point is where the stable geometry of the molecule stands. In fact, this is not a fixed distance, as the atoms vibrate back and forth due to their internal energy and temperature. If the nuclei get close to each other, the repulsion terms prevail over the attraction ones and the total energy increases exponentially. If, on the other hand, they move away from each other, the bond decreases its energy towards zero but, since electrostatic interactions have an infinite range of action, it will theoretically

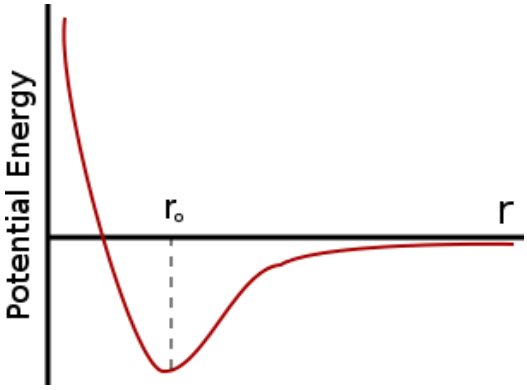

Figure 1.1: Diatomic potential energy curve.

never reach this value.

The attraction forces exerted by the nuclei of one atom to the electrons of another one, apart from bringing the atoms nearer, lightly distort the atom's valence orbitals and so the electronic clouds are displaced, inducing the atom to have more electrons in one zone that it should have, and having less in another one. That creates a charge gradient between the two zones of the atom and generates an *electric dipole moment*. A dipole moment is a vector $\vec{\mu}$ of magnitude $\vec{\mu} = q\vec{R}$ with its origin on the negative charge and pointing towards the positive one, both having the same value q—but different sign—and separated a distance $\vec{R}$. The mean electric dipole density of an atom, or more frequently a molecule, is referred in chemistry as *polarisation*, specially when an atom or a functional group induces the dipole. There are molecules, mainly asymmetric ones, which polarisation is not induced but permanent, e.g. water. However it can be induced as well by an electric field or another nearby polarised compound. The atoms no longer have their charge equally distributed along its orbits, and electrostatic forces are set among the slightly positively-charged part of one molecule to the negatively-charged end of another molecule. Atoms under a induced dipole tend to rearrange their electrons to obtain the most stable configuration, that of minimum energy. This is the first step to different types of bonding. Depending on the electronegativity of the atoms involved, electrons of the outer valence shield can be transferred to, acquired from or shared with other atoms in the dipole, lowering their internal energy and achieving a more stabilised configuration.

1.1.1.1 Strong chemical bonds

One of the possible outcomes of this first steps towards an stable interaction is that one or more electrons leave an atom and are accepted by another one. This case is a *ionic bond* model. Two ions are formed with a strong electrostatic interaction inbetween. The stabilisation of the electronic configuration will drive the atoms tendency to create an ionic bond. Atoms reach the most stable state when all of its electron shells are filled or semi-filled. Atoms with high electronegativities are close to these configurations by acquiring one or two electrons—and becoming *anions*—, while others with lower ones should release them to be more stable—thus being *cations*. When the difference of electronegativities between the atoms in the molecule is large, the most electronegative one takes one or more electrons from the less electronegative, forming the ionic bond. Although the formation of the ions is endothermic, the attraction to each other lowers their total energy.

Another possibility is that both atoms have similar electronegativities. Their configuration is energetically too far from reaching a filled or semi-filled shell, and the energetic lowering due to the strong electrostatic interaction is not enough to counteract the initial energetic investment. What happens in this conditions is that atoms share their electrons with each other and the electronic cloud makes a strong bond, a *covalent bond*.

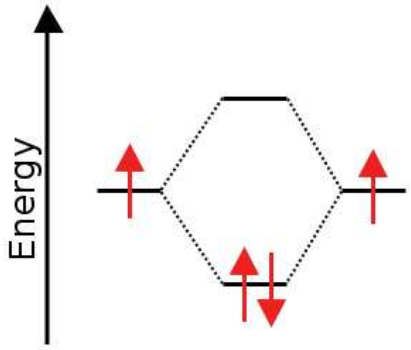

Figure 1.2: Formation of molecular orbitals by combination of two atomic orbitals in a diatomic model. Arrows represent electrons from the two atoms.

The energy stabilisation derives from the combination of the approaching

nuclei atomic orbitals (AO) to form molecular orbitals (MO) into which the covalent bond is coherent. In figure 1.2 a molecular orbital diagram shows qualitatively how two atomic orbitals combine using the linear combination of atomic orbitals (LCAO) method, to form two new molecular orbitals, a bonding one of lower energy and another one of higher energy than the starting ones known as anti-bonding. The electrons are resettled in the new orbitals and, if their total energy is lower than the one they had in the isolated atoms, the bond is set. Then, these electrons can move along the new orbitals around the atoms, and they don't belong to a particular atom, but to both of them. It is said that they are *delocalised*. Even so, electrons are more likely to stay around the most electronegative atom, so the delocalisation is higher when the electronegativities are more similar. Usually electrons are shared in pairs, but the number of shared pairs is not limited to one. The *bond order* is the number of electron pairs shared in a covalent bond. The combination of AOs can lead to MOs of different energy and symmetry which can be occupied by electron pairs. Thus, a single bond involves a pair of electrons and has a bond order of 1, a double bond has two pairs of electrons and a bond order of two, and so on.

A *metallic bond* is another type of electron sharing bond. In this situation a grid of positively charged metal ions are completely immersed in a cloud of electrons. Every valence orbital of each atom participates in the bonding and combines with the other ones, forming a MO around the lattice and allowing all the electrons to move freely around any of the centres. This leads to a complete delocalisation of the electrons among the whole solid and a major decrease in the system's total energy.

1.1.1.2 Weak chemical bonds

Another kind of chemical bond is that of the weak type. In fact, most of them are not much of a bond but mainly an electrostatic interaction between molecules or parts of a molecule. Electrons are neither transferred like the ionic bond nor shared as in the covalent or metallic ones. Instead, the interaction occurs due to the forces formed between dipoles, quadripoles, multipoles, charges, polar molecules or a mix of them. Although they are far less stronger than the ionic, covalent or metallic bonds, they are of major importance, as they are involved in the supra-structure of macromolecules like proteins, docking of proteins in specific zones to activate or deactivate certain processes in living organisms or make water keep its liquid state between 0 and 100 degrees.

There are many types of weak chemical interactions, as any electrostatic interaction set among molecules could be classified in this section, but there are three main types. One of them is the *dipole-dipole* model and is set between two or more molecules with a permanent dipole (or multipole). These are very directional interactions: a small variation in the angle or distance and the strength of the interaction diminishes rapidly. There are subtypes of this interaction, like charge-dipole interaction or dipole-induced dipole. The first one is set between an ion and a dipole and generally is stronger than a dipole-dipole interaction and less direction dependent. The second one occurs when a dipole is near a neutral molecule and polarises it. The dipole's different electronic densities attract or repel the electrons of the other molecule and induce a temporal dipole, which can interact with the permanent dipole. They are weaker than the dipole-dipole interactions and due to the nature of the bond, they usually don't last for a long time and dissociate.

The dipole-induced dipole interaction has its extreme in the induced dipole-induced dipole interactions. This particular case takes place in gas state atoms or non-polar symmetric molecules, where the difference of the composing atoms electronegativity is null or close. In this conditions, an electrostatic interaction should not arise as the compounds doesn't have any dipole and cannot produce any. But due to the quantum distribution of the electrons, there is a small probability where all the electrons are piled together in a certain region of the molecule. This fact produces that a dipole is formed in a moment, and then disappears. In this short time the molecule or atom can interact with another molecules with a multipole or even induce a dipole on another molecule. This phenomenon are the *London dispersion forces* and are the weakest of the chemical bonds. They are short term interactions with weak forces, but they can explain why noble gases still interact even in long distances.

There is the hydrogen bond in the weak interactions as well, but as it is part of the scope of this thesis, it will be thoroughly explained in the next section.

1.1.2 Hydrogen bonds [79, 125, 126, 130, 211]

Many substances have properties related to the "strong" chemical bonding between atoms and ions which cannot be explained by it, but suggest that there are more interactions between them and that they are important enough to keep water in its liquid state while other compounds similar to it are gases at the same temperature. Such interaction is called *hydrogen bonding* (or

HB) and, though normally weak (2.39–14.34 kcal per mol of each hydrogen which is H-bonded), it frequently has a decisive influence on the structure and properties of the substance. Two atoms A and B, which usually would stand at a certain distance, approach more closely to each other and lower the total energy of the system when a bond is set between them with the presence of a hydrogen. The bond is represented as $\mathrm{A}-\mathrm{H}\cdots\mathrm{B}$ and usually occurs when A is sufficiently electronegative to enhance the acidic nature of H (proton donor) and where the acceptor B has a region of high electron density (such as a lone pair of electrons) which can interact strongly with the acidic hydrogen. The interaction can take place in different ways and geometries as shown in figure 1.3. A hydrogen bond is not necessarily linear: it can be linear, bended or it can even interact with two or more acceptors. In the same way, two hydrogens can interact with a single acceptor to produce a two-joined bifurcated interaction. However, the most common structure found in H-bonded systems is the unbranched one, and the others are just a small part present in some complexes.[254]

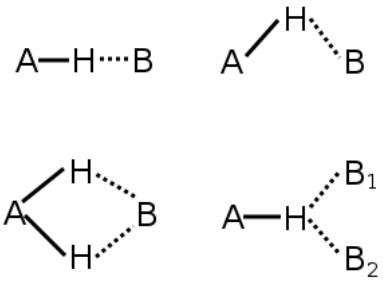

Figure 1.3: Different examples of H-bonds structures.

The strength of the H-bond depends on the different combinations between the atom acceptors and donors. Experimental evidence suggests that strong H-bonds can be formed when the donor A is F, O or N; weaker H-bonds are sometimes formed when A is C or a second row element, P, S, Cl or even Br or I. On the other hand, when the acceptor B is F, O or N the interaction is bigger than when it is Cl, Br or I. However when these last three halogens act as charged species, the hydrogen bond is stronger. Other acceptors can be C, S and P, but they produce weak H-bonds.

1.1.2.1 Influence on properties

It is well known that the melting and boiling points of NH_3, H_2O and HF are anomalously high when compared with the melting and boiling points of the hydrides of other elements in Groups 15, 16 and 17, as shown in figure 1.4. The explanation given normally is that there is some different interaction (i.e. H-bonding) between the molecules of NH_3, H_2O and HF which is absent for methane, and either absent or much weaker for heavier hydrides. This argument is probably correct in outline but is deceptively oversimplified since it depends on the assumption that only some of the H-bonds in solid HF (for example) are broken during the melting process and that others are broken on vaporisation, though not all, since HF is known to be substantially polymerized even in the gas phase. But sometimes, attributing anomalously high melting points to hydrogen bonds can be deceiving. The melting point is the temperature at which there is zero free-energy change on passing from the solid to the liquid state. As the free-energy equation $\Delta G = \Delta H - T\Delta S$ equals to zero, then the melting temperature can be written as directly proportional to the enthalpy of melting and inversely to the entropy of melting $T_m = \frac{\Delta H_m}{\Delta S_m}$. High melting points involve either a high melting enthalpy, a low melting entropy or both of them. Thus, high melting points can not be always related to hydrogen bond in means of high enthalpy of melting, as a small variation in entropy causes a high temperature increment too. Similar arguments can be applied to boiling points and indicate the difficulties in quantifying the discussion.

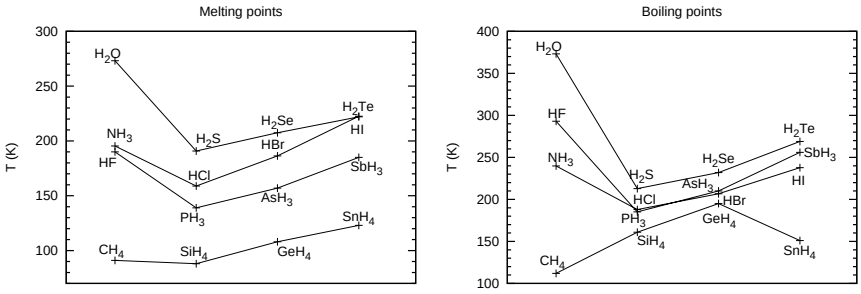

Figure 1.4: Values of melting and boiling points of hydrides.

There are many other properties that depend on H-bonds, like solubility, miscibility, heat of vaporization, heat of mixing, phase-partioning properties,

the existence of azeotropes ad the sensitivity of chromatographic separation. Liquid crystals (or mesophases) which can be regarded as "partly melted" solids also frequently involve molecules that have H-bonded groups (e.g. cholesterols, polypeptides, etc.). Again, H-bonding frequently results in liquids having a higher density and lower molar volume than would otherwise have been expected, and viscosity is also affected (e.g. glycerol, anhydrous H_2SO_4, H_3PO_4, etc.).

Electrical properties of liquids and solids are sometimes crucially influenced by H-bonding. The ionic mobility and conductance of H_3O^+ and OH^- in aqueous solutions are substantially greater than those of other univalent ions due to a proton-switch mechanism in the H-bonded associated solvent, water. For example, at 298 K the conductance of H_3O^+ and OH^- are 350 and 192 $\text{ohm}^{-1}\text{cm}^2\text{mol}^{-1}$, whereas for other ions the values fall mainly in the range of 50–75 $\text{ohm}^{-1}\text{cm}^2\text{mol}^{-1}$. It is also notable that the dielectric constant is not linearly related to molecular dipole moments for H-bonded liquids, being much higher due to the orientating effect of the H-bonds: large quantities of species are able to align in an applied electric field so that the molecular dipoles reinforce one another rather than cancelling each other due to random thermal motion. Even more dramatic are the properties of ferroelectric crystals where there is a stable permanent electric polarisation, as hydrogen bonding is responsible of ordering these molecules in the domain.

Direct information about the nature of the H-bond has come from vibrational spectroscopy (infrared and Raman), proton NMR spectroscopy, and diffraction techniques (X-ray and neutron). In vibrational spectroscopy the presence of a hydrogen bond $\text{A} - \text{H} \cdots \text{B}$ is manifest by diverse effects, all of them related to an interaction taking place between the hydrogen and the acceptor. One of them is that the $\text{A} - \text{H}$ stretching frequency ν shifts to lower wave numbers and its breadth and intensity increase markedly, often more than tenfold. The increase in intensisty and breadth is due to a small amount of electron density (0.01–0.003 electrons) transferred from the proton acceptor B to the proton donor molecule $\text{A} - \text{H}$. The $\text{A} - \text{H}$ bending varies as well shifting to higher wave numbers, and finally sometimes the stretching and bending modes of the H-bond appear at very low wave numbers (20–200 cm^{-1}). Most of these effects correlate roughly with the strength of the H-bond and are particularly noticeable when the bond is strong. For example, for isolated non-H-bonded hydrogen groups, ν(O-H) normally occurs near 3500–3600 cm^{-1} and is less than 10 cm^{-1} broad whereas in the presence of $\text{O} - \text{H} \cdots \text{O}$ bonding ν_{antisym} drops to ∼1700–2000 cm^{-1}, which is several hundred cm^{-1} broad, and much more intense. A similar effect of $\Delta\nu$ ∼1500-2000 cm^{-1} is noted on $\text{F} - \text{H} \cdots \text{F}$

formation and smaller shifts have been found for $N-H\cdots F(\Delta\nu \leq 1000\ cm^{-1})$, $N-H\cdots O(\Delta\nu \leq 400\ cm^{-1})$, $O-H\cdots N(\Delta\nu \leq 100\ cm^{-1})$, etc. Besides, there is as well an important effect coming from the solvent, concentration, temperature and pressure. The magnitude of the effect is much grater then expected on a simple electrostatic theory of hydrogen bonding, and this implies an appreciable electron delocalisation, related to covalency, particularly for the stronger H-bonds. This effect is known as *red shift*. It includes elongation of the $A-H$ bond in the complex $A-H\cdots B$ and its correlated lower stretching frequency.

But there are reports of hydrogen bonded systems showing a *blue shift*. In blue shifting, opposed to the red one, the $A-H$ bond length decreases and the $A-H$ frequency increases. It is the reverse effect of the classical hydrogen bond: there is a shortening of the $A-H$ bond while interacting with the proton acceptor B instead of a lengthening, referring them as *improper hydrogen bonds*. In many blue-shift cases, the hydrogen is bonded to a carbon in the donor molecule, but other examples are known in which it is on an atom of a different element, like nitrogen or sulphur. The IR spectrum of triformylmethane in chloroform has a distinct, sharp band close to the $C-H$ stretch of chloroform but slightly shifted toward higher wavenumbers: 3028 cm^{-1} compared to 3021 cm^{-1}, the typical $C-H$ stretch value for chloroform). There are other reported shifts in chloroform, deuterochloroform, and bromoform in mixed systems containing proton acceptors such as carboxy, nitro, and sulfo compounds which present shifts of 3–8 cm^{-1} to higher frequency compared to their position in CCl_4. Larger shifts in the $C-H$ stretch frequency can be found in the $Cl^-\cdots H_3CBr$ and $I^-\cdots H_3CI$ ionic complexes with a blue shift bigger than 100 cm^{-1}.

Proton NMR spectroscopy has also proved to be valuable in studying H-bonded systems. In NMR the nuclei are under a magnetic field that rises different energy levels and resonance frequencies, which are the same for each atom. But these nuclei have electrons with a magnetic moment of their own and other local magnetic fields from the surrounding molecules or solvent. The *chemical shift* is the variation of the resonance frequencies of the same nucleus due to variations in the electron distribution. As might be expected, substantial chemical shifts are observed and information can be obtained concerning H-bond dissociation, proton exchange times and other relaxation processes. The chemical shift always occurs to low (magnetic) field and some typical values are tabulated below for the shifts which occur between the gas and liquid phases or on dilution in an inert solvent:

The low field shift is generally interpreted, at least qualitatively, in terms

Table 1.2: Chemical shifts of diverse compounds.

Compound	CH_4	C_2H_6	$CHCl_3$	HCN	NH_3	PH_3
δ ppm	0	0	0.30	1.65	1.05	0.78
Compound	H_2O	H_2S	HF	HCl	HBr	HI
δ ppm	4.58	1.50	6.65	2.05	1.78	2.55

of a decrease in diamagnetic shielding of the proton: the formation of a $A-H\cdots B$ tends to draw H towards B and to repel the bonding electrons in A-H towards A thus reducing the number of electrons in H and reducing the shielding too. The strong electric field produced by B also inhibits the diamagnetic circulation within the H atom and this further reduces the shielding. In addition, there is a magnetic anisotropy effect due to B; this will be positive (upfield shift) if the principal symmetry axis of B is towards the H bond, but the effect is presumably small since the overall shift is always downfield.

Ultraviolet and visible spectra are also influenced by H-bonding, but the effects are more difficult to quantify and have been rather less used than IR and NMR. It has been found that the $n \rightarrow \pi^*$ transition of the base B always moves to high frequency* on H-bond formation, the magnitude of $\Delta\nu$ being $\sim$300–4000 cm^{-1} for bands in the region 15000–35000 cm^{-1}. By contrast, $\pi \rightarrow \pi^*$ transitions on the base B usually move to lower frequencies and shifts are in the range from -500 cm^{-1} to -2300 cm^{-1} for bands in the region 30000–47000 cm^{-1}. Detailed interpretations of these data are somewhat complex and obscure, but it will be noted that the shifts are approximately of the same magnitude as the enthalpy of formation of many H-bonds (83.59 cm^{-1} per atom $\equiv$ 0.24 kcal/mol).

1.1.2.2 Influence on structure [202, 269]

The crystal structure of many compounds is dominated by the effect of H-bonds. Ice is perhaps the classic example, but the layer lattice structure of $B(OH)_3$ and the striking difference between the α- and β-forms of oxalic and other dicarboxylic acids is notable. The more subtle distortions can lead to ferroelectric phenomena in KH_2PO_4 and other crystals. Hydrogen bonds between fluorine atoms result in the formation of infinite zigzag chains in crystalline

*Although it's a blue shift, it only refers to the higher frequencies, not the shortening between of the covalent bond between the hydrogen and the proton donor.

hydrogen fluoride with $F-H\cdots F$ distance 2.49 Å between fluorines and the angle H-F-H 120.1°. Likewise, the crystal structure of NH_4HF_2 is completely determined by H-bonds, each nitrogen atom being surrounded by 8 fluorines, 4 in tetrahedral array at 2.80 Å due to the formation of $N-H\cdots F$ bonds, and 4 further away at about 3.10 Å; the two sets of fluorine atoms are themselves bonded pairwise at 2.32 Å by $F-H-F$ interactions. Ammonium azide NH_4N_3 has the same structure as NH_4HF_2, with $N-H\cdots N$ distance between nitrogens of 2.98 Å. Hydrogen bonding also leads NH_4F to crystallise with a structure different from that of the other ammonium (and alkali) halides: NH_4Cl, NH_4Br and NH_4I each have a low-temperature CsCl-type structure and a high-temperature NaCl-type structure, but NH_4F adopts the wurtzite (ZnS) structure in which each NH_4^+ group is surrounded tetrahedrally by 4 F to which it is bonded by 4 $N-H\cdots F$ bonds at 2.71 Å. This is a very similar to the structure of ordinary ice. Typical values of $A-H\cdots B$ distances found in crystals are given in table 1.3.

The precise position of the H atom in crystalline compounds containing H-bonds has raised considerable experimental and theoretical interest. In situations where a symmetric H-bond is possible in principle, it is frequently difficult to decide whether it is vibrating with a smaller amplitude about a single potential minimum or whether it is vibrating with a smaller amplitude but is also statistically disordered between the two sites being small.[79, 126] It now seems well established that the $F-H-F$ bond is symmetrical in $NaHF_2$ and KHF_2, and that the O-H-O bond is symmetrical in $HCrO_2$.

In summary, we can see that H-bonding influences crystal structure by linking atoms or groups into larger structural units. These may be finite groups (HF_2^-, dimers of carboxylic acids like formic acid, etc.), infinite chains (HF, HCN, HCO_3^-, HSO_4^-, etc.), infinite layers ($N_2H_6F_2$, $B(OH)_3$, $B_3O_3(OH)_3$, $H-2SO_4$, etc.) and three-dimensional nets (NH_4F, H_2O, H_2O_2, etc.). H-bonding also vitally influences the conformation and detailed structures of the polypeptide chains of protein molecules and the complementary intertwined polynucleotide chains which form the double helix in nucleic acids.[141, 202] Thus, proteins are built up from polypeptide chains using the peptide bonds which are amides linking a carboxylic acid and an amine.

These chains are coiled in a precise way which is determined to a large extent by $N-H\cdots O$ hydrogen bonds of length 2.79 ± 0.12 Å depending on the amino-acid residue involved. Each amide group is attached by such a hydrogen bond to the third amide group from it in both directions along the chain, resulting in a α-helix of pitch about 5.38 Å per turn, corresponding to

Table 1.3: Length of typical H-bonds.[126, 269]

Bond	Length (Å)	Σ (Å)*	Examples
F – H – F	2.27	(2.70)	$NaHF_2$, KHF_2
F – H ··· F	2.45–2.49	(2.70)	KH_4F_5, HF
O – H ··· F	2.65–2.87	(2.75)	$CuF_2 \cdot 2H_2O$, $FeSiF_6 \cdot 6H_2O$
O – H ··· Cl	2.95–3.10	(3.20)	$HCl \cdot 2H_2O$, $(NH_3OH)Cl$, $CuCl_2 \cdot 2H_2O$
O – H ··· Br	3.20–3.40	(3.35)	$NaBr \cdot 2H_2O$, $HBr \cdot 4H_2O$
O – H – O	2.40–2.63	(2.80)	Ni dimethylglyoxime, KH maleate, $HCrO_2$, $NaH(CO_3)_2 \cdot 2H_2O$
O – H ··· O	2.48–2.90	(2.80)	KH_2PO_4, $NH_4H_2PO_4$, KH_2AsO_4, AlOOH, $\alpha - HIO_3$
O – H ··· S	3.10–3.40	(3.25)	$MgS_2O_3 \cdot 2H_2O$
O – H ··· N	2.68–2.79	(2.90)	$N_2H_4 \cdot 4MeOH$, $N_2H_4 \cdot 4H_2O$
N – H ··· F	2.62–2.96	(2.85)	NH_4F, $N_2H_6F_2$, $(N_2H_6)SiF_6$
N – H ··· Cl	3.00–3.20	(3.30)	Me_3NHCl, Me_2NH_2Cl, $(NH_3OH)Cl$
N – H ··· I	3.46	(3.65)	Me_3NHI
N – H ··· O	2.81–3.04	(2.90)	HSO_3NH_2, $(NH_4)_2SO_4$, $NH_4OOCHCl$, $CO(NH_2)_2$
N – H ··· S	3.23, 3.29	(3.35)	$N_2H_5(HS)$
N – H ··· N	2.94–3.15	(3.00)	NH_4N_3, $NCNC(NH_2)_2$
P – H ··· I	4.24	(4.05)	PH_4I

*Σ = Sum of van der Waals' radii (in Å) of A and B (ignoring H which has a value of ∼1.20 Å) and using the values F 1.35, Cl 1.80, Br 1.95, I 2.15; O 1.40, S 1.85; N 1.50, P 1.90.

3.60 amino-acid residues per turn. These helical chains can, in turn, become stretched and form hydrogen bonds with neighbouring chains to generate either parallel-chain pleated sheets (repeat distances 6.50 Å) or antiparallel-chain pleated sheets (7.00 Å).

Nucleic acids, which control the synthesis of proteins in the cells of living organisms and which transfer heredity information via genes, are also dominated by H-bonding. Their structure involves two polynucleotide chains intertwined to form a double helix. The complementariness in the structure of the two chains is ascribed to the formation of H-bonds between the pyrimidine residue (thymine or cytosine) in one chain and the purine residue (adenine or guanine)

in the other. Whilst there is still some uncertainty as to the precise configuration of the $N-H\cdots O$ and $N-H\cdots N$ hydrogen bonds in particular cases, the extraordinary fruitfulness of these basic ideas has led to a profusion of developments of fundamental importance in biochemistry.[141]

1.1.2.3 Strength of hydrogen bonds and theoretical description [160]

Measurement of the properties of H-bonded systems over a range of temperatures leads to experimental values of ΔG, ΔH and ΔS for H-bond formation, and these data have been supplemented in recent years by increasingly reliable *ab initio* quantum-mechanical calculations. Some typical values for the enthalpy of dissociation of H-bonded pairs in the gas phase are in table 1.4.

Table 1.4: Enthalpy of dissociation of H-bonded pairs in the gas phase, $\Delta H_{298}(A-H\cdots Y)$, in kcal/mol.

Weak		Medium		Strong	
$HSH\cdots SH_2$	1.673	$FH\cdots FH$	6.931	$HOH\cdots Cl^-$	13.145
$NCH\cdots NCH$	3.824	$ClH\cdots OMe_2$	7.170	$HOCNH_2\cdots OCHNH_2$	14.101
$H_2NH\cdots NH_3$	4.063	$FH\cdots OH_2$	9.082	$HCOOH\cdots OCHOH$	14.101
$MeOH\cdots OHMe$	4.541			$HOH\cdots F^-$	23.422
$HOH\cdots OH_2$	5.258			$H_2OH^+\cdots OH_2$	36.089
				$FH\cdots F^-$	40.391
				$HCO_2H\cdots F^-$	∼48

The uncertainty in these values varies between ±0.2 and ±1.5 kcal/mol. In general, H-bonds of energy < 6 kcal/mol are classified as weak; those in the range 6–10 kcal/mol are medium; and those having $\Delta H > 10$ kcal/mol are strong. Until recently, it was thought that the strongest H-bond was that in the hydrogenfluoride ion $[F-H\cdots F]^-$; this is difficult to determine experimentally and values in the range 36–60 kcal/mol have been reported. A recent theoretically computed value is 40.391 kcal/mol which agrees well with the value of 39 ±1 kcal/mol from ion cyclotron resonance studies.[80] In fact, it now seems that the H-bond between formic acid and the fluoride ion, $[HCO_2H\cdots F^-]$, is some 7.1 kcal/mol stronger than that calculated on the same basis for HF_2^-.[81]

Early discussions on the nature of the hydrogen bond tended to adopt an electrostatic approach in order to avoid the implication of a covalency greater

than one for hydrogen. Indeed, such calculations can reproduce the experimental H-bond energies and dipole moments, but this is not a particularly severe test because of the parametric freedom in positioning the charges. However, the purely electrostatic theory is unable to account for the substantial increase in intensity of the stretching vibration ν(A-H) on H-bonding or for the lowered intensity of the bending mode δ(A-H). More seriously, such a theory does not account for the absence of correlation between H-bond strength and dipole moment of the base, and it leaves the frequency shifts in the electronic transitions unexplained. Nonlinear $\mathrm{A-H\cdots B}$ bonds would also be unexpected, though numerous examples of angles in the range 150-180° are known.[126]

Valence-bond descriptions predict up to five contributions to the total bond wave function,[211] but these are now considered to be merely computational devices for approximating to the true wave function. Perturbation theory has also been employed and it shows that the resultant energy bond is composed of different parts. First there is the electrostatic energy of interaction between the fixed nuclei and the electron distribution of the component molecules, second is the Pauli exchange repulsion energy between spin-like electrons, third is polarisation energy resulting from the attraction between the polarisable charge cloud of one molecule and the permanent multipoles of the other molecule, fourth is the quantum-mechanical charge-transfer energy, and fifth is the dispersion energy, resulting from second-order induced dipole-induced dipole attraction. The results obtained by Umeyama and Morokuma suggest that in general electrostatic effects predominate, particularly for weak bonds, but that covalency effects increase in importance as the strength of the bond increases.[263] It is also possible to tell the contributions of the energy obtained from *ab initio* SCF-MO calculations in this way. For example, in one particular calculation for the water dimer $\mathrm{HOH\cdots OH_2}$, the five energy terms enumerated above were calculated to be: $E_{electstat}$ = –6.33, E_{Pauli} = 4.3, E_{polar} = –0.5, $E_{ch\ tr}$ = –1.8, E_{disp} = 0 kcal/mol. There was also a coupling interaction E_{mix} = –0.1, making in all a total attractive force $\Delta E_0 = E_{dimer} - E_{monomers}$ = –4.4 kcal/mol. To calculate the enthalpy change ΔH_{298} it is also necessary to consider the work of expansion and the various spectroscopic degrees of freedom:

$$\Delta H_{298} = E_0 + \Delta(PV) + \Delta E_{trans} + \Delta E_{vibr} + \Delta E_{rot}$$

Other methods able to decompose the molecules energy to its different parts, like ADF or SAPT, render similar results. Such calculations can also give an indication of the influence of H-bond formation on the detailed electron distribution within the interacting components. There is general agreement

that in the system $X-A-H\cdots B-Y$ as compared with the isolated species XAH and BY, there is a net gain of electron density by X, A and B and a net loss of electrons by H and Y. There is also a small transfer of electronic charge (∼0.05 electrons) from BY to XAH in moderately strong H-bonds (5–10 kcal/mol). In virtually all neutral dimers, the increase in the A-H bond length on H-bond formation is quite small (< 0.05 Å), with an exception as $ClH\cdots NH_3$, where the proton position in the H-bond is half-way between completely transferred to NH_3 and completely fixed on HCl.

It follows from the preceding discussion that the unbranched H-bond can be regarded as a 3-centre 4-electron bond $A-H\cdots B$ in which the 2 pairs of electrons involved are the bond pair in A-H and the lone pair on B. The degree of charge separation on bond formation will depend on the nature of the proton donor group AH and the Lewis base B. The relation between this 3-centre bond formalism and the 3-centre bond descriptions frequently used for boranes, polyhalides and compounds of xenon is particularly instructive. Numerous examples are also known in which hydrogen acts as a bridge between metallic elements in binary and more complex hydrides.

1.2 Dihydrogen bonds [15, 56, 68, 219]

A *dihydrogen bond* (or DHB) is a kind of unconventional hydrogen bond, established between a metal hydride and a proton donor like OH or NH. It can be represented as $A-H\cdots H-M$, where A is an electronegative element which enhances the proton acidity as in the typical hydrogen bond, and M is a metal less electronegative than H and makes the σ electron pair of the $H-M$ bond act as an acceptor. A possible scheme could be:

Scheme 1.1.

$$A\text{–}H\cdots \begin{array}{|} H \\ M \end{array}$$

Although the interactioning elements are the hydride σ bond and the protonic hydrogen, a dihydrogen bond is usually depicted as an hydric-to-protonic interaction between hydrogens. Thus, the latter scheme is usually depicted as:

Scheme 1.2.

$$A\text{–}H\cdots H\text{–}M$$

By this sort dihydrogen bonds are also called proton-hydride bonding, $H \cdots H$ hydrogen bonding or hydrogen-hydrogen bonding. This interaction has a weaker strength but similar to a regular hydrogen bond, as well as its directionality. Thus, it can influence structure, reactivity and selectivity in solution and solid state, and so it has a potential in catalysis, crystal engineering and materials science.

1.2.1 Structural and energetic characterisation

After Moore and Winmill found the hydrogen bonds in 1912,[184] the possibility of a hydrogen-hydrogen interaction was not out of place. In 1934 there was a possible evidence found by Zachariasen and Mooney when they characterized the crystal structure of ammonium hypophosphite $NH_4^+H_2PO_2^-$ and stated that "the hydrogen atoms of the hypophosphite group behave toward ammonium as if they were H^- ions".[277] A paper published in 1964 by Burg suggested a hydrogen bond inbetween the hydrogens bonded to a nitrogen and those of the borane ($N - H \cdots H_3 - B$) in liquid $(CH_3)_2NH \cdot BH_3$, this time using IR spectroscopy band perturbation.[51] Four years later, a work by Titov and co-workers use as an explanation to the enhanced chemical reactivity of aminoboranes toward H_2 loss, the "close spatial arrangement of the oppositely charged hydrogen atoms".[258]

The first dihydrogen bond was reported in 1968 by Brown and Heseltine while working on of the boron coordination compounds $L \cdot BH_3$ ($L = Me_3N$, Et_3N, Py, Et_3P) and $Me_3N \cdot BH_2X$ ($X = Cl$, Br, I) in the presence of proton donors such as MeOH, PhOH, and $p - F - C_6H_4 - OH$ in CCl_4.[45, 46] They observed two intense absorption bands in the IR wavelengths of 3300 cm^{-1} and 3210 cm^{-1}, in a solution of $Me_2NH \cdot BH_3$ and $(RNH \cdot BH_2)_3$ ($R = Pr$, Bu) in CCl_4. The first one was assigned as a normal $N - H$ vibration, and the second one was assigned to the same bond, but they theorised that it could be interacting with the $B - H$ group. At lower dilutions, the band at 3210 cm^{-1} reduced its intensity and the one at 3300 cm^{-1} increased its, which is indicative of intermolecular association. They proposed the formation of a novel type of hydrogen bond in which the BH_3 and BH_2 groups acted as proton acceptors, despite their lack of lone pairs or π electrons. They measured the strengths of these interactions by variable temperature IR spectroscopy, finding association

energies in the range of 1.7–3.5 kcal/mol, comparable with moderately strong conventional hydrogen bonds.[47]

An intramolecular example of dihydrogen bond was first found in the complex $cis-[IrH(OH)(PMe)_4][PF_6]$ in 1986.[182] A low temperature neutron diffraction study was carried out later,[251] showing a short $O-H\cdots H-Ir$ distance of 2.40 Å, a short $Ir-O-H$ angle of 104.4° and an eclipsed $H-Ir-O-H$ conformation, which was thought to be a result of a dipole-dipole interaction and indicating an attractive $H\cdots H$ interaction. Another $O-H\cdots H-Ir$ interaction was discovered by Crabtree and co-workers in the iridium complex shown in figure 1.5a, based on NMR evidence, as no hydrogen atoms could be detected in the X-ray crystal structure.[159] The $H\cdots H$ distance was estimated as ca. 1.8 Å from the NMR data. Other related complexes were prepared and the first $N-H\cdots H-Ir$ (figure 1.5b) interaction was observed.

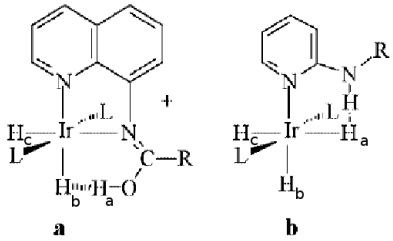

Figure 1.5: Scheme of Crabtree and co-workers' Ir complex.[159]

Theoretical HF calculations were performed on a model of complex 1.5b.[208] The energy of the model $IrH_3(PH_3)_2(HNCHNH_2)$ was lower by 14.4 kcal/mol when the N-H group was in the same plane as IrH_3, as in 1.5b, showing a rotation barrier due to the break of the $N-H\cdots H-Ir$ interaction. This value was corrected to 9.9 kcal/mol to account for the difference between formamidine (model) and 2-aminopyridine, which results are in good agreement with the experimental value of 10.8 kcal/mol. The strength of the hydrogen bond was estimated as 7.1 kcal/mol. The ligand *trans* to the hydride participating in the hydrogen bond may affect the bond; a poorer σ donor will cause the hydride to be less negatively charged, decreasing the electrostatic interaction between the H_2 and the H^+, and therefore leading to a weaker hydrogen bond.

At the same time, Morris and co-workers discovered another intramolec-

ular $H\cdots H$ interaction example in another iridium hydride complex, using X-ray diffraction in the solid-state and NMR spectroscopy in solution.[170] The crystal structure of figure 1.6a indicated a close contact between the pyridinium protons and the Ir-H hydridic hydrogens, which unfortunately could not be located precisely from the electron density difference maps. Nevertheless, their ^1H NMR data provided clear evidence for $N-H\cdots H-Ir$ hydrogen bonding in CD_2Cl-2, with a $H\cdots H$ contact distance of about 1.75 Å, calculated from the observed T_1 (spin-lattice relaxation time) relaxation times of the protonic and hydridic hydrogens. Theoretical calculations by Hoffmann et al. on the model complex 1.6b confirmed the attractive $H\cdots H$ interaction and concluded that its nature is mostly electrostatic.[169] Interestingly, when THF was used as a solvent, the dihydrogen bonds were switched off in 1.6a, presumably due to the formation of conventional $N-H\cdots O$ hydrogen bonds with the solvent.[170]

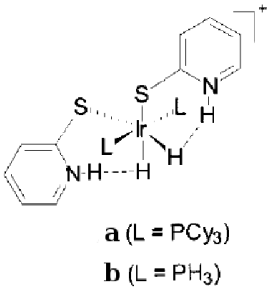

Figure 1.6: Scheme of Morris and co-workers' Ir complex.[170]

Bifurcated $N-H\cdots H(Ir)\cdots H-N$ dihydrogen bonds were also detected by Morris et al. in complexes depicted in figures 1.7a and 1.7b by X-ray crystallography and NMR spectroscopy, and their $H\cdots H$ contact distances were estimated around 1.80 and 1.86 Å, respectively, in solution.[197] The same group also found an interesting bifurcated $Ir-H\cdots H(N)\cdots F-B$ interaction in figure 1.7c complex, in which the N-H proton is shared by a hydridic Ir-H hydrogen and a conventional B-F electron donor from the BF_4^- counterion.[196]

The search for an intermolecular $H\cdots H$ dihydrogen bond had the first univocal result in the co-crystallisation of the complex $ReH_5(PPh_3)_3$ with indole. A neutron diffraction structure showed that two of the hydrides were interacting with the N-H bond of the indole ($H\cdots H$ distances of 1.75 and

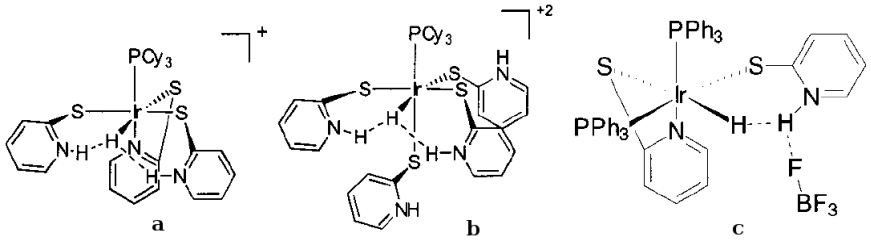

Figure 1.7: Different styles of bifurcated H···H interaction in an Ir complex.[170]

2.25 Å). Theoretical calculations led to a relatively good reproduction of the geometrical features (H···H distances 1.92 and 2.48 Å) and gave an interaction energy of 8.0 kcal/mol.[270] Reaction of the Re precursor with imidazole afforded $ReH_5(PPh_3)_2$(imidazole), where two of the hydrides were involved in hydrogen bonding with the N-H of a free imidazole molecule (H···H distances 1.68 and 1.99 Å).[201] The strength of the interaction was estimated from IR data to be 5.4 kcal/mol. The related derivatives containing pyridine and *o*- or *p*- NHR substituted pyridine, were prepared and the hydride fluxionality studied by NMR and theoretically.[37, 200] The rate was accelerated with the introduction of the *o*-NHR substituent in pyridine, and ascribed to intramolecular dihydrogen bond formation. Comparisons were made with the *p*-NHR derivative as this substituent cannot form intramolecular hydrogen bonds but electronic substituent effects are similar. The turnstile mechanism, with simultaneous rotation of three hydrides, was found to be the preferred both from experimental and theoretical results, leading to comparable barriers. A detailed study of the reaction mechanism showed that, for the 2-aminopyridine complex, strong hydrogen bonding was found in an intermediate along the reaction pathway. There was a barrier before reaching the transition state, owing to repulsion between two hydrides, and this prevented more powerful consequences of hydrogen bond toward lowering the activation barrier for hydride rotation.

In a thorough analysis, Epstein, Berke, and co-workers surveyed dihydrogen bonding in solution in the tungsten hydride-alcohol octahedric complexes $W(CO)_2(ON)L_2H\cdots HOR$, where HOR is a phenol, hexafluoro-2-propanol (HFIP), or perfluoro2-methyl-2-propanol (PFTB).[238] Using IR and NMR spectroscopies, they ruled out hydrogen bonding to the CO or NO groups and proved the exclusive formation of the unconventional $O-H\cdots H-W$ interac-

tions. As expected, the strengths of these dihydrogen bonds increase with the donor abilities of the ligand L ($PMe_3 > PEt_3 > P(Oi-Pr)_3 > PPh_3$) and are directly proportional to the acidities of the proton donors (PFTB > HFIP > PhOH). Their association energies fall in the estimated range 4.1–6.9 kcal/mol, based on both the observed shifts in the corresponding ν(O-H) bands, and the variation of the association constants K with temperature. In addition, NMR experiments (δ shifts, NOE, and T_1 relaxation times) all supported the formation of $O-H\cdots H-W$ dihydrogen bonds, with $H-H$ contact distances as short as 1.77 Å, as observed in the case of HFIP. A linear $O-H\cdots H-W$ orientation was arguably suggested for these interactions, in sharp contrast to the previously established propensity of dihydrogen bonds for a strongly bent geometry.

In an analogous series of rhenium hydride complexes ($ReH(CO)_2(ON)L_2H$), the same two research groups proved the occurrence of intermolecular $O-H\cdots H-Re$ dihydrogen bonding in solution.[24, 181] When PFTB was used as proton donor, interaction energies between 4.5 and 6.1 kcal/mol were calculated from the observed ν(O-H) shifts in the IR spectra in hexane. In toluene, however, the ΔH values, derived from variable temperature NMR spectroscopy, are smaller by about 3.0 kcal/mol, apparently due to competitive $O-H\cdots\pi$ interactions with the solvent.[181] The $H\cdots H$ contact distances calculated from T_1 relaxation times range between 1.78 and 1.94 Å. The phosphine ligand appears to have an important influence over the regioselectivity of the H-bonding formation. Thus, when $L = PMe_3$, an interaction with one of the hydridic hydrogens is preferred, but the NO group competes more and more effectively for the proton donor as the bulkiness of L increases, to the point where only $O-H\cdots O-N$ hydrogen bonds are observed for $L = P\mathit{i}Pr_3$. DFT calculations on a $ReH_2(CO)(NO)(PH_3)_2\cdot H_2O$ model indicated that the $H\cdots H$ interaction is energetically preferred by about 3.0–3.5 kcal/mol.[24] Also, a stronger interaction is predicted with the Re-H hydride *trans* to the NO group, with a $H\cdots H$ distance of 1.49 Å, as compared to the Re-H *trans* to CO, $H\cdots H$ distance 1.79 Å, and confirmed experimentally by the high regioselectivity displayed by both PFTB and HFIP alcohols toward the former, as shown by NMR spectroscopy.

The experimental results obtained by Epstein and Berke on the intermolecular dihydrogen bonding in solution were complemented by the theoretical work by Scheiner et al. on the Mo and W hydride complexes $M(CO)_2L_2L^1H\cdots HA$, where M = Mo and W, $L = PH_3$ and NH_3, L^1 = NO, Cl and H and A = F, OH and H_2O^+.[191] Their theoretical calculations with

different methods confirmed that the $H \cdots H$ interactions are favoured over conventional hydrogen bonding involving the NO group. The dihydrogen bonds in this complex become stronger and shorter as the donating ability of the *cis*-ligand or the acidity of the proton donor increase, which is consistent with experiment. However, the strongly acidic H_3O^+ induces complete proton transfer, resulting in the formation of an $\eta^2 - H_2$ dihydrogen complex. The $H - H - M$ angles are strongly bent in all the optimized structures. For the $Mo(CO)_2(PH_3)_2(ON)H \cdots HF$ dihydrogen-bonded system, a 2.6 kcal/mol destabilisation energy was calculated for a linear $F - H \cdots H - Mo$ orientation.

As seen with the boron hydrides, C-H sites may interact as the protonic partners with transition metal hydrides. Recent X-ray structural studies and CSD surveys confirmed the existence of intra-[134, 144, 220] as well as intermolecular[43] $C - H \cdots H - M$ close contacts in transition metal hydride complexes. A large number of these examples were observed in complexes containing $R_{3-x}(Ph)_xP$ (x = 1–3) ligands, in which one or more ortho C-H bonds point toward the M-H hydridic hydrogens.

While the $H \cdots H$ distances and $M - H \cdots H$ angles in these complexes were found to fall essentially in the same range as observed for the more "conventional" dihydrogen bonds involving N-H or O-H proton donors, the $C - H \cdots H$ angles usually tend to be smaller, due to the inherent constraints imposed by the chelation.[220] Caution is advisable in interpreting some of these $C - H \cdots H - M$ short contacts, however, as steric compression by bulky ligands or packing forces may make a significant contribution to the observed $H \cdots H$ close proximities. Additional evidence is needed before close $H \cdots H$ contacts may be interpreted as attractive dihydrogen bonding interactions in such questionable cases.

The comprehensive analysis of the manganese hydride complex $HMn(CO)_4P(Ph)_2C_6H_5$ carried out by Brammer and collaborators provided convincing evidence for an intramolecular $C - H \cdots H - Mn$ dihydrogen bond.[2] Their combined low-temperature neutron and X-ray diffraction study revealed a short intramolecular $C - H \cdots H - Mn$ contact of 2.10 Å, with $H \cdots H - Mn$ and $C - H \cdots H$ angles of 126.5 and 129.0°, respectively, and an essentially coplanar relative orientation of the Mn-H and C-H bonds (approximately 0.7°). The experimental atomic charges found for the Mn-H hydridic and ortho CH protonic hydrogens, of -0.40 and +0.32 e, clearly indicate an attractive electrostatic interaction, whose magnitude was calculated to be 5.7 kcal/mol. Moreover, topological analysis of the experimental charge density using the "atoms in molecules" theory unequivocally supported the existence of a moderately

strong intramolecular C − H ··· H − Mn hydrogen bond.

Several searches in the CSD for crystals exhibiting short intra- and intermolecular H ··· H contacts were made.[40, 44, 237] Many of the examples refer to intramolecular interactions involving X − H ··· H − M, where *X* is an electronegative atom (O, N, S), starting with the already mentioned *cis* − [IrH(OH) (PMe_3)$_4$][PF_6]. Other cationic complexes belong to this group, such as [IrH_2 (CO)(PPh_3)$_2$(pzH − N)][BF_4] · C_6H_5Me with H ··· H 1.998 Å,[16] [IrH(Cl)(L)] [PF_6] (L = 7-methyl-3,7,11,17-tetraazabicyclo[11.3.1]heptadeca-1(17),13,15--triene) with H ··· H 2.335 Å,[31] as well as the neutral compounds IrH(Cl) (PEt_3)$_2$ [NHPh(C_7H_{10})] with H ··· H 2.242 Å,[59] Ru(H)$_2$ − (CO)$_2$($PHPh_2$) ($PPri_3$)$_2$, with H ··· H 2.63 Å, and the *cis*-dicarbonyl [OsH(CO)$_2$($PHPh_2$) ($PPri_3$)$_2$][BF_4] with H ··· H 3.04 and 2.83 Å.[50] Spectroscopic evidence suggested the presence of M − H ··· H − N interactions in Ru complexes (NMR),[60] although no crystals of the product could be obtained. Polynuclear complexes and clusters also exhibit short H ··· H distances between a hydride and a X-H hydrogen. Examples are given by $Cp_2Zr(NHAr)(\mu - H)(\mu - NBut)IrCp*$, with an H ··· H distance of 1.717 Å,[17] the two related complexes [Rh_2H_2 ($\mu - SH_2$)$_2$MeC(CH_2PPh_2)$_3$][BPh_4] · HCONMe$_2$ [25] and [($\mu - H$)$_2$$Ir_2$ ($\mu - NH_2$)$_2$(PEt_3)$_4$(NH_3)$_2$]·Me_2CO,[58] with H ··· H 1.891 Å and 2.260, 2.189 Å, respectively for the Rh and the Ir complex, ($\mu - H$)Ru_3(CO)$_9$($\mu - C_6H_2-$ $-1 - NH - 2 - NH_2 - 4, 5 - Me_2$), with H ··· H 2.383 Å,[55] [Ru_6 ($\mu - H$)$_6$ ($\mu^3 - \eta^2$ − ampy) (CO)$_1$4] (ampy = 2-aminopyridine), with H ··· H 2.064 Å.[54] N − H ··· H − M interactions have also been detected in compounds without structural characterization, such as OsH (NH_3) (CO)$_9$,[3] and [{$\eta^5 - C_5H_4$ CH (CH_2)$_4$ NMe} Ir(PPh_3)H_2].[1] The observation of these interactions in the polynuclear complexes containing bridging hydrides is particularly interesting, as these hydrides often behave like acids. A close observation of the structure, however, suggests that steric constraints are responsible for the observed short H ··· H contacts.[44] The M-H bond can also participate in M − H ··· O hydrogen bonding,[41] as seen from many structures, but most of the hydrides involved are doubly or triply bridging hydrides which are very likely to carry a positive charge, so that the situation is not so surprising from an electrostatic point of view.

Theoretical studies were performed on some of the complexes, the most interesting results relating to the two cationic species, *cis* − [IrH(OH) (PMe_3)$_4$] [PF_6] and [IrH_2 − (CO) (PPh_3)$_2$ (pzH − N)] [BF_4].[44, 177] The geometries of the cations were optimised (using PH_3 instead of PMe_3 or PPh_3) and the agreement with the experimental structures was not particularly good. Intro-

duction of the counter ion (PF_6^- or BF_4^-) in the calculations led to a better geometry as the charge distribution in these complexes is compatible with an electrostatic interaction between the negatively charged hydride and the positive hydrogen attached to N or O. When the torsion angle H-Ir-O-H changes from 0 to 180°, thus making the $H \cdots H$ interaction vanish, the energy increases by 5.0 kcal/mol in the cation. The corresponding energy difference is 10.5 kcal/mol when the PF_6^- anion is present. The relevant conclusion is of a non-negligible role of the counter ion in helping to stabilise the short $H \cdots H$ arrangements.

The effect of charges in hydrogen bonds has also been assessed in the study of $O - H^- \cdots O^-$ interactions in chains of oxalate anions which are repulsive interactions. The reason why the atoms hold together is that they simultaneously participate in attractive interactions with the counter ion K^+.[42] This is a situation where a short $O - H^- \cdots O^-$ distance does not indicate a hydrogen bond.[43] The point is controversial, and brings forward the question whether distances by themselves provide an answer to the existence of a bond.[249] As the previous example shows, short distances in $O - H^- \cdots O^-$ chains can coexist with repulsive interactions, because a stronger cation-anion electrostatic attraction holds all ions in their place. A similar effect seems to take place in the dihidrogen bonded $cis - [IrH(OH)(PH_3)_4][PF_6]$.

So far the different examples of dihydrogen bonding molecules presented here have been complexes, but there are other simpler structures which have an $H \cdots H$ interaction. Boron is an atom whose hydrides can act as a proton acceptor in hydrogen bonds, as pointed out by Epstein and co-workers.[83, 235, 239] They studied the interaction of neutral NEt_3BH_3 and $P(OEt)_3BH_3$ as well as ionic $Bu_4N^+BH_4^-$ with different alcohols as proton donors, by IR and NMR spectroscopy in CH_2Cl_2, C_6H_{14}, and C_6D_{12}, and concluded that the properties of these unconventional $O - H \cdots H - B$ interactions are similar to those found in classical hydrogen bonds. Their association energies were found to increase proportionally with the proton donors' acidities, being situated in the range 1.1–3.7 and 2.3–6.5 kcal/mol, for the neutral and ionic boron hydrides, respectively. Theoretical calculations confirmed the attractive nature of these proton-hydride interactions.

The solution studies, however, cannot unambiguously establish whether these unusual interactions involve the boron atom, the hydridic hydrogen, or the BH group as a whole. It has been determined the X-ray and neutron crystal structures of $NaBH_4 \cdot 2H_2O$ and $NaBD_4 \cdot 2D_2O$ to probe the existence of $O - H \cdots H - B$ dihydrogen bonding in the solid state and provide a detailed

structural description of it.[69] Three close $H \cdots H$ contacts of 1.79, 1.86, and 1.94 Å, respectively were found, substantially shorter than the 2.4 Å distance corresponding to twice the van der Waals radius of a hydrogen atom. The O-H vectors clearly point toward the middle of the B-H bonds, suggesting association with the σ-bond electrons, rather than B or H atoms.

The same conclusion can be drawn from the systematic CSD search done by Richardson et al. for boron-nitrogen compounds.[219] There were found 26 $N - H \cdots H - B$ intermolecular short contacts in the range of 1.7 to 2.2 Å, for which the term "dihydrogen bonds" was suggested, and they showed a strong preference for a bent geometry, with $NH \cdots H - B$ angles typically within 95 and 120°, and $N - H \cdots H$ angles from the $N - H \cdots H - B$ interaction tending to be larger, most of them ranging from 150 to 170°. These side-on structures from bigger compounds were rationalised in terms of negative density charges on both B and H atoms, with the bending allowing the protonic NH to approach the partially negative B atom, thus maximising the attractive electrostatic interaction. They also investigated theoretically the NH_3BH_3 dimer, whose C_2 symmetrical geometry (figure 1.8a) optimized using theoretical methods (PCI-80/B3LYP) showed two identical $H \cdots H$ interactions, with contact distances of 1.82 Å and $NH \cdots H - B$ and $N - H \cdots HB$ angles of 98.8 and 158.7°, respectively, falling in the range found by the CSD search. The calculated dimerisation energy of -12.1 kcal/mol corresponds to 6.1 kcal/mol per $N - H \cdots H - B$ interaction, which, as suggested by Richardson, could account for the strikingly higher melting point of aminoborane, +104℃, relative to the isoelectronic ethane, -181℃.[219]

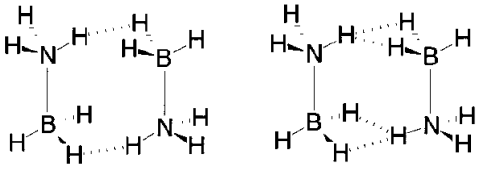

(a) C_2 symmetry (b) C_{2h} symmetry

Figure 1.8: Isomers of the NH_3BH_3 dimer.

A similar head-to-tail arrangement was also found by Cramer and Gladfelter in their theoretical study of the $(NH_3BH_3)_2$ dimer.[66] However, using different theoretical methods from the ones used by Richardson, mainly

HF, DFT and MP2 levels of theory, they found a C_{2h} symmetrical structure as the global minimum (figure 1.8b), which lies only 0.2 kcal/mol under the C_2 isomer reported by Richardson et al. This geometry allows the formation of bifurcated dihydrogen bonds with $H-H$ distances of 1.990 Å, and $NH\cdots H-B$ and $N-H\cdots HB$ angles of 88.6 and 144.8°, respectively, as calculated at the MP2/cc-pVDZ level. The association energy obtained at the same level of theory is -15.1 kcal/mol.

Experimental data obtained using neutron diffraction on the crystal structure of NH_3BH_3 by Crabtree and co-workers in 1999, shows a packing that results in three short intermolecular $N-H\cdots H-B$ interactions, with the shortest one exhibiting a $H-H$ distance of 2.02 Å and values for the $NH\cdots H-B$ and $N-H\cdots HB$ angles of 106 and 156°, respectively.[149] Again, the $N-H$ vectors point toward the middle of the $B-H$ bonds, suggesting that the σ-bond as a whole represents in fact the proton acceptor partner in these interactions.

Further insight into the nature of the $N-H\cdots H-B$ interaction was provided by Popelier, who applied the "atoms in molecules" theory on the same $(NH_3BH_3)_2$ dimer and concluded that this interaction can indeed be classified as a hydrogen bond.[216] Other intermolecular $N-H\cdots H-B$ interactions have also been described in other molecules, for example the $(CH_3)_2NH-BH_2-$ $-N(CH_3)_2-BH_3$ crystal determined by Noth et al., which self-assembles into dihydrogen-bonded dimers, different enough from the NH_3BH_3 crystal, which can produce a grid.

There are also examples of an intramolecular $N-H\cdots H-B$, as found in the crystal structure of the 2'-deoxycytidine-N(3)-cyanoborane, which shows a close $H\cdots H$ contact of 2.05 Å.[243, 281] These close contacts can be responsible to the stabilisation of molecules. In aminoboron hydrides there are $C-H\cdots C-H$ intramolecular interactions that are thought to lead to a stabilisation, which otherwise could not be achieved.[194] Their X-ray crystal structures show multiple $H-H$ distances below 2.65 Å, which was considered as the threshold intermolecular distance for $H\cdots H$ due to be less than the van der Waals radius. The heterocyclic rings adopt almost coplanar orientations relative to the B-H bonds, maximising thus the intramolecular $H\cdots H$ associations. The relatively small H-C-N exocyclic angles next to the B-H bonds in some of these complexes, as compared to the free heterocycles, also suggest attractive interactions between the protonic hydrogens on the α-carbons and the hydridic BH hydrogens. Intramolecular $C-H\cdots H-B$ dihydrogen bonds were also proposed to play an important role in controlling the conformation

of the azacyclohexane-borane adducts.[91] Thus, the BH_3 groups are always found in the equatorial position in these complexes, which appears to be the result of favourable attractive interactions between the hydridic B-H hydrogens and the positively charged H atoms of the α-CH_2 groups. Associations with the C-H hydrogens of the $N-CH_3$ group also seem to stabilise these structures, as indicated by the short $H-H$ distances and the decrease of the $H_3C-N-BH_3$ angles relative to the $H_3C-N-CH_3$ angle in the $(CH_3)_2N^+$ derivative.

The hydrides of the heavier group 3 elements are also capable of forming dihydrogen bonds. Thus, in 1994, Raston and co-workers provided X-ray crystallographic evidence for an intramolecular $N-H\cdots H-Al$ interaction in an alane-piperidine.[9] The H-Al-N-H unit has an eclipsed conformation in the solid state, allowing the two oppositely charged hydrogen atoms to approach to 2.31 Å, in direct contrast to the previously reported structures of aminoalanes, which are known to exhibit a staggered conformation about the Al-N bond. This arrangement, Raston noted, represents an intermediate prior to H_2 evolution, to form an amidometal species. Gallium can also be involved in dihydrogen bonding, as Gladfelter's neutron diffraction crystal structure of cyclotrigallazane (a three member N-Ga ciclohexane-type ring, $Ga_3N_3H_{12}$) demonstrates.[57] In the solid state, it forms an α-network, by participating in four $N-H\cdots H-Ga$ intermolecular interactions, with $H-H$ distances of 1.97 Å. The observed $NH\cdots H-Ga$ and $N-H\cdots HGa$ angles are rather close, with values of 131 and 145°, respectively. The strength of these dihydrogen bonds was estimated by theoretical calculations on the $[(NH_2GaH_2)_3]_2$ dimer. As in the aluminium analogue, the monomer prefers the twist-boat conformation by 2.6 kcal/mol, favouring thus intramolecular $H\cdots H$ interactions involving the oppositely charged H atoms from the flagpole positions. However, for direct comparison with the solid-state structure, the chair conformation was considered for the geometry optimization of the dimer. The highest dimerisation energy was found for the C_s symmetrical structure, from which an interaction energy of about 3.0 kcal/mol could be estimated for each $N-H\cdots H-Ga$ dihydrogen bond. In the case of the $(NH_3GaH_3)_2$ dimer, theoretical calculations by Cramer and Gladfelter predicted a C_2 symmetrical geometry similar to the one found in the aluminium analogue, with $N-H\cdots H-Ga$ dihydrogen bonds of approximately 7.2 kcal/mol in strength.[66]

Formation of dihydrogen-bonded complexes by other main group hydrides such as LiH, BeH_2, or the recently discovered XeH_2, has been investigated theoretically by a number of researchers.[4, 154, 155, 169, 171, 218] A theo-

retical study at MP2 and B3LYP level of the dihydrogen-bonded complexes between the hydrides LiH, NaH, BeH_2, MgH_2, CH_4, SiH_4, GeH_4, SnH_4, and hydrofluoric acid demonstrated the existence of direct correlations between $H\cdots H$ distances and H-bonding energies.[123] Also, the $H\cdots H$ separations have been found to be inversely proportional to the F-H bond lengths, as is seen in conventional $O-H\cdots O$ or $N-H\cdots O$ hydrogen bonds.[115, 123]

1.2.2 Reaction control and selectivity with dihydrogen bonds

As it has been previously stated in section 1.1.2.2, weak interactions are involved on molecular suprastructures like the secondary, ternary and quaternary conformation of proteins. Nevertheless, dihydrogen bonds have been regarded also as a useful tool to control reactivity and selectivity in some reactions. Thanks to their substantial strength and directionality they are used in supramolecular molecule synthesis. However, what makes dihydrogen bonding particularly interesting is the special reactivity conferred by its peculiar nature. It has been recently demonstrated that $H\cdots H$ bonds have a role in the formation of dihydrogen η^2-H_2 complexes and the reverse heterolytic splitting of H_2, as well as σ-bond metathesis (see scheme 1.3). In the solid state, this transformation can be topochemical, transferring the initial order present in the starting dihydrogen-bonded crystal to the newly formed covalent network, thus providing access to novel crystalline materials with desired structures and properties.

Scheme 1.3.

$$M\text{–}H \;+\; H\text{–}A \;\rightarrow\; M\text{–}H\cdots H\text{–}A \;\rightleftharpoons\; M\cdots \begin{vmatrix} H \\ A \\ H \end{vmatrix}^{+} \quad \begin{matrix} -H_2 \\ \rightleftharpoons \\ +H_2 \end{matrix} \quad M\text{–}A$$

The Ir-H_b bond in 1.5a has been found to be activated by dihydrogen bonding for a number of reactions.[158] Thus, the hydridic and protonic hydrogens H_a and H_b involved in the $H\cdots H$ interaction can interchange relatively easily, whereas the noninteracting H_c is exchanged much more slowly with H_a and H_b. The $\Delta H^{\not=}$ for the H_a/H_b exchange was estimated by variable temperature NMR spectroscopy at around 14.0–15.9 kcal/mol and found to go down as the R group becomes more electron-withdrawing, consistent with a mechanism involving proton transfer from the OH group to the Ir-H_a bond, to give

an η^2-H_2 intermediate complex. Rotation of the H_2 ligand in this complex and transfer of the proton back to the oxygen completes the exchange.

The first direct observation of a dynamic equilibrium between a $H\cdots H$ bonded system and an η^2-H_2 complex resulting from proton transfer along a dihydrogen bond was made by Chaudret and coworkers, using NMR spectroscopy on $(dppm)_2HRuH\cdots H-OR$.[10] Thus, the ruthenium hydride complex $RuH_2(dppm)_2\cdot PhOH$ exists as a mixture of dihydrogen-bonded *cis* and *trans* isomers in benzene or toluene solutions. The *trans* isomer is also involved in a dynamic equilibrium with the dihydrogen forming a σ bond with Ru, which lies 17.0 kcal/mol lower in enthalpy than the initial complex showing a $Ru-H\cdots H-OR$. It was proposed that the reversibility of the process originates in the strong dihydrogen bonding in $(dppm)_2HRuH\cdots H-OR$. In the presence of the more acidic hexafluoro-2-propanol, the corresponding dihydrogen complex showing the η^2-H_2 further reacts by H_2 loss, to ultimately give $(dppm)_2Ru(OR)_2$. Theoretical calculations by Scheiner et al. on a $HOH\cdots H_2Ru(PH_2CH_2PH_2)_2$ model confirmed the higher stability of the dihydrogen complex, which lies 10.7 kcal/mol lower in energy than the dihydrogen-bonded adduct in this case.[192] The activation energy for the proton transfer was estimated around 10.0 kcal/mol. However, when the stronger proton donor HF was used in the calculations, no $F-H\cdots H-Ru$ adduct could be identified, and the system evolved directly toward a dihydrogen complex, which in this case was found to be 23.8 kcal/mol lower in energy than the separated HF and ruthenium hydride complex.

Using IR and NMR spectroscopy techniques, Epstein et al. studied the reversible proton transfer in the dihydrogen-bonded complexes between $(triphos)-$ $-Re-(CO)_2H$ and phenol, tetrafluoroboric acid ($HBF_4\cdot OMe_2$), chloroacetic acid ($ClCH_2CO_2H$), hexafluoro-2-propanol (HFIP), or perfluoro-2-methyl-2-propanol (PFTB), as proton donors, at 200-260 K.[236] The η^2-H_2 complexes were found again to be thermodynamically more stable than their $H\cdots H$ bonded precursors. Higher temperatures induced H_2 loss with the formation of the covalent products with $O-R$. The proton transference to form a η^2-H_2 in a complex is dependent on the proton donor capacity of the protonated species as found by Scheiner et al.[190] They used the $HRu(Cp)(CO)(PH_3)$ ruthenium hydride model, and made it interact with H_3O^+, CF_3OH, or H_2O, representing strong, moderate, and weak proton donors, respectively. While in the first case spontaneous transfer of proton with the formation of a corresponding hydrated η^2-H_2 complex was observed, the other two weaker acids did not transfer the proton at all, suggesting that the activation barrier for this process is largely determined by the proton donor ability of the acidic

partner. The critical role of the proton donor acidity has also been recently recognised by Lau et al., who concluded that strongly acidic conditions give η^2-H_2 complexes, while weakly acidic conditions favour dihydrogen-bonded species.[61]

Other examples of dihydrogen bonds involved in a reaction were shown by Lau et al., intramolecular $N-H\cdots H-Ru$ dihydrogen bonds also appear to mediate proton transfer and subsequent formation of N-Ru bonds in the first complex depicted in scheme 1.4, which illustrates the H_2 loss.[60] H/D exchange of both protonic and hydridic hydrogen atoms with D_2O strongly suggest the existence of η^2-H_2 intermediate species in equilibrium with the $H\cdots H$ bonded complexes. H_2 loss with the formation of a Ru-N bonded chelate structure is easy in the second form, and the reverse Ru-N bond hydrogenolysis can be done at 60°C under 60 atm. This system was found to catalyse the reduction of CO_2 to formic acid, although with low yields.

Scheme 1.4.

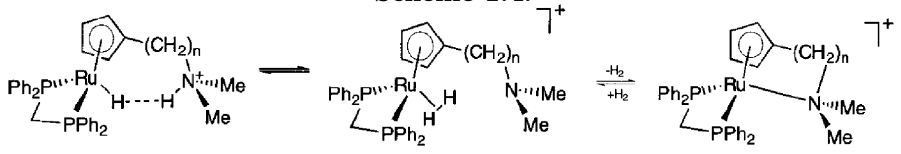

A very interesting dihydrogen-bonded system and its hydrogen exchange dynamics have been recently described by Jalon et al.[53] They reported a three centre $py_2H\cdots H-Ru$ intramolecular interaction in the first complex in shceme 1.5, in which fast scrambling between the hydridic and protonic hydrogens occurs most probably via an η^2-H_2 complex intermediate. An activation energy of about 13.6 kcal/mol was determined for this process, using variable temperature ^1H NMR spectroscopy. Moreover, this system proved to be a very active catalyst for D^+/H_2 exchange. Thus, when a solution of the species in scheme 1.5 in CD_3OD as solvent was exposed to a hydrogen atmosphere at room temperature and 1 atm, more than 90% of H_2 was exchanged for D_2 in about half an hour.

The last examples show many studies regarding the dynamics of dihydrogen-bonded systems in solution, and conclude that proton transfer from the acidic AH partners to the transition metal hydrides MH, along the $H\cdots H$ bonds, generally leading to η^2-H_2 nonclassical complexes, which subsequently eliminate hydrogen upon heating, with the formation of covalent M-A bonds (scheme 1.3). An analogous process appears to occur in the case of the borohydride an-

Scheme 1.5.

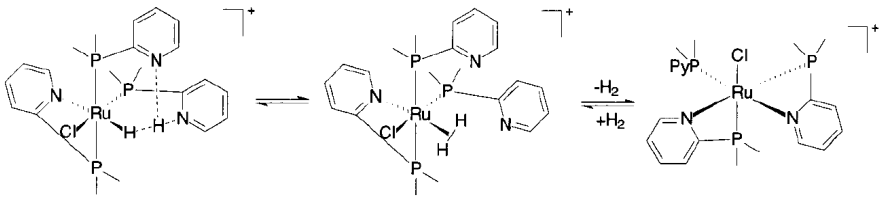

ion. In aqueous solutions, BH_4^- is very likely dihydrogen-bonded to H_2O, as suggested by the crystal structure of $NaBH_4 \cdot 2H_2O$, as well as theoretical and experimental studies by Epstein et al.[83, 235, 239] Under neutral or acidic conditions, borohydrides undergo hydrolysis to boric acid ($B(OH)_3$), for which the established mechanism involves slow proton transfer resulting in a BH_5 intermediate, followed by fast H_2 loss and B-O bond formation.[72, 152, 180, 204] Theoretical work by Elguero et al. indicates that H_2 generation from dihydrogen-bonded borohydrides can also be induced by the internal forces within a crystal.[224] This considerations, added to the proven ability of borohydrides to self-assemble into extended dihydrogen-bonded networks, suggested that $A-H\cdots H-B$ dihydrogen bonds could be employed in topochemical assembly of covalent materials.[67] Such weak $H\cdots H$ interactions, in principle, may be used to organise and hold a structure form while it is more firmly fastened together by A-B bond formation, transferring thus the initial order from the starting crystal to the newly formed covalent frame. This strategy makes dihydrogen bonding a potentially powerful tool for rational assembly of new crystalline covalent materials with controlled structures and properties.

Cyclotrigallazane, which its solid structure is reviewed in page 35, is an example of topochemical control by dihydrogen bonding with its solid-state conversion into nanocrystalline gallium nitride, reported by Gladfelter and coworkers.[137] Initial loss of H_2 at 150°C resulted in an amorphous GaN phase, which upon annealing at 600°C led to the metastable crystalline cubic gallium nitride, as a 1:1 mixture with the thermodynamically favoured hexagonal GaN. The crystallisation in the cubic system appears to be dictated by the initial crystal packing in the cyclotrigallazane, consisting of $N-H\cdots H-Ga$ dihydrogen-bonded chains (figure 1.9), which can be considered essentially "hydrogenated" cubic GaN. For comparison, decomposition of cyclotrigallazane in thin films obtained by vapour deposition, a process that presumably disrupts the dihydrogen-bonded network, yields exclusively hexagonal GaN. It is re-

markable that despite the huge contraction of the unit cell accompanying the conversion of cyclotrigallazane into cubic GaN, the reaction still maintains partial topochemical character. The price to pay, however, was the initial loss of crystallinity and the consequent requirement for high annealing temperatures to restore it. Although this thermal treatment had no detrimental effect upon the robust GaN, more delicate structures would not tolerate such high temperatures, limiting the general applicability of this approach.

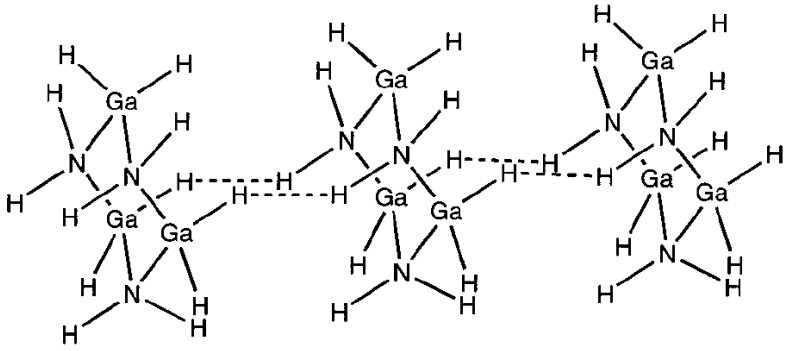

Figure 1.9: Solid state self-assembled cyclotrigallazane.

A low temperature procedure for topochemical dihydrogen to covalent bonding transformations would allow the extension of this strategy into the structurally more diverse domain of organic materials. Like many solid-state processes, this reaction includes two threats to the crystalline order. One is the geometry change upon bond reorganisation, and the other is gas release within the lattice. Clearly, careful design of the starting dihydrogen-bonded networks is necessary to meet these challenges. Success, however, would mean that the well-developed tools of molecular synthesis could now be applied to the rational construction of crystalline covalent solids with desired structures and functions.

One step beyond of the reaction selectivity leads to the field of hydrogen storage.[62, 275, 278, 75, 146] The convenience of stabilizing large quantities of hydrogen for storage and transportation is paramount as it has a low-temperature ignition, ease of leakage and metal embrittling properties. One of the trends to deal with this problem is the use of solid surface adsorbents to fix or even break the hydrogen molecules and recover them when

needed.[146, 173, 183, 189, 250, 129, 248] Most of the reactions involve steps where a dihydrogen bond is established. Pyykkõ and Wang made a study on the boron-nitrogen compound $N-\mathrm{TMPN}-\mathrm{CH_2C_6H_4B(C_6F_5)_2}$, TMPN is $2,2,6,6-$tetramethylpiperidine and N is the place where the ligand is attached, which reversibly adsorbs hydrogen.[217] Their study remarks that without using bulky ligands, the energy of the hydrogenated system would be lower than using them, as well as that a relatively tiny dihydrogen bonding contribution has the potential to influence the process too. But the most studied compounds are the amino borane complexes, as it will be further studied in this thesis too. They have good hydrogen storage properties as their potential active hydrogen content is very high and the release of hydrogen at 25℃ is almost thermoneutral,[76, 124] although the reverse reaction is unlikely to happen at moderate pressures.[183] The different studies of this group of molecules point to a formation of dihydrogen bonds during the adsorption and desorption of hydrogen molecules, a facet which will be extended in this work.

1.3 Overview of the thesis

Through this chapter different aspects and points of interest about dihydrogen bonds have been showed and highlighted, exposing them as the key to important changes in the structure and properties of different compounds. They can be responsible for the geometry of not only small molecules like the $\mathrm{NH_3BH_3}$ dimer, but also for higher structures like metallic complexes or solids. They can also change the boiling and melting points, magnetic and spectroscopic properties and other characteristics like hydrogen bonds, although hydrogen-hydrogen bonds are not as strong as the former. It is in this fashion that dihydrogen bonds can be profitable, up to a plausible extent, when they can be used in certain molecules or certain syntheses to obtain new materials with particular or even tailored properties or geometries. The work developed in this thesis is aimed to have a deeper understanding of dihydorgen bonds, deepening on certain aspects using methods that have not been used up to date, and working towards having reliable models to set a basis for further investigations.

The chapters in this thesis are arranged in an increasing system size scale. This chapter has been a general picture to introduce where does the dihydrogen bond stand with respect to other forces and its general properties. It has followed a deeper insight in the first hints of dihydrogen bonds, mainly in complexes, and the consequent research in both experimental and theoretical level, giving further information of them. Chapter 2 provides an overview of

the theory and methods used in this thesis. In the first section there is a general explanation of quantum theory and some mathematical representations which will be used later in the theoretical methods. Next, the *ab initio* Hartree-Fock or self-consistent field methods are first explained as they provide the basis for the other post-hartree-fock methods like Møller-Plesset or any other algorithms which include it. Other methods and theories briefly explained in chapter 2 are density functional theory, perturbation theory, a small part of the wide basis set superposition error correction problem and a way to correct a potential energy surface, Bader's atoms in molecules theory which is useful for knowing the topology of the interactions, Kohn-Sham orbital theory to study the orbital interactions which are taking place, and finally some hints of solid state simulation.

Chapters 3, 4, 5 and 6 apply all the aforementioned theories and methods to different systems, starting from simple model systems and increasing their complexity to solid state. In chapter 3 small systems are used to understand the behaviour and properties which later will help us understand bigger systems. First a geometric and energetic analysis is performed on dimers which are known to have dihydrogen bonds. The basis set superposition error is important in systems like these, which have really small interaction energies and its potential energy surfaces are smooth and flat. In specific cases a small change of energy might represent a drastic geometry reorganisation. It follows a deeper insight in chapter 4 on the electronic structure using atoms in molecules theory to describe the bond through bond critical points, electron densities, electron delocalizations and other related properties. From this data, a $H \cdots H$ can be classified as a hydrogen molecule, a typical hydrogen bond, or a dihydrogen bond. Afterwards, the same systems have been studied at orbital level using Kohn-Sham orbital theory, looking at the different energy contributions to the system and finding which is responsible for the system's stabilisation.

Chapter 5 focus on the reactive importance of dihydrogen bonds while needing to increase the size of the model systems, using experimental molecules known to have DHB interactions in the intermediate species of the reaction, usually resulting in a dehydrogenation. There is a small discussion in this chapter dealing with H_2 storage, as DHBs have a small interaction energy, they could be used as an easy energetically-inexpensive way to store and release hydrogen. Finally, chapter 6 deals with the simulation of a solid state BH_3NH_3 simulation, whose DHBs differ each other in range and energy depending on the position they occupy the crystal, but are interactions of the branched type. An analysis on geometry, energies and frequencies is commented in order to

find new characteristics in these DHBs and define the strengths of each DHB interaction separately. The last chapter resumes the conclusions obtained from all the previous sections.

Chapter 2

Methodology

Karma police
arrest this man
he talks in maths
he buzzes like a fridge
he's like a detuned radio

— Radiohead
Karma police (1997)

2.1 From continuum to quantum [8, 203, 210]

Right in the beginning of the twentieth century, physics was thought to be thoroughly set and described. The macroscopic world had been studied and models on matter and waves could describe and predict their motion or other behaviours. It was thought to be just a matter of time to perfect the theories and increase the precision of the different universal constants found up to date.

But there were several evidences for which the Newtonian physics could not account. When models were applied to a scale different from the human-size one in which they were observed, they failed repeatedly to predict the expected results. The smallest and the most massive bodies, as well as interactions at the highest speeds, looked as if they were not subjected to those models. Two objects approaching at more than the speed of light cannot be approaching each other at more of the speed of light itself, matter can be transformed into energy, time progresses slower in the proximity of a massive object, really small bodies cannot be traced as an entity but a probability... scales which were thought to be constant didn't behave as such.

2.1.1 Old quantum theory

Huygens, Newton, Young and Fresnel, Maxwell and Hertz made different experiments regarding the nature of light. Its characteristics were in a controversy between some who thought of it as a particle (Newton) and others who devised it as a wave (Huygens), which was an inconvenience since in classical physics these theories are contradictory. Their different experiments led to think that the corpuscular model which Newton came up with was not adequate to explain all of them. Hints were taken from photoconductivity: when light hits certain electrical conductors, it creates an electron flow. If the intensity is raised, more electrons move, but they do not move faster as it was thought in the corpuscular model. Instead, intensity controls current that translates to energy. On the other hand, light frequency controls electron speed or voltage. A packet or quantum model was needed.

2.1.1.1 Planck constant

Max Planck was the first scientist to shed the idea of quantized energy in his theoretical hypothesis of the black body radiation.[213] In physics, a *black body* is an impermeable object capable of absorbing any type of radiation without reflecting it, and at the same time should emit all the absorbed radiation, thus being in thermal equilibrium with the surroundings. Rayleigh and Jeans used classical physics while assuming that the whole black body as a group of electromagnetic oscillators of all possible frequencies, obtaining:

$$\rho = \frac{8\pi kT}{\lambda^4} \tag{2.1}$$

where ρ represents the energy density (or the density of states), k is the *Boltzman's constant* ($k = 1.381{\cdot}10^{-23}$ J·K^{-1}), T is the temperature and λ is the wavelength. Rayleigh-Jeans law checks with experimental data at long wavelengths, but predicts infinite energy density at short wavelengths. This implies that, for example, at room temperature, there is a large quantity of energy radiated in high-frequency modes (ultraviolet and X-rays) which has not any experimental back-up. This is known as the *ultraviolet catastrophe*.

Planck used a different approach to the energy density distribution: he postulated that the harmonic oscillators (i.e. the vibrating particles of matter) do not emit or absorb light continuously but instead they do it in discrete quantities of magnitude $h\nu$ proportional to the frequency ν of the light, that is:

$$E = nh\nu \qquad n = 1, 2, 3 \ldots \tag{2.2}$$

$$\rho = \frac{8\pi hc}{\lambda^5 \left(e^{hc/\lambda kT} - 1\right)} \tag{2.3}$$

There are two new constants compared with equation 2.1: c is the speed of light, and the proportionality constant h is *Planck's constant* and has a value of $6.626{\cdot}10^{-34}$ J·s. It is what quantizes the energy of the oscillator, forbidding it to take any value independently from the frequency at which it moves, describing the wave as small packets which Planck named as *quanta*. In some sense this discovery was an approach of the wave to the particle. Later, Einstein suggested that the quantity of radiant energy sent out in the process of emission of light was not emitted in all directions but instead unidirectionally, like a particle.[78] In the same work, he described a possible explanation for the photoelectric effect, postulating the energy in a beam of light occurs in concentrations that he called light quanta, later known as *photons*. Photons can have more or less energy, but that only depends on their frequency.

2.1.1.2 Bohr atom

In 1909 Geiger and Marsden under the direction of Rutherford came up with an experiment which discarded the Thomson's plum pudding atomic model, where the electrons, discovered back in 1897 by Thomson himself, were surrounded by a soup of positive charges. The experiment is known as *Geiger-Marsden, Gold foil* or *Rutherford experiment*.[109] They fired a flux of α-particles through a

thin gold foil looking for deviations in the particles beams, expecting none or few to happen if the Thomson model was correct. They found that few rays were deflected, but some rays were deflected back, which should not happen and thus discarding the model. Rutherford processed the data from the experiment, and two years later he devised a simple atomic model where a dense positively charged centre was orbited by small electrons.[225] The model fit in the Geiger-Marsden experiment as there was much empty space between the nucleus and the electrons, thus avoiding the deflection of the α-particles, but the dense nucleus made for the explanation of the returning beams. Yet it had one flaw: if electrons were to move in orbits, they should radiate energy which would precipitate them towards the nucleus.

Niels Bohr joined the Rutherford atomic model and Planck's quantization to produce a new model of the atom. The model was based on Rutherford's one but avoided the electron fall into the nucleus by issuing two postulates:

1. *The Existence of Stationary States.* An atomic system can exist in certain stationary states, each one corresponding to a definite value of the energy E of the system; and transition from one stationary state to another is accompanied by the emission or absorption as radiant energy, or the transfer to or from another system, of an amount of energy equal to the difference in energy of the two states.

2. *The Bohr Frequency Rule.* The frequency of the radiation emitted by a system on transition from an initial state of energy E_2 to a final state of lower energy E_1 (or absorbed on transition from the state of energy E_1 to that of energy E_2) is given by the equation 2.4:

$$\nu = \frac{E_2 - E_1}{h} \tag{2.4}$$

With these postulates, Bohr gave a method of determining the quantized states of motion of the stationary states of atoms. It explained the orbits electrons can take by relating the angular momentum of electrons in each allowed orbit to Planck's constant h and considered one revolution in orbit to be equivalent to one cycle in an oscillator, which is in turn similar to one cycle in a wave. The number of revolutions per second is the frequency of that electron or orbital. Each orbit is described by its frequency which must be an integer multiple of Planck's constant and hence, quantized. At that time, scientists were looking at hydrogen spectra and trying to model the hydrogen atom. Working with the Balmer series of spectra, Bohr introduced that

the electrons angular momentum in its orbit, L, was quantized as well. This method of quantization involving the restriction of the angular momentum of circular orbits to integral multiples of the quantum $h/2\pi$ lead to satisfactory energy levels related to spectrographic information, but was soon superseded by a more powerful method, described in next section 2.1.2.

The old quantum theory did not provide a satisfactory method of calculating the intensities of spectral lines emitted or absorbed by a system, that is, the probabilities of transition from one stationary state to another with the emission or absorption of a photon. Qualitative information was provided by an auxiliary postulate, known as *Bohr's correspondence principle*, which correlated the quantum-theory transition probabilities with the intensity of the light of various frequencies which would have been radiated by the system according to classical electromagnetic theory. In particular, if no light of frequency corresponding to a given transition would have been emitted classically, it was assumed that the transition would not take place. The results of such considerations were expressed in selection rules. In Bohr's atomic model, comparing with the experimental data, the transition between orbitals was only possible if $\Delta n = \pm 1$: an electron can jump one orbital at a time.

2.1.1.3 Wave-particle duality

The way an electron jumps in a transition happening between orbitals is far from a classic problem. In Bohr's model, electrons disappeared from one orbit and appeared in the other one, without moving through the space inbetween orbitals. The electrons taking one quantum of energy leap automatically to the orbital above them, more energetic; and the ones emitting one quantum of energy fall to the orbital under them, closer to the nucleus and with less energy. A fraction of quanta is not possible, so there is no trip from one orbital to the other.

Up to the point where Bohr had his model set, the nature of light, and by extension the behaviour of electrons, was still in doubt whether it was a wave or a particle. Bohr enunciated the *complementarity principle*, where he stated that wave and particle were paired, i.e. sometimes subatomic particles behaved following the wave analogy, sometimes reacted like particles, but never simultaneously as both. It allows wave and particle attributes to co-exist, but postulates that a stronger manifestation of the particle nature leads to a weaker manifestation of the wave nature and vice versa. Luis de Broglie worked on this theory, adding Planck's and Einstein's discoveries as well, and pushed for its

application beyond hydrogen and tried to find an equation which could explain the wavelength characteristics of all matter. He postulated in his thesis—and latter in the journal Annales de Physique—that subatomic entities have properties of both waves and particles.[73] He generalised Planck's equation 2.2 to all matter:

$$\lambda = \frac{h}{p} \tag{2.5}$$

De Broglie conclusions applied to electrons implied that they could only appear under conditions that permit a standing wave. The only standing waves that can occur are those with zero amplitude at two fixed ends if they are not continuous. A standing wave can only be formed when the wavelength fits the available vibrating entity. In other words, no partial fragments of wave crests or troughs are allowed. In a round vibrating medium, the wave must be a continuous formation of crests and troughs all around the circle. Each electron must be its own standing wave in its own discrete orbital.

The decline of the old quantum theory began with the introduction of half-integral values for quantum numbers in place of integral values for certain systems, in order to obtain agreement with experiment. There were cases in which agreement with the observed energy levels could not be obtained by the methods of the theory developed by Bohr or by any such subterfuge or arbitrary procedure, and cases where the methods of the old quantum theory led to definite qualitative disagreement with experiment. Moreover, the failure of the old quantum theory to provide a method of calculating transition probabilities and the intensities of spectral lines was recognised more and more clearly as a fundamental flaw. This dissatisfaction culminated in the formulation by Heisenberg in 1925 of his quantum mechanics, as a method of treatment of atomic systems leading to values of the intensities as well as frequencies of spectral lines.

2.1.2 New quantum theory

Werner Heisenberg approached the problem left by Bohr in a slightly different way as his academical advisor had done. He made correlations with observable quantities from spectrographic experiments, where the transition between known orbitals and its frequency of occurrence could be discerned. The findings differed from the classic point of view, as the relations were not always commutative, like matrices. Besides, filling in the arrays of information was not a simple fact, as any observation made on one single quantum system gives

one value but has the potential of changing other values. This leads to a problem: a precise determination of one characteristic's value necessarily creates an uncertainty in the value of its correlate. Heisenberg stated the fact that to observe unobservable quantities, i.e. quantum properties such as the position and period of an electron, was not possible without using mathematics, as they predicted the relations actually observed in experiments that worked different depending on the sequence they were applied.[127] The mathematical apparatus suitable for this kind of operations are matrices, which he used to understand the relations between momentum and position of electrons obtaining intensity. It proved that the math gave an exact description of the quantum behaviour of the electron. Matrix mechanics was the first complete definition of quantum mechanics, its laws, and properties that described fully the behaviour of the electron. It was later extended to apply to all subatomic particles.

2.1.2.1 Wave function

Then again, and at the same time, Erwin Schrödinger used a different approach to obtain information from the electrons in an atom using mathematics as well.[234] However, instead of attempting to find equations such as Newton's equations, which enable a prediction to be made of the exact positions and velocities of the particles of a system in a given state of motion, he devised a method of calculating a function of the coordinates of the system and the time (and not the momenta or velocities), with the aid of which probable values of the coordinates and of other dynamical quantities can be predicted for the system. Particles could be described as waves, as stated by Bohr and de Broglie, so Schrödinger formulated an equation for an electron like a wave around the nucleus of the atom. Each electron had its own wave function, Ψ, called the *Schrödinger wave function* or *probability amplitude function*. Originally, this representation included three properties: the principal quantum number n referred to the proximity of the electron to the nucleus, the shape of the orbital l referred to the angular momentum of the orbital, and the magnetic moment of the orbital m_l that depends upon l. Later, Pauli introduced a fourth quantum number m_s, which is the spin projection referred to the angular momentum of the electron, because spectroscopic experiments had showed that two electrons could occupy a single orbital. The square of the absolute value of a given wave function is interpreted as a *probability distribution function* for the coordinates of the system in the state represented by this wave function. It was later recognised that the acceptance of dynamical equations of this type in-

volves the renunciation of the hope of describing in exact detail the behaviour of a system. Although it is referred to a wave due to the similitude its second order derivative on the coordinates has with the wave equation of the classical theory, there are no further similarities.

The wave equation of Schrödinger used previous mathematical developments made by Newton, Lagrange and Hamilton. Thus, it's still applicable on a system consisting of N point particles of masses $m_1, m_2, \ldots, m_n$ moving in a three-dimensional space under the influence of forces expressed by the potential function $V(x_1, x_2, \ldots, y_1, y_2, \ldots z_N, t)$, being $x_1, \ldots, z_N$ the $3N$ Cartesian coordinates of the N particles. The potential function V represents the interaction of the particles with one another, with an external field or both, and may be time dependent or not, in the latter case corresponding to a conservative system. The wave function describing the system depends on the $3N$ Cartesian coordinates and time as well: $\Psi(x_1, \ldots, z_N, t)$. The energy of the system, dependent on time, is assumed to be

$$-\frac{h^2}{8\pi^2}\sum_{i=1}^{N}\frac{1}{m_i}\left(\frac{\partial^2\Psi}{\partial x_i^2}+\frac{\partial^2\Psi}{\partial y_i^2}+\frac{\partial^2\Psi}{\partial z_i^2}\right)+\hat{V}\Psi=-\frac{h}{2\pi i}\frac{\partial\Psi}{\partial t} \tag{2.6}$$

The *Laplace operator* or *Laplacian* is the second derivative of all Cartesian coordinates and can be written for the ith particle as:

$$\nabla_i^2=\frac{\partial^2}{\partial x_i^2}+\frac{\partial^2}{\partial y_i^2}+\frac{\partial^2}{\partial z_i^2}$$

so equation 2.6 is written like:

$$-\frac{h^2}{8\pi^2}\sum_{i=1}^{N}\frac{1}{m_i}\nabla_i^2\Psi+\hat{V}\Psi=-\frac{h}{2\pi i}\frac{\partial\Psi}{\partial t}$$

Schrödinger wave function resembles much to the equation of classical Newtonian mechanics:

$$\hat{H}\left(p_{x_1}\ldots p_{z_N}, x_1\ldots z_N, t\right)=\hat{T}\left(p_{x_1}\ldots p_{z_N}\right)+\hat{V}\left(x_1\ldots z_N, t\right)=E \tag{2.7}$$

Equation 2.7 is referred to as the *Hamilton operator* or *Hamiltonian*. It states that the total energy of the system E is expressed as the sum of the kinetic energy from the $\hat{T}$ operator and the potential energy from the $\hat{V}$ operator.

Introducing explicitly the momenta $p_{x_1} \dots p_{z_N}$ becomes:

$$\hat{H}\left(p_{x_1} \dots p_{z_N}, x_1 \dots z_N, t\right) = \sum_i \frac{1}{2m_i}\left(p_{x_i}^2 + p_{y_i}^2 + p_{z_i}^2\right) + \hat{V}\left(x_1 \dots z_N, t\right) = E \tag{2.8}$$

Each term of each particle's momentum in Cartesian form $p_{x_1} \dots p_{z_N}$ can be arbitrarily substituted by the corresponding differential operators $\frac{h}{2\pi i}\frac{\partial}{\partial x_1}, \dots, \frac{h}{2\pi i}\frac{\partial}{\partial z_N}$, and the total energy E can be substituted by $-\frac{h}{2\pi i}\frac{\partial}{\partial t}$, and applied to the function $\Psi\left(x_1, \dots, z_N, t\right)$:

$$\hat{H}\left(\frac{h}{2\pi i}\frac{\partial}{\partial x_1}, \dots, \frac{h}{2\pi i}\frac{\partial}{\partial z_N}, x_1 \dots z_N, t\right) = -\frac{h^2}{8\pi^2}\sum_{i=1}^{N}\frac{1}{m_i}\nabla_i^2\Psi + \hat{V}\Psi = -\frac{h}{2\pi i}\frac{\partial\Psi}{\partial t} \tag{2.9}$$

which is identical to equation 2.6, and is usually symbolically written in the conspicuous expression:

$$\hat{H}\Psi = E\Psi \tag{2.10}$$

The Schrödinger wave function including time can be split into two functions: the $3N$ coordinate part times the time dependent function:

$$\Psi\left(x_1, \dots, z_N, t\right) = \psi\left(x_1, \dots, z_N\right)\varphi\left(t\right) \tag{2.11}$$

After introducing this in equation 2.6 and dividing through by $\psi\left(x_1, \dots, z_N\right)\varphi\left(t\right)$, it becomes

$$\frac{1}{\psi}\left(-\frac{h^2}{8\pi^2}\sum_{i=1}^{N}\frac{1}{m_i}\nabla_i^2\psi + \hat{V}\psi\right) = -\frac{h}{2\pi i}\frac{\partial\psi}{\partial t} \tag{2.12}$$

The right side of this equation is a function of the time t alone and the left side a function of the $3N$ Cartesian coordinates. It is consequently necessary that the value of the quantity to which each side is equal be dependent on neither the $3N$ coordinates nor t that is, that it must be a constant, called arbitrarily as E. Equation 2.12 can then be written as two equations, namely:

$$\frac{d\varphi\left(t\right)}{dt} = -\frac{2\pi i}{h}E\varphi\left(t\right) \tag{2.13}$$

$$-\frac{h^2}{8\pi^2}\sum_{i=1}^{N}\frac{1}{m_i}\nabla_i^2\psi + \hat{V}\psi = E\psi \tag{2.14}$$

Equation 2.14 is known as the Schrödinger wave function, explained before in this chapter, and determines the amplitude of the function $\Psi(x_1, \ldots, z_N, t)$ for a conservative system of point particles. The equation has various satisfactory solutions, when limited to a certain set of conditions, for each of the $3N$ coordinates that generate $3N$ quantum numbers, which correspond to the various values of the constant E, all them denoted as E_n. Each value of E_n has a ψ_n function associated.

Equation 2.13 can be forwardly integrated as

$$\varphi(t) = e^{-2\pi i \frac{E_n}{h} t} \tag{2.15}$$

and the various particular solutions of the wave equation are hence

$$\Psi_n(x_1, \ldots, z_N, t) = \psi_n(x_1, \ldots, z_N)\, e^{-2\pi i \frac{E_n}{h} t} \tag{2.16}$$

which turns into the general solution of the wave equation as

$$\Psi(x_1, \ldots, z_N, t) = \sum_n a_n \Psi_n(x_1, \ldots, z_N, t) = \sum_n a_n \psi_n(x_1, \ldots, z_N)\, e^{-2\pi i \frac{E_n}{h} t} \tag{2.17}$$

where a_n are constants. The symbol $\sum_n$ represents summation for all discrete values of E_n and integration over all continuous ranges of values.

The conditions on which a good wave function can be constructed are based on the following auxiliary postulates regarding the nature of wave functions:

> To be a satisfactory wave function, a solution of the Schrödinger wave equation must be continuous, single-valued, and finite throughout the configuration space of the system.

The functions ψ which satisfy equation 2.14 and this auxiliary conditions are variously called *wave functions* or *eigenfunctions* (from German Eigenfunktionen), or sometimes amplitude functions, characteristic functions, or proper functions. It is found that satisfactory solutions ψ_n of the wave equation exist only for certain values of the parameter E_n (which is interpreted as the energy of the system). These values E_n are *characteristic energy values* or *eigenvalues* (from German Eigenwerte) of the wave equation.

In page 51 the probability distribution function was defined as the square of the absolute value of a wave function. This is true when the wave functions don't have an imaginary part, but when they do, the probability distribution

function is defined as the product of the Ψ function and its complex conjugate (changing the sign of the imaginary part of the function) Ψ^*. A new postulate is introduced:

> The quantity $\Psi^*(x_1, \ldots, z_N, t)\,\Psi(x_1, \ldots, z_N, t)\,dx_1, \ldots, dz_N$ is the probability that the system in the physical situation represented by the wave function $\Psi(x_1, \ldots, z_N, t)$ have at the time t the configuration represented by a point in the volume element $dx_1, \ldots, dz_N$ of configuration space.

and the volume element $dx_1, \ldots, dz_N$ can be represented as $d\tau$. Thus, $\Psi^*\Psi dx$ is the probability that the particle lie in the region between x and $x+dx$ at the time t. In order that this postulate can be made, the wave function Ψ must be *normalised* to unity. To do so, the constants a_n of equation 2.17 must be chosen to satisfy the relation

$$\int \Psi^*(x_1, \ldots, z_N, t)\,\Psi(x_1, \ldots, z_N, t)\,d\tau = 1 \tag{2.18}$$

which is integrated in the whole space from $-\infty$ to $+\infty$. The amplitude functions $\psi_n(x_1, \ldots, z_N, t)$ should also be normalised:

$$\int \psi_n^*(x_1, \ldots, z_N)\,\psi_n(x_1, \ldots, z_N)\,d\tau = 1 \tag{2.19}$$

Moreover it is found that the independent solutions of any amplitude equation can always be chosen in such a way that for any two of them, $\psi_m(x_1, \ldots, z_N)$ and $\psi_n(x_1, \ldots, z_N)$, are orthogonal, satisfying the orthogonality equation:

$$\int \psi_m^*(x_1, \ldots, z_N)\,\psi_n(x_1, \ldots, z_N)\,d\tau = 0 \qquad m \neq n \tag{2.20}$$

Following the equality in equation 2.16, a wave function is normalised if it satisfies the equation

$$\sum_n a_n^* a_n = 1 \tag{2.21}$$

The probability function depends on the time, except when the coefficients a_n are zero for all except one value of E_n. Then $\Psi^*\Psi$ is independent of t, and the state is called a *stationary state*.

2.1.2.2 Heisenberg uncertainty principle

After Schrödinger released his research on quantum mechanics, Heisenberg was still on the subject of the momentum and position of electrons. Working through his data, he found out that the difference of momentum times position and position times momentum was of $h/4\pi$. The more certain is the position of a particle, the less certain is its momentum. Two years later releasing his article about the mathematical apparatus that should be used for subatomic particles, he published a new paper exposing the *Heisenberg uncertainty principle*:[128]

> The values of two dynamical quantities f and g of a system can be accurately measured at the same time only if their commutator is zero; otherwise these measurements can be made only with an uncertainty $\Delta f \Delta g$ whose magnitude is dependent on the value of the commutator. In particular, for a canonically conjugate coordinate q and momentum p the uncertainty $\Delta q \Delta p$ is of the order of magnitude of Planck s constant h, as is $\Delta E \Delta t$ for the energy and time.

A *commutator* of two operators or matrices is defined as

$$[f, g] = fg - gf \tag{2.22}$$

and what Heisenberg uncertainty principle establishes is when $fg - gf \neq 0$ the dynamical variables f and g cannot be accurately measured at the same time: applied to a stationary wave function Ψ, due to the nature of it and its probability distribution function, the energy and momentum can be known; but the uncertainty in the position is infinite as the probability distribution function $\Psi^*\Psi$ is constant for all values of the coordinates. On the contrary, when $fg - gf = 0$, both variables can be measured.

2.1.3 Approximate solutions of wave equations

The solution of the wave equation for any molecule is a very difficult problem. Only the simplest ones like atomic hydrogen can be solved exactly. The Born-Oppenheimer approximation explained in section 2.1.3.1 reduces drastically its complexity by cutting out the nuclei movement from the Hamiltonian operator, but the interactions between electrons and nuclei sum up to $\binom{n}{2}$ terms, considering just pair-interactions. However, the information extracted

from molecular spectra points that the energy of the molecule can be split in several parts: the *electronic energy*, the *vibrational energy* and the *rotational energy*. Each one can be described as an independent wave function which can be combined to approximately solve the molecular wave equation. Even then, system information cannot be conveniently treated by direct solution of the wave function. Nevertheless, there are methods available which enable approximate values for the energy of certain of the states of the system to be computed.

2.1.3.1 Born-Oppenheimer approximation [36]

The mass of an electron is about two thousand times smaller than the mass of a proton, and this rate increases as an atom's atomic number raises. Moreover, the speed of the electrons moving around the nuclei is much faster than their translation speed, which is affected by the nucleus own translation. Thus, the nucleus can be considered as a reference point in a fixed frame by the electrons. Born and Oppenheimer were able to show that an approximate solution of the complete wave equation for a molecule can be obtained by first solving the wave equation for the electrons alone and then solving a wave equation for the nuclei alone, in which a characteristic energy value of the electronic wave equation, regarded as a function of the internuclear distances, occurs as a potential function. Let us suppose a molecule consisting of r nuclei and s electrons. The $3r$ coordinates of the r nuclei are represented by $\vec{\xi}$, relative to a frame of reference fixed in space, and the $3s$ coordinates of the s electrons are represented with letter $\vec{x}$, relative to the nuclei axes. The wave function of the system is represented as $\psi_{n,\nu}\left(\vec{x},\vec{\xi}\right)$, where ν are the quantum numbers associated with the motion of the nuclei, and n are those associated with the motion of the electrons. The complete wave equation for this molecule is

$$-\frac{h^2}{8\pi^2}\left(\sum_{A=1}^{r}\frac{1}{M_A}\nabla_A^2+\frac{1}{m_0}\sum_{i=1}^{s}\nabla_i^2\right)\psi+\hat{V}\psi=E\psi \tag{2.23}$$

in which M_A is the mass of the Ath nucleus, m_0 the mass of each electron, ∇_A^2 the Laplace operator in terms of the coordinates of the Ath nucleus, and ∇_i^2 the same operator for the ith electron. $\hat{V}$ is the potential energy of the system, of the form

$$\hat{V}=\sum_{i,j>i}\frac{e^2}{r_{ij}}+\sum_{A,A>B}\frac{Z_AZ_Be^2}{r_{AB}}-\sum_{i,A}\frac{Z_Ae^2}{r_{iA}} \tag{2.24}$$

the sums including each pair of particles once (indicated by the $j > i$ term). Here Z_A is the atomic number of the Ath nucleus. Applying the Born-Oppenheimer approximation, a solution of equation 2.23 can be obtained of the form:

$$\psi_{n,\nu}\left(\vec{x},\vec{\xi}\right) = \psi_n\left(\vec{x},\vec{\xi}\right)\psi_{n,\nu}\left(\vec{\xi}\right) \tag{2.25}$$

The different functions $\psi_n\left(\vec{x},\vec{\xi}\right)$, which may be called the *electronic wave functions*, correspond to different sets of values of the electronic quantum numbers n only, being independent of the nuclear quantum numbers ν. On the other hand, each of these functions is a function of the nuclear coordinates $\vec{\xi}$ as well as the electronic coordinates $\vec{x}$. These functions are obtained by solving a wave equation for the electrons alone, the nuclei being restricted to a fixed configuration. This wave equation is

$$-\frac{h^2}{8\pi^2}\frac{1}{m_0}\sum_{i=1}^{s}\nabla_i^2\psi_n\left(\vec{x},\vec{\xi}\right) + \hat{V}\left(\vec{x},\vec{\xi}\right)\psi_n\left(\vec{x},\vec{\xi}\right) = U_n\left(\vec{\xi}\right)\psi_n\left(\vec{x},\vec{\xi}\right) \tag{2.26}$$

and is known as the *electronic wave equation*. It is a variation of the complete wave equation 2.23, omitting the terms involving the kinetic energy of nuclei and replacing the time independent wave function for the electronic part, giving the electronic energy $U_n\left(\vec{\xi}\right)$. It is seen that for any fixed set of values of the s nuclear coordinates this equation is an ordinary wave equation for the s electrons, the potential energy function $\hat{V}$ being dependent on the values selected for the nuclear coordinates. In consequence the characteristic electronic energy values U_n and the electronic wave functions ψ_n will also be dependent on the values selected for the nuclear coordinates; accordingly written as $U_n\left(\vec{\xi}\right)$ and $\psi_n\left(\vec{x},\vec{\xi}\right)$. The first step in the treatment of a molecule is to solve this electronic wave equation for all configurations of the nuclei. It is found that the characteristic values $U_n\left(\vec{\xi}\right)$ of the electronic energy are continuous functions of the nuclear coordinates $\vec{\xi}$.

After having evaluated the characteristic electronic energy $U_n\left(\vec{\xi}\right)$, the expressions for the *nuclear wave functions* $\psi_{n,\nu}\left(\vec{\xi}\right)$ should be found. These functions are the acceptable solutions of a wave equation in the nuclear coordinates $\vec{\xi}$ where the characteristic electronic energy function $U_n\left(\vec{\xi}\right)$ plays the

role of the potential energy; that is, the nuclear wave equation is

$$-\frac{h^2}{8\pi^2}\sum_{A=1}^{r}\frac{1}{M_A}\nabla_A^2\psi_{n,\nu}\left(\vec{\xi}\right)+\hat{V}\psi_{n,\nu}\left(\vec{\xi}\right)=E_{n,\nu}\psi_{n,\nu}\left(\vec{\xi}\right) \tag{2.27}$$

There is one such equation for each set of values of the electronic quantum numbers n, and each of these equations possesses an extensive set of solutions, corresponding to the allowed values of the nuclear quantum numbers ν. The values of $E_{n,\nu}$ are the characteristic energy values for the entire molecule: they depend on the electronic and nuclear quantum numbers n and ν.

This approximation does not consider the electron-nucleus coupling term due to their movement. When these terms are critical enough to be considered, like systems with two potential energy surfaces close to each other, the approximation cannot be applied. Some systems may present multiconfigurational crossings between potential energy surfaces and the movement of the nuclei should be taken into consideration.

2.1.3.2 The variation method

Finding a suitable wave equation is a question of solving the Schrödinger integral $E=\int\Psi^*\hat{H}\Psi d\tau$, where $\hat{H}$ is the complete Hamiltonian operator and Ψ is a normalised wave function. It can be applied to the time-independent wave function ψ as well, obtaining the energy of a stationary state. This equality has to observe the Schrödinger's postulates for a wave function (see page 54) and so a set of eigenfunctions is generated as suitable solutions, some exactly describing the different energy levels of the system and others being mere approximations to those. The variation theorem states that *any wave function ϕ from this set will always have an energy higher than that of the basal state*, this being described by ψ_0 and with an energy equal to E_0. The *variation function* ϕ can be constructed as a linear combination of the *orthonormalised* (orthogonal and normalised) functions $\psi_0,\psi_1,\ldots,\psi_n,\ldots$:

$$\phi=\sum_n a_n\psi_n \qquad \sum_n a_n^*a_n=1 \tag{2.28}$$

Substitution to the Schrödinger energy integral, leads to

$$E=\sum_n\sum_{n'}a_n^*a_{n'}\int\psi_n^*\hat{H}\psi_{n'}d\tau=\sum_n\sum_n a_n^*a_nE_n \tag{2.29}$$

as each ψ_n is an eigenfunction of the Hamiltonian operator. The lowest energy E_0 can be subtracted to both sides

$$E - E_0 = \sum_n \sum_n a_n^* a_n \left(E_n - E_0\right) \tag{2.30}$$

and since E_n is greater than or equal to E_0 for all values of n and the coefficients $a_n^* a_n$ are all positive or zero, the right side of equation 2.30 is positive or zero. E is always an upper limit to E_0 that is,

$$E \geq E_0 \tag{2.31}$$

This theorem can be used to calculate the lowest energy level of a system. Given a set of variation functions $\phi_1, \phi_2, \ldots, \phi_n$ the corresponding energy to each one will be $E_1, E_2, \ldots, E_n$, neither of them greater than the energy level E_0, and the lowest energy one being the nearest to E_0. This is useful in theoretical and computational chemistry as ϕ functions only differ from each other on the values of some parameters. The process consists to achieve the lowest E trying different variation functions. If E is equal to E_0 then ϕ is identical with ψ_0, so that it is natural to assume that if E is nearly equal to E_0 the function ϕ will approximate closely to the true wave function ψ_0.

2.1.3.3 Perturbation theory

When a wave function Ψ cannot be solved exactly, an approximate solution can be obtained from a solvable wave equation ψ^0 similar to the time-independent exact one ψ but differing from it in the omission of certain terms whose effect on the system is small. The approximate equation is solved and then small correction terms are added. This is the *Rayleigh-Schrödinger perturbation theory* (RSPT). It should stick as always to the Schrödinger equation $\hat{H}\psi = E\psi$. In RSPT the Hamiltonian operator is expanded in a Taylor series in terms of some parameter λ

$$\hat{H} = \hat{H}^{(0)} + \lambda \hat{H}^{(1)} + \lambda^2 \hat{H}^{(2)} + \ldots \tag{2.32}$$

The first term of the equation $\hat{H}^{(0)}$ is the *unperturbed* part of the Hamiltonian, whereas the terms to its left $\lambda \hat{H}^{(1)} + \lambda^2 \hat{H}^{(2)} + \ldots$ are called the *perturbation*. Any of its possible solution eigenfunctions ψ_i—non-degenerate—and

associated eigenvalues E_i can be expanded in a Taylor series like the Hamiltonian, as the perturbation introduced is small enough and the series will converge. So:

$$\psi_i = \psi_i^{(0)} + \lambda\psi_i^{(1)} + \lambda^2\psi_i^{(2)} + \dots \tag{2.33}$$

$$E_i = E_i^{(0)} + \lambda E_i^{(1)} + \lambda^2 E_i^{(2)} + \dots \tag{2.34}$$

The parameter λ has been chosen in such a way that when $\lambda \to 0$, the Schrödinger equation reduces to $\hat{H}^{(0)}\psi_i^{(0)} = E_i^{(0)}\psi_i^{(0)}$. The wave functions of $\hat{H}^{(0)}$ are chosen normalised and at the same time they normalise with the exact function ψ_i so

$$\int \psi_i^{(0)*}\psi_i d\tau = \int \psi_i^{(0)*}\psi_i^{(0)} d\tau + \lambda \int \psi_i^{(0)*}\psi_i^{(1)} d\tau + \lambda^2 \int \psi_i^{(0)*}\psi_i^{(2)} d\tau + \dots = 1 \tag{2.35}$$

which is called an intermediate normalisation and can always be made unless $\psi_i^{(0)}$ and ψ_i are orthogonal. It holds for all values of λ and therefore, coefficients of λ^n on both sides must be equal, and hence

$$\int \psi_i^{(0)*}\psi_i^{(n)} d\tau = 0 \qquad n = 1, 2, 3, \dots \tag{2.36}$$

Combining equations 2.32, 2.33 and 2.34 to the Schrödinger wave equation:

$$\begin{aligned}\left(\hat{H}^{(0)} + \lambda\hat{H}^{(1)} + \lambda^2\hat{H}^{(2)} + \dots\right)\left(\psi_i^{(0)} + \lambda\psi_i^{(1)} + \lambda^2\psi_i^{(2)} + \dots\right) \\ = \left(E_i^{(0)} + \lambda E_i^{(1)} + \lambda^2 E_i^{(2)} + \dots\right)\left(\psi_i^{(0)} + \lambda\psi_i^{(1)} + \lambda^2\psi_i^{(2)} + \dots\right)\end{aligned} \tag{2.37}$$

developing and equating the λ^n coefficients of each side and grouping them,

$$\hat{H}^{(0)}\psi_i^{(0)} = E_i^{(0)}\psi_i^{(0)} \qquad n = 0 \tag{2.38}$$

$$\hat{H}^{(0)}\psi_i^{(1)} + \hat{H}^{(1)}\psi_i^{(0)} = E_i^{(0)}\psi_i^{(1)} + E_i^{(1)}\psi_i^{(0)} \qquad n = 1 \tag{2.39}$$

$$\hat{H}^{(0)}\psi_i^{(2)} + \hat{H}^{(1)}\psi_i^{(1)} + \hat{H}^{(2)}\psi_i^{(0)} = E_i^{(0)}\psi_i^{(2)} + E_i^{(1)}\psi_i^{(1)} + E_i^{(2)}\psi_i^{(0)} \qquad n = 2 \tag{2.40}$$

Let us consider as a first step to a general perturbation expression the equation 2.39. The unknown function $\psi_i^{(1)}$ can be constructed as a linear

combination of a known orthonormal function from another state $\psi_k^{(0)}$,

$$\psi_i^{(1)} = \sum_k a_k \psi_k^{(0)} \tag{2.41}$$

which when substituted in the first term of equation 2.39 it becomes

$$\hat{H}^{(0)}\psi_i^{(1)} = \sum_k a_k \hat{H}^{(0)}\psi_k^{(0)} = \sum_k a_k E_k^{(0)}\psi_k^{(0)} \tag{2.42}$$

and the same is done on the first term on the left:

$$E_i^{(0)}\psi_i^{(1)} = \sum_k a_k E_i^{(0)}\psi_k^{(0)} \tag{2.43}$$

Joining all the pieces, 2.42 and 2.43, to 2.39, the expression becomes:

$$\sum_k a_k E_k^{(0)}\psi_k^{(0)} + \hat{H}^{(1)}\psi_i^{(0)} = \sum_k a_k E_i^{(0)}\psi_k^{(0)} + E_i^{(1)}\psi_i^{(0)} \tag{2.44}$$

When each side is multiplied by $\psi_i^{(0)*}$ and integrated over the whole configuration space, the terms containing the known function $\psi_k^{(0)}$ vanish since

$$\int \psi_i^{(0)*} \sum_k a_k E_k^{(0)}\psi_k^{(0)} d\tau = 0$$

$$\int \psi_i^{(0)*} \sum_k a_k E_i^{(0)}\psi_k^{(0)} d\tau = 0$$

and as they are orthonormal, when $i \neq k$ their integral is zero, and when $i = k$, both integrals have the same value and they cancel each other as they are on different sides of the equality 2.44. Hence, the equation 2.44 is reduced to

$$\int \psi_i^{(0)*}\hat{H}^{(1)}\psi_i^{(0)} d\tau = \int \psi_i^{(0)*} E_i^{(1)}\psi_i^{(0)} d\tau \tag{2.45}$$

and since $E_i^{(1)}$ is a constant and $\int \psi_i^{(0)*}\psi_i^{(0)} d\tau = 1$, the first correction to the unperturbed energy can be written as

$$E_i^{(1)} = \int \psi_i^{(0)*}\hat{H}^{(1)}\psi_i^{(0)} d\tau \tag{2.46}$$

Following the same steps, the second correction is $E_i^{(2)} = \int \psi_i^{(0)*}\hat{H}^{(1)}\psi_i^{(1)} d\tau$, and the nth as well:

$$E_i^{(n)} = \int \psi_i^{(0)*}\hat{H}^{(1)}\psi_i^{(n-1)} d\tau \tag{2.47}$$

2.1.3.4 Density functional theory

An alternative to the conventional *ab initio* methods* is the *density functional theory* (DFT)[198] which introduces the electronic correlation† effects to the electronic Schrödinger equation. The method was developed initially by Hohenberg and Kohn[131] for non-degenerate ground states in the absence of a magnetic field and later generalised by Levy.[163] In this method, the energy calculation for the fundamental state of a many-electron system is based on the probability distribution function of the system. Traditional methods in electronic structure theory, in particular Hartree-Fock theory and its descendants, are based on the complicated many-electron wave function. The main objective of density functional theory is to replace the many-body electronic wave function with the electronic density as the basic quantity. Whereas the many-body wave function is dependent on $3N$ variables, three spatial variables for each of the N electrons, the density is only a function of three variables and is a simpler quantity to deal with both conceptually and practically. Unfortunately the exact relation between the electronic density and the energy is not known, and approximate expressions are needed. Even so, these approximations still lead to a different range of acceptable results, although there is no systematic way to improve them.

As explained in section 2.1.2.1, the probability of finding an electron (any electron) belonging to an N-electron system described by the spatial orbital wave function—see page 68 for further reference—$\psi_a(\vec{r}_1, \vec{r}_2, \ldots, \vec{r}_N) = \psi_a(\vec{r})$ in the $\vec{r}_1 + d\vec{r}_1$ space region is the integral

$$\int \psi_a^*(\vec{r}_1)\, \psi_a(\vec{r})\, d\vec{r}_2 \ldots d\vec{r}_N \tag{2.48}$$

and due to the indistinguishability of the electrons

$$\rho(\vec{r}_1) = N \int \psi_a^*(\vec{r})\, \psi_a(\vec{r})\, d\vec{r}_2 \ldots d\vec{r}_N = N \int |\psi_a(\vec{r})|^2\, d\vec{r}_2 \ldots d\vec{r}_N \tag{2.49}$$

it calculates the probability of finding an electron in a region independently of the situation of the other electrons and is known as the *first order density* . Over integration the spin coordinate ω, the *electronic density* $\rho(\vec{x})$ or *charge*

*The *ab initio* methods are those able to compute chemical properties based on quantum chemistry.

†The electronic correlation is the interaction between the different electrons in a system.

density is obtained:

$$\rho\left(\vec{x}_1\right) = \int \rho\left(\vec{r}\right) d\omega_1 = N \int \psi_a^*\left(\vec{r}\right) \psi_a\left(\vec{r}\right) d\omega_1 d\vec{r}_2 \ldots d\vec{r}_N$$
$$= N \int \left|\psi_a\left(\vec{r}\right)\right|^2 d\omega_1 d\vec{r}_2 \ldots d\vec{r}_N \quad (2.50)$$

Provided that $\psi_a\left(\vec{x}\right)$ is a normalised function, the integral of this electronic density $\rho\left(\vec{x}\right)$ is the number of electrons N:

$$\int \rho\left(\vec{x}\right) d\vec{x} = N \quad (2.51)$$

Equation 2.49 can be expressed in the form of the molecular orbital expansion in 2.88 using a Slater determinant (see page 72) in a restricted closed shell system :

$$\begin{aligned}
\rho\left(\vec{x_1}\right) &= N \int \psi_a^*\left(\vec{x}\right) \psi_a\left(\vec{x}\right) d\vec{x}_2 \ldots d\vec{x}_N = \\
&= 2 \sum_a^{N/2} \psi_a^*\left(\vec{x}\right) \psi_a\left(\vec{x}\right) = \\
&= 2 \sum_a^{N/2} \sum_\nu C_{\nu a}^* \phi_\nu^*\left(\vec{x}\right) \sum_\mu C_{\mu a} \phi_\mu\left(\vec{x}\right) = \\
&= \sum_{\mu\nu} \left[\sum_a^{N/2} C_{\mu a} C_{\nu a}^* \right] \phi_\mu\left(\vec{x}\right) \phi_\nu^*\left(\vec{x}\right) = \\
&= \sum_{\mu\nu} P_{\mu\nu} \phi_\mu\left(\vec{x}\right) \phi_\nu^*\left(\vec{x}\right)
\end{aligned} \quad (2.52)$$

where $\mathbf{P}$ is the *first order density matrix*, its elements defined as

$$P_{\mu\nu} = 2 \sum_a^{N/2} C_{\mu a} C_{\nu a}^* \quad (2.53)$$

From 2.52, given a set of known basis functions $\{\phi_\mu\}$ the matrix $\mathbf{P}$ specifies completely the charge density $\rho\left(\vec{x}\right)$. It is directly related to the expansion

coefficients $\mathbf{C}$ by 2.53. For a non-restricted Slater determinant, the density matrix distinguishes from α and β electrons, and its definition becomes

$$P^{\alpha}_{\mu\nu} = \sum_{a=1}^{N_\alpha} C_{\mu a} C^*_{\nu a} \quad , \quad P^{\beta}_{\mu\nu} = \sum_{a=1+N_\alpha}^{N_\alpha+N_\beta} C_{\mu a} C^*_{\nu a} \quad , \quad P^{T}_{\mu\nu} = P^{\alpha}_{\mu\nu} + P^{\beta}_{\mu\nu} \tag{2.54}$$

On the other hand, it is possible to define a probability to find two electrons in two different space regions $\vec{r}_1 + d\vec{r}_1$ and $\vec{r}_2 + d\vec{r}_2$, and again it does not depend on the coordinates of the other electrons:

$$\gamma_2(\vec{r}_1, \vec{r}_2) = N(N-1) \int |\psi_a(\vec{r})|^2 \, d\vec{r}_3 \ldots d\vec{r}_N \tag{2.55}$$

where $N(N-1)$ are all the possible electron pairs and $\gamma_2(\vec{r}_1, \vec{r}_2)$ is known as the *second order density*. Integrating over the spin coordinates

$$\gamma_2(\vec{x}_1, \vec{x}_2) = \int \gamma_2(\vec{r}_1, \vec{r}_2) \, d\omega_1 d\omega_2 \tag{2.56}$$

gives $\gamma_2(\vec{r}_1, \vec{r}_2)$, which is the *bielectronic density*. The difference between this density and the second order one is that this one considers all the spin combinations of the paired electrons, i.e. $\alpha\alpha$, $\alpha\beta$, $\beta\alpha$ and $\beta\beta$. Similar to the unrestricted first order density matrix, the *second order density matrix* or *pair density* is defined in the all possible spin combinations of the paired electrons:

$$\begin{aligned} \Gamma^{\alpha\alpha}_{\mu\nu\sigma\lambda} &= P^{\alpha}_{\sigma\mu} P^{\alpha}_{\lambda\nu} + P^{\alpha}_{\lambda\mu} P^{\alpha}_{\sigma\nu} \\ \Gamma^{\alpha\beta}_{\mu\nu\sigma\lambda} &= P^{\alpha}_{\sigma\mu} P^{\beta}_{\lambda\nu} \end{aligned} \tag{2.57}$$

The $\alpha\alpha$ and $\beta\beta$ combinations are identical except for the electrons used.

On both cases of electronic and bielectronic densities is possible to restrict the density and refer it to the electronic spin part. In the electronic density it is as simple as to consider the number of α (N_α) or β (N_β) electrons instead of the total number of electrons N. The total electronic density will be the sum of the two separate densities. In the bielectronic density the possible combinations of the electronic spins increase the number of adding terms up to four.

Then, the energy or any observable of a polielectronic system can be extracted from the first and second order densities using the appropriate operators. Hohenberg and Kohn set the guidelines of the DFT and announced two theorems,[131] the first one being

> It exists a one-to-one relation between the ground state electronic density and the ground state wave function of a many-particle system, thus any observable can be written as a functional of the ground state electronic density.

As the electronic density determines the total number of electrons in the system (from equation 2.51) and also sets the external electron-nucleus potential $\hat{V}_{iA}[\rho]$ (electron-electron potential and kinetic energy do not depend on the external potential), according to the first theorem it is concluded that the electronic density determines the Hamiltonian and the wave function of the fundamental state, and by extension all observable properties of the fundamental state, including the kinetic energy of the electrons, the coulombic repulsion, and so on. In particular, $E = E[\rho]$. Thus, there is a direct correlation between the density and the wave function through the external potential. It is important to note that this theory only holds for the non-degenerate fundamental states, $\rho(\vec{r})$ must be defined as positive in all the space and its integral must be equal to the total number of electrons in the system. In addition, there must be an external potential from which this $\rho(\vec{r})$ density could be derived. In the cases which this theorem is valid it can be written that

$$E[\rho] = \hat{T}[\rho] + \hat{V}_{iA}[\rho] + \hat{V}_{ij}[\rho] \left(+\hat{V}_{AB}\right) \tag{2.58}$$

The operators $\hat{T}[\rho]$ and $\hat{V}_{ij}[\rho]$ do not depend on the external potential and usually gets included in the *Hohenberg-Kohn functional* $F_{HK}[\rho]$ term, and so

$$E_{\nu}[\rho] = \int \rho(\vec{r})\, \nu(\vec{r})\, d\vec{r} + F_{HK}[\rho] \tag{2.59}$$

where $F_{HK}[\rho]$ stands for

$$F_{HK}[\rho] = \int \rho^{*}(\vec{r}) \left(\hat{T} + \hat{V}_{ij}\right) \rho(\vec{r})\, d\vec{r} \tag{2.60}$$

The second theorem proves that the ground state density minimises the total electronic energy of the system:

> The exact electronic density of a non-degenerate fundamental state can be calculated by determining the density which minimises the energy of the ground state.

It sets the variation method for the DFT. Given a test density function $\tilde{\rho}(\vec{r})$ defined in the same conditions as in the first theorem, it holds that:

$$E_o \leq E_\nu \left[\tilde{\rho}(\vec{r})\right] \tag{2.61}$$

Eighteen years later Levy proposed a new formulation on the topic.[164] It is another proof that a bijective function exists between the electronic density and the ground state wave function. In Levy's demonstration the electronic density does not need an external potential to be derived. Moreover, it can also be applied to degenerate ground states. Even choosing a restricted set of base functions, it can be applied to excited states.[198]

In order to minimise the energy with respect to the electronic density, its is needed that $\delta E_\nu [\rho] = 0$. Furthermore, the electronic density must keep the premises of being positive all along its space and its integral must result to the total number of electrons. This last premise is secured by the equation

$$\int \rho(\vec{r})\, d\vec{r} - N = 0 \tag{2.62}$$

and is introduced using the Lagrange multipliers in an expression which has to be minimised:

$$\delta \left[E_\nu [\rho] - \lambda \left(\int \rho(\vec{r})\, d\vec{r} - N \right) \right] = 0 \tag{2.63}$$

The differential of any functional $F[f]$ can be written as

$$\delta F = \int \frac{\delta F}{\delta f(x)} \delta f(x)\, dx \tag{2.64}$$

and after combining it into equation 2.63 and working with the expression, it leads to the condition of restricted minimisation and the value of λ that minimises the functional:

$$\lambda = \frac{\delta E_\nu [\rho]}{\delta \rho(\vec{r})} = \nu_n(\vec{r}) + \frac{\delta F_{HK}[\rho]}{\delta \rho(\vec{r})} \tag{2.65}$$

2.2 Theoretical chemistry methods

The exact wave function for many-electron atoms remains unknown up to date. Nevertheless, there are many methods and approximations that can lead to a

sufficiently accurate wave function for energy levels calculation. Increasing the number of atoms and electrons leads to an exponential growth of the Hamiltonian complexity due to the proliferation of the possible interactions between single particles to other particles. The general Hamiltonian for a N-electron M-atom system can be expressed as

$$\hat{H} = -\frac{h^2}{8\pi^2}\left(\frac{1}{m_0}\sum_{i=1}^{N}\nabla_i^2 + \sum_{A=1}^{M}\frac{1}{M_A}\nabla_A^2\right) + \sum_{i,i>j}^{N}\frac{e^2}{r_{ij}} + \sum_{A,A>B}^{M}\frac{Z_A Z_B e^2}{r_{AB}} - \sum_{i,A}^{N,M}\frac{Z_A e^2}{r_{iA}} \quad (2.66)$$

which is formed from equations 2.23 and 2.24. The first two left terms in the parentheses are the operator for the kinetic energy of the electrons and the nuclei, respectively; the other ones are the potential energy operators due to coulombic attractions or repulsions: the third term is repulsion between electrons, the fourth is the repulsion between nuclei and the fifth is the attraction between electrons and nuclei. Applying the Born-Oppenheimer approximation, the second term of equation 2.66 can be neglected as the nuclei are static, and the fourth term, the repulsion of the nuclei, can be considered to be a constant; and so it becomes the electronic Hamiltonian:

$$\hat{H} = -\frac{h^2}{8\pi^2}\frac{1}{m_0}\sum_{i=1}^{N}\nabla_i^2 + \sum_{i,j>i}^{N}\frac{e^2}{r_{ij}} - \sum_{i,A}^{N,M}\frac{Z_A e^2}{r_{iA}} \quad (2.67)$$

This equation still can't be solved for more than one electron, even considering the coulomb attraction between electrons and nuclei as a dependence on the electrons under a constant electric field. Thus, the wave functions should be approximate. One way to treat this problem is to construct the wave function as a linear combination of monoelectronic wave functions. This wave functions are known as the *spin orbitals* $\chi(\vec{x})$ and describe the position of one electron—a non-relativistic property—and its spin—a relativistic property—,both combined in $\vec{x}$, a four dimensional variable. The wave function can be defined as a product of the three dimensional *spatial orbital* part, $\psi(\vec{r})$, which describes the spatial distribution of the electron, and the spin function, which can be $\alpha(\omega)$ or $\beta(\omega)$ for spin up ($\uparrow$) or down ($\downarrow$) respectively. If the spatial orbitals are orthonormal, so are the spin orbitals. Then, each spatial function can generate two spin orbitals:

$$\chi(\vec{x}) = \begin{cases} \psi(\vec{r})\alpha(\omega) \\ \psi(\vec{r})\beta(\omega) \end{cases} \quad (2.68)$$

Now that each electron can be defined with a spin orbital wave function, a group of electrons can be defined in turn as a combination of the spin orbitals of each electron interacting independently

$$\phi_1(\vec{x}_1, \vec{x}_2, \ldots, \vec{x}_N) = \chi_i(\vec{x}_1)\,\chi_{i'}(\vec{x}_2)\cdots\chi_{i^N}(\vec{x}_N) \tag{2.69}$$

Such a many-electron wave function is termed a *Hartree product*, with electron one being described by the spin orbital χ_i, electron two being described by the spin orbital $\chi_{i'}$ and so on. As each spin orbital is independent and an eigenfunction of its Hamiltonian $\hat{h}_i$, the Hamiltonian of the collective wave function and its eigenvalues is:

$$\hat{H} = \sum_{i=1}^{N} \hat{h}_i \tag{2.70}$$

$$\hat{h}_i\chi_{i'}(\vec{x}_i) = \varepsilon_{i'}\chi_{i'}(\vec{x}_i) \tag{2.71}$$

$$E = \varepsilon_i + \varepsilon_{i'} + \cdots + \varepsilon_{i^N} \tag{2.72}$$

But the wave function obtained from a Hartree product is not a valid one as it is uncorrelated for the electrons. Another acceptable solution for the electronic wave function 2.69 is

$$\phi_2(\vec{x}_1, \vec{x}_2, \ldots, \vec{x}_N) = \chi_i(\vec{x}_2)\,\chi_{i'}(\vec{x}_1)\cdots\chi_{i^N}(\vec{x}_N) \tag{2.73}$$

and all the other possible permutations of electrons and positions, as the electrons are indistinguishable. In general, the solution wave function for an energy level can be written as

$$\phi(\vec{x}_1, \vec{x}_2, \ldots, \vec{x}_N) = \frac{1}{\sqrt{N!}} \sum_{P} (-1)^P P\chi_i(\vec{x}_1)\,\chi_{i'}(\vec{x}_2)\cdots\chi_{i^N}(\vec{x}_N) \tag{2.74}$$

where P represents all the possible permutations of the electron coordinates and the term $1/\sqrt{N!}$ is the normalisation factor (as there are $N!$ possible combinations) and $(-1)^P$ is introduced to apply the antisymmetry principle. An antisymmetric wave function is that one which changes its sign when two electrons are interchanged:

$$\phi(\chi_1, \ldots, \chi_i, \ldots, \chi_j, \ldots, \chi_N) = -\phi(\chi_1, \ldots, \chi_j, \ldots, \chi_i, \ldots, \chi_N) \tag{2.75}$$

, A symmetric wave function, on the other hand, does not change its sign in the same circumstances. The antisymmetry is used in the *antisymmetry principle*

to comply with the *Pauli exclusion principle*[‡] to choose those functions with a physical significance:

> A many-electron wave function must be antisymmetric with respect to the interchange of the coordinate $\vec{x}$ (both space and spin) of any two electrons.

The wave function 2.74 is an antisymmetric function, thus the $(-1)^P$ term. It may be also written as a *Slater determinant*:

$$\phi\left(\vec{x}_1, \vec{x}_2, \ldots, \vec{x}_N\right) = \frac{1}{\sqrt{N!}} \begin{vmatrix} \chi_i\left(\vec{x}_1\right) & \chi_{i'}\left(\vec{x}_1\right) & \cdots & \chi_{i^N}\left(\vec{x}_1\right) \\ \chi_i\left(\vec{x}_2\right) & \chi_{i'}\left(\vec{x}_2\right) & \cdots & \chi_{i^N}\left(\vec{x}_2\right) \\ \vdots & \vdots & \ddots & \vdots \\ \chi_i\left(\vec{x}_N\right) & \chi_{i'}\left(\vec{x}_N\right) & \cdots & \chi_{i^N}\left(\vec{x}_N\right) \end{vmatrix} \tag{2.76}$$

This Slater determinant does not specify which electron is in which orbital. Note that the rows of an N-electron Slater determinant are labeled by electrons and the columns are labeled by spin orbitals. Interchanging the coordinates of two electrons corresponds to interchanging two rows of the Slater determinant, which changes the sign of the determinant. Hence Slater determinants meet the requirement of the antisymmetry principle. Having two electrons occupying the same spin orbital corresponds to having two columns of the determinant equal, which makes the determinant zero. Therefore no more than one electron can occupy a spin orbital (Pauli exclusion principle).

As it has been pointed out before, the Hartree product is an independent-electron wave function. The probability of finding electron one in $d\vec{x}_1$ at $\vec{x}_1$, electron two $d\vec{x}_2$ at $\vec{x}_2$, etc. is equal to the product of probabilities of finding these electrons in their $d\vec{x}$. Antisymmetrising a Hartree product to obtain a Slater determinant introduces exchange effects, so-called because they arise from the requirement that the probability of ψ ($\int \psi^* \psi d\tau$) be invariant to the exchange of the space and spin coordinates of any two electrons. In particular, a Slater determinant incorporates *exchange-correlation*, which means that the motion of two electrons with parallel spins is correlated. Since the motion of electrons with opposite spins remains uncorrelated, it is customary to refer to a single determinantal wave function as an uncorrelated wave function.

[‡]The Pauli exclusion principle was formulated by Wolfgang Pauli in 1925 and it states that two identical fermions cannot have the same quantum state simultaneously. It relates to the antisymmetry principle as for two identical fermions the total wave function must be anti-symmetric. Electrons are fermions, so in a single atom two electrons cannot have the same four quantum numbers.

2.2.1 The Hartree-Fock approximation

The Hartree-Fock method is a simple approach to find an approximate solution to the electronic Schrödinger equation. It is also the first step for an approximation for other methods towards more accurate results. The method uses the Slater determinants as an antisymmetric wave function and the variation principle to choose the best wave function in a given range. Starting with an electronic wave function constructed from spin orbitals of N electrons like the one described at 2.69

$$\phi = \chi_1(\vec{x}_1)\,\chi_2(\vec{x}_2)\cdots\chi_N(\vec{x}_N) \tag{2.77}$$

the terms $\chi_i(\vec{x}_i)$ are varied to determine each one. This variation has to lead to lower energies than the previous ones, resolving $E = \int \phi^* \hat{H} \phi d\tau$ and supposing that ϕ is normalised, and thus using the variational principle explained in section 2.1.3.2. The operator $\hat{H}$ can be written as:

$$\hat{H} = \sum_i \hat{h}(\vec{x}_i) + \sum_{i,j>i} \frac{e^2}{r_{ij}} \tag{2.78}$$

where the first term is a core-Hamiltonian and creates all the one-electron integrals. Each core-Hamiltonian describes the kinetic and potential energy in the field of the nuclei:

$$\hat{h}(\vec{x}_i) = -\frac{h^2}{8\pi^2 m_0}\nabla_i^2 - \sum_A^M \frac{Z_A e^2}{r_{iA}} \tag{2.79}$$

All the spin orbitals are integrated upon all their complex conjugates, producing 1 when the spin orbital, Hamiltonian applied if suited, and its complex conjugate are the same or 0 when they are not equal. Thus, from the last equation, the one-electron integrals only affect the spin orbitals to whom the operator affects.

The second term of equation 2.78 refers to the repulsion between electrons and involves the spin orbital functions χ_i and $\chi_{i'}$ of two electrons and their positions $\vec{x}_i$ and $\vec{x}_j$, which can be interchanged between orbitals. When this operator acts on the ϕ wave function, it generates two two-electron integrals, due to the antisymmetric nature of the determinantal wave function. For example, in a two electron wave function, the application of the e^2/r_{12} repulsion

term leads to:

$$\int \phi^* \frac{e^2}{r_{12}} \phi \, d\tau = \int \frac{1}{\sqrt{2}} \left\{ \chi_1(\vec{x}_1) \chi_2(\vec{x}_2) - \chi_2(\vec{x}_1) \chi_1(\vec{x}_2) \right\}^* \times \frac{e^2}{r_{12}} \frac{1}{\sqrt{2}} \left\{ \chi_1(\vec{x}_1) \chi_2(\vec{x}_2) - \chi_2(\vec{x}_1) \chi_1(\vec{x}_2) \right\} d\vec{x}_1 d\vec{x}_2$$
$$= \frac{1}{2} \int \chi_1^*(\vec{x}_1) \chi_2^*(\vec{x}_2) \frac{e^2}{r_{12}} \chi_1(\vec{x}_1) \chi_2(\vec{x}_2) + \chi_2^*(\vec{x}_1) \chi_1^*(\vec{x}_2) \frac{e^2}{r_{12}} \chi_2(\vec{x}_1) \chi_1(\vec{x}_2)$$
$$- \chi_1^*(\vec{x}_1) \chi_2^*(\vec{x}_2) \frac{e^2}{r_{12}} \chi_2(\vec{x}_1) \chi_1(\vec{x}_2) - \chi_2^*(\vec{x}_1) \chi_1^*(\vec{x}_2) \frac{e^2}{r_{12}} \chi_1(\vec{x}_1) \chi_2(\vec{x}_2) \, d\vec{x}_1 d\vec{x}_2 \tag{2.80}$$

Since $r_{12} = r_{21}$, the dummy variables of integration can be interchanged in the second term of the expression and show that it is equal to the first term. Similarly, the third and fourth terms are equal.

$$\int \phi^* \frac{e^2}{r_{12}} \phi \, d\tau = \int \chi_1^*(\vec{x}_1) \chi_2^*(\vec{x}_2) \frac{e^2}{r_{12}} \chi_1(\vec{x}_1) \chi_2(\vec{x}_2) \, d\vec{x}_1 d\vec{x}_2 - \int \chi_1^*(\vec{x}_1) \chi_2^*(\vec{x}_2) \frac{e^2}{r_{12}} \chi_2(\vec{x}_1) \chi_1(\vec{x}_2) \, d\vec{x}_1 d\vec{x}_2 \tag{2.81}$$

In systems with more than two electrons the deductive steps of the equation are the same but the number of combinations which make up the ϕ function escalates to N^2 possible combinations, but the equation of the two-electron integral is the same as 2.81. The first integral is the *coulomb integral* and the second one is the *exchange integral*. The coulomb and the exchange integrals take, respectively, this general form:

$$J_{ii'} = \int \chi_i^*(\vec{x}_1) \chi_{i'}^*(\vec{x}_2) \frac{e^2}{r_{12}} \chi_i(\vec{x}_1) \chi_{i'}(\vec{x}_2) \, d\vec{x}_1 d\vec{x}_2 \tag{2.82}$$

$$K_{ii'} = \int \chi_i^*(\vec{x}_1) \chi_{i'}^*(\vec{x}_2) \frac{e^2}{r_{12}} \chi_{i'}(\vec{x}_1) \chi_i(\vec{x}_2) \, d\vec{x}_1 d\vec{x}_2 \tag{2.83}$$

The coulomb integral can be written as the *Coulomb operator* applied to a spin orbital $\chi_i(\vec{x}_1)$

$$\hat{J}_{i'}(\vec{x}_1) \chi_i(\vec{x}_1) = \left[\int \chi_{i'}^*(\vec{x}_2) \frac{e^2}{r_{12}} \chi_{i'}(\vec{x}_2) \, d\vec{x}_2 \right] \chi_i(\vec{x}_1) = \left[\int |\chi_{i'}(\vec{x}_2)|^2 \frac{e^2}{r_{12}} d\vec{x}_2 \right] \chi_i(\vec{x}_1) \tag{2.84}$$

The coulomb term has a simple interpretation. Electron 1 feels a potential associated with the instantaneous position of electron 2, but is replaced by a one-electron potential, obtained by averaging the interaction e^2/r_{12} of electron 1 and electron 2, over all space and spin coordinates $\vec{x}_2$ of electron 2, weighted by the probability $\chi_{i'}(\vec{x}_2)|^2 d\vec{x}_2$ that electron 2 occupies the volume element $d\vec{x}_2$ at $\vec{x}_2$. The total averaged potential acting on the electron in χ_i arising from the $N-1$ electrons in the other spin orbitals is obtained by summing over all $i \neq i'$.

The Coulomb operator can be defined as a local stand-alone operator, but the *exchange operator* needs another spin orbital to be defined as it swaps electrons from one orbital to the other:

$$\hat{K}_{i'}(\vec{x}_1)\chi_i(\vec{x}_1) = \left[\int \chi^*_{i'}(\vec{x}_2)\frac{e^2}{r_{12}}\chi_i(\vec{x}_2)\,d\vec{x}_2\right]\chi_{i'}(\vec{x}_1) \tag{2.85}$$

Applying operator $\hat{K}_{i'}$ on $\vec{x}_1$ involves an "exchange" of electron 1 for electron 2 on the right of the e^2/r_{12} in 2.85, relative to 2.84. $\hat{K}_{i'}$ is a non-local operator, since there does not exist a simple potential $\hat{K}_{i'}(\vec{x}_1)$ uniquely defined at a local point in space $\vec{x}_1$. The result of operating with $\hat{K}_{i'}(\vec{x}_1)$ on $\chi_i(\vec{x}_1)$ on the value of χ_i throughout all space, not just at $\vec{x}_1$.

The core-Hamiltonian, coulomb and exchange operators act only on one electron at a time, and thus the Hartree-Fock equation is summed up in a operator including summation over all the spin orbitals, named the *Fock operator*, which is

$$\hat{f}(\vec{x}_1) = \hat{h}(\vec{x}_1) + \sum_{i'}\hat{J}_{i'}(\vec{x}_1) - \sum_{i'}\hat{K}_{i'}(\vec{x}_1) \tag{2.86}$$

so that the Hartree-Fock equations become

$$\hat{f}(\vec{x}_1)\chi_i(\vec{x}_1) = \varepsilon_i\chi_i(\vec{x}_1) \tag{2.87}$$

the equation onto which the variational principle has to be applied to minimise the energy and obtain the best spin orbital combination. The solving procedure starts from a starting spin orbital group guess the equation 2.87 is solved and the process is repeated—*iterated*—with the new set of spin orbitals until the energetic difference between one set and its predecessor is lower than an accepted error. For this reason, Hartree-Fock approximation is also known as *self-consistent field* (SCF) method.

2.2.1.1 Restricted Hartree-Fock method (RHF)

Many-electron systems have a complexity which can be numerically solved when they are atomic calculations. Otherwise, in a molecular system there is no method of calculus to obtain a numerical solution. Roothaan[223] constructed the molecular orbitals from a known spatial set of basis functions, using the LCAO method. This way the differential equations can be solved by standard matrix techniques. It restricts the spin orbitals of two electrons in a same atomic or molecular orbital to have the same spatial function and differ only in the spin part. Dropping the spin function $\alpha(\omega)$ and $\beta(\omega)$ from the spin orbital $\chi_i(\vec{x}_1)$, a spatial orbital $\psi_i(\vec{r}_1)$ can be expanded in a set of K known *basis functions* $\{\phi_\mu(\vec{r}_1)\}$:

$$\psi_i = \sum_{\mu=1}^{K} C_{\mu i}\phi_\mu \qquad i = 1, 2, \ldots, K \tag{2.88}$$

The description of ψ_i improves as the number of basis set functions $\{\phi_\mu\}$ is increased. If the set was complete, the expansion would be provide the "exact" molecular orbitals, i.e. the molecular orbitals would converge to those of equation $\hat{f}\psi_i = \varepsilon_i\psi_i$, the true eigenfunction of the Fock operator. Unfortunately, computational restrictions oblige to truncate the complete basis set to a few basis, leading to an approximate description of the spatial orbital ψ_i. Moreover, this truncation is one of the origins of the *basis set superposition error* (BSSE) artifact, which will be explained later in section 2.3. Nevertheless, it is important to choose a basis set that will provide, as far as possible, a reasonably accurate expansion for the exact molecular orbitals ψ_i, particularly for those orbitals ψ_a which are occupied in Ψ_o and determine the ground state E_o. Thus, now the problem is to calculate the set of expansion coefficients:

$$\hat{f}(\vec{r}_1)\sum_{\nu} C_{\nu i}\phi_\nu(\vec{r}_1) = \varepsilon_i \sum_{\nu} C_{\nu i}\phi_\nu(\vec{r}_1) \tag{2.89}$$

operator $\hat{f}(\vec{r}_i)$ being:

$$\hat{f}(\vec{r}_i) = -\frac{h^2}{8\pi^2 m_o}\nabla_i^2 - \sum_{A}^{M}\frac{Z_A e^2}{r_{iA}} + \sum_{b}^{N/2}\left[2\hat{J}_b(\vec{r}_i) - \hat{K}_b(\vec{r}_i)\right] \tag{2.90}$$

The $N/2$ factor on the second summation appears as a consequence of the restriction of the spin orbitals to have the same spatial function, as it only

needs to be solved for half the electrons. Thus this technique can be only applied to closed shell configurations, which have two electrons in each atomic or molecular orbital. The coulomb and exchange integrals J_{ab} and K_{ab} are the same as in equations 2.82 and 2.83 but instead of spin orbitals χ_i they use the spatial orbitals ψ_i. The summation term including them is sometimes represented as $\hat{\nu}^{HF}$.

By multiplying equation 2.89 by $\phi_\mu^* (\vec{r}_1)$ on the left and integrating:

$$\sum_\nu C_{\nu i} \int \phi_\mu^* (\vec{r}_1) \hat{f} (\vec{r}_1) \phi_\nu (\vec{r}_1) d (\vec{r}_1) = \varepsilon_i \sum_\nu C_{\nu i} \int \phi_\mu^* (\vec{r}_1) \phi_\nu (\vec{r}_1) d (\vec{r}_1) \tag{2.91}$$

two matrices can be defined from this expression. The *overlap matrix* $\mathbf{S}$ is an Hermitian matrix of elements

$$S_{\mu\nu} = \int \phi_\mu^* (\vec{r}_1) \phi_\nu (\vec{r}_1) d (\vec{r}_1) \tag{2.92}$$

and is a positive-definite matrix as its eigenvalues are necessarily positive numbers. The other matrix is Hermitian as well and it is the *Fock matrix* $\mathbf{F}$, its elements defined as

$$F_{\mu\nu} = \int \phi_\mu^* (\vec{r}_1) \hat{f} (\vec{r}_1) \phi_\nu (\vec{r}_1) d (\vec{r}_1) \tag{2.93}$$

where $\hat{f} (\vec{r}_1)$ is a one-electron operator, and any set of one-electron functions defines a matrix representation of this operator. The Fock matrix $\mathbf{F}$ is the matrix representation of the Fock operator with the set of basis functions $\{\phi_\mu\}$. Now equation 2.91 can be written in terms of $\mathbf{F}$ and $\mathbf{S}$:

$$\sum_\nu F_{\mu\nu} C_{\nu i} = \varepsilon_i \sum_\nu S_{\mu\nu} C_{\nu i} \qquad i = 1, 2, \ldots, K \tag{2.94}$$

known as the *Roothan equations*, which can be written more compactly as the single matrix equation

$$\mathbf{FC} = \mathbf{SC}\boldsymbol{\varepsilon} \tag{2.95}$$

where $\mathbf{C}$ is a $K \times K$ square matrix of the expansion coefficients $C_{\nu i}$ and ε is a diagonal matrix of the orbital energies ε_i.

A variation of the RHF method can be applied to open shell systems which, apart from having spin orbitals doubly occupied, they have one or more atomic or molecular orbitals with a single electron. This is the *restricted open-shell*

Hartree Fock method (ROHF). In this case the Fock operator in 2.90 could not be applied because the Fock matrix **F** is not unique: it can take different forms leading to different orbitals and different orbital energies, but the same total eigenfunctions, energy, and other observables.

2.2.1.2 Unrestricted Hartree-Fock method (UHF)

Not all molecules, nor all states of closed-shell molecules, can be described by pairs of electrons in closed-shell orbitals, so the previous closed-shell formalism should be generalised to accommodate situations in which a molecule has one or more open-shell (unpaired) electrons. an unrestricted set of spin orbitals has the form:

$$\chi_i(\vec{x}) = \begin{cases} \psi_j^{\alpha}(\vec{r})\,\alpha(\omega) \\ \psi_j^{\beta}(\vec{r})\,\beta(\omega) \end{cases} \tag{2.96}$$

There are different spatial orbitals for α or β spin electrons. In restricted Hartree-Fock $\psi_j^{\alpha} = \psi_j^{\beta} = \psi_j$. Now electrons of α and β spin are described by different spatial functions and thus have a different set of orbital energies. The general Hartree-Fock equations when χ_i equals to ψ_j^{α} and ψ_j^{β} are respectively

$$\begin{aligned} \hat{f}(\vec{r}_1)\,\psi_j^{\alpha}(\vec{r}_1)\,\alpha(\omega_1) &= \varepsilon_j^{\alpha}\psi_j^{\alpha}(\vec{r}_1)\,\alpha(\omega_1) \\ \hat{f}(\vec{r}_1)\,\psi_j^{\beta}(\vec{r}_1)\,\beta(\omega_1) &= \varepsilon_j^{\beta}\psi_j^{\beta}(\vec{r}_1)\,\beta(\omega_1) \end{aligned} \tag{2.97}$$

which multiplied respectively by $\alpha^*(\omega_1)$ and $\beta^*(\omega_1)$ and integrated over spin is

$$\begin{aligned} \hat{f}^{\alpha}(\vec{r}_1)\,\psi_j^{\alpha}(\vec{r}_1) &= \varepsilon_j^{\alpha}\psi_j^{\alpha}(\vec{r}_1) \\ \hat{f}^{\beta}(\vec{r}_1)\,\psi_j^{\beta}(\vec{r}_1) &= \varepsilon_j^{\beta}\psi_j^{\beta}(\vec{r}_1) \end{aligned} \tag{2.98}$$

where the Fock operators are defined as

$$\begin{aligned} \hat{f}^{\alpha}(\vec{r}_1) &= \int \alpha^*(\omega_1)\,\hat{f}(\vec{r}_1,\omega_1)\,\alpha(\omega_1)\,d\omega_1 \\ \hat{f}^{\beta}(\vec{r}_1) &= \int \beta^*(\omega_1)\,\hat{f}(\vec{r}_1,\omega_1)\,\beta(\omega_1)\,d\omega_1 \end{aligned} \tag{2.99}$$

This operator includes the kinetic energy, nuclear attraction and effective potential of an electron of α or β spin. The effective potentials of the α-spin

electron are calculated as the addition of the coulomb and exchange interactions with all other α-spin electrons plus only a coulomb interaction with electrons of β-spin.

$$\begin{aligned}\hat{f}^{\alpha}(\vec{r}_1) &= \hat{h}(\vec{r}_1) + \sum_{a}^{N^{\alpha}} \left[\hat{J}_a^{\alpha}(\vec{r}_1) - \hat{K}_a^{\alpha}(\vec{r}_1)\right] + \sum_{a}^{N^{\beta}} \hat{J}_a^{\beta}(\vec{r}_1) \\ \hat{f}^{\beta}(\vec{r}_1) &= \hat{h}(\vec{r}_1) + \sum_{a}^{N^{\beta}} \left[\hat{J}_a^{\beta}(\vec{r}_1) - \hat{K}_a^{\beta}(\vec{r}_1)\right] + \sum_{a}^{N^{\alpha}} \hat{J}_a^{\alpha}(\vec{r}_1)\end{aligned} \tag{2.100}$$

The formalism includes the interaction of an electron with itself, but in this case the coulomb and exchange terms are the same, and the resulting interaction is zero.

Again, the Fock operators $\hat{f}^{\alpha}$ and $\hat{f}^{\beta}$ cannot be solved independently, for they are coupled, and they should be solved by an iterative process. As in the Roothaan's equations, an expanded basis set is linearly combined to obtain the spatial functions ψ_i^{α} and ψ_i^{β} and solve equation 2.98. The expansion is defined in orthonormal sets of $\{\psi_i^{\alpha}\}$ and $\left\{\psi_i^{\beta}\right\}$, but not necessarily between them, although they overlap with each other. The set is defined as

$$\psi_i^{\alpha} = \sum_{\mu=1}^{K} C_{\mu i}^{\alpha}\phi_{\mu} \qquad \psi_i^{\beta} = \sum_{\mu=1}^{K} C_{\mu i}^{\beta}\phi_{\mu} \qquad i = 1, 2, \ldots, K \tag{2.101}$$

Using ψ_i^{α} and substituting in 2.98

$$\sum_{\nu} C_{\nu j}^{\alpha}\hat{f}^{\alpha}(\vec{r}_1)\,\phi_{\nu}(\vec{r}_1) = \varepsilon_j^{\alpha}\sum_{\nu} C_{\nu j}^{\alpha}\phi_{\nu}(\vec{r}_1) \tag{2.102}$$

then multiplying by $\phi_{\mu}^{*}(\vec{r}_1)$ and integrating over the spatial coordinates of electron-one

$$\sum_{\nu} F_{\mu\nu}^{\alpha} C_{\nu j}^{\alpha} = \varepsilon_j^{\alpha}\sum_{\nu} S_{\mu\nu j} C_{\nu j}^{\alpha} \qquad j = 1, 2, \ldots, K \tag{2.103}$$

where $\mathbf{S}$ is the overlap matrix and $\mathbf{F}^{\alpha}$ is the matrix representation of $\hat{f}^{\alpha}$ in the basis $\{\phi_{\mu}\}$

$$F_{\mu\nu}^{\alpha} = \int \phi_{\mu}^{*}(\vec{r}_1)\,\hat{f}^{\alpha}(\vec{r}_1)\,\phi_{\nu}(\vec{r}_1)\,d(\vec{r}_1) \tag{2.104}$$

For β-spin electrons, the procedure is identical. This equations can be combined into two matrix expressions:

$$\begin{aligned} \mathbf{F}^{\alpha}\mathbf{C}^{\alpha} &= \mathbf{S}\mathbf{C}^{\alpha}\varepsilon^{\alpha} \\ \mathbf{F}^{\beta}\mathbf{C}^{\beta} &= \mathbf{S}\mathbf{C}^{\beta}\varepsilon^{\beta} \end{aligned} \tag{2.105}$$

Roothaan equations are a particular case of the unrestricted ones, known as *Pople-Nesbet equations*. The solution method is similar to the Roothaan equations, but $\mathbf{F}^{\alpha}$ and $\mathbf{F}^{\beta}$ depend both on $\mathbf{C}^{\alpha}$ and $\mathbf{C}^{\beta}$ so the two matrix eigenvalue problems must be solved simultaneously.

The application of the Hartree-Fock method has its main flaw in neglecting the electron correlation due to the mean field approximation, and leads to large deviations from experimental results. Alternatives exist and are known as the *post-Hartree-Fock methods*, devised to include electron correlation and which usually use the Hartree-Fock method to provide a starting wave function which will be later corrected. One of these approaches is the Møller-Plesset perturbation theory, which treats correlation as a perturbation of the Fock operator.

2.2.2 Møller-Plesset perturbation theory

The idea behind the Møller-Plesset perturbation theory is improving the Hartree-Fock energy using RSPT (see section 2.1.3.3 for more details) and use the perturbation to obtain the correlation energy, i.e. the energy difference between the Hartree-Fock energy and the exact one. The unperturbed Hamiltonian $\hat{H}^{(0)}$ is the summation of all the N one-electron Hartree-Fock operators

$$\begin{aligned} \hat{H}^{(0)} &= \sum_{i}^{N} \hat{f}\left(\vec{x}_i\right) = \\ &= \sum_{i}^{N} \left\{ -\frac{h^2}{8\pi^2 m_o}\nabla_i^2 - \sum_{A}^{M} \frac{Z_A e^2}{r_{iA}} + \sum_{b}^{N/2} \left[2\hat{J}_b\left(\vec{x}_i\right) - \hat{K}_b\left(\vec{x}_i\right) \right] \right\} = \\ &= \sum_{i}^{N} \left[\hat{h}\left(\vec{x}_i\right) + \hat{\nu}^{HF}\left(\vec{x}_i\right) \right] \end{aligned} \tag{2.106}$$

The perturbation term $\hat{H}^{(1)}$ is defined as the difference between the Coulomb operator describing the exact electron-electron interactions and the potential

operator from RHF:

$$\hat{H}^{(1)} = \sum_{i<j}^{N} \frac{e^2}{r_{ij}} - \sum_{i}^{N} \sum_{b}^{N/2} \left[2\hat{J}_b(\vec{x}_i) - \hat{K}_b(\vec{x}_i) \right] = \sum_{i<j}^{N} \frac{e^2}{r_{ij}} - \sum_{i}^{N} \hat{\nu}^{HF}(\vec{x}_i) \quad (2.107)$$

The zeroth-order perturbation energy is the sum of the one-electron energies, as the eigenfunction of the Hamiltonian $\hat{H}^{(0)}$ is $\Psi_0^{(0)}$ and its eigenvalue $E_0^{(0)}$:

$$\hat{H}^{(0)}\Psi_0^{(0)} = E_0^{(0)}\Psi_0^{(0)} \qquad E_0^{(0)} = \sum_a \varepsilon_a \quad (2.108)$$

Subindex a refers to the occupied spin orbitals. They are labeled as $a, b, c, \ldots$, while unoccupied ones are labeled as $r, s, t, \ldots$. The first-order correction of the energy is:

$$\begin{aligned} E_0^{(1)} &= \int \Psi_0^{(0)*} \hat{H}^{(1)} \Psi_0^{(0)} d\tau \\ &= \int \Psi_0^{(0)*} \sum_{i<j} \frac{e^2}{r_{ij}} \Psi_0^{(0)} d\tau - \int \Psi_0^{(0)*} \sum_i \hat{\nu}^{HF}(\vec{x}_i) \Psi_0^{(0)} d\tau \\ &= \frac{1}{2} \sum_{ab} \int \chi_a^*(\vec{x}_1) \chi_b^*(\vec{x}_2) \frac{e^2}{r_{ij}} \chi_a(\vec{x}_1) \chi_b(\vec{x}_2) d\tau - \\ &\qquad - \sum_a \int \chi_a^*(\vec{x}_1) \sum_b \left(\hat{J}_b - \hat{K}_b \right) \chi_a(\vec{x}_1) d\tau = \\ &= -\frac{1}{2} \sum_{ab} \int \chi_a^*(\vec{x}_1) \chi_b^*(\vec{x}_2) \frac{e^2}{r_{ij}} \chi_a(\vec{x}_1) \chi_b(\vec{x}_2) d\tau \end{aligned} \quad (2.109)$$

The sum of the zeroth and the first-order energies is the Hartree-Fock energy

$$E_0 = E_0^{(0)} + E_0^{(1)} = \sum_a \varepsilon_a - \frac{1}{2} \sum_{ab} \int \chi_a^*(\vec{x}_1) \chi_b^*(\vec{x}_2) \frac{e^2}{r_{ij}} \chi_a(\vec{x}_1) \chi_b(\vec{x}_2) d\tau \quad (2.110)$$

and thus the first correction to the Hartree-Fock energy occurs in the second order of perturbation theory. The second-order energy corrections from section 2.1.3.3 can be rewritten to

$$E_0^{(2)} = {\sum_n}' \frac{\left| \int \Psi_0^{(0)*} \hat{H}^{(1)} \Psi_n^{(0)} d\tau \right|^2}{E_0^{(0)} - E_n^{(0)}} \quad (2.111)$$

where $\Psi_n^{(0)}$ represents the excitations of the system. Single and triple excitations are forbidden due to the two-particle nature of the perturbation. Thus, only double excitations are allowed represented by Ψ_{ab}^{rs} and the eigenvalues of the Hamiltonian for this eigenfunction are

$$\hat{H}_0 \Psi_{ab}^{rs} = \left(E_0^{(0)} - (\varepsilon_a + \varepsilon_b - \varepsilon_r - \varepsilon_s) \right) \Psi_{ab}^{rs} \tag{2.112}$$

and because all possible double excitations are added by summing over all a and all $b > a$ states and over all r and all $s > r$ excitations, the second-order energy is

$$E_0^{(2)} = \sum_{\substack{a<b \\ r<s}} \frac{\left| \int \Psi_0^{(0)*} \left(\sum_{i<j} \frac{e^2}{r_{ij}} \right) \Psi_{ab}^{rs} d\tau \right|^2}{\varepsilon_a + \varepsilon_b - \varepsilon_r - \varepsilon_s} \tag{2.113}$$

and expressed as a spin-orbital combination is

$$E_0^{(2)} = \sum_{\substack{a<b \\ r<s}} \frac{\left| \begin{array}{l} \int \chi_a^*(\vec{x}_1)\chi_b^*(\vec{x}_2)\left(\sum_{i<j} \frac{e^2}{r_{ij}}\right)\chi_r(\vec{x}_1)\chi_s(\vec{x}_2) d(\vec{x}_1) d(\vec{x}_2) \\ - \int \chi_a^*(\vec{x}_1)\chi_b^*(\vec{x}_2)\left(\sum_{i<j} \frac{e^2}{r_{ij}}\right)\chi_s(\vec{x}_1)\chi_r(\vec{x}_2) d(\vec{x}_1)(\vec{x}_2) \end{array} \right|^2}{\varepsilon_a + \varepsilon_b - \varepsilon_r - \varepsilon_s} \tag{2.114}$$

This is the energy which Møller-Plesset theory uses in its second-order correction and is referred to as MP2. Clearly, through second-order in the correlation potential, the total electronic energy is given by the Hartree-Fock energy plus second-order Møller-Plesset correction: $E \approx E_{HF} + E_{MP2}$. A zeroth-order degenerated energy can be observed between occupied and virtual orbitals. When these orbitals do not have a sensible energy gap between them, MPPT cannot be used for these systems. MPPT can also use third and upper orders of correction, but generally the computational costs are too high to the small corrections they get.

2.2.3 Exchange-correlation functionals

In section 2.1.3.4 it has been pointed out that the main problem in DFT is to establish a relationship between the electronic density and the energy. The kinetic energy functional is known exactly, but the exact functional for exchange and correlation (XC) is not known except for the free electron gas.

Nevertheless it exists a relation between the XC potential and the XC energy although the exact operator is unknown:

$$E_{XC}[\rho] = \int \rho(\vec{r})\,\hat{\nu}_{XC}(\vec{r})\,d(\vec{r}) = \int \rho(\vec{r})\,\varepsilon_{XC}[\rho]\,d(\vec{r}) = \int e_{XC}[\rho]\,d(\vec{r}) \tag{2.115}$$

$$\hat{\nu}_{XC}(\vec{r}) = \frac{\delta E_{XC}[\rho]}{\delta\rho(\vec{r})} = \frac{\delta(\rho(\vec{r})\,\varepsilon_{XC}[\rho])}{\delta\rho(\vec{r})} = \frac{\delta e_{XC}[\rho]}{\delta\rho(\vec{r})} \tag{2.116}$$

where the variable ε_{XC} is the XC energy per particle, whereas e_{XC} is the XC energy per volume.

However there are several approximations which make the calculation of certain physical properties possible in a quite accurate way. The simplest and at the same time most widely used is the *local density approximation*(LDA). In this method, the functional ε_{XC} depends only on the local electronic density. The exchange and correlation parts are treated separately: the exchange part uses the exact exchange energy for a uniform electron gas[245] and fitting its correlation part by an interpolating method.[267] LDA is a good approximation for systems where the electronic density is approximately homogeneous. In other cases where important variations exist, an approach using infinitesimal portions from Monte Carlo simulations of the electron gas is used. Open-shell systems where α and β densities are not the same need a different treatment than the LDA. The *local spin density approximation*(LSDA) is similar to the treatment used in UHF and minimises both densities independently. Although a simple approximation, LDA and LSDA reproduce geometries, frequencies and charge densities reasonably well, but are not appropriate for systems with weak interactions, zones near the nucleus or making thermodynamic calculations. They have a tendency to elongate distances and overvalue the bond energy. Furthermore, one of the turndowns of LDA is that it undervalues the exchange energy by 10–15%.

One way to improve LDA is to introduce the density gradient in the XC effects using the *generalized gradient approximation*(GGA) This method accounts for how density varies around a coordinate, besides the local density. The LDA XC energy is modified so it has an adequate asymptotic behaviour and escalates correctly. GGA improves the geometries, frequencies and charge density compared to LDA, and it works reasonably well with hydrogen bonded systems, although complexes presenting van der Waals interactions are not so well described.

There are many corrections to the GGA for the different exchange and

correlation parts. Becke improved the GGA exchange energy adding a correction term to the LDA expression, defining it as the sum of the LDA exchange energy plus a parameter which depends on the density gradient to introduce the gradient effects.[20] This is the most used correction to the exchange part up to date. The correlation parts have other corrections, those most widely applied are the ones proposed by Perdew[205] and those by Lee, Yang and Parr.[156]

The *hybrid functionals* are a type of approximations to the XC energy functional in DFT that incorporate a portion of exact exchange from Hartree-Fock theory with exchange and correlation from other sources (*ab initio*, such as LDA, or empirical). The justification of the connection between the exact exchange from Hartree-Fock goes through the adiabatic connection for the XC energy using an external potential exponentiation with a variable set between 0 and 1. The hybrid approach to constructing density functional approximations was introduced by Becke in 1993.[21] Hybridisation with Hartree-Fock exchange—which is exact— provides a simple scheme for improving many molecular properties, such as atomisation energies, bond lengths and vibration frequencies, which tend to be poorly described with simple *ab initio* functionals.

2.3 Basis set superposition error

The molecular orbitals used in theoretical chemistry methods are expanded on a set of functions or *basis set*, whose linear combination creates the whole function space in which the MO are defined with the weights of the coefficients to be determined. Usually these functions are AOs as they are centred on the atomic nuclei and form orbitals, but they can be centred in bonds, lone pairs or in the two lobes of a p-orbital as well, all them known as *floating functions*.[136] The first basis sets used in molecular calculations were typically *Slater-type orbitals*(STO),[244] which correspond to a set of functions which decay exponentially with distance from the nuclei. Later, this approximation was in turn approximated as linear combinations of *Gaussian-type orbitals*(GTO),[38] which overlap and other integrals are easier to calculate, leading to huge computational savings. The minimum basis sets are those which a single basis function is set on each atom in the molecule in a Hartree-Fock calculation on free atoms. More functions can be added to obtain a better description of the atom, for example basis functions of the p-type to atoms which have p orbitals. Furthermore, auxiliary functions can be introduced to add some

additional needed flexibility within the basis set. These *polarisation functions* add one more node to the valence orbitals: they can be from the p-type orbitals for hydrogen atoms to the f-type for heavier ones. Polarisation allow atoms to be more asymmetric about the hydrogen nucleus. This is an important result when considering accurate representations of bonding between atoms, because the very presence of the bonded atom makes the energetic environment of the electrons spherically asymmetric. Another improvement to the basis sets are the addition of *diffuse functions*, which are a very shallow type of Gaussian basis functions, which more accurately represent the tail portion of the atomic orbitals, distant from the atomic nuclei. Diffuse functions can be important when considering anions and other large, "soft" molecular systems.

As it has been pointed out early in section 2.2.1.1, using an infinite set of basis functions leads to an exact description of the system's atomic orbitals, but on the other hand it needs, at least to date, an infinite time to compute. Thus, the infinite basis sets are truncated to obtain finite basis sets which allow calculations with finite time, but with an error associated to the observable—e.g. energy. Usually bigger basis sets lead to better system descriptions[§] but in turn increase calculation time exponentially. If the finite basis is expanded towards an infinite complete set of functions, calculations using such a basis set are said to approach the basis set limit.

The use of finite basis sets leads to a mathematical artifact known as the *basis set superposition error* (BSSE) when used to calculate interaction energies of separate molecules, different parts of the same one or approaching molecules. In order to obtain the binding energy of two interacting fragments $A \cdots B$ the usual method is to calculate the energy of the complex and then substract the corresponding energy of the isolated fragments. The total basis set used by the complex is the sum of these of the two separated fragments, obtaining a bigger basis set and thus a potentially better, lower energy for the complex than these of the fragments. This effect was first pointed out by Jansen and Ros,[140] although the terminology BSSE was first introduced by Liu and McLean.[168] The expression used to calculate the interaction energy is, without taking into account the nuclear relaxation,

$$\Delta E(AB) = E_{AB}^{\alpha\cup\beta}(AB) - E_{AB}^{\alpha}(A) - E_{AB}^{\beta}(B) \tag{2.117}$$

where superindices α and β are the basis sets of the A and B fragments, respectively; and the expression $\alpha \cup \beta$ refers to the union of the two basis

[§]Remember that in variational methods, the lower the energy obtained, the better the description of the system.

sets or the extended basis set. Inbetween parenthesis there is the fragment to which the energy term refers, being AB the complex. Subindices refer to the geometry of the fragment in which the energy has been calculated. Thus, $E^{\alpha}_{AB}(A)$ is the energy of the fragment A using its own base α and the geometry it has in the complex AB (not isolated as A).

Taking into account that as the basis set grows, the energy of the complex diminishes, the resulting interaction as for the expression 2.117 will be much more attractive (lower energy) than the real value. This is the BSSE, and the magnitude of this error is related to the size of the basis set used, the geometry of the system and the definition of the fragments. In complexes where the bonding energy is small, BSSE can account for the same value as the interaction energy.

2.3.1 BSSE correction

Over the years different approaches, methods and strategies have been developed to avoid or at least minimise the BSSE effects. Most of these methods are based on modifying or adapting the basis set they use. The most immediate approach is to increase the size of the basis sets used, with the consequent increase of the calculation costs. Introducing diffuse functions the BSSE is reduced for a small expense in computing time.[229, 231, 195] Another option is to saturate the system's space with basis sets and fix them through the molecule optimization process, but this model would not be valid as the system wave function would change if translated or rotated, apart from the fact that linear dependencies in the basis set could arise if the space was too saturated with them. Another option is the use of the plane waves (PW) as basis set. Plane waves are expanded independently of the position and number of nuclei of the molecule, and the real space representation of the wave function is obtained after the application of fast Fourier transform techniques. Unfortunately, the results obtained are not so good as the ones using atom-centred functions.

A different approach to solve the problem is to develop a methodology which takes into account the BSSE. They are called *a priori* methods, and there exists a wide range of possibilities, all of them more or less successful and/or accepted. One of these methods is developed by Mayer,[174] applying the second quantization theory to split the Hamiltonian into the sum of all the intramolecular terms as well as the pure-energy terms of the intermolecular operator. The BSSE is eliminated by projecting all the intramolecular terms

into the subspace spawned by the basis functions of the corresponding complex fragment. This method is known as the *chemical Hamiltonian approach* (CHA)

Another *a priori* method is the *constrained dimer function*[226] (CDF), which removes the BSSE by introducing constraints to the wave function at SCF level. The constraints made that the occupied orbitals of the dimer would not mix with those of the monomers which are approximate solutions of the system, as the orbitals of the fragments are orthogonal with each other. On the other hand, this produces modelled results which sometimes are artifacts. Calculations made on this method pointed out flaws in the supermolecule geometry description[175, 227], and thus is no longer used.

There are other *a priori* methods working on different methodologies. Some modify the SCF methodology, constraining it, locating or imposing conditions to the basis set or wave functions, so the result is usually an under-correction of the BSSE compared to better established methods.[89, 110, 187] Others focus on electron correlation, the most successful ones are called local correlation methods although they started as a way to reduce computational costs.[222, 228, 271] The electronic excitations of the correlation are restricted to those occurring in the same fragment and the ones from the ground level of a fragment to the virtual orbitals of the other are excluded.

Finally, corrections can be made *a posteriori* as well. The counterpoise method falls in this group and nowadays is the most used to correct BSSE and is the one used in this thesis.

2.3.2 The counterpoise correction

The *counterpoise correction* (CP) was developed by Boys and Bernardi in 1970 as an *a posteriori* correction of the BSSE.[39] The idea behind CP is to use the same basis for all the calculations: the complex and fragments. As the supermolecule basis set is the combination of the fragments ones, it is easier to use the complex extended basis to calculate the energy of the fragments. At practical effects that means using the extended basis set for each fragment, or eliminating the other fragment from the complex setting its nuclear charges to zero and omitting its electrons. Thus the expression 2.117 is now written as:

$$\Delta E^{CP}(AB) = E_{AB}^{\alpha\cup\beta}(AB) - E_{AB}^{\alpha\cup\beta}(A) - E_{AB}^{\alpha\cup\beta}(B) \tag{2.118}$$

Of course, one of the drawbacks of this method is that the calculation time

used for the fragments will be longer than the fragments with the original basis.

As it has been stated before, the interaction energy is the difference between the the energies of isolated objects and their assembly. This includes the deformation energy that the monomers undergo to adapt to the interacting geometry. The CP correction in 2.118 does not consider this effect, thus the *fragment relaxation* term is introduced to take into account the deformation energy which is always positive.[264] It's counterpart is the *fragment preparation*, which energy is the same as the relaxation energy but with its sign changed. The total interaction energy including the deformations of the monomers is

$$\Delta E(AB) = E_{AB}^{\alpha\cup\beta}(AB) - E_A^{\alpha}(A) - E_B^{\beta}(B) \tag{2.119}$$

which is different of that in 2.117 in the geometry used. This energy can be divided into two terms: the interaction energy E_{int} and the relaxation energy E_{rel}

$$\Delta E(AB) = \Delta E_{int}(AB) - \Delta E_{rel}(A,B) \tag{2.120}$$

where the interaction energy is that of equation 2.117. The relaxation term includes the energy needed by the monomer to modify its geometry to the complex one

$$\Delta E_{rel}(A,B) = -\Big(E_{AB}^{\alpha}(A) - E_A^{\alpha}(A) + E_{AB}^{\beta}(B) - E_B^{\beta}(B)\Big) \tag{2.121}$$

The CP idea is to calculate all the fragments in the extended basis set, including the relaxation terms, and the only term which has to be BSSE corrected is the interaction term. Thus,

$$\begin{aligned}\Delta E^{CP}(AB) = &\Big[E_{AB}^{\alpha\cup\beta}(AB) - E_{AB}^{\alpha\cup\beta}(A) - E_{AB}^{\alpha\cup\beta}(B)\Big] + \\ &+ \Big[E_{AB}^{\alpha}(A) + E_{AB}^{\beta}(B) - E_A^{\alpha}(A) - E_B^{\beta}(B)\Big]\end{aligned} \tag{2.122}$$

which can be rearranged in

$$\begin{aligned}\Delta E^{CP}(AB) = &\Big[E_{AB}^{\alpha\cup\beta}(AB) - E_A^{\alpha}(A) - E_B^{\beta}(B)\Big] + \\ &+ \Big[E_{AB}^{\alpha}(A) + E_{AB}^{\beta}(B) - E_{AB}^{\alpha\cup\beta}(A) - E_{AB}^{\alpha\cup\beta}(B)\Big] = \Delta E(AB) + \delta_{AB}^{CP}\end{aligned} \tag{2.123}$$

where now the interaction energy $\Delta E(AB)$ is corrected by the CP-BSSE correction term δ_{AB}^{CP}, which can also be considered as a sum of each of the fragments BSSE, $\delta_{AB}^{CP} = \delta_A + \delta_B$. The value of this correction is usually positive

due to the variational principle, producing more attractive uncorrected interactions; it diminishes as the monomer basis grows to the upper basis set limit, approaching to that of the complex; and depends on the geometrical properties of the complex, as indicated in the subindex (AB). This dependence on the geometry makes this term nor constant nor additive for all the systems calculated on the same basis sets.

Note that in the initial energy equation 2.121 the calculation of three terms was needed to obtain the interaction energy, and after applying the CP correction and the fragments relaxation, the number of terms needed to compute the interaction is seven, four of which are in the δ_{AB}^{CP} term. In case of a trimer or superior aggregate, CP can also be applied considering all the combinations of all the fragments with their basis and the extended one, increasing even more the number of terms needed. In this situation the calculation time increases exponentially.[82, 229] When a single atom is defined as a fragment, there is no need to calculate its own energy in its basis set more than once.

2.3.3 CP corrected PES [241]

The CP correction is usually applied as a one-point correction of a system at a particular geometry, usually the minimum interaction energy obtained from the potential energy surfaces (PES). The PES is constructed using the different approaches to solve the electronic Schrödinger wave function at different geometries, using iteration methods until a stationary state energy—a minimum energy state, but not necessarily—is found, which complies with the condition to be an absolute minimum. But CP-correcting this point leads to a higher energy which could not correspond to the system absolute minimum energy, as the BSSE depends on the geometry, the PES are anharmonic potentials and basis sets extensions increase as the fragments come close together. Thus, the geometry will have associated energies which might not be the minimum for the system, and geometry might have longer interaction distances. Nevertheless, the CP correction can be applied to the whole PES, adding the δ_{AB}^{CP} term along the PES, and use the CP-BSSE free PES for finding the stationary points. This can be easily seen in scheme 2.1, where points **a** and **c** represent the optimized structures on the uncorrected and corrected PES, respectively, while points **b** and **d** are the energy of those two geometries on the other PES.

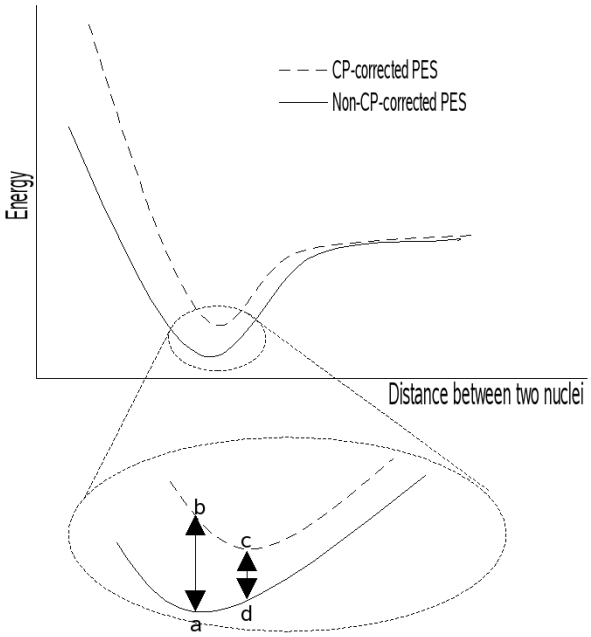

Scheme 2.1.

Point **c**, representing the corrected minimum energy and where the stable geometry lies, is different from point **b** which is the punctual energy correction. The whole PES changes, and it can lead to different geometries and energies from those on the uncorrected PES. BSSE magnitude depends on the geometry where it is calculated, making it change its position and topology. Usually, the fact that the corrected energy is less attractive induces longer intermolecular distances for the system. This new PES curvature will also change due to the correction, and so will the corrected vibration energies.

Anyway, any stationary point on the corrected PES is a correction of the same stationary point on the uncorrected PES. From this fact, the CP-corrected interaction PES can be used to find stationary geometries. To do

so, equation 2.123 should be derived:

$$\begin{aligned}\frac{\partial\left(\Delta E^{CP}(AB)\right)}{\partial q_i} &= \frac{\partial\left(\Delta E(AB)\right)}{\partial q_i} + \frac{\partial\left(\delta_{AB}^{CP}\right)}{\partial q_i} \\ &= \frac{\partial\left(E_{AB}^{\alpha\cup\beta}(AB)\right)}{\partial q_i} - \frac{\partial\left(E_{A}^{\alpha}(A)\right)}{\partial q_i} - \frac{\partial\left(E_{B}^{\beta}(B)\right)}{\partial q_i} + \frac{\partial\left(E_{AB}^{\alpha}(A)\right)}{\partial q_i} \\ &\quad + \frac{\partial\left(E_{AB}^{\beta}(B)\right)}{\partial q_i} - \frac{\partial\left(E_{AB}^{\alpha\cup\beta}(A)\right)}{\partial q_i} - \frac{\partial\left(E_{AB}^{\alpha\cup\beta}(B)\right)}{\partial q_i} \\ &= \frac{\partial\left(E_{AB}^{\alpha\cup\beta}(AB)\right)}{\partial q_i} + \frac{\partial\left(E_{AB}^{\alpha}(A)\right)}{\partial q_i} + \frac{\partial\left(E_{AB}^{\beta}(B)\right)}{\partial q_i} \\ &\quad - \frac{\partial\left(E_{AB}^{\alpha\cup\beta}(A)\right)}{\partial q_i} - \frac{\partial\left(E_{AB}^{\alpha\cup\beta}(B)\right)}{\partial q_i} \qquad ,\forall q_i \in \{AB\}\end{aligned} \tag{2.124}$$

Note that the partial derivatives on the isolated fragments $\frac{\partial(E_A^{\alpha}(A))}{\partial q_i}$ and $\frac{\partial\left(E_B^{\beta}(B)\right)}{\partial q_i}$ are null with respect to the variation of the geometry of the complex as their stationary points are calculated independently of each other and are constants. Besides, it can be seen that a point on the uncorrected PES will be stationary also on the CP corrected PES when the CP correction surface δ_{AB}^{CP} is stationary as well, i.e. $\frac{\partial\left(\delta_{AB}^{CP}\right)}{\partial q_i} = 0$.

However, in order to obtain the interaction energies between fragments, the corrected PES of the complex must be constructed, d can be constructed adding the correction CP term to the energy of the supermolecule:

$$\begin{aligned}\Delta E^{CP}(AB) = E_{AB}^{\alpha\cup\beta}(AB) + \delta_{AB}^{CP} &= E_{AB}^{\alpha\cup\beta}(AB) \\ &+ \left[E_{AB}^{\alpha}(A) + E_{AB}^{\beta}(B) - E_{AB}^{\alpha\cup\beta}(A) - E_{AB}^{\alpha\cup\beta}(B)\right]\end{aligned} \tag{2.125}$$

This is the description of the complex corrected PES and from this the CP-BSSE free interaction should be calculated. The difference between equation 2.123 and 2.125 is a BSSE-free constant term which depends only on the system and the definition of the fragments, the terms of the monomers stationary points pointed out before. Then, this equation can be derived and

generalized to the N^{th}-order energy derivatives:

$$\begin{aligned}\frac{\partial^n\left(E^{CP}(AB)\right)}{\partial^n q_i} &= \frac{\partial^n\left(E_{AB}^{\alpha\cup\beta}(AB)\right)}{\partial^n q_i} + \frac{\partial^n\left(\delta_{AB}^{CP}\right)}{\partial^n q_i} \\ &= \frac{\partial^n\left(E_{AB}^{\alpha\cup\beta}(AB)\right)}{\partial^n q_i} + \left[\frac{\partial^n\left(E_{AB}^{\alpha}(A)\right)}{\partial^n q_i} + \frac{\partial^n\left(E_{AB}^{\beta}(B)\right)}{\partial^n q_i}\right. \\ &\quad \left. - \frac{\partial^n\left(E_{AB}^{\alpha\cup\beta}(A)\right)}{\partial^n q_i} - \frac{\partial^n\left(E_{AB}^{\alpha\cup\beta}(B)\right)}{\partial^n q_i}\right]\end{aligned} \tag{2.126}$$

Second and third derivatives are used to calculate the harmonic and anharmonic vibration frequencies. Unfortunately, there is no definition for a CP-corrected electronic density for the complex.

2.4 Atoms in molecules theory [11]

Using the first order electronic density $\rho(\vec{r})$, Bader developed the *atoms in molecules theory* (AIM) which can, among other characteristics, analyse the electronic density of a given molecule in atomic fragments. With this analysis, the contributions for every atom to the molecule of a property which depends on the electronic density can be studied; properties like the bond critical points or the bielectronic densities. The methodology to obtain such properties is based on densities, not on the molecular structures, only on the topology of the electronic density. Results should adapt to the quantum molecular model which does not consider "defined" bonds between atoms. Furthermore, as AIM theory is based on first order densities, which are observable magnitudes, its results should have a physical significance that others obtained from analytical methods based for example on LCAO, although Bader uses them as well.

In order to divide the molecule in subatomic spaces it needs to exist a condition of zero flux surface to define these subspaces called basins:

$$\nabla\rho(\vec{r})\cdot n(\vec{r}) = 0 \qquad ,\forall\vec{r}\in S(\vec{r}) \tag{2.127}$$

where $S(\vec{r})$ is the surface defining the atom and $n(\vec{r})$ the normal vector at $\vec{r}$ on the surface. The surface can occupy all the available space, in this case the

zero flux condition will be met at infinite, because is where $\nabla\rho(\vec{r})$ is null, and thus it will be delimited. The other zones where the condition is also observed are those on the limits of the atomic volume, usually containing one single atom. This way, the properties of the atoms can be isolated for a molecule.

Using the gradient of the first order density, the *critical points* of a molecule are the points where the gradient of the first order electron density is zero. Critical points can be classified using the values that their diagonalised Hessian[¶] has. The rank ω is the number of the Hessian curvature matrix eigenvalues different from zero; and the signature σ is expressed as the algebraic sum over the signs of these curvatures. Using this nomenclature, critical points with rank 3, whose usually found associated with first order densities, can be described as:

$(3,-3)$ *Attractor*: At these points, all the curvatures of the Hessian are negatives, pointing a density maximum.

$(3,-1)$ *Bond critical point* (BCP): At these points the density has a positive curvature at one direction and two negative ones at the other two. This type of points can be found among atoms separated by zero flux surfaces. When two atoms share a bonding point and an interatomic surface, they can be considered to be bonded. Furthermore, the values of the electronic density and other properties on the bond critical point can give important information on the type of interaction.

$(3,+1)$ *Ring critical point* (RCP): A ring critical point has two positive density curvatures and a negative one. This type of critical points are usually found in the centre of rings, e.g. benzene.

$(3,+3)$ *Cage critical point* (CCP): It is related to a minimum of the electronic density. This type of critical point can only be found inside a group of cage-shaped bonded atoms

At critical points with rank 2 the electronic density curvature is null at one direction. There are three possibilities: $(2,-2)$, $(2,0)$ and $(2,+2)$. In fact, it is

[¶]The Hessian matrix is the square matrix of second-order partial derivatives of a function, i.e. it describes the local curvature of a function of many variables,

$$H_{ij} = \frac{\partial^2\rho(\vec{r})}{\partial x_i \partial x_j}, i \in \{1,2,3\}$$

where 1,2 and 3 represent the Cartesian coordinates.

more appropriate to call them *critical circles* as this is the shape they present. On the other hand, there are the *critical spheres* which correspond to the two possible structures with rank 1: $(1,-1)$ and $(1,+1)$.

Studying the derived functions from the first order density brings forth important data. For example, in the same guidelines of the density gradient flux

$$\nabla\rho\left(\vec{r}\right) = \frac{\partial\rho\left(\vec{r}\right)}{\partial x} + \frac{\partial\rho\left(\vec{r}\right)}{\partial y} + \frac{\partial\rho\left(\vec{r}\right)}{\partial z} \tag{2.128}$$

the molecular connectivity can be established: when two atoms are bonded to each other, there must be some gradient vectors that connect a common BCP of both atoms to each of the attractors. Following these vectors for all the attractors, a molecular graphic can be generated that indicates in which way are bonded the atoms make up the molecule. Gradient vectors which do not come from a $(3,-1)$ critical point can come out from the $(3,+1)$ or $(3,+3)$ critical point types or from infinity.

The density Laplacian is used as well

$$\nabla^2\rho\left(\vec{r}\right) = \frac{\partial^2\rho\left(\vec{r}\right)}{\partial^2 x} + \frac{\partial^2\rho\left(\vec{r}\right)}{\partial^2 y} + \frac{\partial^2\rho\left(\vec{r}\right)}{\partial^2 z} = \lambda_1 + \lambda_2 + \lambda_3 \tag{2.129}$$

particularly its sign shows an electron accumulation or deficiency at any point. When the Laplacian sign is positive there is an electron shortage, and vice versa. The Laplace operator can give a different information than that of the gradient. For example, when applied on a bond critical point, the bond type can be characterized as covalent (negative Laplacian, high electronic density at this point, open shell); or ionic or van der Waals (positive Laplacian, low electronic density, closed shell). Moreover, the accumulation of non-bonding electronic pairs can be detected with the density Laplacian too.

The bond *ellipticity* is a measure that allows to determine if there is a higher charge density in some of the bond directions than others. It is defined as

$$\varepsilon = \frac{\lambda_1}{\lambda_2} - 1 \tag{2.130}$$

where λ_1 and λ_2 represent the eigenvalues of the density Hessian perpendiculars to λ_3, which stands for the bond direction, being λ_3 positive as it is a minimum. Thus, the ellipticity is always positive as $\lambda_1 < \lambda_2 < 0$. In case of a σ-bond, the ellipticity value will be zero due to fact that the charge distribution perpendicular to the bonding path is homogeneous. In case of a π-bond,

its value will be different from zero as in one of the perpendiculars there will be more charge density than in the other one.

Apart from the first order densities, second order densities can be obtained as well. In this case, the function will represent the probability of finding two electrons in two different positions, similar to equation 2.55,

$$\rho\left(\vec{r}_1,\vec{r}_2\right)=\frac{N\left(N-1\right)}{2}\int\psi^*\left(\vec{x}_1,\ldots,\vec{x}_N\right)\psi^*\left(\vec{x}_1,\ldots,\vec{x}_N\right)d\omega_1 d\omega_2 d\vec{x}_3\ldots d\vec{x}_N \tag{2.131}$$

which integrated over the whole space will produce the number of electron pairs of the system. Bear in mind that the equation refers to two electrons leading to four possible combinations of electron pairs: $\alpha\alpha$, $\alpha\beta$, $\beta\alpha$ and $\beta\beta$.

Second order density function can be used to localize electronic pairs in the molecule.[103] The electronic localization and delocalization rate at different space regions can be defined using the Fermi hole, which describes the probability to find an electron in a position $\vec{r}_1$ near another electron with the same spin located in a $\vec{r}_2$ position. Starting from this bielectronic density, the localisation and delocalisation atomic indeces can be defined, which grades the XC importance, depending on the method used, between electrons belonging to different atoms of the same molecule.[215] Hence an *electron localisation index* can be defined by integrating the two electronic coordinates associated to the electronic density that in turn are associated to the XC density inside an atomic basin:

$$\lambda\left(A\right)=\int_A f\left(\vec{r}_1,\vec{r}_2\right)d\vec{r}_1 d\vec{r}_2 \tag{2.132}$$

where $f\left(\vec{r}_1,\vec{r}_2\right)$ is the Fermi correlation function. In a similar way, an interatomic *electron delocaliation index* can be defined integrating over a different atomic basin

$$\delta\left(A,B\right)=\int_A\int_B f\left(\vec{r}_1,\vec{r}_2\right)d\vec{r}_2 d\vec{r}_1 \tag{2.133}$$

$\lambda\left(A\right)$ is an index that represents the number of electrons localized inside the atomic basin of a certain atom. At the extreme possibility of an atom with a null interaction with its neighbours, $\lambda\left(A\right)$ value will be the electronic population of the atom A. On the other hand, $\delta\left(A,B\right)$ refers to the delocalization degree of the electrons between atoms A and B. The value of $\delta\left(A,B\right)$ will be higher for atomic pairs presenting an open-shell or covalent interaction. Take into consideration that the delocalisation index can be applied to any atom pair in a molecule, it does not matter if they are or are not formally bonded.

2.5 Kohn-Sham equations [26]

Equation 2.65 explained in section 2.1.3.4 is the expression to calulate the minimal energy and determine the electronic density of the ground state. The problem is, as it has been yet stated, that the relation between $F_{HK}[\rho]$ and the density is not known exactly. Specifically, $T[\rho]$ is the term which is not known with enough precision, in opposition to the kinetic energy which is easily calculated when ψ is known. Kohn and Sham tried to solve the problem using the Hartree-Fock approximation as a starting point.[151] The model is made up of N-electrons not interacting among them but experiencing the coulombic attraction from the nuclei; and moving under an external potential $\nu_s(\vec{r})$, which generates a wave function ψ_s with the same electron density as the real one. Its Hamiltonian only contains the one-electron operators, and solving the HF equations provides the exact orbital equations for this ideal system, the wave function being the Slater determinant. The exact density for this system is

$$\rho(\vec{r}) = \sum_{i=1}^{N_{occ}} |\chi_i(\vec{r})|^2 \tag{2.134}$$

and the exact kinetic energy

$$T_s[\rho] = -\frac{h^2}{8\pi^2} \sum_{i=1}^{N_{occ}} \int \chi_i^*(\vec{r}) \frac{1}{m_i} \nabla^2 \chi_i(\vec{r})\, d\vec{r}_i \tag{2.135}$$

The total energy for this HF system can be written as

$$E_\nu[\rho] = \sum_{i=1}^{N_{occ}} \varepsilon_i = T_s[\rho] + \int \rho(\vec{r})\, \nu_s(\vec{r})\, d\vec{r} \tag{2.136}$$

which differs from the real one which is

$$E_\nu[\rho] = T[\rho] + \int \rho(\vec{r})\, \nu_n(\vec{r})\, d\vec{r} + V_{ee}[\rho] \tag{2.137}$$

$T_s[\rho]$ and $T[\rho]$ are equal only when the HF solution is the exact one. The real energy equation 2.136 can be reordered and modified introducing the $T_s[\rho]$

term and a new Coulombic repulsion term $J[\rho]$:

$$E_\nu[\rho] = T_s[\rho] + \int \rho(\vec{r})\,\nu_n(\vec{r})\,d\vec{r} + J[\rho] + (T[\rho] - T_s[\rho]) + (V_{ee}[\rho] - J[\rho]) \tag{2.138}$$

$$J[\rho] = \frac{e^2}{2}\int \frac{\rho(\vec{r}_i)\,\rho(\vec{r}_j)}{r_{ij}} d\vec{r}_i d\vec{r}_j \tag{2.139}$$

The total exchange-correlation energy $E_{XC}[\rho]$ can be defined grouping the $T[\rho] - T_s[\rho]$ term into $T_c[\rho]$, which is the kinetic energy difference between the real system and the HF one, and $V_{ee}[\rho] - J[\rho]$ into $W_{XC}[\rho]$, which represents the exchange-correlation energy from the electronic part

$$E_{XC}[\rho] = (T[\rho] - T_s[\rho]) + (V_{ee}[\rho] - J[\rho]) = T_c[\rho] + W_{XC}[\rho] \tag{2.140}$$

and parallelly the same XC energy can be defined similarly to equation 2.59 as

$$E_{XC}[\rho] = \int \rho(\vec{r})\,\nu_{XC}(\vec{r})\,d\vec{r} \tag{2.141}$$

Thus, equation 2.138 will be transformed into

$$E_\nu[\rho] = T_s[\rho] + \int \rho(\vec{r})\,\nu_n(\vec{r})\,d\vec{r} + \frac{e^2}{2}\int \frac{\rho(\vec{r}_i)\,\rho(\vec{r}_j)}{r_{ij}} d\vec{r}_i d\vec{r}_j + E_{XC}[\rho] \tag{2.142}$$

This functional is then minimized with respect to the density with the DFT fundamental equation

$$\lambda = \frac{\delta E_\nu[\rho]}{\delta\rho(\vec{r})} = \frac{\delta T_s[\rho]}{\delta\rho(\vec{r})} + \nu_n(\vec{r}) + \int \frac{\rho(\vec{r}_j)}{r_{ij}} d\vec{r}_j + \frac{\delta E_{XC}[\rho]}{\delta\rho(\vec{r})} \tag{2.143}$$

which is usually shortened as

$$\lambda = \frac{\delta T_s[\rho]}{\delta\rho(\vec{r})} + (\phi(\vec{r}) + \nu_{XC}(\vec{r})) = \frac{\delta T_s[\rho]}{\delta\rho(\vec{r})} + \nu_{eff}(\vec{r}) \tag{2.144}$$

and where $\phi(\vec{r})$ is the *Coulomb potential* defined as

$$\phi(\vec{r}) = \nu_n(\vec{r}) + \int \frac{\rho(\vec{r}_j)}{r_{ij}} d\vec{r}_j \tag{2.145}$$

and $\nu_{XC}(\vec{r})$ is the *exchange-correlation potential* which is

$$\nu_{XC}(\vec{r}) = \frac{\delta E_{XC}[\rho]}{\delta \rho(\vec{r})} \tag{2.146}$$

The reference system used at the beginning of the section has an external potential $\nu_s(\vec{r})$ under which the electrons move, can be applied to the DFT fundamental equation 2.65 as well, in which case it will produce the following equation

$$\lambda = \frac{\delta E_\nu[\rho]}{\delta \rho(\vec{r})} = \frac{\delta T_s[\rho]}{\delta \rho(\vec{r})} + \nu_s(\vec{r}) \tag{2.147}$$

which ressembles the later equation 2.144. The solution to both equations is the same swapping $\nu_s(\vec{r})$ for $\nu_{eff}(\vec{r})$. The Kohn-Sham equations to solve from the effective potential will be

$$\hat{h}_{KS}\chi_i = \varepsilon_i \chi_i \tag{2.148}$$

$$\hat{h}_{KS} = -\frac{e^2}{2}\nabla^2 + \nu_{eff}(\vec{r}) \tag{2.149}$$

and the spin orbitals used must be othogonal with each other. These orbitals are known as the *Kohn-Sham orbitals* and allow to calculate the electron density from expression 2.134. The procedure to obtain the spin orbital wave functions is similar to the used in HF, where a starting set of molecular orbitals is used to begin the iteration process through the different equations exposed lately and repeated until the convergence is reached. Note that the only unknown term is the $\nu_{XC}(\vec{r})$ at the $\nu_{eff}(\vec{r})$. The electronic density will be closer to the real one as long as the exchange-correlation potential gets closer to the real one. The DFT has the property of including the whole XC energy, compared to HF that cannot. Apart from the different approximation at the beginning, both DFT and HF are similar. The fundamental differences are that DFT uses an approximate Hamiltonian to obtain a good approximation of the exact electronic density, while HF is the reverse: it uses an exact Hamiltonian but an Slater determinant as wave function, which is always an approximate solution. Using the Kohn-Sham orbitals to construct the Slater determinant and calculate its energy using the exact Hamiltonian, the energy obtained is higher than that obtained using HF.[13]

2.6 Bloch theorem [138, 212, 232]

The study of *condensed matter* is a subject field of physics focusing on the microscopic and macroscopic properties of matter. Condensed phases appear when the number of constituents in a system is extremely large and the interactions between them are strong. The typical examples are solids and liquids, but there are other less known examples like superfluids. Interactions take place between close and far apart molecules or atoms at different degrees of importance, but in some cases the weaker interactions can modify drastically the behaviour of the system. The background idea is that all the atom distribution and properties usually add up to create the global properties of the condensed phase. A branch of the condensed matter physics, the largest one, is the study of solid-state matter: atoms packed tightly under strong interaction forces responsible of the properties of the solid. Depending on the material involved and the conditions in which it was formed, the atoms may be arranged in a regular, geometric pattern (crystalline solids, which include metals and ordinary water ice) or irregularly (an amorphous solid such as common window glass). Most of the investigations done in this field are made on crystals, as its space regularity due to atom periodicity is an advantage which can be used to simplify mathematical modelling or for engineering purpouses.

Nowadays the application of *ab initio* methods makes possible to calculate PESs and other properties of at most medium-sized molecules, due to the restrictions from computer capacities. Although improvements have been made in the applied quantum theory methodology, molecules composed by more than 50 atoms take a long time to compute using the simplest approximation. Of course, the bottleneck is not only the hardware but the building up complexity as the system increases its constituent atoms. Thus, when it comes to model big systems like those in condensed phase, the aforementioned theoretical chemistry metods are constrained by both complexity and hardware. Alternatives can be designed especifically for each system, coping with the different aspects to be focused on and avoiding an overcharge of atoms. For example, a crystal could be modeled with only a few atoms recreating the *Brillouin zone*—the primitive cell of a structure—or some repetitions of this zone, trying to approximate the model to the data obtained in that piece of solid. These models are called *finite* or *cluster* models. Problems arise when this system must be fine tuned like in catalysis or properties come out from small deficiencies in the crystal, and this approach cannot be used. Besides, the interruption of the sequence at the edges of the model could make up deformed geometries, different electron densities and other inaccuracies.

However, there is a method which uses the periodicity of the crystals to provide wave functions adapted to the symmetry, like that of the molecular orbitals. Bloch constructed the wave function of a particle placed in a periodic crystal using a plane wave $e^{i\vec{k}\vec{r}}$ and a periodic Bloch function $u(\vec{r})$ which has the same periodicity as the potential affecting the particle.[32] The concept is that as the crystal is a periodic structure, the observables of a zone wave function will be the same if a translation operator is applied to this wave function and moves it to the another period, like the limits of the Brillouin zone.

$$\psi^{\vec{k}}(\vec{r}) = u(\vec{r})\, e^{i\vec{k}\vec{r}} \tag{2.150}$$

where $\psi^{\vec{k}}(\vec{r})$ is named *Bloch function*. Bloch used previous work made by Floquet regarding periodic functions in his work. Floquet theorem is referred to ordinary differential equations and basically states that any function $\phi(t)$ which is solution to a periodic system with a period T will be solution again after the period: $\phi(t) = \phi(t+T)$. Translating these concepts into operators and wave functions of the theoretical chemistry, applying a translation operator $\hat{T}$ on a periodic wave function will obtain the same wave function moved a vector $\vec{T}$. At the same time, the translation operator, which can be made of any vector set but they must be eigenvalues of the wave function to be applied to it, holds its own solutions:

$$\hat{T}\psi(\vec{r}) = \psi\left(\vec{r}+\vec{T}\right) = \lambda\left(\vec{T}\right)\psi(\vec{r}) \tag{2.151}$$

In order to this condition to hold true, the electronic density $|\psi|^2$ must be periodic and so $|\psi(\vec{r})|^2 = |\psi\left(\vec{r}+\vec{T}\right)|^2$ and $|\lambda\left(\vec{T}\right)|^2 = 1$. The eigenvalue of the Bloch function must have a quadratic value of one, further on this section a solution is proposed.

On the other hand, a translation operator can be applied as well on the Schrödinger wave equation, with which it can commute as the Hamiltonian doesn't change its form after the translation:

$$\hat{T}\hat{H}\psi(\vec{r}) = \hat{H}\psi\left(\vec{r}+\vec{T}\right) = \hat{H}\hat{T}\psi(\vec{r}) \tag{2.152}$$

For the same reason, two different translation operators $\hat{T}$ and $\hat{T}'$ can commute $\hat{T}\hat{T}' = \hat{T}'\hat{T}$. Commuting makes it possible to choose the eigenvectors of the Hamiltonian and the translation operator separately

$$\hat{H}\psi(\vec{r}) = E\psi(\vec{r}) \qquad \text{and} \qquad \hat{T}\psi(\vec{r}) = \lambda\left(\vec{T}\right)\psi(\vec{r}) \tag{2.153}$$

and hence their transaltion operator eigenvalues are the first translation times the other one as they cover all the space in which they have moved

$$\lambda\left(\vec{T}+\vec{T}'\right)=\lambda\left(\vec{T}\right)\lambda\left(\vec{T}'\right) \tag{2.154}$$

The translation vector $\vec{T}$ can be written as the summatory of all the space basis vectors $\vec{k}$ times an integer n

$$\vec{T}=\sum_{j=1}^{3}n_j\vec{k}_j \tag{2.155}$$

which is known as the *Born-von Karman boundary condition*. The basis set vectors $\vec{k}$ are those of the reciprocal lattice of the Bravais lattice which comply for all the lattice point vectors $\vec{R}$ that $e^{i\vec{k}\vec{R}}=1$. Of course, $\vec{k}$ could be any vector and thus there will be infinite sets of vectors, but it suffices to consider those of the Brillouin cell to produce a non-redundant translation, although they are infinite as well. The translation eigenvalues $\lambda\left(\vec{T}\right)$ are then defined as a product of its basis vectors egienvalues exponentiated to the integer n

$$\lambda\left(\vec{T}\right)=\prod_{j=1}^{3}\lambda\left(\vec{k}_j\right)^{n_j}=e^{i\sum_{j=1}^{3}n_j\vec{k}_j}=e^{i\vec{k}\vec{T}} \tag{2.156}$$

and indeed $|\lambda\left(\vec{T}\right)|^2=|e^{i\vec{k}\vec{T}}|^2=1$, observing the condition aforementioned. Then equation 2.151 can we rewritten as

$$\psi^{\vec{k}}\left(\vec{r}+\vec{T}\right)=e^{i\vec{k}\vec{T}}\psi^{\vec{k}}\left(\vec{r}\right) \tag{2.157}$$

This means that any bloch function $\psi^{\vec{k}}\left(\vec{r}+\vec{T}\right)$ that is a solution to the Schrödinger equation of the problem, differs only by a phase factor of $e^{i\vec{k}\vec{T}}$ between its equivalent positions in the lattice. This implies immediately that the probability of finding an electron is the same at any equivalent position.

Still, a periodic system is an infinite repetitive lattice, and although the wave function is the same, modelling the system involves its infinite repetition, leading in an infinite calculation time. The solution is considering the system as a cyclic system, and any translation vector $\vec{T}_N$ leads to the origin point,

defining it as

$$\vec{T}_N = 2\pi \sum_{j=1}^{3} N_j \vec{k}_j \tag{2.158}$$

which compared to 2.155 should comply that

$$\vec{k}_j = \frac{n_j}{N_j}; \qquad n_j = 0, 1, 2, 3, \ldots, N_j \tag{2.159}$$

and all the $\vec{k}$ vectors in the Brillouin zone are not infinite anymore, their number is equal to the number of crystal cells. In this way, the index has become discrete although the number of cells under consideration should be big to mantain the cyclic conditions true. Equation 2.157 will be newly rewritten to

$$\psi^{\vec{k}}\left(\vec{r} + \vec{T}_N\right) = e^{i\vec{k}\vec{T}_N}\psi^{\vec{k}}\left(\vec{r}\right) \tag{2.160}$$

and as the translation must return to the starting point making $\psi^{\vec{k}}\left(\vec{r} + \vec{T}_N\right) = \psi^{\vec{k}}\left(\vec{r}\right)$, the plane wave $e^{i\vec{k}\vec{T}_N}$ must be 1.

The orbitals used in Bloch waves are linear combinations of Bloch basis sets constructed from localized functions $\phi_\mu^{\vec{k}_{BZ}}\left(\vec{r}\right)$ or plane waves

$$\psi_n^{\vec{k}}\left(\vec{r}\right) = \sum_\mu c_{\mu n}^{\vec{k}_{BZ}} \phi_\mu^{\vec{k}_{BZ}}\left(\vec{r}\right) \tag{2.161}$$

where the n subindices are referred to the different bands whose PES falls into the Brillouin zone. The coefficients $c_{\mu n}^{\vec{k}_{BZ}}$ are determined by solving the equations from the variation principle

$$\mathbf{H}^{\vec{k}_{BZ}}\mathbf{C}^{\vec{k}_{BZ}} = \mathbf{S}^{\vec{k}_{BZ}}\mathbf{C}^{\vec{k}_{BZ}}\varepsilon^{\vec{k}_{BZ}} \tag{2.162}$$

$$\mathbf{C}^{\vec{k}_{BZ}*}\mathbf{S}^{\vec{k}_{BZ}}\mathbf{C}^{\vec{k}_{BZ}} = \mathbf{I} \tag{2.163}$$

in this case assuming a one-electron Hamiltonian.

The translation vector $\vec{k}$ can no longer be taken as a direct representation of momentum $\vec{p}$ of the Bloch wave function as in $\vec{p} = \frac{h}{2\pi}\vec{k}$ or its wavelength $\lambda = \frac{h}{\vec{k}}$. The electronic momentum at the edges fo the Brilluin zone is zero, because velocity is zero, but $\vec{k}$ is not. Thus the momentum is no longer constant through the system. Besides, if a plane wave is used, there is no unique wavelength when chosen arbitrarily with another function, and choosing a good one

to keep the momentum is difficult. To solve this situation, a *crystal momentum* is defined as $\vec{P} = \frac{h}{2\pi}\vec{k}$ which is still a constant and is the combination of the electron and the crystal momenta. It is related to a particular Bloch wave function $\psi^{\vec{k}}(\vec{r})$. Only when the external potential is zero, the electron momentum is equal as the crystal momentum. Although the crystal momentum cannot be concieved as mass times velocity, is an approximation to the momentum and still holds some of its properties like its conservation.

Chapter 3

Counterpoise-corrected PES for dihydrogen-bonded systems

–"What're quantum mechanics?"
–"I don't know. People who repair quantums, I suppose."

— Terry Pratchett
Eric (1990)

3.1 Introduction

There are many studies of series of gas phase dihydrogen-bonded systems which can be found in literature (see for example [5, 115, 120, 123, 154, 155, 172, 176, 218, 221, 224] as the most recent studies). One of the MH molecules mostly used is LiH, where the hydrogen atom has clear hydride behaviour, holding

a charge about -0.8 au. This molecule can interact with a HX molecule, being X a halogen atom, forming a dihydrogen bond. When these dimers are taken into account to describe this kind of interaction, they are considered as a linear arrangement of monomers. One of the features found in the study of $MH\cdots HX$ (M = Li, Na and X = F, Cl, Br) was that this type of complexes are not minima in the gas phase. The calculated stationary points have an imaginary harmonic vibrational frequency, which was already observed previously by different authors.[154, 169, 176] The analysis of these stationary points, as well as those formed with NaH is one of the objectives of this section. In order to study the behaviour these dimers present in gas phase, they have been compared to $MH\cdots HCN$ and $MH\cdots HCCH$, which are known to have a minima with all real harmonic vibrational frequencies.[4, 5, 218] The other series of dihydrogen-bonded systems studied in this section are those with M = Be and B with the same halogens defined before.

An extra problem appears when $H\cdots H$ contacts between monomers are studied. When finite basis sets are used while describing dimer potential energy surfaces, the so-called basis set superposition error (BSSE) appears, as explained in section 2.3. Although these systems exhibit a weak interaction with an important amount of BSSE with finite basis sets, no studies have dealt, to our knowledge, with their BSSE-corrected potential energy surfaces. As it has been studied before, when BSSE is corrected along the whole surface, important changes in the potential energy surface appear and the uncorrected and corrected-PES may indeed be different, not only in the energy but also in the position of the minimum as well as its topology [231, 241]. In this section the counterpoise correction (CP) proposed by Boys and Bernardi [39] is used to correct the potential energy surface BSSE, geometry and frequencies. The study of the influence of CP correction in the position and topology of different minima is the central discussion of this work.

3.2 Methodology

For all complexes, geometry and harmonic vibrational frequencies calculations have been computed using the Hartree–Fock (HF) level, second-order Møller–Plesset perturbation theory (MP2) and the non-local hybrid three-parameter B3LYP density functional approach. The 6-31++G(d,p) basis set was chosen not only for having a smaller BSSE effect, but also because counterpoise-corrected values are in good agreement with those obtained with larger basis set such as 6-311++G(3df,2pd).[39] All calculations, non-CP-corrected

and CP-corrected potential energy surfaces, were performed with the Gaussian 98 package.[104]

3.3 Results and discussion

Tables 3.1 and 3.2 gather interaction energies, geometrical parameters and dihydrogen bond formation harmonic vibrational frequencies for LiH$\cdots$HX and NaH$\cdots$HX complexes, being X = F, Cl, Br, CN, CCH. Superindex CP is used to signal parameters calculated on their correspondent CP-corrected PES (in italic number). Frequency calculations are preformed to confirm the number of imaginary frequencies and the existence of this minimum in gas phase. The number of non-degenerated imaginary frequencies is collected in the last column of tables 3.1 and 3.2.

Different studies about these complexes, LiH$\cdots$HX, can be found, specially about LiH$\cdots$HF.[115, 123, 154, 169] Almost all these complexes, MH$\cdots$HX (M = Li, Na and X = F, Cl, Br), yield to $C_{\infty V}$ complex (linear arrangement of monomers) with two degenerated imaginary frequencies (they are counted as 1 imaginary frequency in tables 3.1 and 3.2). LiH$\cdots$HCl and LiH$\cdots$HBr present minimum stationary points with real frequencies in the non-CP-corrected potential energy surface. However, when CP correction is considered along the whole PES, these minima become stationary points with two degenerated imaginary frequencies. This change in the topology of the PES caused by the inclusion of CP correction along the PES is found as well in the next series of complexes with M = Be and B.

NaH$\cdots$HX complexes have similar behaviour: all the complexes present a linear arrangement of monomers with two degenerated imaginary frequencies. Non-CP-corrected PESs give a better description of the stationary point than LiH$\cdots$HX complexes non-CP-corrected PES, since the inclusion of CP correction along the whole PES does not change its topology (except for NaH$\cdots$HCl at HF level).

To get a better understanding of the stationary point found for these complexes, an intrinsic reaction coordinate (IRC) calculation has been carried out. These calculations have been performed for all complexes, which present imaginary frequencies in the non-corrected PES at each level of theory. Results show that the normal mode corresponding to the imaginary frequencies leads to a weakly bound complex MCl$\cdots$H$_2$, and a posterior dehydrogenation. This reaction can be represented as:

Scheme 3.1.

$$M\text{–}H \;+\; H\text{–}X \;\rightarrow\; [M\text{–}H \;\cdots\; H\text{–}X]^{\ddagger} \;\rightarrow\; M\text{–}X \;\cdots\; H_2 \;\rightarrow\; M\text{–}X \;+\; H_2$$

where [M–H $\cdots$ H–X]‡ are the dimers studied in this section. Figure 3.1 depicts the dehydrogenation IRC for LiH$\cdots$HF complex at B3LYP level of theory. It can be seen from this figure that the flatness of the TS region makes the characterization of the stationary point quite difficult, being the inclusion of CP correction necessary. Vibrational normal mode corresponding to the imaginary frequency is represented for TS complex. All complexes present similar potential energy surfaces with different energetic barriers. The results obtained for these systems are totally in agreement with previous studies made by different authors who noticed the dehydrogenation reaction for these complexes.[169, 224]

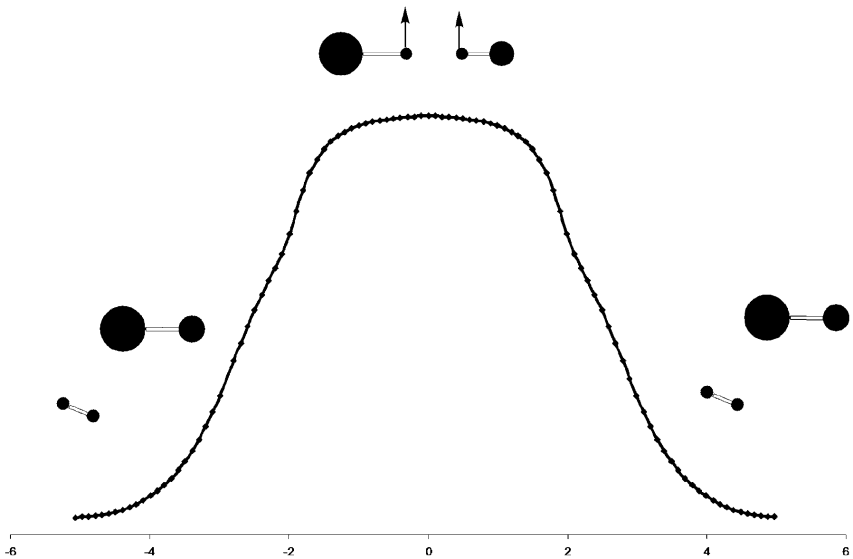

Figure 3.1: Intrinsic reaction path for the dehydrogenation of LiH$\cdots$HF at B3LYP level of theory. Abscissa corresponds to the reaction coordinate.

Significant differences can be found in the dihydrogen bond energies. As it is widely known, interaction energies are related to the intermolecular dis-

tances, i.e. dihydrogen bond distances, and this relation can be observed in tables 3.1 and 3.2. From this point of view MH···HX (X = F, Cl, Br) systems can be mainly separated in two groups depending on the interaction energy and H···H distance. This first geometrical analysis brings up an idea of two different bonding types between hydrogen atoms. Dihydrogen bond distances will decrease, generally, with the increase of the electronegativity of the halogen atom (Pauling values for electronegativities: F=3.98, Cl=3.16 and Br=2.96.), as it can be noticed from results in tables 3.1 and 3.2. For MH···HBr complexes, H···H bond is quite similar to H_2 bond length, which will be related to a more covalent description of this interaction. This fact will be analysed within the atoms in molecules theory in chapter 4 of this thesis. Similar trends were observed by Grabowski for a set of charged dihydrogen-bonded dimer.[120]

Intermolecular stretching frequencies corresponding to the dihydrogen bond formation are collected in tables 3.1 and 3.2 for LiH···HX and NaH···HX complexes, respectively. It can be observed that they follow the same trend as intermolecular distances do. The shorter the dihydrogen bond is, the higher value the dihydrogen bond formation frequency has, being the highest frequencies the ones corresponding to those complexes with dihydrogen bond distance nearer to H_2 bond length.

MH···HCN and MH···HCCH results are collected in tables 3.1 and 3.2 too. These four complexes have been chosen because they are known to have stable minima and they are widely studied. All results agree reasonably well with previous structures of McDowell et al. [176] where the isotope effect of Li···HCN and Li···HCCH was discussed. Li···HCCH and Li···HCN complexes are found to have a linear arrangement of monomers in the non-CP-corrected PES, while Na···HCN and Na···HCCH present a C_s symmetry, with torsion angles about 70–80 degrees. All stationary points present no imaginary frequencies, confirming they are minima in the PES. Although some variations can be observed when a different level of theory is used, they are not as important as they were in the previous complexes (X = F, Cl, Br). All these dimers can be classified as conventional hydrogen bonds as it was shown before in the framework of the atoms in molecules theory.[5] The fact that the electronegativity of X = CN, CCH) is very low compared to (X = F, Cl, Br), causes these complexes to be thermodynamically less stable, with weaker interaction energies, larger dihydrogen bond lengths and lower values of intermolecular formation of vibrational frequencies.

When CP-corrected potential energy surface is calculated it can be ob-

Table 3.1: $Li-H\cdots H-X$ (X = F, Cl, Br, CN, CCH) interaction energies (kcal/mol) and single-point CP-corrected interaction energy (kcal/mol), $Li-H$ bond distances (Å), dihydrogen bond distance (Å), intermolecular frequency corresponding to the formation of the dihydrogen bond (cm^{-1}) and number of imaginary frequencies.

		E_{int}	$E_{int}+CP$	r_{Li-H}	$r_{H\cdots H}$	ν	
		E_{int}^{CP}		r_{Li-H}^{CP}	$r_{H\cdots H}^{CP}$	ν^{CP}	♯
$LiH\cdots HF$	HF	-10.91	-10.79	1.618	1.599	223.8	1
		-10.79		*1.619*	*1.605*	*222.6*	*1*
	B3LYP	-14.72	-14.53	1.599	1.347	282.5	1
		-14.53		*1.603*	*1.353*	*281.8*	*1*
	MP2	-13.56	-12.85	1.605	1.383	260.2	1
		-12.87		*1.613*	*1.414*	*253.0*	*1*
$LiH\cdots HCl$	HF	-7.83	-7.41	1.624	1.686	172.9	0
		-7.42		*1.626*	*1.719*	*167.6*	*1*
	B3LYP	-12.89	-12.37	1.613	1.176	281.5	0
		-12.38		*1.618*	*1.196*	*246.8*	*1*
	MP2	-9.95	-8.82	1.617	1.419	190.6	1
		-8.88		*1.622*	*1.500*	*178.6*	*1*
$LiH\cdots HBr$	HF	-8.35	-6.46	1.620	1.653	151.8	0
		-6.50		*1.629*	*0.986*	*142.7*	*1*
	B3LYP	-15.69	-13.26	1.626	0.981	346.7	0
		-13.28		*1.640*	*0.959*	*347.9*	*1*
	MP2	-13.39	-10.00	1.629	0.935	342.4	0
		-10.05		*1.647*	*0.960*	*357.9*	*1*
$LiH\cdots HCN$	HF	-7.80	-7.54	1.624	1.966	164.3	0
		-7.54		*1.629*	*1.981*	*162.1*	*0*
	B3LYP	-8.63	-8.26	1.605	1.756	185.2	0
		-8.26		*1.613*	*1.771*	*182.8*	*0*
	MP2	-8.40	-7.66	1.616	1.841	176.3	0
		-7.64		*1.624*	*1.887*	*166.7*	*0*
$LiH\cdots HCCH$	HF	-3.38	-3.19	1.625	2.223	119.3	0
		-3.18		*1.629*	*2.251*	*118.3*	*0*
	B3LYP	-4.48	-4.16	1.607	1.980	141.3	0
		-4.16		*1.613*	*2.008*	*135.2*	*0*
	MP2	-4.17	-3.60	1.618	2.045	139.2	0
		-3.58		*1.630*	*2.112*	*126.0*	*0*

Note. Italic numbers correspond to the CP-corrected PES parameters.

Table 3.2: $Na-H\cdots H-X$ (X = F, Cl, Br, CN, CCH) interaction energies (kcal/mol) and single-point CP-corrected interaction energy (kcal/mol), $Na-H$ bond distances (Å), dihydrogen bond distance (Å), intermolecular frequency corresponding to the formation of the dihydrogen bond (cm^{-1}) and number of imaginary frequencies.

		E_{int} E_{int}^{CP}	$E_{int}+CP$	r_{Na-H} r_{Na-H}^{CP}	$r_{H\cdots H}$ $r_{H\cdots H}^{CP}$	ν ν^{CP}	♯
$NaH\cdots HF$	HF	-11.91	-11.81	1.911	1.582	159.2	1
		-11.81		*1.911*	*1.588*	*158.8*	*1*
	B3LYP	-15.21	-15.02	1.871	1.328	194.8	1
		-15.02		*1.876*	*1.335*	*195.7*	*1*
	MP2	-14.78	-14.08	1.901	1.349	185.4	1
		-14.10		*1.903*	*1.377*	*181.2*	*1*
$NaH\cdots HCl$	HF	-8.81	-8.35	1.919	1.611	115.1	0
		-8.36		*1.919*	*1.653*	*111.7*	*1*
	B3LYP	-15.20	-14.58	1.891	0.963	222.2	1
		-14.58		*1.899*	*0.977*	*225.5*	*1*
	MP2	-11.86	-10.06	1.920	0.992	229.0	1
		-10.33		*1.916*	*1.275*	*107.3*	*1*
$NaH\cdots HBr$	HF	-14.19	-11.90	1.921	0.805	151.1	1
		-11.91		*1.921*	*0.811*	*152.2*	*1*
	B3LYP	-19.84	-17.78	1.905	0.881	176.2	0
		-17.80		*1.920*	*0.889*	*178.5*	*0*
	MP2	-20.08	-17.18	1.931	0.832	166.9	1
		-17.19		*1.933*	*0.842*	*171.4*	*1*
$NaH\cdots HCN$	HF	-8.43	-8.27	1.923	1.964	113.8	0
		-8.27		*1.923*	*1.972*	*112.6*	*0*
	B3LYP	-8.70	-8.42	1.884	1.747	124.8	0
		-8.42		*1.888*	*1.767*	*127.4*	*0*
	MP2	-8.90	-8.28	1.916	1.836	121.2	0
		-8.27		*1.916*	*1.873*	*116.6*	*0*
$NaH\cdots HCCH$	HF	-3.55	-3.41	1.920	2.236	82.9	0
		-3.41		*1.921*	*2.259*	*81.2*	*0*
	B3LYP	-4.39	-4.14	1.882	1.977	96.4	0
		-4.14		*1.886*	*2.015*	*93.3*	*0*
	MP2	-4.33	-3.82	1.914	2.051	96.9	0
		-3.80		*1.915*	*2.114*	*89.9*	*0*

Note. Italic numbers correspond to the CP-corrected PES parameters.

served that LiH$\cdots$HX (X = F, Cl, Br) present doubly degenerated frequencies, so they were not real minima in gas phase. The nonphysical attraction produced by basis set superposition error can change the topology of the whole PES, leading to some wrong conclusion. When BSSE is corrected, complexes become less stable with larger optimized intermolecular distances and lower values of dihydrogen bond harmonic frequencies compared to CP-uncorrected optimized systems. NaH$\cdots$HX (X = F, Cl, Br) were found to have a doubly degenerated imaginary harmonic frequency when non-CP-corrected PES was calculated. If CP correction is included, no change in the topology is observed, being NaH$\cdots$HCl at HF level the only exception. MH$\cdots$HCN and MH$\cdots$HCCH complexes present a molecular symmetry change. LiH$\cdots$HCN and LiH$\cdots$HCCH change to an angular geometry, with an angle of torsion about 70 degree, while NaH$\cdots$HCN and NaH$\cdots$HCCH, which had C_s symmetry in non-CP-corrected PES, go in a linear arrangement of monomers when the CP-corrected PES is calculated.

Single-point-corrected energies do not differ very much from those obtained with the CP-corrected PES. Due to the nonphysical attraction that BSSE represents, intermolecular distances will increase with the inclusion of CP correction in the whole PES. The relative change due to the BSSE correction is linearly related to the percentage of CP correction.[240]. It can be observed that MP2 calculations present the largest amount of BSSE, in agreement with previous studies.[242]. Consequently, for all complexes studied, the MP2 CP-corrected potential energy surfaces are those which exhibit largest changes in the dihydrogen bond, M $-$ H distances and the intermolecular stretching frequencies. On the other hand, if different complexes are compared, MH$\cdots$HCCH, which are the weakest ones, are those with largest variation in the geometry and frequencies.

The other series studied are MH$\cdots$HX with M = HBe, H_2B and X = F, Cl, Br. Table 3.3 gathers the results for these complexes. Note that parameters with superindex CP are referred to CP-corrected PES. Furthermore, figure 3.2 shows their structural description. Frequency calculations display that they are actual minima on the CP-uncorrected and corrected PES. Results are in agreement with previous calculations by Grabowski,[115, 114] although in those calculations most of the complexes were restricted to be linear.

Single-point corrected interaction energies in the CP-uncorrected surface are very similar to those obtained in the CP-corrected PES, as it was seen in other studies.[240] The HBeH$\cdots$HBr complex presents the largest difference between energies at MP2 level, but it is mainly due to the change in the

linearity of the dihydrogen bond. This complex presents an angular arrangement in the uncorrected surface while it becomes linear when CP correction is considered in the whole PES.

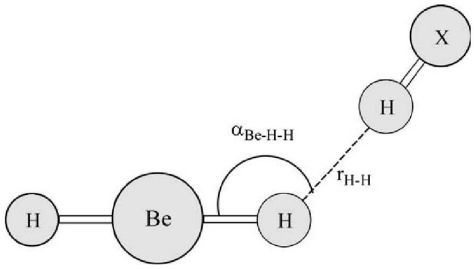

Figure 3.2: Geometrical parameters for HBeH $\cdots$ HX (X = F, Cl, Br).

The linear or angular arrangement of monomers for the different complexes does not change when CP-corrected PESs are considered, except for the HBeH $\cdots$ HBr complex at the MP2 level. Like earlier studies,[240, 242, 241] the most important changes when a CP-corrected PES is used lie in the intermolecular distances, hence the focus on dihydrogen bond distances. As expected, CP-corrected intermolecular distances are larger than CP-uncorrected PES distances. In a recent study of a series of hydrogen bonded systems,[240] it was already found a good linear relationship between the percentage of BSSE and the relative change in intermolecular distances. This relationship is also found for HBeH complexes with the three different proton donors at different levels of theory. HBeH $\cdots$ HF is the system which presents smaller BSSE, leading to less important changes in the intermolecular parameters than HBeH $\cdots$ HBr. For these complexes (HBeH $\cdots$ HBr), the CP correction is about 50% of the interaction energy, resulting in changes on the dihydrogen bond distances about 0.15 Å

The intermolecular stretching frequencies corresponding to the dihydrogen bond formation are collected in table 3.3. It can be observed that they follow the same trend as intermolecular distances do. This value is shifted to lower frequencies when they are calculated on the CP-corrected PES. The change in the frequency is also linearly dependent on the percentage of BSSE, being more important in the HBeH $\cdots$ HBr complex.

MP2 calculations present, in general, a very large amount of BSSE [242] and the results reported in this communication show it. For all three complexes

Table 3.3: $HBe-H\cdots H-X$ (X = F, Cl, Br) interaction energies (kcal/mol) and single point CP-corrected interaction energy (kcal/mol), dihydrogen bond distance (Å), angles (degrees) and intermolecular frequency corresponding to the formation of the dihydrogen bond (cm^{-1}).

		E_{int} E_{int}^{CP}	$E_{int}+CP$	$r_{H\cdots H}$ $r_{H\cdots H}^{CP}$	$\alpha_{Be-H\cdots H}$ $\alpha_{Be-H\cdots H}^{CP}$	ν ν^{CP}
$HBeH\cdots HF$	HF	-2.49	-2.38	1.904	180.0	118.2
		-2.38		*1.915*	*180.0*	*115.8*
	B3LYP	-4.02	-3.85	1.594	131.2	291.5
		-3.86		*1.605*	*130.4*	*292.8*
	MP2	-3.48	-2.92	1.694	130.4	260.5
		-2.98		*1.749*	*141.2*	*214.4*
$HBeH\cdots HCl$	HF	-1.49	-1.26	2.161	180.0	81.2
		-1.27		*2.241*	*180.0*	*73.0*
	B3LYP	-2.30	-2.01	1.786	180.0	117.5
		-2.02		*1.826*	*180.0*	*110.3*
	MP2	-2.13	-1.62	1.974	177.0	101.1
		-1.65		*2.073*	*180.0*	*87.3*
$HBeH\cdots HBr$	HF	-1.90	-0.95	2.174	180.0	79.0
		-1.01		*2.358*	*180.0*	*59.1*
	B3LYP	-2.78	-1.51	1.788	167.9	120.6
		-1.57		*1.908*	*165.8*	*104.5*
	MP2	-2.69	-1.38	1.963	156.7	126.8
		-1.50		*2.123*	*180.0*	*76.6*

Note. Italic numbers correspond to the CP-corrected PES parameters.

studied, the MP2 CP-corrected potential energy surfaces are those which exhibit largest changes, both in the dihydrogen bond distances and the intermolecular stretching frequencies.

The results for $H_2BH\cdots HX$ (X = F, Cl, Br) are collected in table 3.4. Figure 3.3 shows their structural parameters. For these systems, it was also checked that they are minima on the CP-uncorrected and the corrected PES, respectively. All minima exhibit an asymmetric bidentate structure, in agreement with previous calculations performed by Kulkarni.[154, 155].

Table 3.4: $H_2BH\cdots HX$ (X = F, Cl, Br) interaction energies (kcal/mol) and single point CP-corrected interaction energy (kcal/mol), dihydrogen bond distance (Å), angles (degrees) and intermolecular frequencies corresponding to the formation of both dihydrogen bonds (cm^{-1}).

		E_{int} E_{int}^{CP}	$E_{int}+CP$	$r_{H3\cdots H4}$ $r_{H3\cdots H4}^{CP}$	$r_{H2\cdots H4}$ $r_{H2\cdots H4}^{CP}$	$\alpha_{B-H3\cdots H4}$ $\alpha_{B-H3\cdots H4}^{CP}$	$\alpha_{B-H2\cdots H4}$ $\alpha_{B-H2\cdots H4}^{CP}$	ν_1 ν_1^{CP}	ν_2 ν_2^{CP}
$H_2BH\cdots HF$	HF	-0.86	-0.80	2.295	2.666	105.2	86.4	81.0	53.5
		-0.80		*2.335*	*2.644*	*103.6*	*88.0*	*75.0*	*45.8*
	B3LYP	-1.72	-1.58	1.886	2.443	105.6	78.3	151.0	91.9
		-1.58		*1.911*	*2.452*	*105.4*	*78.9*	*142.9*	*88.2*
	MP2	-1.47	-1.17	2.041	2.548	106.7	81.2	127.4	78.5
		-1.17		*2.152*	*2.532*	*103.8*	*84.5*	*96.7*	*66.4*
$H_2BH\cdots HCl$	HF	-0.48	-0.34	2.749	2.749	98.0	98.0	45.3	31.1
		-0.36		*2.824*	*2.879*	*97.4*	*100.4*	*39.3*	*5.4*
	B3LYP	-0.81	-0.60	2.163	2.746	110.7	81.0	99.9	49.3
		-0.61		*2.213*	*2.822*	*112.2*	*81.0*	*93.6*	*44.2*
	MP2	-1.13	-0.62	2.366	2.608	101.9	89.6	72.7	41.4
		-0.67		*2.620*	*2.620*	*96.9*	*96.9*	*57.2*	*9.6*
$H_2BH\cdots HBr$	HF	-1.07	0.14	3.157	4.172	134.3	77.2	28.0	63.6
		-0.77	-0.20	2.713	2.715	97.7	97.6	73.8	47.5
		-0.21		*3.005*	*3.005*	*100.0*	*100.0*	*29.7*	*17.8*
	B3LYP	-1.16	-0.28	2.345	2.416	95.8	92.3	68.8	81.6
		-0.64		*2.309*	*3.117*	*120.3*	*77.6*	*35.5*	*29.7*
	MP2	-1.67	0.02	2.584	3.562	129.8	75.7	127.6	52.7
		-0.40		*2.594*	*2.755*	*101.6*	*93.3*	*99.4*	*40.2*
		-0.51	0.5	2.436	2.437	95.0	95.0	72.9	94.4
		-0.67		*2.670*	*2.673*	*97.5*	*97.3*	*50.0*	*20.1*

Note. Italic numbers correspond to the CP-corrected PES parameters.

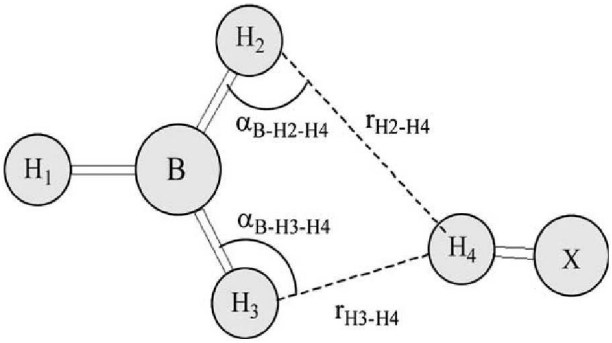

Figure 3.3: Geometrical parameters for $H_2BH\cdots HX$ (X = F, Cl, Br).

In general, like in the HBeH complexes, the single point corrected interaction energy calculated in the CP-uncorrected PES is very similar to the CP-corrected interaction energy. For the $H_2BH\cdots HCl$ complex, the largest difference is found at the MP2 level, where the arrangement of monomers changes from asymmetric to symmetric if geometry is optimized taking into account the CP correction. More important differences are observed in $H_2BH\cdots HBr$ complex, which presents very flat CP-uncorrected and corrected PES. At the HF level there are two different minima when the CP correction is not considered. The asymmetric arrangement of monomers turns out to yield an unphysical positive interaction energy after applying the CP correction, while the symmetric has a single-point CP-corrected interaction energy about -0.20 kcal/mol. When the CP-corrected PES is studied, only the symmetric arrangement of monomers is found, with little change in interaction energy, as expected. At the MP2 level two minima can be found again, one asymmetric and another symmetric. The order of stabilization varies depending on which PES is used, the CP-uncorrected or the corrected one. On the CP-uncorrected PES an asymmetric arrangement of monomers is the most stable system (being unphysically repulsive if single-point CP correction is added), while for the CP-corrected PES a symmetric arrangement becomes the most stable complex. As mentioned above, it is well known that the MP2 level of theory usually overestimates BSSE, hence leading to different kinds of wrong conclusions.

Intermolecular distances for H_2BH complexes are not so easy to compare as they were for HBeH. Not only there is a change in dihydrogen bond dis-

tances, but also different arrangements of monomers appear upon reoptimizing with CP. Most systems show an asymmetric bidentate dihydrogen bond at both CP-uncorrected and corrected PES. All these systems present also a symmetric stationary point with an imaginary frequency, thus not being a true minimum in the PES and not considered in table 3.4. Noteworthy, a linear relationship between the percentage of BSSE and the relative change in $H_3 \cdots H_4$ distance can be generally observed, being $H_3 \cdots H_4$ the shorter dihydrogen bond in the bidentate complex. However, there is no general behaviour for the $H_2 \cdots H_4$ distances. In some complexes it increases when a CP-corrected PES is considered while in others it decreases. This behaviour can be understood considering that the main contribution to the interaction energy arises from the shortest bond.

Two intermolecular stretching frequencies belonging to the formation of dihydrogen bonds are considered in table 3.4. In all cases their related frequencies decrease when CP correction is included in the PES. However, when the symmetry of the bidentate complex changes, these two frequencies are not directly comparable. Frequencies which correspond to the $H_3 \cdots H_4$ stretching show larger changes because the bond distances are those modified most when reoptimizing in the CP-corrected PES.

3.4 Conclusions

The inclusion of the CP correction along the whole PES clarifies the topological characterization of dihydrogen-bonded complexes $MH \cdots HX$ (M = Li, Na and X = F, Cl, Br). In these complexes the BSSE correction has lead to new PES where they are not minima but have imaginary vibrational harmonic frequencies, except $NaH \cdots HBr$ at B3LYP or the ones that yet have them in the non-corrected PES. Almost all complexes present two degenerated imaginary frequencies resulting in transition states systems, which give a posterior dehydrogenation.

On the other hand, dihydrogen-bonded complexes $HBeH \cdots HX$ and $H_2BH \cdots HX$ (X = F, Cl, Br) on the CP-corrected PES do not differ so drastically from the uncorrected PES, as all minima detected on the corrected PES are similar to those on the CP-corrected one. Nevertheless, the interaction lengths and energies changes are important enough to consider the BSSE correction.

The results of calculations presented in this communication show the importance of considering the CP correction over all the whole PES of dihydrogen-bonded systems. Not only changes in the interaction energy are found, but also the arrangement of monomers is modified noticeably. Thus, it is shown that the study of weekly bonded system must be performed on the BSSE-corrected PES.

Chapter 4

Atoms in molecules analysis of dihydrogen bonds

Any sufficiently advanced technology is indistinguishable from magic.

— Arthur C. Clarke
British science fiction writer and inventor
(1917–2008)

4.1 Introduction

Hydrogen bonds (and intermolecular interactions in general) can be classified using energetic or geometrical criteria. For instance, topological characterization of the electron density $\rho(\vec{r})$ in the intermolecular regions allows for an accurate analysis based on quantitative interpretation of the electron density

distribution, its Laplacian, and its principal curvatures at the bond critical points (BCP). Nowadays, such a topological analysis is one of the most useful tools to characterize atomic and molecular interactions; thus, many studies of hydrogen bonding from the point of view of the Atoms in molecules theory (AIM)[11] can be found in the literature. In particular, Koch and Popelier have proposed a set of topological criteria that a bond must fulfill in order to be considered as a hydrogen bond; such criteria were applied to classify the dihydrogen bond interaction.[150, 216]

Among all topological properties used to analyze the electron density, energetic properties of the electron density distribution at the bond critical point ($G(r_{BCP})$ and $V(r_{BCP})$) are quite useful to assess the character of the bond. For instance, Espinosa et al. have discussed the relationship between the principal curvatures of $\rho(\vec{r})$ at the BCP and the energetic properties of $\rho(r_{BCP})$, $G(r_{BCP})$, and $V(r_{BCP})$, thus leading to a new representation of the topological characteristics of electron density in terms of those properties of $\rho(\vec{r})$ and vice versa.[85, 86, 87] Furthermore, the same authors have tried to classify hydrogen bonds using topological and energetic properties of intermolecular BCP derived from experimental electron densities.[88] In another study, Grabowski has used the AIM theory as a measure of hydrogen-bonding strength in conventional and unconventional hydrogen bonds.[119, 116, 117, 118] Moreover, the *electron localization function* (ELF)* has been used to established topological criteria to distinguish between weak, medium, and strong hydrogen bonds.[106, 107]

During the last years, very strong hydrogen-bonded systems have deserved increased attention. One can find in the literature different studies of the covalent contribution to this very short hydrogen bond. Espinosa et al. studied the $X-H\cdots F-Y$ interaction by performing a comprehensive analysis of the intermolecular topology and energetic properties of $\rho(\vec{r})$ from weak to strong hydrogen bonds.[84] Their conclusions were supported by Gálvez et al., who analyzed different intermolecular interactions.[108] Espinosa et al. classified weak and strong hydrogen bonds from pure closed-shell interactions (weak interaction) to pure shared-shell interaction (very strong HB), including various levels of contributions of covalent character. Pacios claimed that topological indices cannot be used to identify equilibrium structures, because their change with intermolecular distances does not show special trends.[193] Concerning dihydrogen-bonded systems, some theoretical and experimental studies

*ELF is a measure of the likelihood of finding an electron in the same neighborhood of space as a reference electron located at a given point and with the same spin.

have recently appeared, where very short H···H distances have been reported, mainly related to a dehydrogenation reaction, including results in the previous section 3.3 of this thesis.[5, 121, 145, 166, 179] Grabowski et al. studied, in the framework of AIM theory and energy decomposition analysis, how short the dihydrogen intermolecular distance contact may be, concluding that very short H···H intermolecular distances are partly covalent.[122, 121]

Very recently, $CH^{\delta+}\cdots\ ^{\delta+}HC$, CH···O, and CH···C weak interactions in three organic crystals have been compared by analyzing experimental densities at the H···H and hydrogen bond critical points.[272] This study stresses also the importance of the assessment of the bond type to understand the conformation of molecules in their crystalline state and their stability.

Indeed, dihydrogen bonds and hydrogen bonds share a common trend; however, dihydrogen bonds are very particular because a bond is formed between two very particular atoms: hydrogens. This special bond has received the focus of earlier studies, especially on the relationship between topological parameters and energetic properties of $\rho(r_{BCP})$; furthermore, their studies have not assessed clearly enough the different trends shown between dihydrogen-bonded systems and other hydrogen-bonded complexes when geometric parameters are considered. Moreover, the Wolstenholme's above-mentioned study[272] on the relationship between H···H electron density at the bond critical point and hydrogen bond length is limited to a few, particular, organic interactions.

In this chapter some general studies of dihydrogen-bonded systems M−H···H−X (M = Li, Na and X = F, Cl, Br) are analyzed using the AIM theory and afterwards they will be complemented on differences between hydrogen- and dihydrogen-bonded systems, focusing especially on the dependence of density parameters with geometries, while dealing with complexes ranging from weak to very strong. For this purpose, the intermolecular electron density, its Laplacian, and also its components at the bond critical point (and optimized equilibrium geometry) will be analyzed. This analysis will be performed first as a function of the hydrogen/dihydrogen equilibrium bond length and later as a function of the interaction energy as a measure of intermolecular strength in order to assess which parameters are the most suitable to separate HB and DHB interactions.

4.2 Methodology

For all monomers and dimers considered in this study, molecular geometries were optimized at the nonlocal three-parameter hybrid B3LYP and at the MP2 levels of theory.[22, 156] MP2 is one of the most economical post-Hartree-Fock methods that account for the full range of intermolecular interactions: electrostatic, induction, and dispersion effects. Even though the B3LYP approach does not account for dispersion interactions, several studies have shown a reasonably good performance of DFT methods.[240] In order to check DFT results, a comparison of both methods will be discussed in the next section. MP2 calculations were performed correlating all the electrons except the inner shells.

The 6-31++G(d,p) basis set was chosen for being one of the most popular basis sets used in the study of medium- and large-sized hydrogen-bonded systems as well as for yielding a very small BSSE with countepoise-corrected values comparable to those of the larger 6-311++G(3df,2pd) basis set.[230] The countepoise correction (CP) proposed by Boys and Bernardi has been calculated to the dimerization and interaction energies in order to compare MP2 and B3LYP energetic data.[39] Vibrational analyses of optimized systems show that their structures are always a minimum on the potential energy surface, except for $XH\cdots HM$ (M = Li, Na) as seen in chapter 3. The latter systems exhibit a double degenerate imaginary frequency which corresponds to the formation of H_2. All calculations were carried out with the Gaussian 03 package.[105]

Bond critical points were characterized using the AIM2000 program based on Bader's Atoms in Molecules Theory.[11, 30] The electron density and its Laplacian were obtained for each intermolecular interaction, as well as the kinetic and potential energy densities ($G(r_{BCP})$ and $V(r_{BCP})$) evaluated at the BCP.

4.3 Results and discussion

This section is split into three parts. The discussion starts with the AIM results and natural charges of linear $M-H\cdots H-X$ dihydrogen bonds with M = Li, Na and X = F, Cl, Br. This first approach is intended to obtain a better understanding of the electronic density of DHBs using different indeces. It will follow a comparison of these properties with those of various hydrogen-bonded

systems, looking for the behavior of topological and energetic properties as an intermolecular distance function. Finally, in order to compare the DHB bond strength, the dimerization energies will be plotted with some of the electronic density indeces to find possible correlations. In figure 4.1 the structure of all different dimers studied in this section and how they are bonded is depicted. In all cases, hydrogen halides ($H-X$, where X = F, Cl, Br) were used as proton donor, while seven different atoms or groups were chosen as proton acceptors. As pointed out before, when the proton acceptor is a hydrogen atom, the interaction is defined as a dihydrogen bond.

Tables 4.1 and 4.2 collect all the energetic, geometric and topological data of the various complexes considered in the present study at the B3LYP and MP2 levels of theory, respectively. Interaction energies (E_{int}, in kcal/mol) correspond to the dimer formation taking into account the nuclear relaxation of each monomer (i.e. to D_e, the difference between the absolute energy of the minimum and separate, optimized monomers) while the dimerization energy (E_{dim}, kcal/mol) does not take into account the nuclear relaxation (i.e. it is the difference in energy between the absolute energy of the minimum and the energies of the monomers with the geometry they have at the dimer minimum). Both energies are single-point-corrected for BSSE using the CP correction ($E_{int} + CP$, and $E_{dim} + CP$). $r_{H\cdots B}$ stands for the intermolecular distance, whereas $\rho(r_{BCP})$ and $\nabla^2\rho(r_{BCP})$ are the electron densities and their Laplacians at the bond critical point. Two of the main three curvatures at the bond critical point are collected as λ_1 and λ_3, the latter being parallel to the bond. Kinetic ($G(r_{BCP})$) and potential energy ($V(r_{BCP})$) densities at the BCP are also reported.

4.3.1 Linear $MH\cdots HX$ with M = Li, Na and X = F, Cl, Br study based on AIM and natural charges.

In chapter 3 of this thesis it was found, from a geometrical point of view, that $MH\cdots HX$ (M = Li, Na and X = F, Cl, Br) complexes can be classified in two different sets. In order to have a deeper insight in these interactions these dihydrogen bond systems are going to be analysed from an electron density point of view, within the atoms in molecules (AIM) formalism. Table 4.3 resumes data from tables 4.1 and 4.2 for the aforementioned complexes and extends it to natural charges. Bond critical point and its topological properties are calculated in the non-corrected potential energy surface. Natural charges for both hydrogen atoms in the complex are collected too. Last columns in

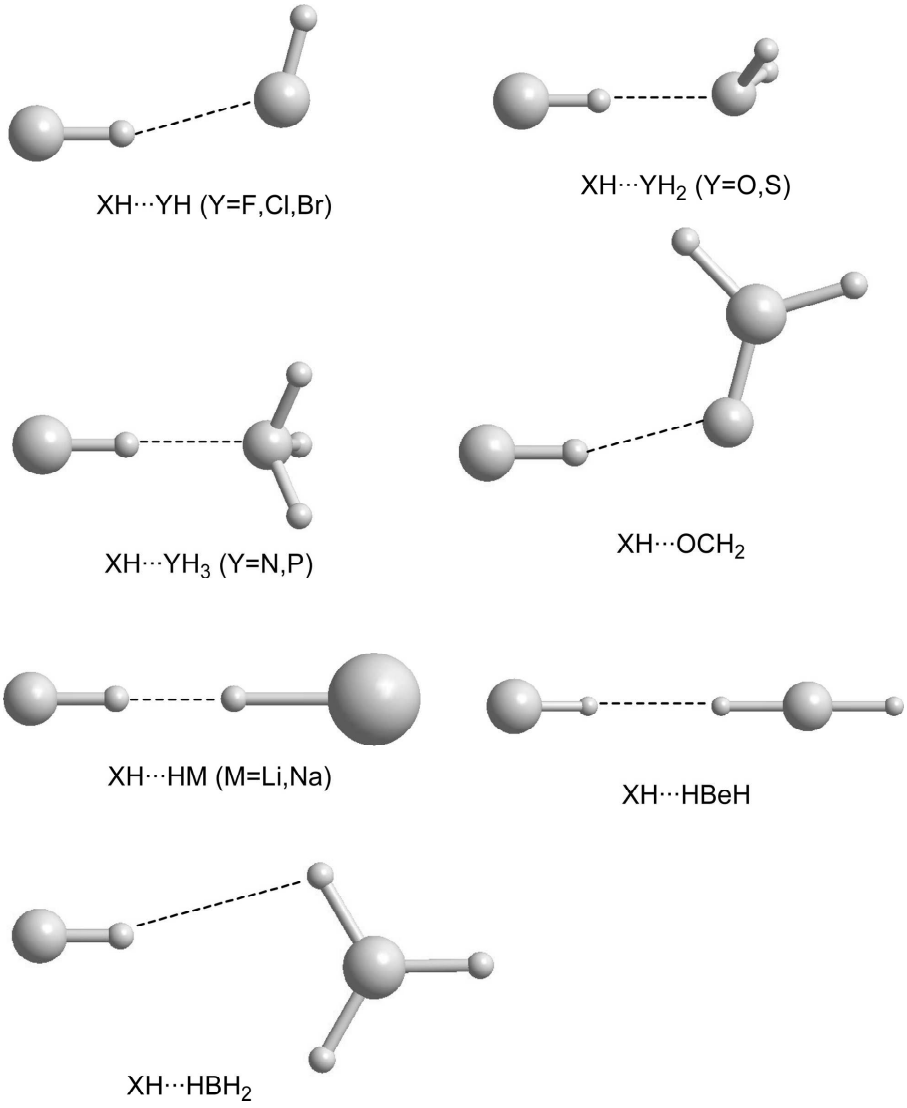

Figure 4.1: Molecular structure of the dimers. Geometrical parameters can be found in references [6, 115, 114, 154, 155, 172, 214, 218, 221, 240], in chapter 3 and in table B.1 in appendix B.

Table 4.1: B3LYP/6-31++G(d,p) CP-corrected interaction and CP-corrected dimerization energies (kcal/mol), intermolecular distances (Å), electron density topological properties at the bond critical point r_{BCP} (e·Å^{-3} and e·Å^{-5}), along with kinetic (G) and potential (V) energy density properties (a.u.).

	$E_{int}+CP$	$E_{dim}+CP$	$r_{H\cdots B}$	$\rho(r_{BCP})$	$\nabla^2\rho(r_{BCP})$	λ_1	λ_3	$G(r_{BCP})$	$V(r_{BCP})$
NH_3-HF	-14.02	-15.18	1.644	0.059	0.114	-0.111	0.335	0.0372	-0.0460
NH_3-HCl	-9.66	-11.27	1.683	0.058	0.102	-0.101	0.303	0.0317	-0.0381
NH_3-HBr	-8.40	-12.26	1.543	0.083	0.073	-0.174	0.420	0.0425	-0.0667
H_2O-HF	-9.37	-9.69	1.673	0.044	0.139	-0.076	0.288	0.0335	-0.0322
H_2CO-HF	-8.25	-8.59	1.699	0.042	0.130	-0.071	0.271	0.0313	-0.0302
H_2O-HCl	-5.78	-5.96	1.840	0.033	0.088	-0.046	0.178	0.0219	-0.0218
H_2O-HBr	-4.73	-4.87	1.895	0.030	0.077	-0.041	0.156	0.0198	-0.0204
PH_3-HF	-5.48	-5.88	2.304	0.024	0.037	-0.027	0.091	0.0106	-0.0121
H_2S-HF	-5.46	-5.62	2.250	0.025	0.046	-0.029	0.104	0.0124	-0.0133
$H_2CO-HCl$	-4.92	-5.12	1.875	0.031	0.079	-0.043	0.164	0.0201	-0.0206
$H_2CO-HBr$	-4.64	-4.09	1.926	0.029	0.071	-0.040	0.150	0.0188	-0.0199
$HF-HF$	-4.38	-4.80	1.808	0.026	0.093	-0.040	0.170	0.0225	-0.0217
$HBr-HF$	-2.70	-2.73	2.447	0.016	0.038	-0.017	0.071	0.0088	-0.0082
PH_3-HCl	-3.24	-3.48	2.476	0.019	0.031	-0.019	0.070	0.0087	-0.0095
H_2S-HCl	-3.21	-3.33	2.420	0.020	0.037	-0.021	0.079	0.0098	-0.0103
$HBr-HCl$	-1.33	-1.35	2.593	0.014	0.033	-0.014	0.059	0.0076	-0.0070
$HBr-HBr$	-0.94	-0.95	2.648	0.013	0.032	-0.012	0.055	0.0071	-0.0062
H_2S-HBr	-2.55	-2.64	2.478	0.018	0.037	-0.018	0.074	0.0093	-0.0093
PH_3-HBr	-2.50	-2.70	2.511	0.018	0.033	-0.018	0.069	0.0086	-0.0090
$HF-HCl$	-2.73	-2.74	2.024	0.018	0.054	-0.024	0.100	0.0144	-0.0153
$HCl-HF$	-2.71	-2.74	2.348	0.016	0.044	-0.018	0.079	0.0100	-0.0090
$HF-HBr$	-2.16	-2.16	2.115	0.015	0.048	-0.019	0.085	0.0124	-0.0127
$HCl-HCl$	-1.44	-1.44	2.583	0.011	0.032	-0.011	0.054	0.0070	-0.0060
$HCl-HBr$	-1.06	-1.06	2.664	0.010	0.030	-0.009	0.048	0.0062	-0.0049
$NaH-HBr$	-17.78	-43.69	0.881	0.174	-0.488	-0.520	0.551	0.0206	-0.1634
$LiH-HBr$	-13.26	-27.02	0.982	0.130	-0.208	-0.339	0.470	0.0252	-0.1023
$NaH-HF$	-15.02	-16.57	1.328	0.051	0.025	-0.088	0.201	0.0192	-0.0321
$NaH-HCl$	-14.58	-32.91	0.963	0.138	-0.251	-0.365	0.479	0.0244	-0.1115
$LiH-HF$	-14.53	-15.75	1.347	0.047	0.033	-0.080	0.193	0.0188	-0.0294
$LiH-HCl$	-12.37	-17.45	1.176	0.078	-0.022	-0.157	0.291	0.0224	-0.0502
$HBeH-HF$	-3.85	-3.95	1.594	0.024	0.048	-0.034	0.114	0.0127	-0.0133
$HBeH-HBr$	-1.51	-1.54	1.788	0.017	0.037	-0.021	0.078	0.0093	-0.0095
$HBeH-HCl$	-2.01	-2.05	1.786	0.017	0.035	-0.020	0.075	0.0089	-0.0092
H_2BH-HF	-1.58	-1.63	1.886	0.013	0.037	-0.015	0.064	0.0080	-0.0067
$H_2BH-HBr$	-0.28	-0.28	2.354	0.007	0.024	-0.007	0.033	0.0047	-0.0035
$H_2BH-HCl$	-0.60	-0.62	2.160	0.008	0.025	-0.008	0.040	0.0051	-0.0038

Table 4.2: MP2/6-31++G(d,p) CP-corrected interaction and CP-corrected dimerization energies (kcal/mol), intermolecular distances (Å), electron density topological properties at the bond critical point r_{BCP} (e·Å^{-3} and e·Å^{-5}), along with kinetic (G) and potential (V) energy density properties (a.u.).

	$E_{int}+CP$	$E_{dim}+CP$	$r_{H\cdots B}$	$\rho(r_{BCP})$	$\nabla^2\rho(r_{BCP})$	λ_1	λ_3	$G(r_{BCP})$	$V(r_{BCP})$
NH_3-HF	-12.05	-12.92	1.673	0.050	0.131	-0.091	0.313	0.037	-0.041
NH_3-HCl	-7.18	-7.79	1.817	0.040	0.098	-0.058	0.213	0.025	-0.025
NH_3-HBr	-6.60	-7.91	1.717	0.051	0.106	-0.085	0.276	0.031	-0.035
H_2O-HF	-8.22	-8.43	1.716	0.035	0.141	-0.057	0.252	0.031	-0.027
H_2CO-HF	-7.23	-7.48	1.743	0.034	0.133	-0.054	0.240	0.030	-0.026
H_2O-HCl	-4.91	-5.00	1.903	0.026	0.079	-0.034	0.146	0.020	-0.019
H_2O-HBr	-4.49	-4.56	1.951	0.024	0.072	-0.031	0.131	0.018	-0.018
PH_3-HF	-4.44	-4.67	2.346	0.021	0.042	-0.022	0.085	0.010	-0.010
H_2S-HF	-4.06	-4.14	2.298	0.020	0.049	-0.022	0.093	0.011	-0.011
$H_2CO-HCl$	-4.25	-4.36	1.936	0.026	0.074	-0.033	0.139	0.019	-0.019
$H_2CO-HBr$	-3.83	-3.95	1.974	0.025	0.070	-0.032	0.132	0.018	-0.019
$HF-HF$	-4.21	-4.23	1.858	0.020	0.090	-0.029	0.147	0.020	-0.018
$HBr-HF$	-2.14	-2.16	2.534	0.012	0.033	-0.012	0.056	0.007	-0.006
PH_3-HCl	-2.43	-2.51	2.586	0.015	0.029	-0.014	0.058	0.007	-0.008
H_2S-HCl	-2.19	-2.21	2.528	0.015	0.034	-0.015	0.062	0.008	-0.008
$HBr-HCl$	-0.99	-1.00	2.666	0.012	0.029	-0.011	0.050	0.007	-0.006
$HBr-HBr$	-1.08	-1.09	2.704	0.011	0.029	-0.010	0.048	0.007	-0.006
H_2S-HBr	-2.00	-2.02	2.559	0.014	0.035	-0.014	0.062	0.008	-0.008
PH_3-HBr	-2.18	-2.26	2.582	0.016	0.032	-0.015	0.061	0.008	-0.008
$HF-HCl$	-2.43	-2.43	2.065	0.016	0.052	-0.019	0.090	0.013	-0.014
$HCl-HF$	-2.01	-2.03	2.377	0.013	0.043	-0.014	0.071	0.009	-0.008
$HF-HBr$	-0.68	-0.70	2.143	0.013	0.048	-0.016	0.079	0.012	-0.012
$HCl-HCl$	-1.11	-1.11	2.603	0.010	0.031	-0.010	0.050	0.007	-0.006
$HCl-HBr$	-1.12	-1.13	2.648	0.010	0.030	-0.009	0.048	0.007	-0.005
$NaH-HBr$	-17.18	-54.65	0.832	0.198	-0.771	-0.631	0.491	0.015	-0.222
$LiH-HBr$	-10.01	-28.52	0.935	0.143	-0.339	-0.396	0.453	0.024	-0.133
$NaH-HF$	-14.08	-15.44	1.349	0.045	0.045	-0.074	0.192	0.020	-0.029
$NaH-HCl$	-10.07	-26.13	0.992	0.123	-0.219	-0.312	0.405	0.025	-0.105
$LiH-HF$	-12.85	-13.78	1.383	0.040	0.052	-0.063	0.177	0.019	-0.025
$LiH-HCl$	-8.83	-9.98	1.420	0.041	0.036	-0.061	0.158	0.016	-0.024
$HBeH-HF$	-2.93	-2.98	1.694	0.018	0.046	-0.022	0.088	0.010	-0.009
$HBeH-HBr$	-1.38	-1.39	1.963	0.008	0.030	-0.008	0.039	0.005	-0.004
$HBeH-HCl$	-1.63	-1.63	1.974	0.011	0.028	-0.011	0.050	0.006	-0.006
H_2BH-HF	-0.76	-0.80	2.041	0.007	0.023	-0.008	0.038	0.005	-0.004
$H_2BH-HBr$	0.03	0.02	2.584	0.006	0.021	-0.006	0.028	0.004	-0.003
$H_2BH-HCl$	-0.46	-0.47	2.138	0.007	0.021	-0.007	0.036	0.005	-0.004

tables 4.1 and 4.2 are referred to the charge transfer between monomers when the dimer is formed. Due to the fact that the tendencies presented by both LiH and NaH complexes is similar, the next discussion will be referred to both of them together.

Table 4.3: $M-H\cdots H-X$ (M = Li, Na and X = F, Cl, Br) dihydrogen bond critical point distance respected to the dihydrogen bond distance, density at the bond critical point (a.u.), Laplacian at the bond critical point (a.u.), natural charges of hydrogen Atoms (a.u.) and difference of monomer charges (a.u.).

	$r_{BCP}/r_{H\cdots H}$	$\rho(r_{BCP})$	$\nabla^2\rho(r_{BCP})$	q_{H1}	q_{H2}	$q_{H2}-q_{MH}$
			LiH − HF			
B3LYP	0.578	0.047	0.033	-0.793	0.558	0.097
MP2	0.597	0.040	0.052	-0.838	0.602	0.072
			LiH − HCl			
B3LYP	0.554	0.078	-0.022	-0.669	0.230	0.221
MP2	0.572	0.041	0.036	-0.804	0.302	0.097
			LiH − HBr			
B3LYP	0.548	0.130	-0.210	-0.533	0.145	0.355
MP2	0.574	0.140	-0.034	-0.547	0.201	0.386
			NaH − HF			
B3LYP	0.578	0.051	0.025	-0.736	0.544	0.117
MP2	0.599	0.046	0.045	-0.814	0.591	0.096
			NaH − HCl			
B3LYP	0.551	0.014	-0.250	-0.471	0.166	0.386
MP2	0.576	0.120	-0.022	-0.570	0.230	0.359
			NaH − HBr			
B3LYP	0.548	0.017	-0.490	-0.383	0.118	0.459
MP2	0.579	0.200	-0.770	-0.399	0.185	0.553

For all complexes, the relative position of bond critical points is similar. This position is defined from the hydride hydrogen atom, where a value of $r_{BCP}/r_{H\cdots H}$=0.6 means that the BCP is near to the protonic hydrogen. More

interesting is the analysis of the electron density as well as the laplacian at BCP. It can be rapidly observed that the shorter the dihydrogen bond is, a higher value in the electron density is found. As it was seen for the geometrical parameters, the H $\cdots$ H distances in LiH $\cdots$ HBr, NaH $\cdots$ HCl and NaH $\cdots$ HBr were deriving near to the molecular hydrogen distance. These two factors can be analysed as the covalent character becomes more dominant. A similar conclusion can be found when the Laplacian is analysed. Complexes with larger intermolecular distances present a positive laplacian about 0.03 a.u., which is one of the criteria that Popelier defined to characterize a hydrogen bond in the framework of AIM theory.[216] For the second group of complexes, those with shorter intermolecular bond length, a negative Laplacian is found, which describes shared interactions, i.e. covalent bonds. These results totally agree with optimized geometrical parameters, leading to the conclusion that these complexes describe the formation of a hydrogen molecule.

Natural charges can help us in the analysis of the covalent character that presents these complexes. Table 4.3 gathers the natural charges for both hydrogen atoms when they are part of the complex. MH $\cdots$ HF dimer present a very large charge for both hydrogen atoms leading to an electrostatic domination in the intermolecular energy. Last column in table 4.3 is referred to the charge transfer between monomer when the dimer is formed.

From these data, it can be observed that as intermolecular distances get smaller, there is an increase in the charge transfer between monomers. This fact totally agrees with the increment of the covalent character that present this set of complexes.

4.3.2 Dependence on optimized (equilibrium) intermolecular distances.

Figure 4.2 plots electron density values at the bond critical point $\rho(r_{BCP})$ vs. the hydrogen or dihydrogen optimized bond length $r_{H\cdots B}$ at B3LYP/6-31++G(d,p) (solid lines) and MP2/6-31++G(d,p) (dash lines). For both sets of systems (HB and DHB) and both levels of calculation, $\rho(r_{BCP})$ shows a typical exponential behavior with the intermolecular distance. No meaningful differences between the results in tables 4.1 and 4.2 are observed. In general, at the MP2 level the interaction between monomers exhibits lower $\rho(r_{BCP})$ than B3LYP calculations. Analysis of both set of complexes reveals clearly that DHB systems have smaller $\rho(r_{BCP})$ as compared to HB dimers. This general trend is found for all systems, ranging from the weakest to the strongest ones.

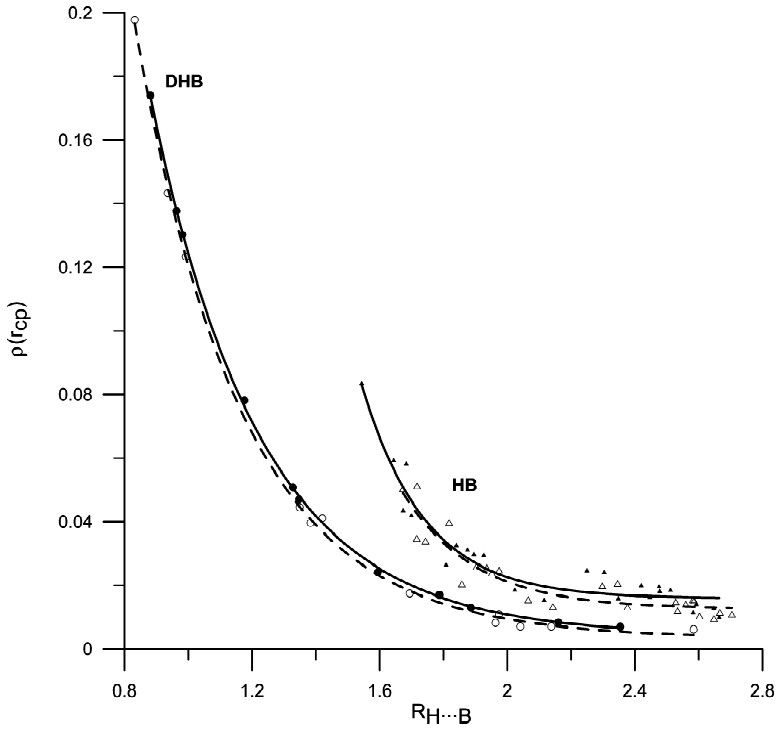

Figure 4.2: Electron density at the bond critical point ($e \cdot Å^{-3}$) versus intermolecular distance (Å). Solid circles and triangles are for B3LYP calculations (DHB and HB, respectively), the solid lines being their fitted curves. Empty circles and triangles are for MP2 calculations (DHB and HB, respectively), the dashed lines being their fitted curves.

Since all dihydrogen-bonded systems consist of the same proton acceptor (a hydrogen atom), the change of its $\rho(r_{BCP})$ with the intermolecular distance is much more homogeneous ($R^2 = 0.999$) than it is for hydrogen-bonded systems ($R^2 = 0.936$ and 0.870 for B3LYP and MP2, respectively), where different proton acceptors are considered.

Some authors have classified interaction energies by means of $\nabla^2\rho(r_{BCP})$.[11, 84] It is well-known that not only $\rho(r_{BCP})$ is interesting to be analyzed, but also the way that this electronic charge density is distributed around the intermolecular region. The sign of the Laplacian will determine if the electronic

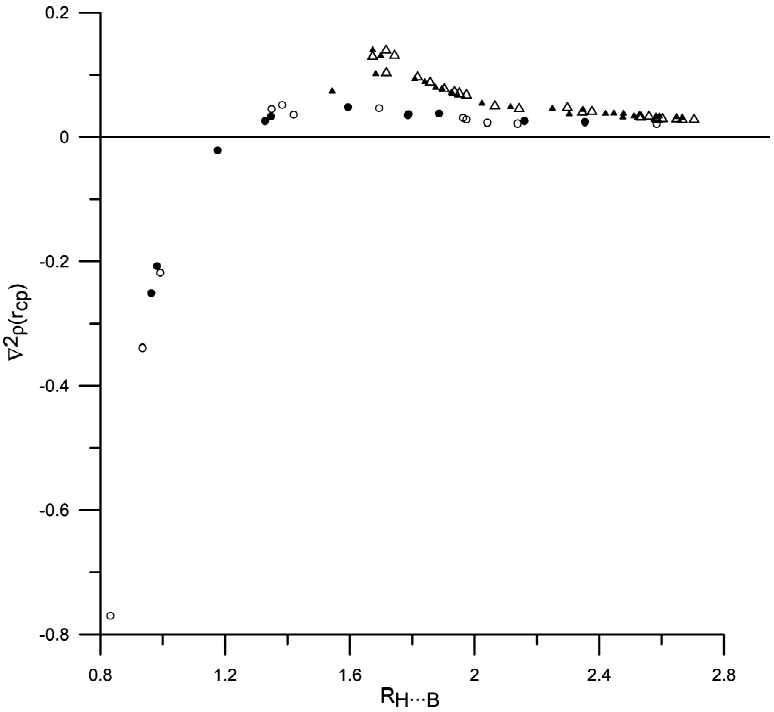

Figure 4.3: Laplacian of the electron density at the bond critical point ($e \cdot Å^{-5}$) versus intermolecular distance (Å). Solid circles and triangles are for B3LYP calculations (DHB and HB, respectively), while empty circles and triangles are for MP2 (DHB and HB, respectively).

charge is locally concentrated ($\nabla^2\rho(r_{BCP}) < 0$) or depleted ($\nabla^2\rho(r_{BCP}) > 0$). Figure 4.3 plots $\nabla^2\rho(r_{BCP})$ vs. equilibrium $r_{H\cdots B}$ for this purpose.

The discussion of figure 4.3 can be focused on two different aspects: first, the comparison between HB and DHB $\nabla^2\rho(r_{BCP})$, and second, the observed change of Laplacian sign. Regarding topological differences between both intermolecular bonds (HB and DHB), it can be seen that DHB display lower Laplacian values than HB complexes. The different electronic structure of the atoms involved in the intermolecular interactions will bring about a different behavior when the classification is based merely on $\rho(r_{BCP})$ values. This is the main reason that DHB systems have a smaller $\rho(r_{BCP})$ than HB systems.

A more interesting analysis can be carried out by checking the sign of Laplacian values. It is well-known that positive values indicate a closed-shell interaction, while negative values correspond to shared-shell interactions. All studied hydrogen-bonded complexes exhibit a positive value of the Laplacian, thus indicating a depletion of the charge. This fact, along with the low values of $\rho(r_{BCP})$, allows classifying the HB interaction as closed-shell. On the contrary, for dihydrogen-bonded systems both positive and negative values of the Laplacian are founds the stronger complexes having the most negative values. This behavior was already found in earlier studies and in chapter 3 for very strong hydrogen and dihydrogen bonds.[5, 120, 145, 166, 179] Likewise, the trend of Laplacian as a function of distance is in very good agreement with previous studies.[84, 108] Starting from large intermolecular distances (pure closed-shell systems), there is a smooth increase of $\nabla^2\rho(r_{BCP})$ while shortening the bonds, the Laplacian value reaching a maximum; from this point, $\nabla^2\rho(r_{BCP})$ starts decreasing along with the distance, being very steep when the Laplacian becomes negative. Interestingly, the largest difference between MP2 and B3LYP results can be found for very short intermolecular distances.

To get a deeper insight on the different behavior of the $\nabla^2\rho(r_{BCP})$ in HB and DHB systems, the Laplacian has been decomposed into its three curvatures: λ_1 and λ_2 (negative curvatures perpendicular to the bond) and λ_3 (positive parallel curvature), and analyzed independently. The curvatures perpendicular to the bond (λ_1 and λ_2) will be discussed together, as they have a similar value due to the cylindrical symmetry of the bond.

In figure 4.4 λ_1 and λ_3 are plotted as a function of the intermolecular distance, $rH\cdots B$. It can be noted that the dependence of curvature vs bond length is again more homogeneous for DHB systems than for HB complexes for both the MP2 and B3LYP levels of theory (i.e. at the MP2 level of theory $R^2 = 0.9997$ for DHB/λ_1 while $R^2 = 0.926$ for HB/λ_1). At large distances of DHB systems, λ_3 is more sensitive than λ_1 to the decrease of the equilibrium bond length, as compared with the corresponding decrease in HB complexes. The fact that the variation of λ_3 values vs. λ_1 values is more noticeable in HB complexes is the reason for the decrease in the Laplacian values of DHB complexes (recall that the Laplacian is calculated as the sum of the three curvatures). For both curvatures, DHB values are always much lower, exhibiting larger differences as the intermolecular distance becomes shorter. It is worth mentioning that these curvatures show a very well-defined trend versus intermolecular distances, which is in very good agreement with earlier works where the positive curvature was found to be the most meaningful parameter for hydrogen bond characterization and classification.[88]

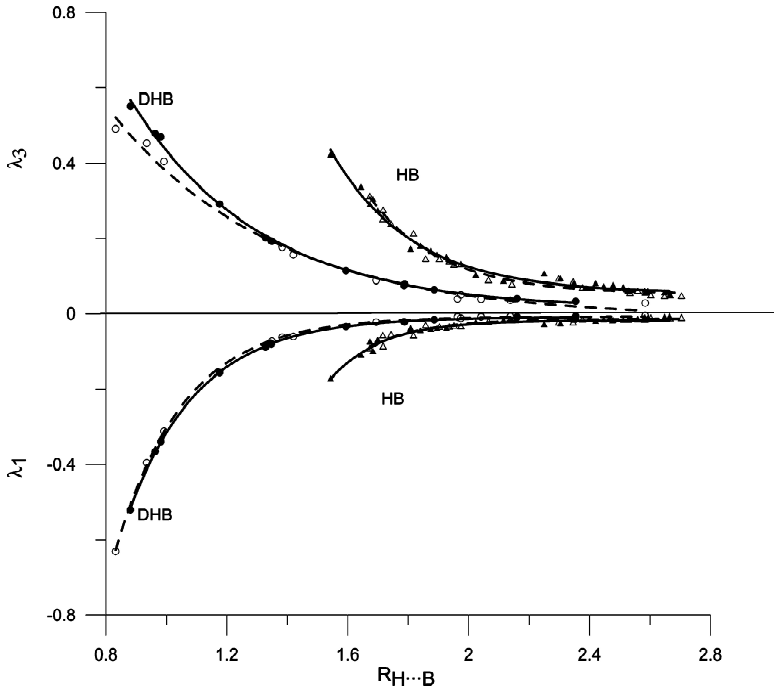

Figure 4.4: λ_1 and λ_3 (e·Å^{-5}) at the bond critical point versus the intermolecular distance (Å). Solid circles and triangles are for B3LYP calculations (DHB and HB, respectively), the solid lines being their fitted curves. Empty circles and triangles are for MP2 calculations (DHB and HB, respectively), the dashed lines being their fitted curves.

Among all topological characteristics that can be considered, the energetic properties of $\rho(r_{BCP})$ at the bond critical point are a good representation of the intermolecular interaction. In this scope is centered the discussion of the HB and DHB systems in terms of energy component densities, that is, kinetic and potential energies ($G(r_{BCP})$ and $V(r_{BCP})$). Thus, in figure 4.5 the relation between $G(r_{BCP})$ and $V(r_{BCP})$ with the intermolecular distance is plotted at the B3LYP/6-31++G(d,p) and MP2/6-31++G(d,p) levels of theory. As Espinosa et al. showed, for closed-shell systems there is a linear relationship between $G(r_{BCP})$ and λ_3, while $V(r_{BCP})$ is linearly related to the sum of the other two curvatures $(\lambda_1 + \lambda_2)$.[85, 86, 87] Having this fact in mind, at

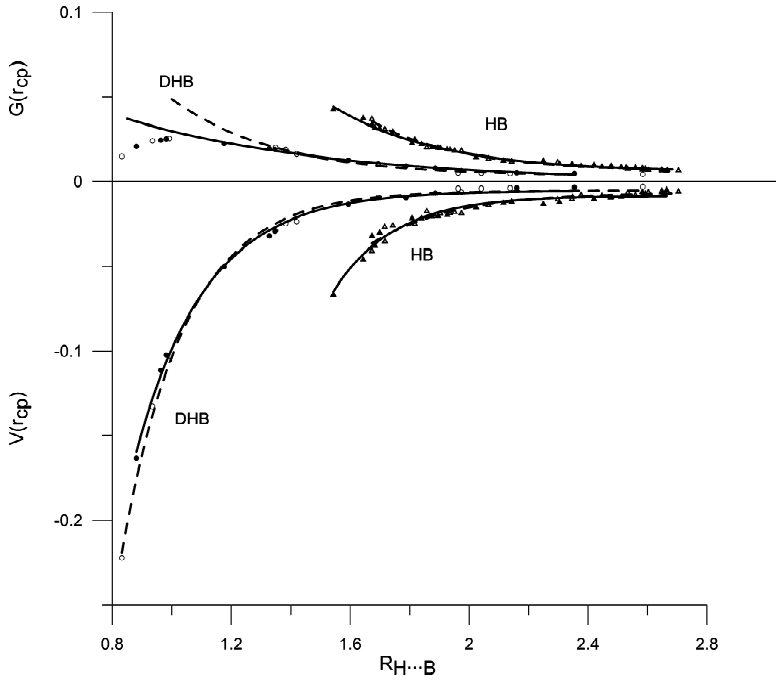

Figure 4.5: Potential ($V\left(r_{BCP}\right)$) and kinetic ($G\left(r_{BCP}\right)$) energy densities (a.u.) at the bond critical point versus the intermolecular distance (Å). Solid circles and triangles are for B3LYP calculations (DHB and HB, respectively), the solid lines being their fitted curves. Empty circles and triangles are for MP2 calculations (DHB and HB, respectively), the dashed lines being their fitted curves.

large intermolecular distances, figure 4.5 shows a shape similar to that in figure 4.4. $G\left(r_{BCP}\right)$ can be interpreted as a contribution of the electron dilution involved in the bond formation. As pointed out above, DHB systems display high $\rho\left(r_{BCP}\right)$ values as well as lower concentration/depletion of this electron density. This fact is in full agreement with the lower value of $G\left(r_{BCP}\right)$ shown by DHB complexes. There is also a decrease of DHB $V\left(r_{BCP}\right)$ as compared to HB dimers. In that way, a lower $\rho\left(r_{BCP}\right)$ is related to $V\left(r_{BCP}\right)$, due to weaker capacity to accumulate electrons. Once again, there is a similar behavior for both MP2 and B3LYP levels of calculation.

A second point to be considered here concerns the distance shortening and $\nabla^2\rho(r_{BCP})$ becoming negative. While λ_3 keeps increasing when shortening the distance (see figure 4.4), $G(r_{BCP})$ presents a maximum for DHB with a final decrease for $NaH\cdots HBr$; this is actually the complex with the shortest intermolecular distance. Espinosa et al. had already found this behavior for $XH\cdots FY$, hence classifying the shorter distance complexes as shared-shell interactions.[84]

A very appealing separation between HB and DHB systems can be obtained for complexes characterized as closed-shell (figure 4.5). Note that the correlation between $G(r_{BCP})$ and $r_{H\cdots B}$ is very good at both levels of theory and all systems ($R^2 = 0.988$ for DHB/MP2 and $R^2 = 0.992$ for the others).

4.3.3 HB/DHB strength dependence.

So far, the characterization of dihydrogen-bonded systems has been analyzed in terms of intermolecular distances ($r_{H\cdots B}$) and electronic densities. However, another usual attractive point of view can be considered in terms of strength, that is, considering the energy implied in the formation of DHB.

Figure 4.6 shows how the CP-corrected dimerization energy (with no nuclear relaxation) correlates with intermolecular distance. As found in previous studies, there is an exponential relationship between geometrical parameters ($r_{H\cdots B}$) and the interaction strength ($E_{dim} + CP$).[119] Figure 4.6 shows how DHB complexes with dimerization energy similar to HB systems present shorter distances. Since in the first part of this section it was concluded that, in general, DHB have lower $\rho(r_{BCP})$ and also a lower curvature, the present conclusion fully agrees with the fact that DHB are weaker at the same interatomic distance. A common behavior is found for the B3LYP and MP2 levels of theory. It must be noted that the $NH_3 - HBr$ complex presents a $r_{H\cdots B}$ distance (1.543 Å) which is too short compared to complexes of similar dimerization energy. The reason may be found in its very large BSSE (2.45 kcal/mol estimated by CP). In a previous paper,[214, 240] it was shown that there is a linear relationship between the amount of CP correction to the energy and the change in the intermolecular distance if the geometry is reoptimized using the CP-corrected scheme.[214, 240] In this particular case, reoptimizing in a CP-corrected surface would increase the $NH_3 - HBr$ distance and thus improve the correlation with that of others complexes.

As a result of the trend shown in figure 4.6, it was interesting to reanalyze

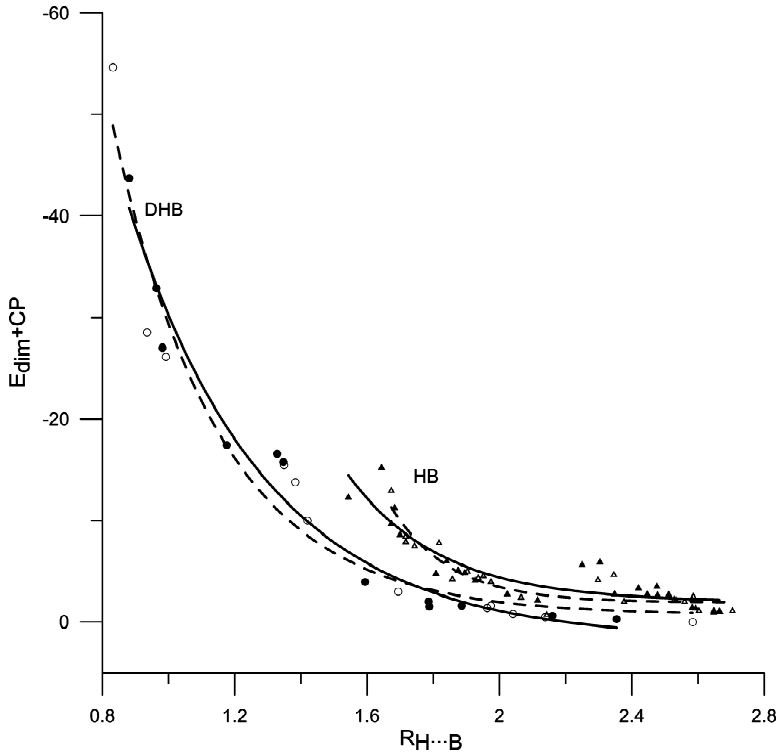

Figure 4.6: BSSE-corrected dimerization energy (kcal/mol) versus intermolecular distance (Å). Solid circles and triangles are for B3LYP calculations (DHB and HB, respectively), the solid lines being their fitted curves. Empty circles and triangles are for MP2 calculations (DHB and HB, respectively), the dashed lines being their fitted curves.

the topology of the HB/DHB interactions and energy density values $V(r_{BCP})$ and $G(r_{BCP})$ at the bond critical point as a function of the energetic criteria. Therefore, $\rho(r_{BCP})$ was plotted as a function of the dimerization energy $(E_{dim} + CP)$ (figure 4.7). Comparing this graphic with 4.2 (electron density represented as a function of $r_{H\cdots B}$), it can readily be observed that there is no actual, clear separation between HB and DHB systems. Furthermore, comparing the solid line (B3LYP data) with the dashed line (MP2 data), one can assess again that no significant differences are observed, as far as topological

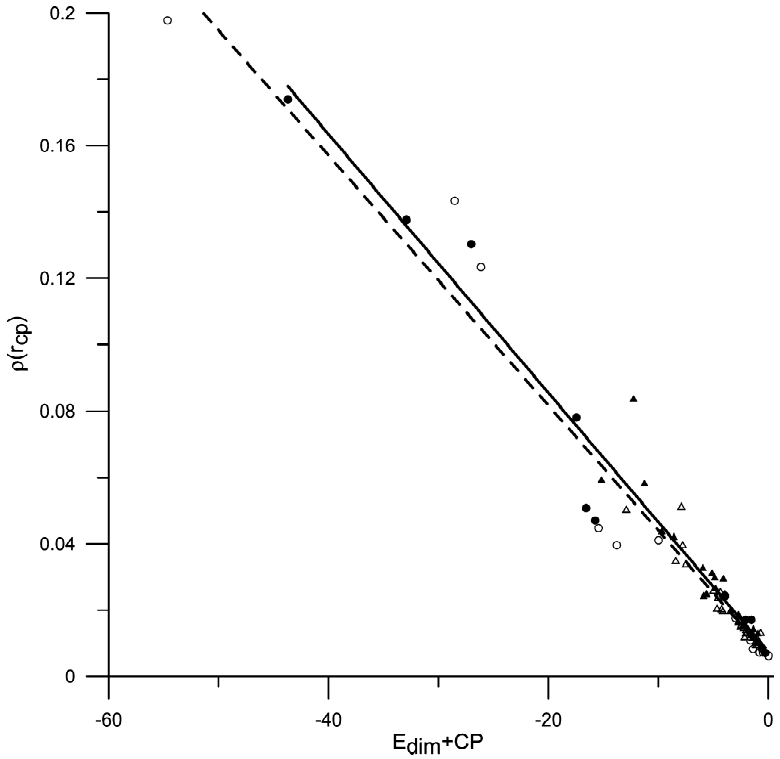

Figure 4.7: Electron density at the bond critical point ($e \cdot Å^{-3}$) versus dimerization energy (kcal/mol). Solid circles and triangles are for B3LYP calculations (DHB and HB, respectively), the solid line being their fitted curve. Empty circles and triangles are for MP2 calculations (DHB and HB, respectively), the dashed line being their fitted curve.

behavior is concerned. A similar behavior is observed by plotting the Laplacian ($\nabla^2 \rho(r_{BCP})$) or the two curvatures λ_1 and λ_3 vs. E_{dim}.

To further assess the relationship between density topological parameters and energetic data, a final analysis of the kinetic and potential energy densities at r_{BCP} is made. Because of the linear relationship existing for closed-shell interactions between the curvatures ($\lambda_1 + \lambda_1$ and λ_3) at the BCP and $V(r_{BCP})$ and $G(r_{BCP})$, respectively, it might be expected from figure 4.8 that no significant differences will be found between HB and DHB when en-

ergy densities are analyzed. This fact can be verified in figure 4.8, where $V(r_{BCP})$ and $G(r_{BCP})$ are represented vs. the dimerization energy. Focusing on the systems with larger intermolecular distances, there is no actual difference between HB and DHB. However, when the distance decreases there is a maximum in $G(r_{BCP})$. Espinosa et al. claimed that this fact (the increase and further decrease of $G(r_{BCP})$ while shortening the intermolecular distance) is related to the covalent contribution to the bond.[84] Comparing figure 4.8 and figure 4.5 ($G(r_{BCP})$ versus $r_{H\cdots X}$ and CP-corrected dimerization energy, respectively), one can observe that, for DHB complexes, all $MH\cdots HX$ (M = Li, Na) systems deviate significantly from the HB set. As mentioned above, all these systems have very short intermolecular distances, which can be translated into an important covalent contribution. In that way, the representation of $G(r_{BCP})$ versus dimerization energies assess in a better way the separation between closed-shell and shared-shell systems.

The results presented so far show that hydrogen- and dihydrogen-bonded systems have topological and energetic properties which show a similar dependence with intermolecular strength, that is, with dimerization energies.[123, 216] This fact is in complete agreement with previous studies which found a similar behavior for HB and DHB. The present study evidence that, on the contrary, when the intermolecular distance is considered, meaningful differences can be found between the set of HB or DHB complexes; such differences, induced by lower density and concentration/depletion electron charge density, allow for a remarkable separation of both sets of intermolecular bonds and thus provide a nice way for their classification. Overall, they provide a neater way to understand HB and DHB systems, which enhances earlier studies.

4.4 Conclusions

B3LYP/6-31++G(d,p) and MP2/6-31++G(d,p) calculations for various different hydrogen-bond and dihydrogen-bond systems have been carried out in order to analyze their electron density topological and local energetic properties at the bond critical point at the optimized geometries. MP2 and B3LYP topological and energetic data give rise to very similar conclusions. Both levels of calculations predict the same topological differences between HB and DHB complexes.

Electron density and geometrical analysis of the $MH\cdots HX$ (M = Li, Na and X = F, Cl, Br dimers show mainly two different set of complexes depending

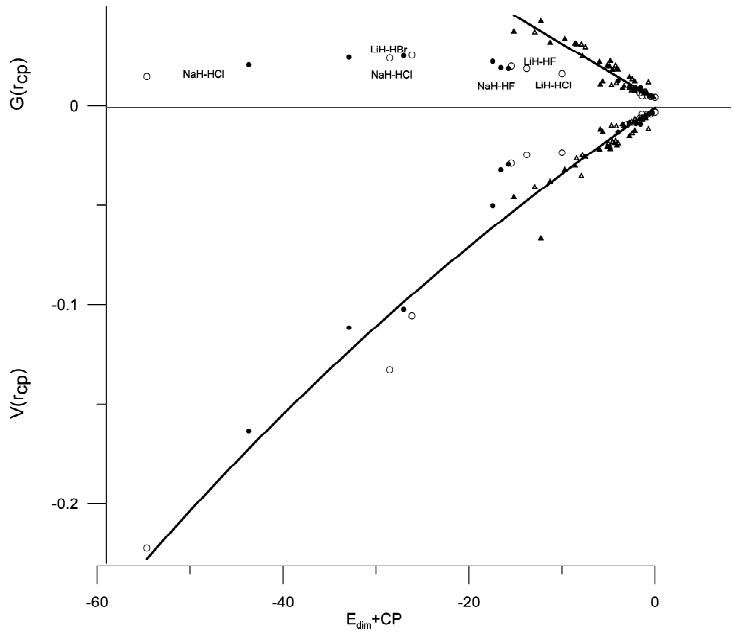

Figure 4.8: Potential ($V\left(r_{BCP}\right)$) and kinetic ($G\left(r_{BCP}\right)$) energy densities (a.u.) at the bond critical point versus the dimerization energy (kcal/mol). Solid circles and triangles are for B3LYP calculations (DHB and HB, respectively), and empty circles and triangles are for MP2 calculations (DHB and HB, respectively). Solid lines correspond to fitted curves for all MP2 and B3LYP data together. For $G\left(r_{BCP}\right)$, only purely closed-shell data are considered in the fitted data.

on the covalent contribution to the dihydrogen bond. From both points of view it can be concluded that the set with larger dihydrogen distances, can be classified as hydrogen bond, while the second one present a covalent hydrogen bond.

H$\cdots$H interactions exhibit shorter dihydrogen bond lengths as compared with hydrogen-bonded systems with the same strength. This behavior can be rationalized from the lower $\rho\left(r_{BCP}\right)$, as well as a lower concentration/depletion of that density, which is due to the different electronic structure of both atoms taking part in the interaction. The proton acceptor hydrogen has a smaller radius than the hydride hydrogen of a hydrogen bond, and thus the difference.

While there are no significant differences when properties are represented as a function of the dimerization energy, they can be separated into two well-defined sets when intermolecular hydrogen bond distances are considered.

For dihydrogen-bonded complexes it can be observed that their trends are more homogeneous, due to both atoms involved in the intermolecular interaction being the same in all complexes. Ranging from very weak to very strong dihydrogen-bonded complexes, it has been found that results for the topological and energetic values of $\rho(r_{BCP})$ are similar to those found earlier for density by Espinosa et al. for $XH\cdots FY$ complexes, thus revealing important covalent contribution for very strong systems.

All in all, the relationship between $\rho(r_{BCP})$ properties and intermolecular distances has been characterized; this relationship is different for the set of dihydrogen-bonded systems and for the set of other standard hydrogen-bond complexes. Thus it has been possible to assess the differences between these two types of systems and to stress the importance of taking into account hydrogen-bond-optimized equilibrium distances instead of energetic (i.e. dimerization energies) values. The latter parameters do not give rise to a classification and separation of both sets of hydrogen-bonded systems. Plotting against bond length does, and hence it allows for better understanding of the different properties of HB and DHB complexes.

Chapter **5**

Kohn-Sham density functional theory analysis of dihydrogen bonds

The saddest aspect of life right now is that science gathers knowledge faster than society gathers wisdom.

— Isaac Asimov
Russian-born professor of biochemistry and english science fiction writer (1920-1992)

5.1 Introduction

The electronic nature of classical hydrogen bonds has been researched a lot in recent years, in particular the question as to the extent of covalent (orbital interaction) versus electrostatic character.[111, 112, 113, 214] Morokuma and

Scheme 5.1.

$A-H^{\delta-}\cdots{}^{\delta+}H-X$ *(a)* $\qquad A^{+}\cdots H-H\cdots{}^{-}X$ *(b)* $\qquad A^{\bullet}\cdots H-H\cdots{}^{\bullet}X$ *(c)*

coworkers have found that hydrogen bonds in simple dimers, e.g., of water, have a dominant electrostatic but a non-negligible contribution of some 20% from donor-acceptor orbital interactions.[147] Fonseca Guerra et al. showed that the hydrogen bonds in Watson-Crick pairs as well as in mismatches of DNA bases receive a contribution of some 40% from donor-acceptor orbital interactions between N or O lone pairs and N − H σ^* acceptor orbitals.[92, 95, 94, 93, 97, 96, 98, 101] Furthermore, Isaacs and coworkers confirmed through X-ray scattering measurements that the hydrogen bonds in ice have indeed partial covalent character.[139] Likewise, the driving force of DHB formation has been ascribed to a combination of a larger term of electrostatic attraction and a smaller but non-negligible term of donor-acceptor interactions between the hydridic and protonic hydrogens.[5, 70, 121, 145, 166, 179, 191]

In the last chapters complexes with very strong DHBs were studied, and recently there has been some interest on this subject in other works as well.[71, 120, 121] These complexes feature extremely short H···H distances of 1.2 to 1.4 Å and relatively high binding energies of some 20 kcal/mol. Theoretical analyses have classified these DHBs as partially covalent (see chapter 4 and citation [71]). They appear as precursor complexes AH···HX to a proton transfer reaction yielding cationic dihydrogen complexes $A(H_2)^+\cdots X^-$.[23, 111, 133] Very strong DHBs can achieve H − H bond distances not much longer than that in the H_2 molecule. Interestingly, based on this H − H distance, it has been argued that the H···H share in a DHB is a more loose donor-acceptor bond between A − H and H − X (scheme 5.1a) or that it can be conceived as a H_2 molecule with a strong H − H electron-pair bond, interacting with A and X (schemes 5.1b and 5.1c). Liao, for example, classified the H − H moiety in microsolvated LiH···HF either as a DHB or a H_2 molecule, based on the computed H − H distance which varies as a function of the number of water molecules.[165]

There are three objectives developed in this chapter. The first one is the question if the formation of a DHB (scheme 5.1a) or a molecular hydrogen (schemes 5.1b and 5.1c) can be distinguished, and how can it be distinguished. For this fundamental issue, the linear H_4 is used, as it is the simplest model system possible. In second place, more realistic (but still simple) model

systems are used, such as $LiH\cdots HX$ with X = Cl, F and CN, as well as $BH_4^- \cdots HF$, which feature hydridic and protonic hydrogens forming a DHB. The discussion of how the electronic structure and the bonding of these species differ from that of H_4 is introduced as well. The third and last objective is, after having examined the basic principles of DHB, modelling more realistic complexes, some of which have been studied experimentally, namely, $BH_4^- \cdots HX$ and $AlH_4^- \cdots HX$. These bonding analyses are based on the quantitative molecular orbital (MO) model contained in Kohn-Sham density functional theory (DFT)[12, 14, 20, 18, 33, 90, 100, 102, 153, 205, 245, 246, 255, 256, 265, 267] at the BP86/TZ2P level. For selected model systems, a quantitative bond-energy decomposition was carried out as a function of the $H-H$ bond distance, into the classical electrostatic interaction, Pauli repulsive orbital interactions (between closed shells), and bonding orbital interactions (e.g., donor–acceptor and electron-pair bonding).

5.2 Methodology

All calculations were performed using the Amsterdam Density Functional (ADF) program developed by Baerends and others.[12, 14, 20, 18, 33, 90, 100, 102, 153, 205, 245, 246, 255, 256, 265, 267] The numerical integration was performed using the procedure developed by te Velde et al.[33, 255] The MOs were expanded in a large uncontracted set of Slater-type orbitals (STOs) containing diffuse functions: TZ2P (no Gaussian functions are involved).[246] The basis set is of triple-ζ quality for all atoms and has been augmented with two sets of polarization functions, i.e. $3d$ and $4f$ on C, N and O; and $2p$ and $3d$ on H. The $1s$ core shells of carbon, nitrogen and oxygen were treated by the frozen-core approximation.[12] An auxiliary set of s, p, d, f and g STOs was used to fit the molecular density and to represent the Coulomb and exchange potentials accurately in each self-consistent field cycle.[153]

All the equilibrium structures were optimized using analytical gradient techniques.[265] Geometries and energies were calculated at the BP86 level of the generalized gradient approximation (GGA): exchange is described by Slater's $X\alpha$ potential [245] with nonlocal corrections due to Becke [20, 18] added self-consistently and correlation is treated in the Vosko-Wilk-Nusair (VWN) parameterization [267] with nonlocal corrections due to Perdew [205] added, again, self-consistently (BP86).[90]

5.2.1 Bonding energy analysis

The overall bond energy E is made up of two major components,

$$\Delta E = \Delta E_{prep} + \Delta E_{int} \tag{5.1}$$

where the preparation energy ΔE_{prep} is the amount of energy required to deform the separate molecular fragments from their equilibrium structure to the geometry that they acquire in the DHB complex. The interaction energy ΔE_{int} corresponds to the actual energy change when the prepared fragments are combined to form the DHB complex. It is analyzed in the framework of the Kohn-Sham MO model using a decomposition of the bond into electrostatic interaction, exchange repulsion (or Pauli repulsion), and (attractive) orbital interactions,[26, 27, 28, 147, 185, 280, 279]

$$\Delta E_{int} = \Delta V_{elstat} + \Delta E_{Pauli} + \Delta E_{oi} \tag{5.2}$$

in which ΔV_{elstat} corresponds to the classical electrostatic interaction between the unperturbed charge distributions of the prepared (i.e. deformed) molecular fragments and is usually attractive. The Pauli repulsion ΔE_{Pauli} comprises the destabilizing interactions between occupied orbitals and is responsible for the steric repulsion. The orbital interaction ΔE_{oi} in any MO model, and therefore also in Kohn-Sham theory, accounts for charge transfer (i.e., donor-acceptor interactions between occupied orbitals on one moiety with unoccupied orbitals of the other, including the HOMO-LUMO interactions) and polarization (empty/occupied orbital mixing on one fragment due to the presence of another fragment). Since the Kohn-Sham MO method of DFT in principle yields exact energies and, in practice, with the available density functionals for exchange and correlation, rather accurate energies, we have the special situation that a seemingly one-particle model (an MO method) in principle completely accounts for the bonding energy.[256] In particular, the orbital-interaction term of the Kohn-Sham theory comprises the often distinguished attractive contributions charge transfer, induction (polarization) and dispersion. One could in the Kohn-Sham MO method try to separate polarization and charge transfer, as has been done by Morokuma in the Hartree-Fock model, but this distinction is not sharp. In fact, contributions such as induction and charge transfer, and also dispersion, can be given an intuitive meaning, but whether, or with what precision, they can be quantified, remains a controversial subject. In view of the conceptual difficulties, further decomposing the Kohn-Sham orbital interaction term is not adequate in this work, except by symmetry. It has been observed that the orbital interactions are mostly of

the donor-acceptor type, and it is therefore justified to denote the full orbital interaction term for brevity just as "charge transfer" or "covalent" contribution, as opposed to the electrostatic and Pauli repulsion contributions. However, the straightforward denotation "orbital interaction" avoids confusion with the charge-transfer energy, which features in other elaborate decomposition schemes [253, 252] that also give rise to induction and dispersion contributions, which are not attempted to be quantified here but which are all lumped together in the Kohn-Sham orbital interaction.

5.2.2 Analysis of the charge distribution

The electron density distribution is analyzed using the *Voronoi deformation density* (VDD) method.[29, 99] The VDD charge Q_A is computed as the (numerical) integral of the deformation density $\Delta\rho(\vec{r}) = \rho(\vec{r}) - \sum_B \rho_B(\vec{r})$ associated with the formation of the molecule from its atoms over the volume of the Voronoi cell of atom A,

$$Q_A = -\int_{\substack{\text{Voronoi}\\ \text{cell A}}} \rho\left(\vec{r}\right) \sum_B \rho_B\left(\vec{r}\right) d\vec{r} \tag{5.3}$$

The Voronoi cell of atom A is defined as the compartment of space bounded by the bond midplanes on and perpendicular to all bond axes between nucleus A and its neighboring nuclei (cf. the Wigner-Seitz cells in crystals).[148, 266] Here, $\rho(\vec{r})$ is the electron density of the molecule and $\sum_B \rho_B(\vec{r})$ the superposition of atomic densities ρ_B of a fictitious promolecule without chemical interactions that is associated with the situation in which all atoms are neutral. The interpretation of the VDD charge Q_A is rather straightforward and transparent. Instead of measuring the amount of charge associated with a particular atom A, Q_A directly monitors how much charge flows, due to chemical interactions, out of ($Q_A > 0$) or into ($Q_A < 0$) the Voronoi cell of atom A, i.e., the region of space that is closer to nucleus A than to any other nucleus.

The chemical bond between two molecular fragments can be analyzed by examining how the VDD atomic charges of the fragments change due to the chemical interactions. In reference [98] however, Fonseca and coworkers have shown that equation 5.3 leads to small artifacts that prohibit an accurate description of the subtle changes in atomic charges that occur in case of weak chemical interactions, such as hydrogen bonds or dihydrogen bonds. This is

due to the so-called front-atom problem that, in fact, all atomic-charge methods suffer from. To resolve this problem and, thus, enabling a correct treatment of even subtle changes in the electron density, the change in VDD atomic charges ΔQ_A is defined by equation 5.4, which relates this quantity directly to the deformation density $\Delta\rho(\vec{r}) = \rho_{complex}(\vec{r}) - \rho_{fragment_1}(\vec{r}) - \rho_{fragment_2}(\vec{r})$ associated with forming the overall molecule (i.e., the DHB complex) from the joining the molecular fragments, fragment 1 and fragment 2.

$$\Delta Q_A = -\int_{\substack{\text{Voronoi}\\ \text{cell A in}\\ \text{complex}}} \rho_{complex}\left(\vec{r}\right) - \rho_{fragment_1}\left(\vec{r}\right) - \rho_{fragment_2}\left(\vec{r}\right) d\vec{r} \qquad (5.4)$$

Again, ΔQ_A has a simple and transparent interpretation: it directly monitors how much charge flows out of ($Q_A > 0$) or into ($Q_A < 0$) the Voronoi cell of atom A as a result of the chemical interactions between fragment 1 and fragment 2 in the complex.

5.3 Results and discussion

5.3.1 Linear H_4: donor-acceptor $H_2 - H_2$ dihydrogen bond versus electron-pair bonded central hydrogen molecule $^{\bullet}H\cdots H_2\cdots H^{\bullet}$

The formation of linear H_4 from two hydrogen molecules is a generic and idealized model for analyzing the nature of dihydrogen bonding and, in particular, for addressing the question if one can distinguish qualitatively between donor–acceptor $H\cdots H$ bonding and the formation of a hydrogen molecule with an electron-pair bond. Interestingly, this turns out indeed to be the case. This follows from the quantitative Kohn-Sham MO analyses at BP86/TZ2P which are schematically illustrated in figure 5.1 for the frontier-orbital interactions between two H_2 fragments in H_4.

Thus, two closed-shell hydrogen molecules approaching each other in a linear manner yield an H_4 molecule (see figure 5.2) with a closed-shell singlet (S) ground state that is essentially unbound. Pushing the H_2 fragments together, i.e., reducing the central $H - H$ bond leads to 2-orbital–4-electron (or Pauli) repulsion between the occupied H_2 σ orbitals which go into the occupied bonding H_4 1σ and occupied antibonding H_4 $1\sigma^*$ MOs (see figure 5.1a). In this situation, any stabilizing contribution to the net interaction, besides

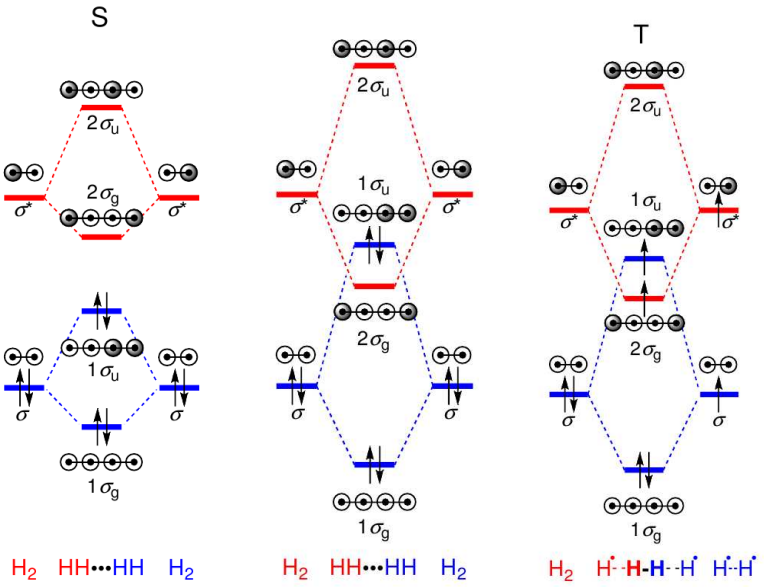

Figure 5.1: Schematic orbital-interaction diagram for linear H_4 in terms of two H_2 molecules.

electrostatic attraction, is provided by donor-acceptor interaction between the occupied 1σ of one H_2 fragment with the unoccupied σ^* of the other H_2 fragment and vice versa. Due to the relatively large HOMO-LUMO gap between σ and σ^* in molecular hydrogen, this donor-acceptor interaction is weak and therefore dominated by the $\sigma \pm \sigma$ Pauli repulsion; for clarity, figure 5.1a only shows the latter.

If the two H_2 fragments are pushed together, below a certain, critical central $H - H$ distance, the $H_2 - H_2$ antibonding $\sigma - \sigma$ combination ($1\sigma_u$ in H_4) rises above the $H_2 - H_2$ bonding $\sigma^* + \sigma^*$ combination ($2\sigma_g$ in H_4) as shown in figure 5.1b. The original closed-shell singlet configuration is no longer the ground state at such shorter central $H - H$ distance. Instead, as shown in figure 5.1c, an open-shell triplet ground state occurs as one of the electrons drops from the $H_2 - H_2$ antibonding $1\sigma_u$ into the $H_2 - H_2$ bonding $2\sigma_g$. This

substantially reduces the $\sigma \pm \sigma$ Pauli repulsion and introduces a $\sigma^* + \sigma^*$ one-electron bond. Thus, effectively, a central $H - H$ electron-pair bond emerges in the linear $^{\bullet}H \cdots H_2 \cdots H^{\bullet}$ diradical.

The discussion so far highlights the important role of the HOMO-LUMO gap between σ and σ^* in each of the two H_2 fragments. This, in turn, depends on the internal $H - H$ distance in the H_2 fragments, i.e., the terminal $H - H$ distance in linear H_4. In the following text, an overview of numerical experiments is provided. The objective is to explore how the relative energy of the singlet (S) and triplet state (T) of H_4 depends in central and terminal $H - H$ distances (see figure 5.2). First, two H_2 molecules are considered, each with a frozen internal $H - H$ distance R_H of 0.75 Å, that are brought together from a central $H - H$ distance $R_{central}$ in the resulting linear H_4 (see figure 5.2a). At any dihydrogen bond distance $R_{central}$ that we probe, singlet H_4 is significantly more stable than triplet H_4. Both configurations present a minimum on the PES, the singlet at about $R_{central} = 3$ Å whereas the higher-energy triplet state, with its effective electron-pair bond, achieves a minimum at $R_{central} = 0.75$ Å. Note that this corresponds to the H_2 equilibrium distance.

Next, two H_2 molecules that are brought together in linear H_4 are considered again, but now each of these H_2 fragments has a somewhat longer frozen internal $H - H$ distance $R_{terminal}$ of 1.25 Å (see figure 5.2b). Still, singlet H_4 is more stable than triplet H_4, at any dihydrogen bond distance $R_{central}$, but the energy difference has become smaller.

Finally, the experiment is repeated with long terminal $H - H$ distances bond distance $R_{terminal}$ of 2.5 Å (see figure 5.2c). In this situation, in which the $\sigma - \sigma^*$ gap in the terminal H_2 moieties has become relatively small (1.3 eV as compared to 11.3 eV in the equilibrium H_2 molecule), the inversion of orbital energies between the H_4 $1\sigma_u$ and H_4 $2\sigma_g$ occurs at an early stage of approach and the triplet state is thus easily reached. Indeed, as can be seen in figure 5.2c, the triplet state drops below the singlet state at all central $H - H$ distances probed. In other words, H_4 with long terminal $H - H$ bonds has a ground state with an effective central $H - H$ electron-pair bond. Note that the formation of a central H_2 molecule nicely agrees with the optimum central $H - H$ distance of about 0.75 Å. Note also that the optimum central $H - H$ distance in the singlet state also becomes shorter as the terminal $H - H$ distances get longer (compare figures 5.2a–5.2c). Likewise, the energy wells get deeper. The reason is that, as the $\sigma - \sigma^*$ orbital-energy gap in H_2 becomes smaller, also $\sigma + \sigma^*$ donor-acceptor bonding between the H_2 moieties in H_4 becomes stronger and eventually overrules the $\sigma \pm \sigma$ Pauli repulsion.

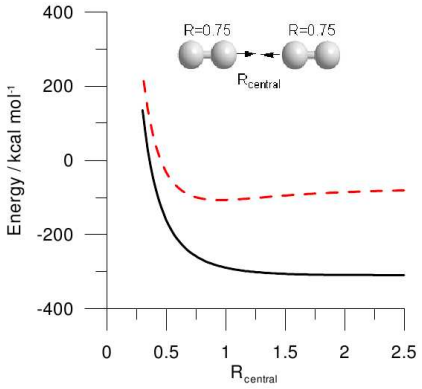

(a) Central $H-H$ distance with terminal bonds kept frozen to 0.75 Å

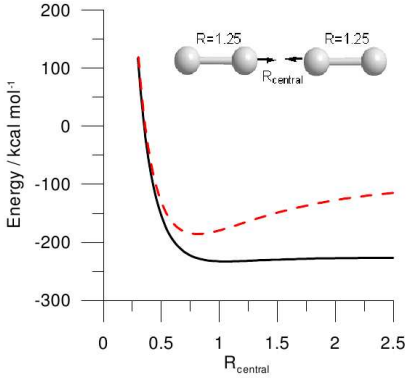

(b) Central $H-H$ distance with terminal bonds kept frozen to 1.25 Å

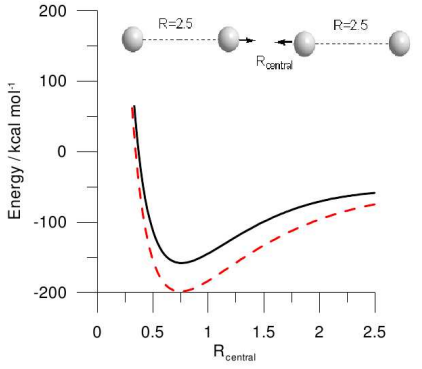

(c) Central $H-H$ distance with terminal bonds kept frozen to 2.50 Å

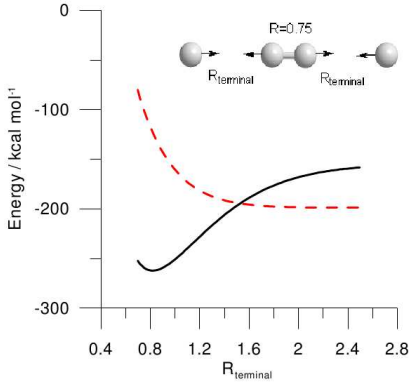

(d) Terminal H–H distances with the central bond kept frozen to 0.75 Å

Figure 5.2: Energy of the singlet (black curves) and triplet groundstate (dashed curves) of linear H_4 as a function of different geometry parameters, computed at BP86/TZ2P relative to ADF basic atoms.

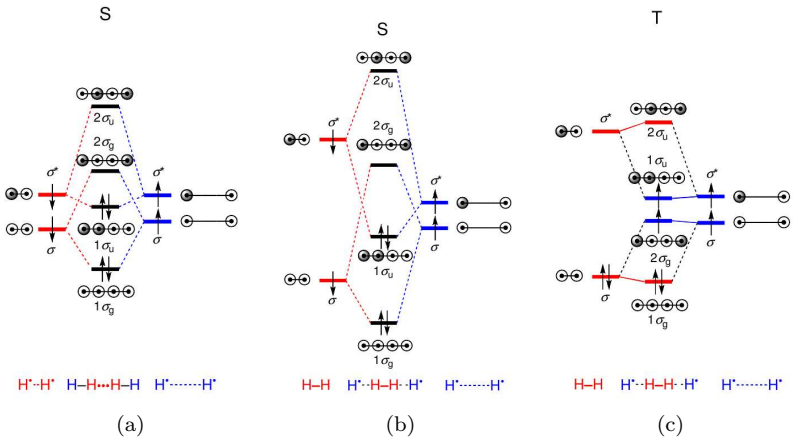

Figure 5.3: Schematic orbital-interaction diagram for linear H_4 in terms of a central H_2 molecule interacting with two outer $H^\bullet$ radicals, one to the left and one to the right.

The question whether the *central* H_2 moiety has a donor–acceptor DHB character or is best described as a covalent H_2 molecule clearly depends on the terminal $H-H$ distances. It is therefore instructive to consider an alternative decomposition of linear H_4, namely, the central H_2 fragment interacting on each side with a hydrogen atom, i.e., $H_4 =^\bullet H + H_2 + H^\bullet$. Figure 5.2d shows the corresponding energies of closed-shell singlet and open-shell triplet H_4 (relative to $^\bullet H + H_2 + H^\bullet$ as a function of the terminal $H-H$ distances (i.e., the approach of the $H^\bullet$ atoms) for a central H_2 moiety with its $H-H$ distance frozen to the equilibrium value of molecular hydrogen, 0.75 Å. The corresponding frontier-orbital interactions that emerge from our quantitative Kohn-Sham MO analyses are schematically represented in figure 5.3.

When the outer H atoms are far away from the central H_2 moiety (i.e., at large terminal R_H), the overall H_4 species has a triplet ground state: the dashed curve is below the solid curve in figure 5.2d. Importantly, the central H_2 moiety in this situation has effectively an electron-pair bonding valence configuration that interacts with two hydrogen radicals, as shown in figure 5.3c.

As the two outer H atoms are brought closer to the central, frozen H_2 moiety (i.e., as $R_{terminal}$ decreases while $R_{central}$ remains fixed at 0.75 Å), the

singlet configuration is stabilized and, around $R_{terminal} < 1.5$ Å, it becomes the ground state of H_4 (see figure 5.2d). Note that this corresponds to a change of the valence configuration of the central H_2 moiety from an electron-pair bonded hydrogen molecule to an excited triplet state $^{\bullet}H - H^{\bullet}$ which is intrinsically unbound. Such a valence excitation is facilitated as the central $H - H$ distance is expanded because this leads to a small HOMO-LUMO ($\sigma - \sigma^*$) orbital-energy gap in the central H_2 moiety (see figure 5.3a).

In conclusion, the central $H - H$ bond in linear H_4 can exist in two qualitatively different bonding modes. The first one as donor–acceptor DHB (with no net bonding in this model system), and the second one as a central H_2 molecule with an electron-pair bond. Short terminal $H - H$ distances in H_4 favor a central donor–acceptor DHB whereas long terminal $H - H$ bonds lead to an effectively electron-pair bonded central H_2 molecule. In the "$H_2 + H_2$ perspective", this is can be understood in terms of a large (DHB) or small HOMO–LUMO gap (central electron-pair bond) within the two terminal H_2 fragments. In the "$^{\bullet}H + H_2 + H^{\bullet}$ perspective", on the other hand, the same phenomenon arises from either strong Pauli repulsion, which leads to valence excitation of the central H_2 molecule from bound singlet to unbound triplet, or weak Pauli repulsion, which keeps the central H_2 molecule in the electron-pair bonded singlet state. Both descriptions are, of course, equivalent.

5.3.2 Dihydrogen bonding in linear $AH \cdots HX$

The above analyses show that weak donor-acceptor DHB bonding between two hydrogen molecules is the most stable global situation for linear H_4, and that this bonding cannot surmount closed-shell Pauli repulsion between the two fragments in this particular model system (see figure 5.2a). The next step is to modify the linear $A - H \cdots H - X$ model system from A, X = H towards somewhat more realistic DHB model systems involving a hydridic hydrogen bound to an electropositive A = Li, BH_3 and a protonic hydrogen bound to an electronegative X = Cl, F, CN. Results for the model systems $LiH \cdots HX$ and linear $BH_4^- \cdots HF$ are collected in table 5.1 (bond analyses) and figure 5.4 (geometries). Orbital-interaction diagrams, as they emerge from our quantitative Kohn-Sham MO analyses, are schematically illustrated in figure 5.5. For clarity, the latter has been simplified to showing the essential frontier-orbital interactions in the σ-electron system.

Donor-acceptor DHB is significantly stabilized, compared to H_4, in the linear $AH - HX$ model systems $LiH \cdots HCl$, $LiH \cdots HF$, $LiH \cdots HCN$ and linear

Table 5.1: Analysis of H $\cdots$ H dihydrogen bond in selected complexes.[†]

	LiH $\cdots$ HCl	LiH $\cdots$ HF	LiH $\cdots$ HCN	BH_4^- $\cdots$ HF (linear)
$R_{central}$(H $\cdots$ H)	1.13	1.30	1.70	1.27
		Energy decomposition (in kcal/mol)		
ΔE_{oi}	-40.9	-19.1	-8.1	-18.8
ΔE_{Pauli}	42.7	21.1	11.8	18.2
ΔV_{elstat}	-22.2	-18.9	-12.7	-21.3
$\Delta E_{Pauli} + V_{elstat}$	20.6	2.2	-0.9	-3.1
ΔE_{int}	-20.4	-16.9	-8.9	-21.9
ΔE_{prep}	6.7	1.8	0.4	2.4
ΔE	-13.7	-15.1	-8.5	-19.5
$\%\Delta E_{oi}$ [‡]	65	50	39	47
		Fragment orbital overlaps		
$\langle\sigma_{AH}\|\sigma_{HX}\rangle$	0.26	0.16	0.15	0.14
$\langle\sigma_{AH}\|\sigma^*_{HX}\rangle$	0.56	0.67	0.59	0.44
$\langle\sigma^*_{AH}\|\sigma_{HX}\rangle$	0.08	0.05	0.04	0.08
$\langle\sigma^*_{AH}\|\sigma^*_{HX}\rangle$	0.04	0.01	0.01	0.43
		Fragment orbital energy (in eV)		
		AH		
σ_{AH}	-4.4	-4.4	-4.4	-0.5
σ^*_{AH}	-1.3	-1.3	-1.3	0.2
		HX		
σ_{HX}	-11.3	-13.3	-9.3	-13.6
σ^*_{HX}	-2.1	-1.1	-1.1	-1.1
		Fragment orbital population (in a.u.)		
		AH		
σ_{AH}	1.71	1.95	1.97	1.82
σ^*_{AH}	0.01	0.01	0.00	0.01
		HX		
σ_{HX}	2.00	2.00	2.00	1.95
σ^*_{HX}	0.34	0.07	0.05	0.19
		Fragment VDD Charge (in a.u.)[§]		
$\Delta Q_{AH} = -\Delta Q_{HX}$	0.15	0.07	0.03	0.08

[†]Computed at BP86/TZ2P.
[‡]$\Delta E_{oi} = \frac{\Delta E_{oi}}{(\Delta E_{oi}+\Delta V_{elstat})} \times 100\%$
[§]Sum of atomic charges ΔQ_A of all atoms A in a fragment as defined in equation 5.4, i.e., *net change* in charge relative to separate AH and HX.

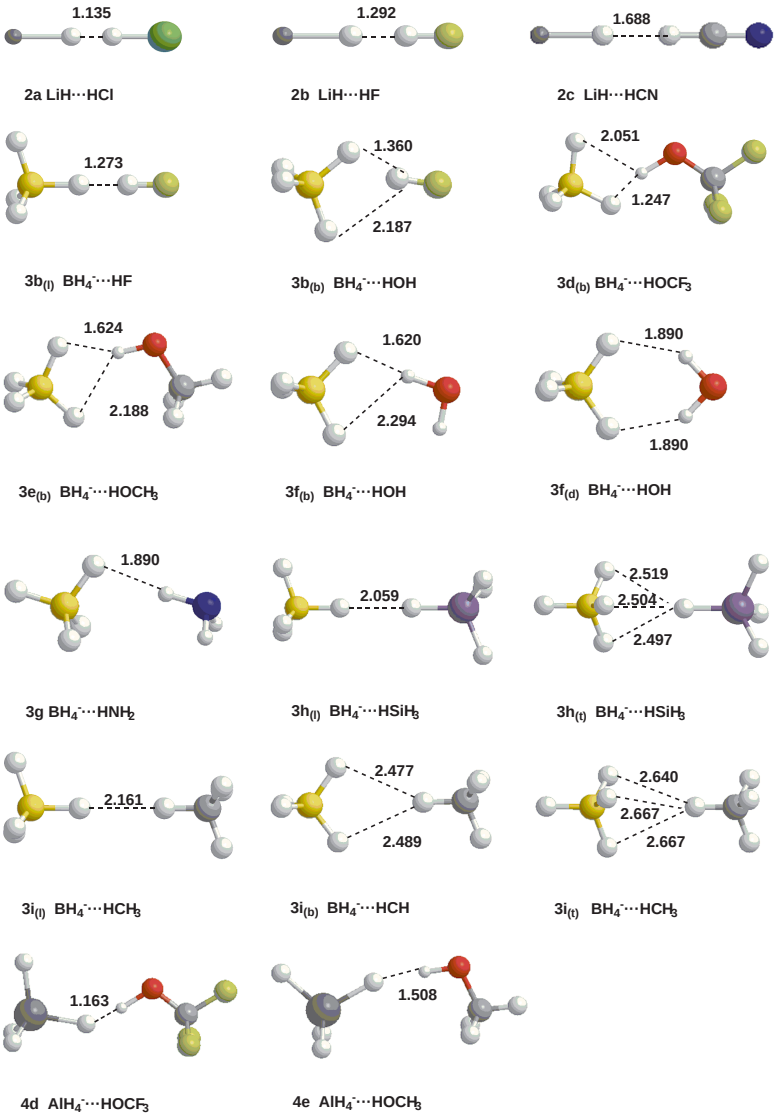

Figure 5.4: Structures (in Å) of dihydrogen-bonded complexes, computed at BP86/TZ2P. Numbers correspond to different proton acceptors (*2*: LiH, **3**: BH_4^-, **4**: AlH_4^-), letters to different proton donors (**a**: HCl, **b**: HF, **c**: HCN, **d**: CF_3OH, **e**: CH_3OH, **f**: H_2O, **g**: NH_3, **h**: SiH_4, **i**: CH_4). Subscripts refer to connectivity: (l) = linear DHB, (b) = bifurcated DHB, (t) = trifurcated DHB, (d) = double DHB.

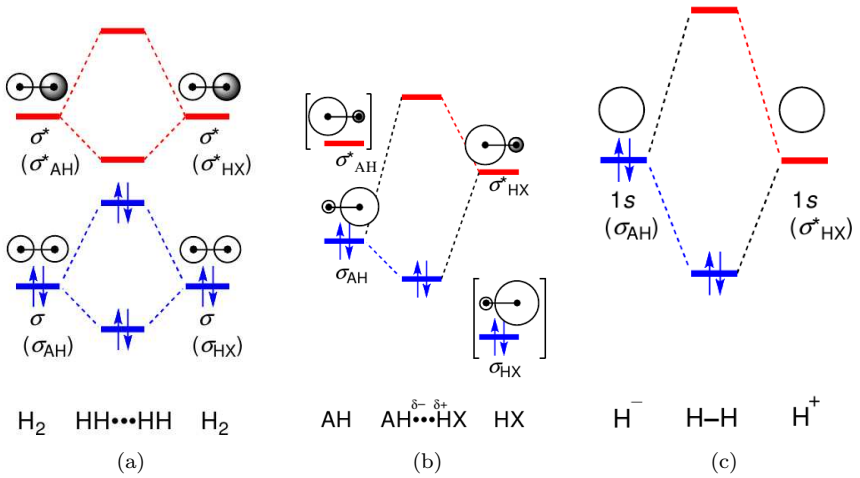

Figure 5.5: Schematic orbital-interaction diagram showing relationships and differences between dihydrogen bonding (DHB) in: (a) $HH\cdots HH$, (b) $AH\cdots HX$ and (c) $H-H$.

$BH_4^-\cdots HF$ which are all bound with respect to dissociation into AH and HX with central $H-H$ bonds of 1.13 Å and -13.7 kcal/mol in $LiH\cdots HCl$ to 1.70 Å and -8.5 kcal/mol in $LiH\cdots HCN$ (see table 5.1). Thus, except $LiH\cdots HCN$, these DHB complexes present relatively short DHB distances, in agreement with the difference in the proton-donor acidity constant, as pointed out by Gilli et al. in the qualitative electrostatic-covalent model.[112]

In the cases of $LiH\cdots HCl$, $LiH\cdots HF$ and linear $BH_4^-\cdots HF$, these linear stationary structures are second-order saddle points with doubly degenerate transition vectors with pronounced $A-H-H$ and $H-H-X$ bending amplitude, such that molecular hydrogen is eliminated from $LiH\cdots HCl$ and $LiH\cdots HF$ (scheme 5.2) whereas a bent, but still dihydrogen-bonded structure bifurcated $BH_4^-\cdots HF$ emerges from linear $BH_4^-\cdots HF$ (see figure 5.4).

Scheme 5.2.

$$A-H\cdots H-X \longrightarrow AX \ + \ H_2$$

The essential change in electronic structure and DHB bonding mechanism, from model H_4 to $LiH\cdots HX$ or $BH_4^-\cdots HX$, is that the σ^*_{AH} and σ_{HX} orbitals leave the scene of frontier orbital interactions. The interactions are then constituted, in good approximation, by a $\sigma_{AH}+\sigma^*_{HX}$ donor-acceptor orbital interaction (compare figure 5.5a and 5.5b). This interaction is reinforced as the σ_{AH} gets destabilized and localized on the hydridic H while the σ^*_{HX} is stabilized and more localized on the protonic H (see figure 5.5b). The σ^*_{AH} and σ_{HX} are still present, of course, but the point is that their orbital energies have moved out off the HOMO-LUMO regime and, in addition, they have only little amplitude on the hydridic and protonic hydrogens, respectively, which together form the DHB.

In line with this, we find that the $\langle\sigma_{AH}|\sigma^*_{HX}\rangle$ overlaps of 0.44–0.67 are up to one order of magnitude larger than the $\langle\sigma^*_{AH}|\sigma_{HX}\rangle$ which range from 0.04–0.08 (see table 5.1). Also, the gross populations of the σ^*_{AH} and σ^*_{HX} fragment orbitals show a donation of a few hundredths ($LiH\cdots HCN$) up to one third of an electron ($LiH\cdots HCl$) from the former to the latter. This is furthermore consistent with the net fragment VDD charges $\Delta Q_{AH}=-\Delta Q_{HX}$ of 0.03 ($LiH\cdots HCN$) to 0.15 a.u. ($LiH\cdots HCl$).

The corresponding DHB energy decomposition shows that the interaction energy ΔE_{int} receives an important part of its stabilizing character from the orbital interaction term ΔE_{oi} (see table 5.1). Thus, electrostatic attraction ΔV_{elstat} amounts to -12.7 ($LiH\cdots HCN$) to -22.2 kcal/mol ($LiH\cdots HCl$) whereas the corresponding orbital interaction ΔE_{oi} is -8.1 ($LiH\cdots HCN$) to -40.9 kcal/mol ($LiH\cdots HCl$). Note that the stronger the DHB, the greater the relative importance of the orbital interactions. For example, along the series $LiH\cdots CN$, $LiH\cdots HF$ and $LiH\cdots HCl$, the interaction energy goes from -8.9 to -16.9 to -20.4 kcal/mol while the percentage ΔE_{oi} of all bonding forces (i.e., $\Delta E_{oi}+\Delta V_{elstat}$) increases from 39% to 50% up to 65%. Interestingly, the latter is even larger than the highest percentage (some 40%) orbital interactions found, so far, for regular hydrogen bonds.[92, 95, 94, 93, 97, 96, 98, 101] Important covalent contributions to dihydrogen bonding also agree with topological analyses of the electron density (see chapter 4).

The variation from apolar $H-H\cdots H-H$ to more polar (and stable) $AH\cdots HX$ species $LiH\cdots HCl$, $LiH\cdots HF$, $LiH\cdots HCN$ and linear $BH_4^-\cdots HF$ constitutes a spectrum of donor-acceptor dihydrogen bonding mechanisms that ranges from clear donor-acceptor bonding, i.e., at variance to the qualitatively different electron-pair bonded central H_2 molecule, to a situation in which the hydridic and protonic character if the respective hydrogen atoms becomes

strong. The polar extreme of this spectrum corresponds to a hydride H^- that enters into a $1s + 1s$ donor-acceptor interaction with the proton H^+ (figure 5.5c). Thus, the clear-cut difference between donor–acceptor DHB and central hydrogen molecule turns into a more gradually changing spectrum in asymmetric model systems AH $\cdots$ HX.

5.3.3 Dihydrogen bonding in $MH_4^- \cdots HX$

To broaden the scope of the above analyses, our set of model systems has been extended (from LiH $\cdots$ HCl, LiH $\cdots$ HF, LiH $\cdots$ HCN and linear and bifurcated $BH_4^- \cdots$ HF) to include more DHB complexes involving boron hydride (BH_4^-) and aluminum hydride (AlH_4^-) fragments as hydride donors, and HCl, HF, HCN, CF_3OH, CH_3OH, H_2O, NH_3, SiH_4 and CH_4 as proton donors. Geometries and bond analyses are collected in figure 5.4 and table 5.2, respectively. Note that all species discussed in this section are stable equilibrium structures with zero imaginary frequencies, except $BH_4^- \cdots$ HOH with a double DHB which is a TS for the automerization reaction between two equivalent bifurcated $BH_4^- \cdots$ HOH.

Our set of model system covers the full range from very strong and short DHB (e.g., $AlH_4^- \cdots HOCF_3$: ΔE = -22.6 kcal/mol and $R_{central}$ = 1.16 Å) to very weak and long (e.g., trifurcated $BH_4^- \cdots HCH_3$: ΔE = -1.8 kcal/mol and $R_{central}$ = 2.64 Å). Important donor-acceptor bonding is again revealed by a strong orbital interaction component ΔE_{oi} in combination with a sizeable transfer of charge from BH_4^- or AlH_4^- to the various proton donors HX (see table 5.1). Note that the three methane complexes $BH_4^- \cdots HCH_3$—linear, bifurcated and trifurcated—are only very weakly bound, due to the high energy of the methane σ^*_{HX} acceptor orbitals.

As the energy of this σ^*_{HX} acceptor orbital decreases, e.g., along bifurcated $BH_4^- \cdots HOCF_3$, bifurcated $BH_4^- \cdots H_2O$ and bifurcated $BH_4^- \cdots HOCF_3$, the DHB bond contracts, becomes stronger and acquires a higher percentage of donor–acceptor orbital interactions. This trend in bonding may serve as the basis for a design principle of hydrogen storage materials. Thus, by varying the electronegativity difference between H and X in H − X (but also between A and H in AH), one can tune the stability or lability of the DHB system towards conservation or elimination of the central H_2 unit, i.e., uptake or release of molecular hydrogen as shown in scheme 5.2.

5.4 Conclusions

The nature of strong dihydrogen bonds ($M-H\cdots H-X$) that occur, e.g. in organometallic reaction mechanisms and potential hydrogen-storage materials, is very similar to that of regular hydrogen bonds ($Y\cdots H-X$): it is provided by roughly 40–60% donor-acceptor orbital interactions and a complementary percentage of electrostatic attraction. This follows from our analyses of the central $H-H$ bond in $LiH\cdots HX$, $BH_4^-\cdots HX$ and $AlH_4^-\cdots HX$ complexes using the quantitative molecular orbital (MO) model contained in Kohn-Sham density functional theory (DFT) at BP86/TZ2P.

It has also been shown that, in principle, there can be a qualitative difference between donor-acceptor DHB and H_2 formation which, in the generic (and idealized) case of H_4, correspond to two different electronic states, namely, closed-shell $H-H\cdots H-H$ and open-shell $^{\bullet}H\cdots H-H\cdots H^{\bullet}$. This clear-cut difference can, however, turn into a more gradually changing spectrum in asymmetric model systems $AH\cdots HX$ that feature hydridic and protonic hydrogens.

The results of our analyses suggest a design principle for hydrogen storage materials. Thus, by varying the electronegativity difference between H and X in $H-X$ (but also between A and H in AH), the stability or lability of the DHB system can be tuned towards conservation or elimination of the central H_2 unit, i.e., uptake or release of molecular hydrogen.

Table 5.2: Analysis of the H···H bond in $BH_4^- \cdots HF$ to $AlH_4^- \cdots HOCH_3$ in the order of ascending H − H bond length.**

AH··· ···HX	AlH_4^- $HOCF_3$	BH_4^- $HOCF_3$*	BH_4^- HF*	AlH_4^- $HOCH_3$	BH_4^- $HOCH_3$*	BH_4^- HOH*	BH_4^- HOH†	BH_4^- HNH_2	BH_4^- $HSiH_3$‡	BH_4^- HCH_3‡	BH_4^- HCH_3*	BH_4^- $HSiH_3$§	BH_4^- HCH_3§
$R_{central}(H\cdots H)$	1.16	1.25	1.36	1.51	1.62	1.62	1.89	1.89	2.06	2.16	2.48	2.50	2.64
						Energy decomposition (in kcal/mol)							
ΔE_{oi}	-36.7	-32.1	-17.6	-10.8	-10.4	-8.8	-7.1	-5.2	-4.4	-2.5	-2.5	-4.9	-2.6
ΔE_{Pauli}	34.5	33.3	19.8	13.6	13.4	12.4	11.7	6.8	4.5	2.7	2.5	4.3	2.2
ΔV_{elstat}	-31.6	-36.5	-25.0	-14.5	-16.7	-17.3	-18.3	-8.7	-2.3	-1.7	-1.7	-2.7	-1.4
$\Delta E_{Pauli} + V_{elstat}$	2.9	-3.2	-5.2	-1.0	-3.3	-4.9	-6.6	-1.9	2.2	1.0	0.9	1.7	0.8
ΔE_{int}	-33.8	-35.4	-22.8	-11.7	-13.7	-13.7	-13.7	-7.1	-2.2	-1.4	-1.7	-3.2	-1.8
ΔE_{prep}	11.2	9.5	2.3	0.8	0.7	0.8	1.3	0.3	0.4	0.0	0.0	0.6	0.0
ΔE	-22.6	-25.9	-20.5	-10.9	-13.0	-12.9	-12.4	-6.8	-1.7	-1.4	-1.7	-2.6	-1.8
$\%\Delta Eoi$‡‡	54	47	41	43	38	34	28	37	66	60	60	65	65
						Fragment orbital overlaps							
$\langle\sigma_{AH}\|\sigma^*_{HX}\rangle$	0.53	0.42	0.41	0.31	0.33	0.30	0.32	0.19	0.20	0.17††	0.17††	0.17	0.15††
										0.34††	0.30††		0.27††
						Fragment orbital energy (in eV)							
σ_{AH}	-1.0	-0.4	-0.5	-1.2	-0.6	-0.6	-0.6	-0.7	-0.7	-0.7	-0.7	-0.7	-0.7
σ^*_{HX}	-2.0	-1.9	-1.1	-0.2	-0.2	-0.7	-0.7	-0.3	-0.1	0.4††	0.5††	-0.1	0.4††
										2.3††	2.3††		2.3††
						Fragment orbital population (in a.u.)							
σ_{AH}	1.74	1.80	1.89	1.89	1.93	1.93	1.94	1.96	1.94	1.97	1.98	1.95	1.97
σ^*_{HX}	0.29	0.23	0.12	0.10	0.08	0.07	0.07	0.04	0.05	0.02	0.02	0.05	0.02
										0.02	0.01		0.02
						Fragment voronoi charge (in a.u.)‖							
$\Delta Q_{AH} = -\Delta Q_{HX}$	0.14	0.13	0.08	0.05	0.05	0.05	0.05	0.03	0.03	0.01	0.01	0.03	0.01

Types of geometry: *Bifurcated, †Double, ‡Linear, §Trifurcated

**Computed at BP86/TZ2P.

††CH_4 has two σ^*_{HX} acceptor orbitals available, from A and T symmetry, and values are displayed for these LUMO and LUMO+1, respectively

‡‡$\Delta E_{oi} = \frac{\Delta E_{oi}}{(\Delta E_{oi}+\Delta V_{elstat})} \times 100\%$

‖Sum of atomic charges ΔQ_A of all atoms A in a fragment as defined in equation 5.4, i.e., *net change* in charge relative to separate AH and HX.

Chapter 6

Periodic systems

L'univers desconegut ès una cadena
d'esdeveniments
que ens afecten més o menys.

— Antònia Font
Astronauta rimador (2004)

6.1 Introduction

Obtaining a safe, reliable hydrogen storage system is one of the backbones of the air pollution reduction and one of the trend topics in science nowadays.[62, 75, 157, 189, 275, 278] Hydrogen gas combustion is highly exothermic, it doesn't liberate greenhouse gases and its production through electrolysis is efficient and easy to implement. Thus, hydrogen has been thought as a way to store energy not only on static uses, but also on mobile ones, as cars, trucks

and other nowadays fuel-powered engines. But as a turndown, storing it is difficult and dangerous for everyday use, especially with automobiles. Traditional tanks and gas cylinders have problems with leakages and can explode when their walls broke as a consequence of a strong impact. More secure means of storage include absorption of the hydrogen gas on different compounds, which will avoid the immediate release of the gas in case of structural fail. But the space the absorber occupies, the ratio between the hydrogen captured in the absorber and the absorber itself, sometimes makes it ineffectual to use it as a valid practical holder. Besides, the speed at which the material can liberate hydrogen is another bottleneck on developing the technology, as sometimes this speed is slower than the needs of the combustion system. Some other materials could not be recycled and others need too much temperature to release the hydrogen, making the energetic balance too negative. A promising compound for hydrogen storage is ammonia borane, (AB), named also as boraneamine or amineborane.[183] Amineborane has a rate of 194 g of H_2 per kg, is stable at room temperature and starts the release of hydrogen at 70°C. Heldebrant and coworkers released an study on synthesizing boraneamine to exploit it as hydrogen storage.[129]

Those recent investigations on boraneamine are not the only ones using this molecule as the focus of study. One of the early evidences of dihydrogen bonds were found in mid-fifties in different boraneamine structural X-ray study [135, 167] but were overlooked as DHBs until Richardson et al. conducted a search on the CSD looking for complexes with $N-H\cdots H-B$ distances less than 2.2 Å,[219] as exposed in section 1.2.1. Indeed, the solid structure of BH_3NH_3, a molecular crystal, has been studied and checked for a long time in literature, not only experimentally but theoretically as well. Lippert and Lipscomb [167] used X-ray to determine the structure of ammonia borane at room temperature and deducted it to have a body-centered tetragonal structure, which was later supported by Hughes.[135] Nevertheless, Sorokin and co-workers published in their results that BH_3NH_3 structure was face-centred orthorhombic unit cell.[247] Hoon and Reynhardt used powder X-ray data for BH_3NH_3 both to confirm that the body-centered tetragonal structure at room temperature and also to show that the compound undergoes a phase transition to a low-temperature primitive orthorhombic form at ca. 200 K, also in the primitive orthorhombic space group.[49, 34, 132] Klooster and co-workers refined the boraneamine structure using neutron diffraction scattering and established that the structure of boron and nitrogen atoms is reversed from the ones published in the last studies, being boron paired with nitrogen and not a boron-boron/nitrogen-nitrogen pair.[149]

Although tridimensional solid state BH_3NH_3 structure is well defined, the interactions keeping it altogether are not so deeply studied. The hydrogen interactions within a single BH_3NH_3 molecule are of a σ-bond type: three hydrogens bonded to the boron atom, giving them hydride character, and three hydrogens bonded with the nitrogen, giving them the acid properties.[143] Boron is bonded to nitrogen through a dative bond, formed by the donor-acceptor complex between the lone pair of electrons from NH_3 and the *2p* empty orbital of BH_3.[7] Intermolecular interactions can be set between different atoms or groups of atoms. Long distances and sterical impediments prevent boron and nitrogen atoms from different molecules to interact. A classical hydrogen bond between the acidic hydrogen from the amine group and boron is discarded as well, as the interaction distance is again too long. The most sterically probable interaction is the weak dihydrogen bond between the proton from the NH part and the hydride from BH, as pointed out by Cramer [66] and later Klooster [149]. Klooster and co-workers discussed that in principle, a classical hydrogen bond should be strong enough to hold the crystal altogether depending on the species involved (see table 1.4) if the acceptor was a strong one. But weaker acceptors like π-bonds yield to weaker interactions and are worse interacting with acidic hydrogens,[162] and thus the interaction which could be established between the much weaker σ-bond acceptor should be null and the crystal would be not stable at room temperature. Klooster found out that the interaction which takes place is actually a dihydrogen bond, but they could not be sure if it was a σ-type. Four years earlier Richardson and co-workers had studied—combined with their CSD search for DHBs—the $[BH_3NH_3]_2$ dimer using PCI-80/B3LYP methodology and the optimized geometry found had features seen in other typical boron compounds. A particularly interesting aspect of these bonds with boron is that a linear $B-H\cdots H-X$ arrangement is an exception. The boraneamine dimer has a calculated $B-H-N$ angle of 98.8° and $N-H-H$ is 158.7°. Although bent bonds were observed in other cases for weak bonds, here they seem to be the rule. An explanation lies in the large negative charge carried by the boron atom, compared to the small negative charge carried by the hydrogen. In order to take advantage of the charge distribution, the $H-N$ points toward the $B-H$ bond rather than toward H.

Then again, BH_3NH_3 has remarkable solid/gas structural differences and is not suitable to study it as a single gas molecule and extrapolate the results to solid state. Differences between solid and gas states in other weak donor-acceptor complexes have been discussed in many works [49, 52, 143, 149, 161, 209, 216, 219, 236, 238, 257, 276] and boraneamine has the less sig-

nificant structural differences due to its strong $B-N$ bond. This complex has a shorter $B-N$ bond length in the solid (1.58 Å [149]) than in the gas phase (1.657 Å [257]). Yokoyama and co-workers noted that the dihydrogen bonding might play an important role in molecular aggregations affecting crystal packing and supramolecular assembly.[276] In the case of BH_3NH_3, it has the proton from the amine group partnering with the hydride from the borane group, providing the means of self-association. Merino et al. studied the boraneamine molecule, and furthermore the dimer, trimer and tetramer aggregates, applying the atoms in molecules theory and the topological analysis of the electron density.[179] The PESs obtained were flat and with various stationary points, similar to these of DHB (see chapter 3), and distances between hydrogens at the aggregates systems were less than the van der Waals radi of hydrogen. The electron density analysis showed bond critical points only along the shorter $H\cdots H$ directions, although hydrogens are geometrically set on the triangle vertices, and closed-shell interactions (see chapters 4 and 5). Besides, they also found ring critical points in the cells formed by the interacting hydrogens. Their final conclusions were that the cooperative dihydrogen interactions are not the main organizing factors in the molecular aggregations, but dipole-dipole interactions are.

Previous results published in this thesis indicate that the interactions that hold the boraneamine crystal together are possibly dihydrogen bonds, as Merino et al. suggested. However, this study is focused on simulating a whole crystal using *ab initio* periodic methods, not only a portion of it. Morrison and Siddick performed the first boraneamine crystal modelling approach using plane waves density functional theory.[186] The average interactions inside the solid-state structure their models showed were dihydrogen bonds of the weak kind. In the boraneamine crystal, each hydrogen could interact with more than two hydrogens from other molecules and thus leading to a more attractive energy within the lattice and a stronger crystal. BH_3NH_3 is a relatively simple structure and has a small unit cell which allows to perform a large number of calculations with a small computational cost associated. Geometries, energies and $M-H$ frequencies will be calculated in order to obtain data about the intermolecular interaction type and to clarify if the crystal presents DHBs and if they are important to its binding. The downside of the periodic *ab initio* method is that right now the topological analysis and use of the Kohn-Sham density functional theory are not implemented, thus depriving from good characterization parameters. The theoretical geometries will be compared with the experimental data, not to reproduce them, as this would mean to include long-range dispersion effects that are missing in the functionals used here,[268, 273, 274],

but for a better study completness.

6.2 Methodology

All calculations in this chapter were made using the CRYSTAL03 periodic code.[233] CRYSTAL is able to use local Gaussian-type orbitals (GTO) as basis sets in all crystalline levels: molecules, one-dimensional periodic polymers, two-dimensional periodic surfaces (*slabs*), and three-dimensional crystals (*bulks*).

The selection of Gaussian-type orbitals or plane waves basis sets depend on the level of accuracy desired and computational power at hand. Both types of basis sets have different properties which make them able to describe some systems better than others. Plane waves were commonly used in former calculations on periodic systems as their computational time expense was lesser than using Gaussian-type orbitals. Energies and geometries converge faster and accuracy is achieved introducing a pseudopotential to account for core electrons. In PW there are only Hellmann-Feyman forces present, in contraposition with GTOs where the calculation of Pulay forces consumes much more time and their implementation is more complex. Plane waves are easier to define with the inclusion of the electronic kinetic energy cutoff E_{kin}, a single parameter. The larger the E_{kin}, the better the basis set. GTOs, on the other hand, are more difficult to adjust for condesed matter systems. In particular, the diffuse functions overlapping in the GTOs could cause linear dependence problems if exponents are not correctly set. One of the most interesting characteristics of PWs is that they do not include the BSSE effect. It is worth using them while studying systems presenting weak interactions as the energies and geometries do not need to be corrected. On the other hand, GTOs do have BSSE but this effect can be corrected using the counterpoise method, explained in chapter 2.3.2. As stated before, the counterpoise effect is an *a posteriori* method and thus the corrected energy could not correspond to a stationary point. CRYSTAL03 includes a BSSE correction based on the counterpoise method, but does only a point correction and not a whole corrected PES optimization.

But although PWs do not have BSSE, they create other artifacts. Plane waves occupy the whole space where the molecule is modelled, a periodic wave repeating uniformly through all three dimensions, whenever the system modelled is a molecule, a slab or a polymer. This causes specious results as electronic interactions between molecules or slabs and their replica images are created. Using Gaussian-type orbitals the dimensionality of the system is

complied and such artifacts are not present. While energies and geometries converge faster, they require to store much more data when norm-conserving potentials were adopted. Finally, plane waves can be used in hybrid functionals but at high computational costs because of the Fock-exchange; and even now, the number of PWs used in those methods is limited. That can be a turndown as hybrid functionals like B3LYP are more accurate than the standard GGA functionals. GTOs, on the other hand, allow exact exchange calculations as well as hybrid functionals.

The basis set chosen in this work was the Gaussian-type orbital 6-311G(d,p) as recommended by Tosoni et al. [259]. It is well balanced between BSSE effect and computational costs. Bigger basis sets only increase the computational time without obtaining more accurate results.[39] Plane waves were discarded as the computational costs to avoid periodic images were bigger than those of the GTOs, although not having BSSE could have been a major advantage.

Choosing an appropriate functional to model systems with a hydrogen interaction in their structure is primordial as former studies have shown.[260, 261, 262] Five different functionals have been chosen to model the boraneamine periodic system in its different dimensional geometries: HF, B3LYP,[156, 19] PW91,[207] PBE[206] and PBE0. Studies on alcoholic molecules with hydrogen bond interactions report that B3LYP is more reliable than PW91,[199, 262] and another work using formic acid and urea as test crystal structures report that structural features are well reproduced by hybrid methods and GGA.[63] Specifically, for acid formic and urea, results of structure, BSSE-corrected interaction energies and vibrational analysis show that hybrid methods are more accurate than HF and both LDA and GGA functionals, with a trend in the computed properties similar to that already described in the hydrogen bonded molecular complexes. But although dihydrogen bonds resemble to hydrogen bonds (see former chapters), one of the scopes of this work is to obtain more data for a better discussion of the results. For further computational details, see appendix C.

Specifically previous *ab-initio* works on formic acid and urea, although not dihydrogen bond examples, with these functionals in a periodic structure depict a good reproduction by hybrid methods and GGA.

6.3 Results and discussion

Molecular structure of boraneamine is depicted in figure 6.1. Reference boraneamine molecule has been optimized at different levels of theory in order to have data to compare to the crystallographic structure, and computed distances and angles can be found in table 6.1. The boraneamine crystal has an orthorhombic lattice and falls into the $Pmn2_1$ space group, with 2 molecules in the conventional cell. The initial parameters used in the calculations are taken from the experimental results of Klooster and coworkers in determining the BH_3NH_3 structure using neutron diffraction techniques.[149] Figure 6.2 shows the ammonia borane crystal with the unit cell. Moreover, calculations on the boraneamine slab have been made as well in order to complete the experiment as a two-closest-molecule thick layer on the [010] plane.

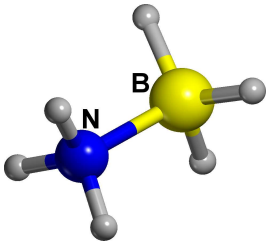

Figure 6.1: Boraneamine molecule.

Table 6.1: Distances (Å) and angles (degrees) of the BH_3NH_3 molecule, optimized at different levels of theory.

	HF	B3LYP	PW91	PBE	PBE0
		Distances			
N – H	1.003	1.019	1.025	1.026	1.016
B – H	1.208	1.210	1.217	1.219	1.213
N – B	1.687	1.668	1.656	1.657	1.647
		Angles			
B – N – H	110.6	111.0	111.2	111.2	110.9
N – B – H	104.4	104.6	104.8	104.9	105.0

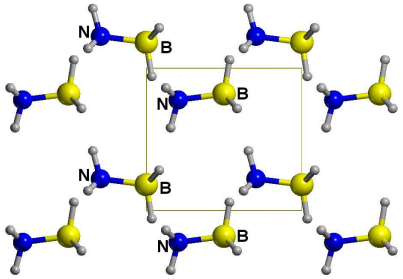

(a) [100]

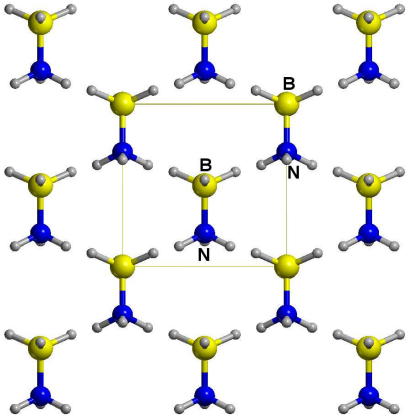

(b) [010]

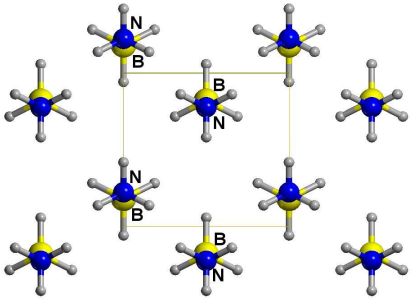

(c) [001]

Figure 6.2: Boraneamine crystal structures oriented at different planes, Miller indices indicated. Unit cell defined by thin lines.

6.3.1 Structure analysis

Relevant geometric parameters for the ammonia borane crystal dihydrogen bonds, theoretical and experimental data from citation [149], are listed in table 6.2 and their reference nomenclature for the different molecules, atoms, bonds and angles can be seen in figure 6.3. Due to the the point group of ammonia borane, symmetry restrictions produce some of the $N-H$, $B-H$ and $H\cdots H$ distances are equal although they are from different hydrogens and repeat in different ways in the crystal. In this case, there are two different bonding distances for each hydrogen-nonmetal pair, i.e. $B-H$ and $N-H$. Distances and angles in table 6.2 have been grouped, and thus the $N-H_{b,c}$ row means that the bonding lengths between $N-H_b$ and $N-H_c$ are equal at the same level, experimental or theoretical.

Comparing the intramolecular crystalline distances to the molecular ones there is a minuscule elongation of the $N-H$ and $B-H$ bond length in the crystal, from 0.001 Å of the $N-H$ at HF level to 0.014 Å of the $B-H$ at PW91 and PBE, opposed to a more significant shrink in the $N-B$ distance, from 0.066 Å at HF to 0.056 Å of the PW91, PBE and PBE0. These variations in the bonding are in agreement with the BH_3NH_3 molecule establishing an interaction with the surrounding molecules. As explained in section 3.3, when molecules interact with each other by means of a dihydrogen bond, as this should be the case, the trend is to elongate their hydrogen covalent bonding distances. On the rebound, the bonds next to those elongated are prone to shorten due to an electron density redistribution (see section 4.3). In this case, although the difference between the distance in the molecule and in the crystal is near to negligible in HF, the shortening of the $N-B$ bonds is more important as it collects the small contributions of all six covalent bonds with hydrogens which have been modified. As for angles, their change is not more than two or three degrees from the isolated molecule to its integration within the crystal. Changes in angles are not known to be notorious as for setting in a DHB, as it is in the boraneamine crystal which gets at least flatter as changing angles tend to increase. The bigger changes are in the borane angle ($N-B-H$), at PW91 and PBE at its maximum, as the $B-H$ distance is longer than the $N-H$ and makes the $N-B-H$ more sensible to variation.

Theoretical results behave accordingly to their original Hamiltonian. Hybrid functional methods (i.e. B3LYP, PW91, PBE and PBE0) have much more similar results compared to HF, as expected. Globally, theoretical results nearly match with the experimental ones. All theoretical methods overestimate the cell boundaries and bonding distances at the intramolecular level,

Table 6.2: Experimental and optimized geometries of the BH_3NH_3 crystal. Distances in Å and angles in degrees. Refer to figure 6.3 for the hydrogens subindeces. Hydrogen atoms H_b and H_c are equivalent in symmetrical terms, as H_d and H_e, and so are the geometric values.

	Experimental [149]	HF	B3LYP	PW91	PBE	PBE0
			Cell parameters			
a	5.40(2)	5.723	5.350	5.283	5.316	5.373
b	4.89(2)	5.173	5.053	4.976	4.969	4.951
c	4.99(2)	5.448	5.412	5.344	5.296	5.214
			Intramolecular distances			
$N-H_a$	1.07(4)	1.004	1.022	1.028	1.029	1.019
$N-H_{b,c}$	0.96(3)	1.006	1.025	1.034	1.035	1.024
$B-H_f$	1.15(3)	1.219	1.222	1.231	1.233	1.226
$B-H_{d,e}$	1.18(3)	1.214	1.215	1.223	1.225	1.219
$N-B$	1.58(2)	1.621	1.608	1.600	1.601	1.591
			Intermolecular distances			
$H_a\cdots H_{d,e}$	2.21(4)	2.488	2.286	2.245	2.243	2.279
$H_b\cdots H_e$, $H_c\cdots H_d$	2.23(4)	2.451	2.302	2.211	2.220	2.215
$H_f\cdots H_{b,c}$	2.02(3)	2.181	1.956	1.895	1.904	1.938
			Intramolecular angles			
$B-N-H_a$	106(4)	111.8	112.4	112.6	112.6	112.5
$B-N-H_{b,c}$	111(2)	111.3	111.2	111.1	111.1	111.0
$N-B-H_f$	114(2)	106.6	106.5	106.6	106.6	106.7
$N-B-H_{d,e}$	112(1)	107.4	108.3	108.7	108.7	108.6
			Intermolecular angles			
$N-H_a\cdots H_{d,e}$	130(1)	131.6	133.0	133.3	132.6	132.4
$N-H_b\cdots H_e$, $N-H_c\cdots H_d$	137(2)	137.4	136.4	135.5	135.5	135.2
$N-H_{b,c}\cdots H_f$	156(3)	163.7	162.6	160.7	160.1	159.8
$B-H_d\cdots H_a$	156(3)	162.3	161.4	160.0	160.0	159.2
$B-H_f\cdots H_{b,c}$	106(1)	104.6	104.2	101.9	101.8	101.3

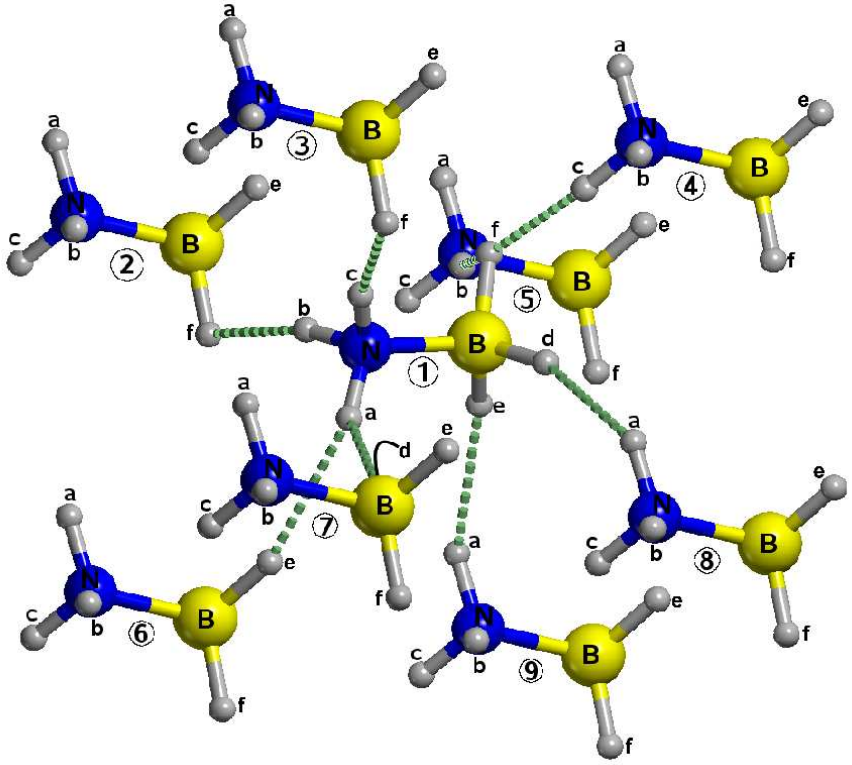

Figure 6.3: Detail of one molecule of the boraneamine crystal interacting with its eight neighbours. Hydrogens have been arbitrarily named clockwise on the [001] plane, starting from the hydrogen bonded to the nitrogen with a different bonding distance.

except for the $N - H_a$ bonds, which are underestimated. The closest distances obtained with a modelling method to the experimental ones come from HF method for nonmetal-hydrogen bonds, but the hybrid methods describe better the $N - B$ covalent bond. It is interesting to note that the $N - B$ dative bond is shorter in the crystal than in the molecule. Allis et al. proposed this effect was due to the short-range dipole-dipole interactions in the molecular ammonia borane crystal.[7] Regarding the cell parameters, differences are more acute than the ones in the bondings but otherwise small, although hybrid methods

get closer to the experimental data than HF. Angles show a different tendency. The $B-N-H_{b,c}$ angles at all levels of theory match to the experimental one, but the other ones have a difference around 6 degrees, leading to wider angles at $B-N-H_a$ and narrower at $N-B-H_{d,e,f}$.

Looking at the intermolecular parameters, it can be seen that they behave accordingly to the intramolecular ones. There is a similitude between parameters from hybrid functional origin with respect to the HF data. Again, angles have a variation compared to the experimental values of 6 degrees or less. Morrison and Siddick obtained shorter intermolecular $H\cdots H$ and $B-N$ bond lengths using plane waves, the intermolecular ones between 1.909 and 2.271 Å and the boron-nitrogen at 1.580 Å.[186] Predicted distances between the closer hydrogens from neighbouring molecules are longer than those experimental, except for the hydrogen bonded to the boron, $H_f\cdots H_{b,c}$, which are shorter. Experimental figures corroborate that the length of the $H_a\cdots H_{d,e}$ bond is similar to those of the $H_f\cdots H_b$ and $H_c\cdots H_d$, with 2.21 and 2.23 Å respectively, which renders the crystal as a continuous grid of molecules equally separated through all the space. However, the difference between these lengths in the theoretically modelled system ranges from 0.3 to 0.4 Å, and the system is no longer homogeneous because one layer of molecules is significantly closer to one of its neighbours on the [100] plane (see figure 6.2a for reference). On the other planes the distances are kept more or less constant and it can be considered that molecules are equally spaced. The gap can be thought as a model artifact, but the fact that all Hamiltonians yield to the same results, within a reasonable interval and all checked as minima, makes the unevenly separated layers model plausible. Extra tests with different Hamiltonians (BLYP, LDA-P86) were preformed obtaining similar geometries, but again they belong to the DFT methods. A possible explanation can be found at the interactions set on the different distances. The hydrogen H_b from molecule ① is near to H_f and H_e from the same molecule ② (distances in the 1.895 Å at PW91 to 2.451 at HF range). On the other hand, the two hydrogens at the same distance from H_a are H_d and H_e, from molecules ⑦ and ⑥ respectively. The next closest ones are H_e from molecule number ⑦ and H_d from number ⑥ which stand around 4 Å. Interactions at such a long distance are not much probable, especially if there are hydrogens at half this length. Thus, having a closed four-atom ring ($\overline{H_e\cdots H_b\cdots H_f-B}$) suggests a stronger interaction than a hydrogen interacting with two others without closing a ring. The interaction energies will be further discussed in the next section 6.3.2.

In order to have a deeper insight on the crystal nature, a slab consisting

of the two closest layers of borazane on the [010] plane was modelled and optimized. The objective is to compare it with the crystal geometry, mainly to check the behaviour of hydrogens H_a, H_d and H_e which in this system will not interact with other hydrogens. The starting geometries were obtained from the optimized crystal at its different levels of theory and results are shown in table 6.3.

Analyzing collected data, HF and DFT methods lead, again, to similar results in intramolecular lengths and angles but show a different tendency for the intermolecular ones, the DFT methods being less different to each other than to HF. The deletion of the molecules in one of the three dimensions over which the crystal spreads out is expected to produce an expansion of the minimum energy cell and the molecules within in the other two dimensions and a constriction in the deleted one.[77] As it can be seen in table 6.3, the expansion is more acute at the cell borders and intermolecular bonds and angles than at the intramolecular bonds and angles. The $N-H$, $B-H$ and $N-B$ covalent bonds length variations with respect to the crystal geometry are zero or close to zero, whereas the $H_f \cdots H_{b,c}$ elongate up to 0.1 Å or more in the DFT methods. On the other hand, $H_b \cdots H_e$ and $H_c \cdots H_d$ interactions shorten more appreciably than the latter. These interactions are nearly parallel to the c border in whose direction the crystal no longer replicates, and the attraction from the surrounding molecules along the c axis has disappeared. The other two cell boundaries, a and b, stretch and become larger as well in order to accommodate the lengthening of the dihydrogen bonds. The only value which does not to grow is the b side calculated at HF level, which shrinks imperceptibly. Angles have a similar tendency as distances: intramolecular angles do not change or change less than one degree, while intermolecular angles bend to more narrower geometries as the $H \cdots H$ increase as well.

6.3.2 Bonding energy analysis

A close-packed crystal structure as boraneamine produces a high number of possible interactions between hydrogens, let alone other atoms. Long-range interactions are part of the crystal and part of its lattice energy. The theoretical methods herein used do not treat this long-range interactions and so a cutoff has been decided in order to define a dihydrogen bond. Most authors [158, 197, 219, 65, 64, 149] set the distance between hydrogens of a dihydrogen bond around 1.7–2.2 Å, shorter than the van der Waals radius of a hydrogen atom, but in former chapters of this thesis it has been demonstrated that DHBs can

Table 6.3: Experimental and optimized geometries of the BH_3NH_3 slab. Text in italics are the variation percentage of the above parameter relative to the crystal equivalent. Distances in Å and angles in degrees. Please refer to figure 6.3 for the hydrogens subindeces.

	HF	B3LYP	PW91	PBE	PBE0
Cell parameters					
a	5.888	5.714	5.670	5.679	5.733
	2.9	*6.8*	*7.3*	*6.8*	*6.7*
b	5.149	5.197	5.079	5.056	5.008
	-0.5	*2.8*	*2.1*	*1.8*	*1.2*
Intramolecular distances					
$N - H_a$	1.004	1.019	1.025	1.026	1.017
	0.0	*-0.3*	*-0.3*	*-0.3*	*-0.2*
$N - H_{b,c}$	1.006	1.025	1.035	1.036	1.025
	0.0	*0.0*	*0.1*	*0.1*	*0.1*
$B - H_f$	1.221	1.222	1.229	1.232	1.225
	0.2	*0.0*	*-0.2*	*-0.1*	*-0.1*
$B - H_{d,e}$	1.213	1.215	1.223	1.226	1.219
	-0.1	*0.0*	*0.0*	*0.1*	*0.0*
$N - B$	1.624	1.613	1.605	1.605	1.595
	0.2	*0.3*	*0.3*	*0.2*	*0.3*
Intermolecular Distances					
$H_b \cdots H_e$, $H_c \cdots H_d$	2.492	2.164	2.043	2.045	2.061
	1.7	*-6.0*	*-7.6*	*-7.9*	*-6.9*
$H_f \cdots H_{b,c}$	2.200	2.051	2.010	2.014	2.048
	0.9	*4.9*	*6.1*	*5.8*	*5.7*
Intramolecular angles					
$B - N - H_a$	112.4	112.7	111.0	113.9	113.3
	-0.5	*-0.3*	*1.4*	*-1.2*	*-0.7*
$B - N - H_{b,c}$	111.4	111.1	112.6	110.8	111.0
	0.0	*0.0*	*-1.4*	*0.3*	*0.0*
$N - B - H_f$	105.9	106.3	106.1	105.8	106.2
	0.7	*0.2*	*0.5*	*0.8*	*0.5*
$N - B - H_{d,e}$	107.4	107.9	108.3	108.6	108.4
	0.0	*0.4*	*0.3*	*0.1*	*0.2*
Intermolecular angles					
$N - H_{b,c} \cdots H_f$	157.5	105.8	146.6	146.7	146.5
	-19.7	*-20.5*	*-10.0*	*-10.6*	*-10.6*
$B - H_f \cdots H_{b,c}$	103.7	95.8	91.9	92.0	91.9
	0.9	*8.0*	*9.8*	*9.7*	*9.2*

be formed even at a longer distance. For those reasons, the dihydrogen bonds cutoff has been set at 2.5 Å between two molecules. The geometry of the BH_3NH_3 crystal discussed in the last section included $H \cdots H$ bond lengths between 1.895 and 2.488 Å. From this upper value, the next possible contact is at more than 3 Å, and it is discarded. With these parameters, there are only 10 possible DHBs contacts, six of which are paired and have a common hydrogen from the ammonia. These interactions are in table 6.2 and depicted in figure 6.3, except the $H_b \cdots H_e$ and $H_c \cdots H_d$ interactions are not depicted.

There are different possible approaches to calculate the DHB interaction energy $E_{H\cdots H}$. One of them is to consider that all of the interactions have the same energy, no matter which distance separates the hydrogens. To calculate it, the energy of one standing-alone optimized borazane molecule $E_{molecule}$ is substracted from the total energy of the crystal cell E_{cell}, leaving the energy of the intermolecular interactions which is then divided by the number of bonds inside the crystal, including those bridging two different cells. In the working example there are two molecules per unit cell which hold twelve DHBs, half of them inside the cell, the other six crossing the borders of the defined cell.

$$E_{H\cdots H} = \frac{E_{cell} - 2E_{molecule}}{12} \tag{6.1}$$

A single point counterpoise correction has been also applied to the optimized bonding energies in order to correct the BSSE. The method is similar to that explained in section 2.3.2 but as it is a periodic system, the extension of the ghost atoms to the whole crystal has some computational and methodological problems. Instead, a zone of ghost atoms is defined and used as an approximate result to the energy of the molecule in its extended basis set. To calculate the mean energy of one bond for this system can be expressed as

$$E^{CP}_{H\cdots H} = \frac{E_{cell} - 2E_{mol|GHOST} + 2E_{mol|CRY} - 2E_{molecule}}{12} \tag{6.2}$$

where $E_{mol|GHOST}$ refers to the energy of one boraneamine molecule in the crystal geometry and neighbouring atoms as ghosts, $E_{mol|CRY}$ is the energy of the boraneamine molecule at crystal geometry, $E_{molecule}$ is the energy of the isolated molecule and E_{cell} the energy of the crystal cell. The molecule referred energies are multiplied by two as there are two identic molecules in the crystalline cell. Were this not the case, the terms should be splitted and would be different for each molecule.

Results for each level are under the *Mean* column in table 6.4. For this energetic distribution the bond strengths are overestimated for the long dihy-

Table 6.4: Dihydrogen bond interaction energies in the optimized boraneamine crystal at different levels of theory, in kcal/mol. $E_{H\cdots H}$ columns refer to the interaction without taking into account the BSSE correction and $E^{CP}_{H\cdots H}$ columns include the BSSE using the counterpoise correction.[39] Under the *Mean* column fall the interaction energies of the DHBs considering that all of them contribute the same amount to the crystal. The other two columns list the interaction energies of the bondings between specific hydrogens.

	Mean		$H_a\cdots H_{d,e}$		$H_f\cdots H_{b,c}$, $H_b\cdots H_e$,$H_c\cdots H_d$	
	$E_{H\cdots H}$	$E^{CP}_{H\cdots H}$	$E_{H\cdots H}$	$E^{CP}_{H\cdots H}$	$E_{H\cdots H}$	$E^{CP}_{H\cdots H}$
HF	-2,21	*-1,97*	-1,03	*-0,92*	-2,80	*-2,49*
B3LYP	-2,81	*-2,36*	-1,26	*-1,07*	-3,58	*-3,12*
PW91	-3,54	*-3,00*	-1,66	*-1,43*	-4,48	*-3,76*
PBE	-3,41	*-2,89*	-1,57	*-1,35*	-4,34	*-3,65*
PBE0	-3,21	*-2,80*	-1,43	*-1,25*	-4,11	*-3,57*

drogen bonds ($H_a\cdots H_{d,e}$) and underestimated for the short ones ($H_f\cdots H_{b,c}$). Their ranges do not fall outside the interval of the molecules studied in previous chapters. In any case, they can not be compared straightly to the borane data (table 3.4 as ammine borane has a covalent bond which makes its electronic distribution different. Plane wave DFT modelling from Morris and Siddick lead to similar mean interaction energies of 12.7 kJ/mol (3.0 kcal/mol).[186] Even so, there is a relation between distance and bond energy: longer bonds have higher energy (less energy). Counterpoise correction increases the bond energy around a half of a kcal. per mol for the DFT methods and less than a quarter of kcal/mol for the HF Hamiltonian. The amount of BSSE is bigger than in other cases of isolated molecules, like the $M-H\cdots H-X$ series in chapter 3.

In order to differentiate the energy contribution to the various bonds inside the crystal, another method has been used. A slab has been cut from the crystal with the same composing molecules and dimensions as that described in table 6.3—cut along the [010] plane between molecule ① and molecules ⑥, ⑦, ⑧ and ⑨. A single point energy calculation from the optimized crystal has been made on this structure. This slab does not have the interactions from $H_a\cdots H_{d,e}$ dihydrogen bonds, but all the others. Thus, if the energy of the crystalline cell E_{cell} is substractd from the energy of this slab $E_{slab|CRY}$, it

results to the whole energy of all of the dihydrogen bonds plus the long-range interactions in the cut axis of the slab, the c axis. The long-range interactions are small enough, especially with the Hamiltonians used, and the contributions to the slab-slab energy can be approximated only to the dihydrogen bonds. As there are four DHBs crossing the [010] plane, four "halves" for each side, the gross total should be divided by four:

$$E_{H_a \cdots H_{d,e}} = \frac{E_{cell} - E_{slab|CRY}}{4} \tag{6.3}$$

Note that this interaction energy does not include the relaxation term usually included in the bonding energy definition, as it uses the slab in the crystal geometry, not the optimized isolated molecule. Using the optimized slab energy would not either lead to the proper binding energy as there are other interactions which deform the original boraneamine molecule. On the other hand, using an isolated molecule will not allow the differentiation with the rest of the dihydrogen bonds.

A similar approach could be used to calculate the $\mathrm{H}_b \cdots \mathrm{H}_e$, $\mathrm{H}_c \cdots \mathrm{H}_d$, both with the same length, and $\mathrm{H}_f \cdots \mathrm{H}_{b,c}$. But the problem is that the definition of the slab cell, which has to measure the same dimensions as the crystal, is not possible without breaking a $\mathrm{B} - \mathrm{H}$ or a $\mathrm{N} - \mathrm{H}$ bond in a molecule. Besides, there will be two different $\mathrm{H} \cdots \mathrm{H}$ bonds broken. Alternatively, the method used to calculate the bonding energy of these interactions uses the energy of the slab previously calculated from which the energy of the molecules forming the slab cell is substracted. The energy obtained contains the intermolecular interactions and the long-range interactions, which are considered negligible in front of the bonding energies. The intermolecular interaction energy is then divided by the number of bonds contributing to it. This slab has two molecules and eight dihydrogen bonds per cell, thus:

$$E_{H_f \cdots H_{b,c}} = E_{H_b \cdots H_c} = E_{H_c \cdots H_d} = \frac{E_{slab|CRY} - 2E_{molecule}}{8} \tag{6.4}$$

In this case the bonding energies include the relaxation term as it uses the optimized isolated boraneamine molecule to calculate the dihydrogen interactions. Moreover, a distinction between $\mathrm{H}_f \cdots \mathrm{H}_{b,c}$ and both $\mathrm{H}_b \cdots \mathrm{H}_c$ and $\mathrm{H}_c \cdots \mathrm{H}_d$ could not be done, although they have different bond length and theoretically each group should have different bonding strength. Counterposie correction has been applied as well to the bonding values using the same method summarized in equation 6.2, but changing the parameters for

the corresponding ones of number of bonds and energies of the crystal, slab, and molecules with and without ghost atoms.

Data from the processes described above is collected under the last columns of table 6.4. As it can be seen, the $H_a \cdots H_{d,e}$ interaction energy approximately halves the bonding energy of all Hamiltonians under the *Mean* column. This difference should be bigger due to the relaxation term, not included in the $H_a \cdots H_{d,e}$ interaction. The BSSE correction rises the interaction energy from 0.1 kcal/mol for HF to 0.23 kcal/mol for PW91, making the interaction weaker. The $H_a \cdots H_{d,e}$ interaction has a longer bond distance in all cases except at B3LYP. Hence, the dihydrogen interaction energies for $H_a \cdots H_{d,e}$ should be the weakest in the crystal. The other listed DHBs are stronger, but they cannot be compared directly as they have different bond length and possibly different bonding energies as well. $H_b \cdots H_c$ and $H_c \cdots H_d$ are longer than $H_f \cdots H_{b,c}$ and should contribute less to the arithmetic mean. PW91, PBE and PBE0 give bigger energies than B3LYP and HF, being the latter the smaller one. The BSSE corrected energies have a similar trend: DFT methods have bonding energies stronger than HF, being PW91 the strongest. The BSSE correction varies around 0.1 and 0.25 kcal/mol which is similar to the values applied to the $H_a \cdots H_{d,e}$ interaction. Still, this BSSE corrected energies are an arithmetic mean calculation, and energies should be different for each distance. The grand total for each interaction energy is 11.8 kcal/mol for HF and between 14.2 and 18 kcal/mol for the DFT methods, having B3LYP the smaller correction and PW91 the bigger. This is not an important error compared to the total binding energy, as it has been intended in choosing the basis set, although the interactions are of a DHB type. This can be possible due to the fact that there are a high number of DHBs formed inside the crystal whose individual flat and shallow PESs add up to make a deeper potential well, with less BSSE.

6.3.3 Dihydrogen bond frequencies analysis

In this last section, $B-H$ and $N-H$ anharmonic frequencies are used to study how do they vary in the crystal with respect to the isolated molecule, as they are a good indicator of the bonding formation and its strength. The $N-H$ stretching frequencies usually fall into the $\sim$3500–3700 cm^{-1}, while $B-H$ stretching falls into the 2500 cm^{-1} region. In table 6.5 there are the stretching anharmonic frequencies for the different Hamiltoninans for the BH_3NH_3 molecule and crystal. Molecular stretching frequencies fall into the aforementioned ranges: $N-H$ frequencies are between 3325 and 3661 cm^{-1} and $B-H$

between 2388 and 2502 cm^{-1}. Meng and coworkers obtained similar results for the ammonia borane molecule and dimer at B3LYP level with a bigger base.[178]

Table 6.5: Anharmonic frequencies (in cm^{-1}) for the $N-H$ and $B-H$ stretching modes in the BH_3NH_3 molecule and crystal at their optimized geometries. Numbers in italics are the frequency shift with respect to the free boraneamine molecule for the crystal.

	Molecule	Crystal		Molecule	Crystal	
	$N-H$	$N-H_a$	$N-H_{b,c}$	$B-H$	$B-H_{d,e}$	$B-H_f$
HF	3661	3648	3617	2502	2491	2399
		-14	*-44*		*-11*	*-103*
B3LYP	3406	3366	3284	2432	2420	2323
		-41	*-122*		*-12*	*-109*
PW91	3329	3272	3142	2395	2369	2277
		-57	*-187*		*-26*	*-118*
PBE	3325	3269	3143	2388	2364	2273
		-56	*-182*		*-24*	*-115*
PBE0	3459	3415	3307	2443	2416	2327
		-44	*-153*		*-26*	*-115*

As well as the molecular frequencies, in table 6.5 there are the data for each of the particular $X-H$ bond stretching in the crystal. Under them there are their differences with molecular values in italics. In all cases HF leads to higher frequencies than DFT methods. The $N-H$ stretching frequency is similar amongst the DFT methods, less than 150 cm^{-1} in both types of hydrogen, and about 200 cm^{-1} between HF and the highest DFT frequency. $N-H_a$ frequencies change less than the $N-H_{b,c}$, and the most acute change occurs in the DFT methods, while HF changes from one third to one fourth of the total DFT variation. $N-H_{b,c}$ has the biggest frequency difference between DFT and HF: 310 cm^{-1} for the PBE0 compared to HF. As for the $B-H$ group, differences between DFT methods and HF are not so important. All molecular frequencies move in a range of 59 cm^{-1}, less than the $N-H$ ones, which is a trend even in the crystalline frequencies. All DFT methods for $B-H_{d,e}$ fall inside the 56 cm^{-1} region and there is a difference 71 cm^{-1} between B3LYP and HF, which is not much. A similar trend is shown for $B-H_f$, where DFT are similar around 54 cm^{-1} and HF is 72 cm^{-1} higher than PBE0.

Focusing on the frequency changes in the crystal and the molecule, hydrogen bonds usually produce a decrease in the value of the $X-H$ stretching with respect to its free counterpart, broadening at the same time its vibrational band. As for dihydrogen bonds, there are reported both red and blue-shifted changes.[5] Meng and coworkers reported that IR intensities for the BH_3NH_3 dimer modelled with the B3LYP Hamiltonian decrease when DHBs are formed.[178]. Furthermore, there is a good correlation between the shift and the strength of the bond.[74] Remember the hypothesis from the last section that H_a interacts with hydrogens H_d and H_e, while H_b and H_c interact with H_f as well as with H_d and H_e. In this case, it can be seen that in all levels of theory there is a shift to the red, more or less acute. Thus, molecules interact with each other in the crystal and as the variation is different for each ammine and borane hydrogens, interactions should be different. The smaller change are in the $N-H_a$ and $B-H_{d,e}$, while the bigger ones happen at the $N-H_{b,c}$ and $B-H_f$ stretching frequencies. It can be induced that the former hydrogens are entangled in weaker interactions than the latter. The frequencies variations are in accordance with the interaction energies obtained in table 6.4. The $H_a\cdots H_{d,e}$ has a weaker interaction energy and the involved hydrogen have a lesser change in the anharmonic frequencies, while the other interactions are stronger and their change in the stretching frequencies are bigger. This ties in with distances too: bond with longer distances usually have smaller frequency changes as their energies are smaller. HF shifts are lower than DFT shifts, in agreement with their lower interaction energy results. As it has been stated before, the $H_b\cdots H_c$, $H_c\cdots H_d$ and $H_f\cdots H_{b,c}$ interaction energies can not be differentiated and frequency results do neither shed a light on this issue. There is a fit between the sum of all their interactions energies and their frequency shift, but otherwise the exact proportion of the shift produced by one interaction or the other remains unknown.

6.4 Conclusions

The present theoretical study on the amminoborane crystal shows that dihydrogen bonds are present amongst its constituent molecules and act as cohesive forces in the crystal. These dihydrogen bonds have different lengths and strengths as evidenced by the anharmonic frequency shifts. There is an inverse proportionality relation between the anharmonic frequency shifts and the interaction strength. The lengths and strengths of these interactions are typical for a dihydrogen bond type of interaction. The crystal structure has

been studied using different Hamiltonians including HF and DFT methods showing that the latter methods group are more similar to each other than to HF. However, DFT methods still tend to underestimate the interaction energy and to elongate the $H \cdots H$ distances, similar to the effect pointed out by other authors.[260, 199]

Basis set superposition error for each single interaction remains unknown as their own exact error could not be distinguished and only a mean approximation for each bond can be obtained. Nevertheless, looking at the total BSSE for all the intermolecular interactions in the crystal, HF leads to a smaller BSSE than DFT methods. There are no radical changes in the total binding energy of the crystal when applying the BSSE correction, leading to think that the CP-corrected PES does not differ much from the uncorrected one near the optimized geometries.

The BH_3NH_3 slab simulation, apart from being useful to calculate the $H_a \cdots H_{d,e}$ interaction, has also provided information on the fact that there is an expansion when there are no crystal restrainments on one of the directions of the primitive cell. This should be taken into account while simulating surface dynamics, e. g. removing hydrogens on from the crystal using heat.

Frequency shifts in the ammonia borane molecule isolated and inside the crystal are red-shifted in all methods. It has been checked that the $H_a \cdots H_{d,e}$ displacement is proportional to the strength of the interaction. The energy of the other interactions could not defined exactly, but frequency shifts reaffirm the idea that $H_f \cdots H_{b,c}$, $H_b \cdots H_e$ and $H_c \cdots H_d$ are stronger than $H_a \cdots H_{d,e}$.

Further investigations on this material, focusing on its hydrogen storage properties, should study the removal and insertion of hydrogens, as the net of interacting intermolecular hydrogens could break or change, leaving the crystal unable to recharge and being reused. There is a high probability that all the interactions can make the crystal a good hydrogen absorbent, even without removing hydrogens beforehand. Also, the ratio at which hydrogens could be transferred outside the crystal is an important factor for its appliance to the hydrogen storage capabilities and should be studied.

Chapter 7

Final conclusions

I ens ha costat Déu i ajuda
arribar fins aquí.

— Manel
Corrandes de la parella estable (2008)

FIRST While calculating dihydrogen bonds, it is important to consider the basis set superposition error as the PESs of the DHBs are flat and shallow. The changes are not only found in the interaction energy, but also the arrangement of monomers is modified noticeably. Thus, the BSSE-corrected PES should be favoured over the non-corrected one in the study of weekly bonded systems.

SECOND Not only distances and energies change from the non-corrected PES to the CP-corrected PES, but their topology changes as well.

THIRD Analysis of the electron density topological and local energetic properties of a series of representative hydrogen-bonded and dihydrogen-

bonded systems at their bond critical point at B3LYP and MP2 level using a double-polarized, double-diffuse Gaussian type base (6-31++G(d,p)) has shown that there are not any noteworthy differences between the results of the two Hamiltoninans. Both levels of calculations predict the same topological differences between HB and DHB complexes.

FOURTH $H \cdots H$ interactions exhibit shorter dihydrogen bond lengths as compared with hydrogen-bonded systems with the same strength. Due to the different electronic structure of the atoms taking part in the interaction, the electronic density has a lower concentration/depletion, as well as that $\rho(r_{BCP})$ has a low value.

The representation of different properties of hydrogen-bonded and dihydrogen-bonded systems versus the dimerization energy lead to no important differences but can be divided into two well-defined groups when intermolecular hydrogen bond distances are included.

SIXTH Dihydrogen $MH \cdots HX$ (M = Li, Na and X = F, Cl, Br) complexes have an homogeneous trend in the electron density topologic analysis. The range of strenghts of the dihydrogen bonded complexes spans from very weak to very strong. In all cases, the topological and energeitc values of $\rho(r_{BCP})$ are similar to those found in other studies from other authors,[84, 85, 86, 88, 87] and reveals the important covalent contribution of very strong systems.

SEVENTH There is a relation between $\rho(r_{BCP})$ properties and intermolecular distances which is different for the dihydrogen-bonded complexes and standard hydrogen-bonded ones. Using these properties and hydrogen-bond-optimized equilibrium distances instead of energetic (i.e. dimerization energies) values, it is possible to find the differences between HBs and DHBs. Although the latter parameters do not give rise to a classification and separation of both groups of hydrogen-bonded systems, when plotted against bond length does, and hence it allows a better understanding of the different properties of HB and DHB complexes.

EIGHTH The analyses of the central $H - H$ bond in $LiH \cdots HX$, $BH_4^- \cdots HX$ and $AlH_4^- \cdots HX$ complexes using the quantitative molecular orbital (MO) model contained in Kohn-Sham density functional theory (DFT) at BP86/TZ2P indicate that there is a similitude in the nature of the dihydrogen bonds in organometallic reaction mechanism and that of regular hydrogen bonds ($Y \cdots H - X$). The donor-acceptor interactions are roughly 40–60% and complemented by a percentage of electrostatic attraction.

NINTH Varying the electronegativity difference between H and X in $H - X$ (but also between A and H in AH) in a dihydrogen interaction, the stability or lability of the DHB system can be modified towards conservation or elimination of the central H_2 unit, i.e., uptake or release of molecular hydrogen.

TENTH Dihydrogen bonds are present in the BH_3NH_3 ammino borane crystal and act as cohesive forces amongst the constituent molecules. These dihydrogen bonds are not identical: they have different lengths and strengths. There is an inverse proportionality between strength and anharmonic frequency shift. The lengths and strenghts of the interactions fall into the dihydrogen bond category type. Data from all Hamiltonians used point to the same conclusion, although the data from the DFT Hamiltonians behave more simlilarly. However, DFT methods tend to underestimate the interaction energy and to elongate the $H \cdots H$ distances.

ELEVENTH The exact amount of BSSE that each interaction has in the ammonia borane crystal can not be known using the method employed in the study, only a mean approximation. The total amount of BSSE per crystal cell is not very important but changes the DHBs interaction energies sensibly. HF method leads to a smaller BSSE than DFT methods.

TWELFTH The slab simulation of the BH_3NH_3 crystal leads to an expansion of the cell in the not occupied direction at all levels of theory, mainly due to the inexistent molecular restrainments in such direction.

THIRTEENTH It has been checked that the frequency shift of the $H_a \cdots H_{d,e}$ in the ammonia borane crystal is proportional to the strength of the interaction. All methods show red-shifted displacements in the $B - H$ and $N - H$ crystalline anharmonic frequencies when compared to those of the isolated ammino borane molecule. The energy of the other interactions in the crystal could not defined exactly, but frequency shifts reaffirm the idea that $H_f \cdots H_{b,c}$, $H_b \cdots H_e$ and $H_c \cdots H_d$ are stronger than $H_a \cdots H_{d,e}$.

Bibliography

[1] M. M. Abad, I. Atheaux, A. Maisonnat, and B. Chaudret. Control of proton transfer by hydrogen bonding in the protonated forms of the binucleophilic complex $[\eta^5 - C_5H_4CH(CH_2)_4NMeIr(PPh_3)H_2]$. *Chem. Commun.*, pages 381–382, 1999. [cited at p. 31]

[2] Y.A. Abramov, L. Brammer, W.T. Klooster, and R.M. Bullock. Experimental Charge Density and Neutron Structural Study of cis-$HMn(CO)_4PPh_3$: Comprehensive Analysis of Chemical Bonding and Evidence for a $C - H \cdots H - Mn$ Hydrogen Bond. *Inorg. Chem.*, 37(24):6317–6328, 1998. [cited at p. 30]

[3] S. Aime, R. Gobetto, and E. Valls. Role of $Os - H \cdots H - N$ Interactions in Directing the Stereochemistry of Carbonyl Cluster Hydride Derivatives. *Organometallics*, 16(24):5140–5141, 1997. [cited at p. 31]

[4] I. Alkorta, J. Elguero, and C. Foces-Foces. Dihydrogen bonds $(A - H \cdots H - B)$. *Chem. Commun.*, pages 1633–1634, 1996. [cited at p. 35, 104]

[5] I. Alkorta, J. Elguero, O. Mó, M. Yáñez, and J. E. Del Bene. Ab Initio Study of the Structural, Energetic, Bonding, and IR Spectroscopic Properties of Complexes with Dihydrogen Bonds. *J. Phys. Chem. A*, 106(40):9325–9330, 2002. [cited at p. 103, 104, 107, 119, 129, 140, 176]

[6] I. Alkorta, I. Rozas, and J. Elguero. Non-conventional hydrogen bonds. *Chem. Soc. Rev.*, 27(2):163–170, 1998. [cited at p. 122]

[7] D.G. Allis, M.E. Kosmowski, and B.S. Hudson. The Inelastic Neutron Scattering Spectrum of $H_3B : NH_3$ and the Reproduction of Its Solid-State Features by Periodic DFT. *J. Am. Chem. Soc.*, 126(25):7756–7757, 2004. [cited at p. 159, 167]

[8] P. Atkins and J. de Paula. *Physical Chemistry; 8th ed.* Oxford University Press, 2006. [cited at p. 45]

[9] J. L. Atwood, G. A. Koutsantonis, F. C. Lee, and C. L. Raston. A thermally stable alane–secondary amine adduct: $[H_3Al(2,2,6,6-\text{tetramethylpiperidine})]$. *Chem. Commun.*, pages 91–92, 1994. [cited at p. 35]

[10] J. A. Ayllon, C. Gervaux, S. Sabo-Etienne, and B. Chaudret. First NMR Observation of the Intermolecular Dynamic Proton Transfer Equilibrium between a Hydride and Coordinated Dihydrogen: $(\text{dppm})_2\text{HRuH}\cdots\text{H}-\text{OR} = [(\text{dppm})_2\text{HRu}(\text{H}_2)]^+(\text{OR})^-$. *Organometallics*, 16(10):2000–2002, 1997. [cited at p. 37]

[11] R.F.W. Bader. *Atoms in Molecules: A Quantum Theory.* Clarendon Press Oxford, UK, 1994. [cited at p. 90, 118, 120, 127]

[12] E. J. Baerends, D. E. Ellis, and P. Ros. Self-consistent molecular Hartree-Fock-Slater calculations I. The computational procedure. *Chem. Phys.*, 2(1):41–51, 1973. [cited at p. 141]

[13] E. J. Baerends and O. V. Gritsenko. A Quantum Chemical View of Density Functional Theory. *J. Phys. Chem. A*, 101(30):5383–5403, 1997. [cited at p. 96]

[14] E. J. Baerends and P. Ros. Evaluation of the LCAO Hartree-Fock-Slater method: applications to transition-metal complexes. *Int. J. Quant. Chem. Symp.*, 12:169–190, 1978. [cited at p. 141]

[15] V. I. Bakhmutov. *Dihydrogen Bond: Principles, Experiments, and Applications.* Wiley & Sons, Inc., April 2008. [cited at p. 24]

[16] A. L. Bandini, G. Banditelli, F. Bonati, G. Minghetti, F. Demartin, and M. Manassero. Heterobimetallic complexes from the reaction of iridium(I) and iridium(III) 3,5-dimethylpyrazolates with gold(I) or gold(III). *Inorg. Chem.*, 26(9):1351–1357, 1987. [cited at p. 31]

[17] A. M. Baranger, F. J. Hollander, and R. G. Bergman. Synthesis of an early-late heterobimetallic imido complex: cooperative reactivity with nitrogen-, oxygen-, and sulfur-hydrogen bonds and formation of a novel aminophosphine complex. *J. Am. Chem. Soc.*, 115(17):7890–7891, 1993. [cited at p. 31]

[18] A. D. Becke. Density functional calculations of molecular bond energies. *J. Chem. Phys.*, 84(8):4524–4529, 1986. [cited at p. 141]

[19] A. D. Becke. A multicenter numerical integration scheme for polyatomic molecules. *J. Chem. Phys.*, 88(4):2547–2553, 1988. [cited at p. 162]

[20] A. D. Becke. Density-functional exchange-energy approximation with correct asymptotic behavior. *Phys. Rev. A*, 38(6):3098–3100, 1988. [cited at p. 82, 141]

[21] A. D. Becke. A new mixing of Hartree-Fock and local density-functional theories. *J. Chem. Phys.*, 98:1372–1377, 1993. [cited at p. 82]

[22] A. D. Becke. Density-functional thermochemistry. III. The role of exact exchange. *J. Chem. Phys.*, 98(7):5648–5652, 1993. [cited at p. 120]

[23] N. V. Belkova, E. Collange, P. Dub, L. M. Epstein, D. A. Lemenovskii, A. Lledós, O. Maresca, F. Maseras, R. Poli, P. O. Revin, E. S. Shubina, and E. V. Vorontsov. Experimental and Computational Studies of Hydrogen Bonding and Proton Transfer to [$Cp^*Fe(dppe)H$]. *Chem. Eur. J.*, 11(3):873–888, 2004. [cited at p. 140]

[24] N.V. Belkova, E.S. Shubina, A.V. Ionidis, L.M. Epstein, H. Jacobsen, A. Messmer, and H. Berke. Intermolecular Hydrogen Bonding of $ReH_2(CO)(NO)L_2$ Hydrides with Perfluoro-tert-butyl Alcohol. Competition between $M-H\cdots H-OR$ and $M-NO\cdots H-OR$ Interactions. *Inorg. Chem.*, 36(7):1522–1525, 1997. [cited at p. 29]

[25] C. Bianchini, C. Mealli, A. Meli, and M.l Sabat. Reversible double addition of hydrogen on a bis(μ-sulfido) binuclear rhodium complex. *Inorg. Chem.*, 25(26):4617–4618, 1986. [cited at p. 31]

[26] F. M. Bickelhaupt and E. J. Baerends. *Reviews in Computational Chemistry*, volume 15, chapter Kohn-Sham Density Functional Theory: Predicting and Understanding Chemistry, pages 1–86. Wiley-VCH, 2000. [cited at p. 94, 142]

[27] F. M. Bickelhaupt, A. Diefenbach, S. P. de Visser, L. J. de Koning, and N. M. M. Nibbering. Nature of the Three-Electron Bond in $H_2S\therefore SH_2^+$. *J. Phys. Chem. A*, 102(47):9549–9553, 1998. [cited at p. 142]

[28] F. M. Bickelhaupt, N. M. M. Nibbering, E. M. Van Wezenbeek, and E. J. Baerends. Central bond in the three $CN^{*\cdot}$ dimers $NC-CN$, $CN-CN$ and $CN-NC$: electron pair bonding and pauli repulsion effects. *J. Phys. Chem.*, 96(12):4864–4873, 1992. [cited at p. 142]

[29] F. M. Bickelhaupt, N. J. R. van Eikema Hommes, C. Fonseca Guerra, and E. J. Baerends. The Carbon-Lithium Electron Pair Bond in $(CH_3Li)_n$ (n = 1, 2, 4). *Organometallics*, 15(13):2923–2931, 1996. [cited at p. 143]

[30] F. Biegler-König, J. Schonbohm, R. Derdau, D. Bayles, and R. F. W. Bader. AIM 2000 Version 2.0, 2002. University of Applied Scence: Bielefeld, Germany. [cited at p. 120]

[31] A. J. Blake, T. I. Hyde, and M. Schröder. Hydrido platinum metal macrocyclic complexes: the synthesis and single-crystal X-ray structure of. *J. Chem. Soc., Dalton Trans.*, pages 1165–1168, 1988. [cited at p. 31]

[32] F. Bloch. Über die Quantenmechanik der Elektronen in Kristallgittern. *Z. Phys. A*, 52(7-8):555–600, 1929. [cited at p. 98]

[33] P. M. Boerrigter, G te Velde, and E. J. Baerends. Three-dimensional numerical integration for electronic structure calculations. *Int. J. Quant. Chem.*, 33(2):87–113, 1987. [cited at p. 141]

[34] R. Boese, N. Niederprum, and D. Blaser. *Molecules in natural science and medicine: an encomium for Linus Pauling*, chapter 5. Ellis Horwood New York, 1991. [cited at p. 158]

[35] N. Bohr. On the Constitution of Atoms and Molecules, Parts I to III. *Philos. Mag.*, 26:1–25, 476–502, 857–875, 1913. [cited at p. 9]

[36] M. Born and R. Oppenheimer. Zur Quantentheorie der Molekeln. *Ann. d. Phys.*, 389:457–484, 1927. [cited at p. 57]

[37] R. Bosque, F. Maseras, O. Eisenstein, B.P. Patel, W. Yao, and R.H. Crabtree. Site Preference Energetics, Fluxionality, and Intramolecular $M-H\cdots H-N$ Hydrogen Bonding in a Dodecahedral Transition Metal Polyhydride. *Inorg. Chem.*, 36(24):5505–5511, 1997. [cited at p. 28]

[38] S. F. Boys. Electronic Wave Functions. I. A General Method of Calculation for the Stationary States of Any Molecular System. *Proc. R. Soc. A*, 200(1063):542–554, 1950. [cited at p. 82]

[39] S. F. Boys and F. Bernardi. The calculation of small molecular interactions by the differences of separate total energies. Some procedures with reduced errors. *Mol. Phys.*, 19:553–566, 1970. [cited at p. 85, 104, 120, 162, 172]

[40] D. Braga, P. De Leonardis, F. Grepioni, E. Tedesco, and M.J. Calhorda. Structural and Theoretical Analysis of $M-H\cdots H-M$ and $M-H\cdots H-C$ Intermolecular Interactions. *Inorg. Chem.*, 37(13):3337–3348, 1998. [cited at p. 31]

[41] D. Braga, F. Grepioni, K. Biradha, V. R. Pedireddi, and G. R. Desiraju. Hydrogen Bonding in Organometallic Crystals. 2. $C-H\cdots O$ Hydrogen Bonds in Bridged and Terminal First-Row Metal Carbonyls. *J. Am. Chem. Soc.*, 117(11):3156–3166, 1995. [cited at p. 31]

[42] D. Braga, F. Grepioni, and J. J. Novoa. Inter-anion $O-H^{-}\cdots O^{-}$ hydrogen bond like interactions: the breakdown of the strength-length analogy. *Chem. Commun.*, pages 1959–1960, 1998. [cited at p. 32]

[43] D. Braga, F. Grepioni, E. Tagliavini, J. J. Novoa, and F. Mota. $C-H\cdots O$ Hydrogen bonds in the mixed-valence salt $[(\eta^6-C_6H_6)_2Cr]^{+}[CrO_3(OCH_3)]^{-}$ and the breakdown of the length/strength analogy. *New J. Chem.*, 22:755–757, 1998. [cited at p. 30, 32]

[44] D. Braga, F. Grepioni, E. Tedesco, M. J. Calhorda, and P. E. M. Lopes. The effect of the counter ion on $M-H\cdots H-X(X=O,N)$ interactions in crystalline transition metal hydrides. *New J. Chem.*, 23:219–226, 1999. [cited at p. 31]

[45] M. P. Brown and R. W. Heseltine. Co-ordinated BH_3 as a proton acceptor group in hydrogen bonding. *Chem. Commun.*, pages 1551–2, 1968. [cited at p. 25]

[46] M. P. Brown, R. W. Heseltine, P. A. Smith, and P. J. Walker. An infrared study of co-ordinated BH_3 and BH_2 groups as proton acceptors in hydrogen bonding. *J. Chem. Soc. A*, pages 410–414, 1970. [cited at p. 25]

[47] M. P. Brown and P. J. Walker. Hydrogen bonds between co-ordinated BH_3 and BH_2 groups and OH groups. Thermodynamics of formation by infrared spectroscopy. *Spectrochim. Acta A*, 30:1125–1131, 1974. [cited at p. 26]

[48] C. G. Broyden. *Math. comput.*, 19:577–593, 1965. [cited at p. 224]

[49] M. Bühl, T. Steinke, P. von Ragué Schleyer, and R. Boese. Solvation effects on geometry and chemical shifts. An ab initio/IGLO reconciliation of apparent experimental inconsistencies on $H_3B \cdot NH_3$. *Angew. Chem. Int. Ed.*, 30:1160–1161, 1991. [cited at p. 158, 159]

[50] M.L. Buil, M.A. Esteruelas, E. Onate, and N. Ruiz. $H \cdots H$ Interaction in Four-Membered $P - H \cdots H - M$ (M = Osmium, Ruthenium) Rings. *Organometallics*, 17(15):3346–3355, 1998. [cited at p. 31]

[51] Anton B. Burg. Enhancement of $P - H$ Bonding in a Phosphine Monoborane. *Inorg. Chem.*, 3(9):1325–1327, 1964. [cited at p. 25]

[52] W. A. Burns and K. R. Leopold. Unusually large gas-solid structure differences: a crystallographic study of $HCN - BF_3$ [hydrogen cyanide-boron trifluoride]. *J. Am. Chem. Soc.*, 115(24):11622–11623, 1993. [cited at p. 159]

[53] A. Caballero and F. A. Jalón. Three-centre dihydrogen bond with fast interchange between proton and hydride: a very active catalyst for $D^+ - H_2$ exchange. *Chem. Commun.*, pages 1879–1880, 1998. [cited at p. 38]

[54] J. A. Cabeza, I. del Rio, J. M. Fernández-Colinas, A. Llamazares, and V. Riera. Synthesis, characterization, reactivity, and catalytic hydrogenation activity of the hexanuclear hexahydrido carbonyl cluster compound $[Ru_6(\mu - H)_60(\mu_3, \nu^2 - ampy)2(CO)14]$ (Hampy = 2-amino-6-methylpyridine). *J. Organomet. Chem.*, 494:169–177, 1995. [cited at p. 31]

[55] J. A. Cabeza, V. Riera, M. A. Pellinghelli, and A. Tiripicchio. μ-Amido complexes of ruthenium carbonyl. Asymmetric versus symmetric bridging preference of the monodeprotonated derivatives of 1,2-arenediamines. Crystal structure of $[Ru_3(\mu - H)(\mu - H_3N_2 - 4, 5 - Me_2 - 1, 2 - phenylene)]$. *J. Organomet. Chem.*, 376:C23–C25, 1989. [cited at p. 31]

[56] M. J. Calhorda. Weak hydrogen bonds: theoretical studies. *Chem. Commun.*, (10):801–809, 2000. [cited at p. 24]

[57] J. P. Campbell, J. W. Hwang, V. G. Young, R. B. Von Dreele, C. J. Cramer, and W. L. Gladfelter. Crystal Engineering Using the Unconventional Hydrogen Bond. Synthesis, Structure, and Theoretical Investigation of Cyclotrigallazane. *J. Am. Chem. Soc.*, 120(3):521–531, 1998. [cited at p. 35]

[58] A. L. Casalnuovo, J. C. Calabrese, and D. Milstein. Nitrogen-hydrogen activation. 1. Oxidative addition of ammonia to iridium(I). Isolation, structural characterization and reactivity of amidoiridium hydrides. *Inorganic Chemistry*, 26(7):971–973, 1987. [cited at p. 31]

[59] Albert L. Casalnuovo, Joseph C. Calabrese, and David Milstein. Rational design in homogeneous catalysis. Iridium(I)-catalyzed addition of aniline to norbornylene via nitrogen-hydrogen activation. *J. Am. Chem. Soc.*, 110(20):6738–6744, 1988. [cited at p. 31]

[60] H. S. Chu, C. P. Lau, K. Y. Wong, and W. T. Wong. Intramolecular $N-H\cdots H-Ru$ Proton-Hydride Interaction in Ruthenium Complexes with (2-(Dimethylamino)ethyl)cyclopentadienyl and (3-(Dimethylamino)propyl)cyclopentadienyl Ligands. Hydrogenation of CO_2 to Formic Acid via the $N-H\cdots H-Ru$ Hydrogen-Bonded Complexes. *Organometallics*, 17(13):2768–2777, 1998. [cited at p. 31, 38]

[61] H. S. Chu, Z. Xu, S. M. Ng, C. P. Lau, and Z. Lin. Protonation of $[tpmRu(PPh_3)_2H]BF_4$ [tpm = Tris(pyrazolyl)methane] - Formation of Unusual Hydrogen-Bonded Species. *Eur. J. Inorg. Chem.*, pages 993–1000, 2000. [cited at p. 38]

[62] H. Chun, D.N. Dybtsev, H. Kim, and K. Kim. Synthesis, X-ray crystal structures, and gas sorption properties of pillared square grid nets based on paddle-wheel motifs: Implications for hydrogen storage in porous materials. *Chem. Eur. J.*, 11(12):3521–3529, 2005. [cited at p. 40, 157]

[63] B. Civalleri, P. Ugliengo, D. Hugas, and S. Simon. Ab-initio modeling of H-Bond features in molecular solids: the cases of urea and formic acid crystals. In *XVIth International Conference Horizons in Hydrogen Bond Research.* Roskilde University, August-September 2005. [cited at p. 162]

[64] R. H. Crabtree. A New Type of Hydrogen Bond. *Science*, 282:2000–2001, 1998. [cited at p. 169]

[65] R. H. Crabtree, P. E. M. Siegbahn, O. Eisenstein, A. L. Rheingold, and T.F. Koetzle. A new Intermolecular interaciton: unconventional hydrogen bonds with element-hydrede bonds as proton acceptor. *Acc. Chem. Res.*, 29(7):348–354, 1996. [cited at p. 169]

[66] C. J. Cramer and W. L. Gladfelter. Ab Initio Characterization of $[H_3N\cdots BH_3]_2$, $[H_3N\cdots AlH_3]_2$, and $[H_3N\cdots GaH_3]_2$. *Inorg. Chem.*, 36(23):5358–5362, 1997. [cited at p. 33, 35, 159]

[67] R. Custelcean and J. E. Jackson. Topochemical Control of Covalent Bond Formation by Dihydrogen Bonding. *J. Am. Chem. Soc.*, 120(49):12935–12941, 1998. [cited at p. 39]

[68] R. Custelcean and J.E. Jackson. Dihydrogen Bonding: Structures, Energetics, and Dynamics. *Chem. Rev.*, 101(7):1963–1980, 2001. [cited at p. 24]

[69] R. Custelcean, M. Vlassa, and J.E. Jackson. Supramolecular Synthesis through Dihydrogen Bonds: Self-Assembly of Controlled Architectures from $NaBH_4 \cdot Poly(2-hydroxyethyl)cyclen$ Building Blocks. *Chem. Eur. J.*, 8:302–308, 2001. [cited at p. 33]

[70] H. Cybulski, M. Pecul, J. Sadlej, and T. Helgaker. Characterization of dihydrogen-bonded $D-H\cdots H-A$ complexes on the basis of infrared and magnetic resonance spectroscopic parameters. *J. Chem. Phys.*, 119(10):5094–5104, 2003. [cited at p. 140]

[71] H. Cybulski, E. Tymińska, and J. Sadlej. The Properties of Weak and Strong Dihydrogen-Bonded $D-H\cdots H-A$ Complexes. *ChemPhysChem*, 7(3):629–639, 2006. [cited at p. 140]

[72] R. E. Davis. Boron Hydrides. IV. Concerning the Geometry of the Activated Complex in the Hydrolysis of Borohydride Ion by Trimethylammonium Ion. *J. Am. Chem. Soc.*, 84(6):892–894, 1962. [cited at p. 39]

[73] L. de Broglie. Recherches sur la théorie des quanta. *Ann. Phys.*, 3:22–128, 1925. [cited at p. 50]

[74] G.R. Desiraju and T. Steiner. *The weak hydrogen bond.* Oxford University Press, New York, 1999. [cited at p. 176]

[75] M. Dincaă, A. Dailly, Y. Liu, C.M. Brown, D.A. Neumann, and J.R. Long. Hydrogen Storage in a Microporous Metal- Organic Framework with Exposed Mn^{2+} Coordination Sites. *J. Am. Chem. Soc.*, 128(51):16876–16883, 2006. [cited at p. 40, 157]

[76] D. A. Dixon and M. Gutowski. Thermodynamic Properties of Molecular Borane Amines and the $[BH4^-][NH4^+]$ Salt for Chemical Hydrogen Storage Systems from ab Initio Electronic Structure Theory. *J. Phys. Chem. A*, 109(23):5129–5135, 2005. [cited at p. 41]

[77] R. Dovesi, B. Civalleri, R. Orlando, C. Roetti, and V. R. Saunders. Ab Initio Quantum Simulation in Solid State Chemistry. In *Reviews in Computational Chemistry*, volume 21, chapter Ab Initio Quantum Simulation in Solid State Chemistry, page 1. John Wiley & Sons, Inc., 2005. [cited at p. 169]

[78] A. Einstein. Über einen die Erzeugung und Verwandlung des Lichtes betreffenden heuristischen Gesichtspunkt. *Ann. D. Phys.*, 322:132–148, 1905. [cited at p. 47]

[79] J. Emsley. Very strong hydrogen bonding. *Chem. Soc. Rev.*, 9(1):91–124, 1980. [cited at p. 14, 20]

[80] J. Emsley. Lattice energies of the alkali metal bifluorides, (MHF_2). *Polyhedron*, 4(3):489–490, 1985. [cited at p. 22]

[81] J. Emsley, O. P. A. Hoyte, and Overill. R. E. The strongest hydrogen-bond? Ab initio-LCAO-MO-SCF calculations. *J. Chem. Soc., Chem. Commun.*, pages 225–226, 1977. [cited at p. 22]

[82] J. Emsley, O. P. A. Hoyte, and R. E. Overill. Ab initio calculations on the very strong hydrogen bond of the biformate anion and comparative esterification studies. *J. Am. Chem. Soc.*, 100(11):3303–3306, 1978. [cited at p. 87]

[83] L. M. Epstein, E. S. Shubina, E. V. Bakhmutova, L. N. Saitkulova, V. I. Bakhmutov, A. L. Chistyakov, and I. V. Stankevich. Unusual Hydrogen Bonds with a Hydride Atom in Boron Hydrides Acting as Proton Acceptor. Spectroscopic and Theoretical Studies. *Inorg. Chem.*, 37(12):3013–3017, 1998. [cited at p. 32, 39]

[84] E. Espinosa, I. Alkorta, J. Elguero, and E Molins. From weak to strong interactions: A comprehensive analysis of the topological and energetic properties of the electron density distribution involving $X - H \cdots F - Y$ systems. *J. Chem. Phys.*, 117(12):5529–5542, 2002. [cited at p. 118, 127, 129, 132, 135, 180]

[85] E. Espinosa, I. Alkorta, I. Rozas, J. Elguero, and E. Molins. About the evaluation of the local kinetic, potential and total energy densities in closed-shell interactions. *Chem. Phys. Lett.*, 336(5-6):457–461, 2001. [cited at p. 118, 130, 180]

[86] E. Espinosa, C. Lecomte, and E. Molins. Experimental electron density overlapping in hydrogen bonds: topology vs. energetics. *Chem. Phys. Lett*, 300(5-6):745–748, 1999. [cited at p. 118, 130, 180]

[87] E. Espinosa, E. Molins, and C. Lecomte. Hydrogen bond strengths revealed by topological analyses of experimentally observed electron densities. *Chem. Phys. Lett.*, 285(3-4):170–173, 1998. [cited at p. 118, 130, 180]

[88] E. Espinosa, M. Souhassou, H. Lachekar, and C. Lecomte. Topological analysis of the electron density in hydrogen bonds. *Acta Cryst. B*, 55:563–572, 1999. [cited at p. 118, 129, 180]

[89] A. Famulari, E. Gianinetti, M. Raimondi, M. Sironi, and I. Vandoni. Modification of Guest and Saunders open shell SCF equations to exclude BSSE from molecular interaction calculations. *Theor. Chem. Acc.*, 99:358–365, 1998. [cited at p. 85]

[90] L. Fan and T. Ziegler. The influence of self-consistency on nonlocal density functional calculations. *J. Chem. Phys.*, 94(9):6057–6063, 1991. [cited at p. 141]

[91] A. Flores-Parra, S. A. Sánchez-Ruiz, C. Guadarrama, H. Nöth, and R. Contreras. $BH^{\delta-} - {}^{\delta+}HC$ Interactions in N-Borane and N-Chloroborane Adducts Derived from 1,3,5-Heterocyclohexanes. *Eur. J. Inorg. Chem.*, page 2069, 1999. [cited at p. 35]

[92] C. Fonseca Guerra, E. J. Baerends, and F. M. Bickelhaupt. Orbital interactions and charge redistribution in weak hydrogen bonds: Watson-Crick GC mimic involving CH proton donor and F proton acceptor groups. *Int. Journ. Quant. Chem.*, 106(12):2428–2443, 2006. [cited at p. 140, 153]

[93] C. Fonseca Guerra and F. M. Bickelhaupt. Charge Transfer and Environment Effects Responsible for Characteristics of DNA Base Pairing. *Angew. Chem. Int. Ed.*, 38(19):2942–2945, 1999. [cited at p. 140, 153]

[94] C. Fonseca Guerra and F. M. Bickelhaupt. Orbital Interactions in Strong and Weak Hydrogen Bonds are Essential for DNA Replication. *Angew. Chem. Int. Ed.*, 41:2092–2095, 2002. [cited at p. 140, 153]

[95] C. Fonseca Guerra and F. M. Bickelhaupt. Orbital interactions and charge redistribution in weak hydrogen bonds: The Watson-Crick AT mimic adenine-2,4-difluorotoluene. *J. Chem. Phys.*, 119:4262–4273, 2003. [cited at p. 140, 153]

[96] C. Fonseca Guerra, F. M. Bickelhaupt, and E. J. Baerends. Orbital Interactions in Hydrogen Bonds Important for Cohesion in Molecular Crystals and Mismatched Pairs of DNA Bases. *Cryst. Growth Des.*, 2(3):239–245, 2002. [cited at p. 140, 153]

[97] C. Fonseca Guerra, F. M. Bickelhaupt, and E. J. Baerends. Hydrogen Bonding in Mimics of Watson-Crick Base Pairs Involving $C-H$ Proton Donor and F Proton Acceptor Groups: A Theoretical Study. *ChemPhysChem*, 5(4):481–487, 2004. [cited at p. 140, 153]

[98] C. Fonseca Guerra, F. M. Bickelhaupt, J. G. Snijders, and E. J. Baerends. The Nature of the Hydrogen Bond in DNA Base Pairs: The Role of Charge Transfer and Resonance Assistance. *Chem. Eur. J.*, 5(12):3581–3594, 1999. [cited at p. 140, 143, 153]

[99] C. Fonseca Guerra, J. W. Handgraaf, E. J. Baerends, and F. M. Bickelhaupt. Voronoi deformation density (VDD) charges: Assessment of the Mulliken, Bader, Hirshfeld, Weinhold, and VDD methods for charge analysis. *J. Comput. Chem.*, 25(2):189–210, 2004. [cited at p. 143]

[100] C. Fonseca Guerra, J. G. Snijders, G. te Velde, and E. J. Baerends. Towards an order-N DFT method. *Theor. Chem. Acc.*, 99(6):391–403, 1998. [cited at p. 141]

[101] C. Fonseca Guerra, T. van der Wijst, and F. M. Bickelhaupt. Supramolecular Switches Based on the Guanine-Cytosine (GC) Watson-Crick Pair: Effect of Neutral and Ionic Substituents. *Chem. Eur. J.*, 12(11):3032–3042, 2006. [cited at p. 140, 153]

[102] C. Fonseca Guerra, O. Visser, J. G. Snijders, G. te Velde, and E. J. Baerends. *In Methods and Techniques in Computational Chemistry*, pages 305–395. STEF: Cagliari, 1995. [cited at p. 141]

[103] X. Fradera, M. A. Austen, and R. F. W. Bader. The Lewis Model and Beyond. *J. Phys. Chem. A*, 103(2):304–314, 1999. [cited at p. 93]

[104] M. J. Frisch, G. W. Trucks, H. B. Schlegel, G. E. Scuseria, M. A. Robb, J. R. Cheeseman, J. A. Montgomery, Jr., T. Vreven, K. N. Kudin, J. C. Burant, J. M. Millam, S. S. Iyengar, J. Tomasi, V. Barone, B. Mennucci, M. Cossi, G. Scalmani, N. Rega, G. A. Petersson, H. Nakatsuji, M. Hada, M. Ehara, K. Toyota, R. Fukuda, J. Hasegawa, M. Ishida, T. Nakajima, Y. Honda, O. Kitao, H. Nakai, M. Klene, X. Li, J. E. Knox, H. P. Hratchian, J. B. Cross, V. Bakken, C. Adamo, J. Jaramillo, R. Gomperts, R. E. Stratmann, O. Yazyev, A. J. Austin, R. Cammi, C. Pomelli, J. W. Ochterski, P. Y. Ayala, K. Morokuma, G. A. Voth, P. Salvador, J. J. Dannenberg, V. G. Zakrzewski, S. Dapprich, A. D. Daniels, M. C. Strain, O. Farkas, D. K. Malick, A. D. Rabuck, K. Raghavachari, J. B. Foresman, J. V. Ortiz, Q. Cui, A. G. Baboul, S. Clifford, J. Cioslowski, B. B. Stefanov, G. Liu, A. Liashenko, P. Piskorz, I. Komaromi, R. L. Martin, D. J. Fox, T. Keith, M. A. Al-Laham, C. Y. Peng, A. Nanayakkara, M. Challacombe, P. M. W. Gill, B. Johnson, W. Chen, M. W. Wong, C. Gonzalez, and J. A. Pople. Gaussian 98, Revision A.11, 1998. Gaussian, Inc., Pittsburgh, PA. [cited at p. 105]

[105] M. J. Frisch, G. W. Trucks, H. B. Schlegel, G. E. Scuseria, M. A. Robb, J. R. Cheeseman, J. A. Montgomery, Jr., T. Vreven, K. N. Kudin, J. C. Burant, J. M. Millam, S. S. Iyengar, J. Tomasi, V. Barone, B. Mennucci, M. Cossi, G. Scalmani, N. Rega, G. A. Petersson, H. Nakatsuji, M. Hada, M. Ehara, K. Toyota, R. Fukuda, J. Hasegawa, M. Ishida, T. Nakajima, Y. Honda, O. Kitao, H. Nakai, M. Klene, X. Li, J. E. Knox, H. P. Hratchian, J. B. Cross, V. Bakken, C. Adamo, J. Jaramillo, R. Gomperts, R. E. Stratmann, O. Yazyev, A. J. Austin, R. Cammi, C. Pomelli, J. W. Ochterski, P. Y. Ayala, K. Morokuma, G. A. Voth, P. Salvador, J. J. Dannenberg, V. G. Zakrzewski, S. Dapprich, A. D. Daniels, M. C. Strain, O. Farkas, D. K. Malick, A. D. Rabuck, K. Raghavachari, J. B. Foresman, J. V. Ortiz, Q. Cui, A. G. Baboul, S. Clifford, J. Cioslowski, B. B. Stefanov, G. Liu, A. Liashenko, P. Piskorz, I. Komaromi, R. L. Martin, D. J. Fox, T. Keith, M. A. Al-Laham, C. Y. Peng, A. Nanayakkara, M. Challacombe, P. M. W. Gill, B. Johnson, W. Chen, M. W. Wong, C. Gonzalez, and J. A. Pople. Gaussian 03, Revision C.02. Gaussian, Inc., Wallingford, CT, 2004. [cited at p. 120]

[106] F. Fuster and B. Silvi. Does the topological approach characterize the hydrogen bond? *Theor. Chem. Acc.*, 104:13–21, 2000. [cited at p. 118]

[107] F. Fuster, B. Silvi, S. Berski, and Z. Latajka. Topological aspects of protonation and hydrogen bonding: the dihydrogen bond case. *J. Mol. Struct. (Theochem)*, 555(1-3):75–84, 2000. [cited at p. 118]

[108] O. Gálvez, P. C. Gómez, and L. F. Pacios. Variation with the intermolecular distance of properties dependent on the electron density in hydrogen bond dimers. *J. Chem. Phys.*, 115(24):11166–11184, 2001. [cited at p. 118, 129]

[109] H. Geiger and E. Marsden. On a Diffuse Reflection of the α-Particles. *Proc. Roy. Soc., Series A*, 82(557):495–500, July 1909. [cited at p. 47]

[110] E. Gianinetti, M. Raimondi, and E. Tornaghi. Modification of the Roothaan equations to exclude BSSE from molecular interaction calculations. *J. Quantum Chem.*, 60:157–166, 1998. [cited at p. 85]

[111] A. Gil, M. Sodupe, and J. Bertran. Unusual hydrogen bonds in $[AH_3 - H_3O]^{+\cdot}$ radical cations (A = C, Si, Ge, Sn and Pb): Single-electron hydrogen bond, proton-hydride hydrogen bond and formation of $[H_2AOH_2]^{+\cdot} - H_2$ complexes. *Chem. Phys. Lett.*, 395(1–3):27–32, 2004. [cited at p. 139, 140]

[112] G. Gilli and P. Gilli. Towards an unified hydrogen-bond theory. *J. Mol. Struct.*, 552(1-3):1–15, 2000. [cited at p. 139, 152]

[113] P. Gilli, V. Bertolasi, V. Ferretti, and G. Gilli. Evidence for resonance-assisted hydrogen bonding. 4. Covalent nature of the strong homonuclear hydrogen bond. Study of the $O - H \cdots O$ system by crystal structure correlation methods. *J. Am. Chem. Soc.*, 116(3):909–915, 1994. [cited at p. 139]

[114] S. J. Grabowski. BeH_2 as a proton-accepting molecule for dihydrogen bonded systems–ab initio study. *J. Mol. Struct.*, 553(1–3):151–156, 2000. [cited at p. 110, 122]

[115] S. J. Grabowski. High-Level Ab Initio Calculations of Dihydrogen-Bonded Complexes. *J. Phys. Chem. A*, 104(23):5551–5557, 2000. [cited at p. 36, 103, 105, 110, 122]

[116] S. J. Grabowski. A new measure of hydrogen bonding strength - ab initio and atoms in molecules studies. *Chem. Phys. Lett*, 338(4-6):361–366, 2001. [cited at p. 118]

[117] S. J. Grabowski. Ab Initio Calculations on Conventional and Unconventional Hydrogen Bonds Study of the Hydrogen Bond Strength. *J. Phys. Chem. A*, 105(47):10739–10746, 2001. [cited at p. 118]

[118] S. J. Grabowski. An estimation of strength of intramolecular hydrogen bonds – ab initio and AIM studies. *J. Mol. Struct.*, 562(1-3):137–143, 2001. [cited at p. 118]

[119] S. J. Grabowski. Hydrogen bonding strength - measures based on geometric and topological parameters. *J. Phys. Org. Chem.*, 17(1):18–31, 2003. [cited at p. 118, 132]

[120] S. J. Grabowski, T. L. Robinson, and J. Leszczynski. Strong dihydrogen bonds - ab initio and atoms in molecules study. *Chem. Phys. Lett.*, 386(1-3):44–48, 2004. [cited at p. 103, 107, 129, 140]

[121] S. J. Grabowski, W. A. Sokalski, and J. Leszczynski. Nature of $X - H^{+\delta} \cdots {}^{-\delta} H - Y$ Dihydrogen Bonds and $X - H \cdots \sigma$ Interactions. *J. Phys. Chem. A*, 108(27):5823–5830, 2004. [cited at p. 119, 140]

[122] S. J. Grabowski, W. A. Sokalski, and J. Leszczynski. How Short Can the $H \cdots H$ Intermolecular Contact Be? New Findings that Reveal the Covalent Nature of Extremely Strong Interactions. *J. Phys. Chem. A*, 109(19):4331–4341, 2005. [cited at p. 119]

[123] S. W. Grabowski. Study of correlations for dihydrogen bonds by quantum-chemical calculations. *Chem. Phys. Lett.*, 312:542–547, 1999. [cited at p. 36, 103, 105, 135]

[124] D. J. Grant and D. A. Dixon. Thermodynamic Properties of Molecular Borane Phosphines, Alane Amines, and Phosphine Alanes and the $[BH4^-][PH4^+]$, $[AlH4^-][NH4^+]$, and $[AlH4^-][PH4^+]$ Salts for Chemical Hydrogen Storage Systems from ab Initio Electronic Structure Theory. *J. Phys. Chem. A*, 109(44):10138–10147, 2005. [cited at p. 41]

[125] NN Greenwood and A. Earnshaw. *Chemistry of the elements*. Butterworth-Heinemann Boston, 2nd edition, 1997. [cited at p. 14]

[126] W.C. Hamilton and J.A. Ibers. *Hydrogen Bonding in Solids: Methods of Molecular Structure Determination*. WA Benjamin, New York, 1968. [cited at p. 14, 20, 21, 23]

[127] W. Heisenberg. Über quantentheoretische Umdeutung kinematischer und mechanischer Beziehungen. *Z. f. Phys.*, 33:879–893, 1925. [cited at p. 51]

[128] W. Heisenberg. Über den anschaulichen Inhalt der quantentheoretischen Kinematik und Mechanik. *Z. f. Phys.*, 43:172–198, 1927. [cited at p. 56]

[129] D. J. Heldebrant, A. Karkamkar, J. C. Linehan, and T. Autrey. Synthesis of ammonia borane for hydrogen storage applications. *Energy Environ. Sci.*, 1:156–160, 2008. [cited at p. 41, 158]

[130] P. Hobza and Z. Havlas. Blue-shifting Hydrogen Bonds. *Chem. Rev.*, 100(11):4253–4264, 2000. [cited at p. 14]

[131] P. Hohenberg and W. Kohn. Inhomogeneous Electron Gas. *Phys. Rev.*, 136(3B):B864–B871, Nov 1964. [cited at p. 63, 65]

[132] C. F. Hoon and E. C. Reynhardt. Molecular dynamics and structures of amine boranes of the type $R_3N.BH_3$. I. X-ray investigation of $H_3N.BH_3$ at 295K and 110K. *J. Phys. C*, 16(32):6129–6136, 1983. [cited at p. 158]

[133] S.-W. Hu, Y. Wang, X.-Y. Wang, T.-W. Chu, and X.-Q. Liu. Gas-Phase Reactions between Silane and Ammonia: A Theoretical Study. *J. Phys. Chem. A*, 107(43):9189–9196, 2003. [cited at p. 140]

[134] L.-Y. Huang, U. R. Aulwurm, F. W. Heinemann, F. Knoch, and . Kisch. Weak $M-H\cdots H-C$ and $M-Cl\cdots H-C$ Interactions in Orthometalated Iridium and Rhodium Complexes. *Chem. Eur. J.*, 4:1641–1646, 1998. [cited at p. 30]

[135] Edward W. Hughes. The Crystal Structure of Ammonia-Borane, H_3NBH_3. *J. Am. Chem. Soc.*, 78(2):502–503, 1956. [cited at p. 158]

[136] A. C. Hurley. *The Molecular Orbital Interpretation of Bond-Length Changes Following Excitation and lonization of Diatomic Molecules.* Löwdin and Pullman, Academic Press, New York, 1964. [cited at p. 82]

[137] J.-W. Hwang, J. P. Campbell, J. Kozubowski, S. A. Hanson, J. F. Evans, and W. L. Gladfelter. Topochemical Control in the Solid-State Conversion of Cyclotrigallazane into Nanocrystalline Gallium Nitride. *Chem. Mater.*, 7(3):517–525, 1995. [cited at p. 39]

[138] F. Illas and J.M. Ricart. *Química cuántica en materia condensada: aplicación al estudio de superficies, quimisorción, catálisis heterogénea y propiedades de sólidos.*, chapter 4, pages 217–279. Universitat Jaume I, Castelòò de la Plana, 2001. [cited at p. 97]

[139] E. D. Isaacs, A. Shukla, P. M. Platzman, D. R. Hamann, B. Barbiellini, and C. A. Tulk. Covalency of the Hydrogen Bond in Ice: A Direct X-Ray Measurement. *Phys. Rev. Lett.*, 82(3):600–603, Jan 1999. [cited at p. 140]

[140] H. B. Jansen and P. Ros. Non-empirical molecular orbital calculations on the protonation of carbon monoxide. *Chem. Phys. Lett.*, 3(3):140–143, 1969. [cited at p. 83]

[141] G. A. Jeffrey and W. Saenger. *Hydrogen Bonding in Biological Structure.* Springer Verlag, Berlin, 1991. [cited at p. 20, 22]

[142] D. D. Johnson. Modified Broyden's method for accelerating convergence in self-consistent calculations. *Phys. Rev. B*, 38(18):12807–12813, 1988. [cited at p. 224]

[143] V. Jonas, G. Frenking, and M. T. Reetz. Comparative Theoretical Study of Lewis Acid-Base Complexes of BH_3, BF_3, BCl_3, $AlCl_3$, and SO_2. *J. Am. Chem. Soc.*, 116(19):8741–8753, 1994. [cited at p. 159]

[144] P. C. Junk and J. W. Steed. Is the unconventional $H\cdots H$ bond more common than expected? Synthesis and X-ray structure of monomeric $[Ru(CO)H_2(PPh_3)_3]$. *J. Organomet. Chem.*, 587:191–194, 1999. [cited at p. 30]

[145] T. Kar and S. Scheiner. Comparison between hydrogen and dihydrogen bonds among H_3BNH_2, H_2BNH_2, and NH_3. *J. Chem. Phys.*, 119(3):1473–1482, 2003. [cited at p. 119, 129, 140]

[146] R. J. Keaton, J. M. Blacquiere, and R. T. Baker. Base Metal Catalyzed Dehydrogenation of Ammonia-Borane for Chemical Hydrogen Storage. *J. Am. Chem. Soc.*, 129(7):1844–1845, 2007. [cited at p. 40, 41]

[147] K. Kitaura and K. Morokuma. A new energy decomposition scheme for molecular interactions within the Hartree-Fock approximation. *Int. J. Quant. Chem.*, 10(2):325–340, 2004. [cited at p. 140, 142]

[148] C. Kittel and P. McEuen. *Introduction to solid state physics*. Wiley, New York, 1986. [cited at p. 143]

[149] W. T. Klooster, T. F. Koetzle, P. E. M. Siegbahn, T. B. Richardson, and R. H. Crabtree. Study of the $N-H\cdots H-B$ Dihydrogen Bond Including the Crystal Structure of BH_3NH_3 by Neutron Diffraction. *J. Am. Chem. Soc.*, 121(27):6337–6343, 1999. [cited at p. 34, 158, 159, 160, 163, 165, 166, 169]

[150] U. Koch and P. L. A. Popelier. Characterization of $C-H-O$ Hydrogen Bonds on the Basis of the Charge Density. *J. Phys. Chem.*, 99(24):9747–9754, 1995. [cited at p. 118]

[151] W. Kohn and L. J. Sham. Self-Consistent Equations Including Exchange and Correlation Effects. *Phys. Rev.*, 140(4A):A1133–A1138, Nov 1965. [cited at p. 94]

[152] M. M. Kreevoy and J. E. C. Hutchins. Acid-catalyzed hydrolysis and isotope exchange in lithium cyanotrihydroborate. *J. Am. Chem. Soc.*, 91(15):4329–4330, 1969. [cited at p. 39]

[153] J. Krijn and E. J. Baerends. *Fit Functions in the* HFS-*Method; Internal Report (in Dutch)*. Vrije Universiteit, Amsterdam, 1984. [cited at p. 141]

[154] S. A. Kulkarni. Dihydrogen Bonding in Main Group Elements: An ab Initio Study. *J. Phys. Chem. A*, 102(39):7704–7711, 1998. [cited at p. 35, 103, 104, 105, 112, 122]

[155] S. A. Kulkarni and A. K. Srivastava. Dihydrogen Bonding in Main Group Elements: A Case Study of Complexes of LiH, BH_3, and AlH_3 with Third-Row Hydrides. *J. Phys. Chem. A*, 103(15):2836–2842, 1999. [cited at p. 35, 103, 112, 122]

[156] C. Lee, W. Yang, and R. G. Parr. Development of the Colle-Salvetti correlation-energy formula into a functional of the electron density. *Phys. Rev. B*, 37(2):785–789, Jan 1988. [cited at p. 82, 120, 162]

[157] H. Lee, J. Lee, J.P. Do Youn Kim, Y.T. Seo, H. Zeng, I.L. Moudrakovski, C.I. Ratcliffe, and J.A. Ripmeester. Tuning clathrate hydrates for hydrogen storage. *Nature*, 434(7034):743–746, 2005. [cited at p. 157]

[158] J. C. Lee, E. Peris, A. L. Rheingold, and R. H. Crabtree. An Unusual Type of $H \cdots H$ Interaction: $Ir - H \cdots H - O$ and $Ir - H \cdots H - N$ Hydrogen Bonding and Its Involvement in σ-Bond Metathesis. *J. Am. Chem. Soc.*, 116(24):11014–11019, 1994. [cited at p. 36, 169]

[159] J. C. Lee Jr., A. L. Rheingold, B. Muller, P. S. Pregosin, and R. H. Crabtree. Complexation of an amide to iridium via an iminol tautomer and evidence $Ir - H \cdots H - O$ hydrogen bond. *J. Chem. Soc., Chem. Commun.*, pages 1021–1022, 1994. [cited at p. 26]

[160] A.C. Legon and D. J. Millen. The nature of the hydrogen bond to water in the gas phase. *Chem. Soc. Revs.*, 21:71–8, 1992. [cited at p. 22]

[161] K. R. Leopold, M. Canagaratna, and J. A. Phillips. Partially Bonded Molecules from the Solid State to the Stratosphere. *Acc. Chem. Res.*, 30(2):57–64, 1997. [cited at p. 159]

[162] M. Levitt and M.F. Perutz. Aromatic rings act as hydrogen bond acceptors. *J. Mol. Biol*, 201(4):751–754, 1988. [cited at p. 159]

[163] M. Levy. Universal Variational Functionals of Electron Densities, First-Order Density Matrices, and Natural Spin-Orbitals and Solution of the ν-Representability Problem. *Proceedings of the National Academy of Sciences*, 76(12):6062–6065, 1979. [cited at p. 63]

[164] M. Levy. Electron densities in search of Hamiltonians. *Physical Review A*, 26(3):1200–1208, 1982. [cited at p. 67]

[165] H. Liao. Computational study on the microsolvation effect of dihydrogen-bonded $LiH \cdots HF$ system. *Chem. Phys. Lett.*, 424(1-3):28–33, 2006. [cited at p. 140]

[166] P. Lipkowski, S. J. Grabowski, T. L. Robinson, and J. Leszczynski. Properties of the $C - H \cdots H$ Dihydrogen Bond: An ab Initio and Topological Analysis. *J. Phys. Chem. A*, 108(49):10865–10872, 2004. [cited at p. 119, 129, 140]

[167] Ernest L. Lippert and William N. Lipscomb. The Structure of H_3NBH_3. *J. Am. Chem. Soc.*, 78(2):503–504, 1956. [cited at p. 158]

[168] B. Liu and A. D. McLean. Accurate calculation of the attractive interaction of two ground state helium atoms. *J. Chem. Phys.*, 59(8):4557–4558, 1973. [cited at p. 83]

[169] Q. Liu and R. Hoffmann. Theoretical Aspects of a Novel Mode of Hydrogen-Hydrogen Bonding. *J. Am. Chem. Soc.*, 117(40):10108–10112, 1995. [cited at p. 27, 35, 104, 105, 106]

[170] A. J. Lough, S. Park, R. Ramachandran, and R. H. Morris. Switching On and Off a New Intramolecular Hydrogen-Hydrogen Interaction and the Heterolytic Splitting of Dihydrogen. Crystal and Molecular Structure of $[IrH(\eta^1 - SC_5H_4NH)_2(PCy_3)_2]BF_4 \cdot 2.7CH_2Cl_2$. *J. Am. Chem. Soc.*, 116(18):8356–8357, 1994. [cited at p. 27, 28]

[171] J. Lundell and M. Pettersson. The dihydrogen-bonded complex $XeH_2 - H_2O$. *Phys. Chem. Chem. Phys.*, 1:1691–1697, 1999. [cited at p. 35]

[172] C. F. Matta, J. Hernández-Trujillo, T. H. Tang, and R. F. W. Bader. Hydrogen-Hydrogen Bonding: A Stabilizing Interaction in Molecules and Crystals. *Chem. Eur. J.*, 9:1940–1951, 2003. [cited at p. 103, 122]

[173] M. H. Matus, K. D. Anderson, D. M. Camaioni, S. T. Autrey, and D. A. Dixon. Reliable Predictions of the Thermochemistry of Boron-Nitrogen Hydrogen Storage Compounds: $B_xN_xH_x$, x = 2, 3. *J. Phys. Chem. A*, 111(20):4411–4421, 2007. [cited at p. 41]

[174] I. Mayer. Towards a Chemical Hamiltonian. *Int. J. Quantum Chem.*, 23:341–363, 1983. [cited at p. 84]

[175] I. Mayer. Comment on: Exact perturbation treatment of the basis set superposition correction. *The Journal of Chemical Physics*, 97(7):5257–5258, 1992. [cited at p. 85]

[176] S. A. C. McDowell and T. S. Forde. Isotope effects in linear dihydrogen bonded complexes containing LiH. *J. Chem. Phys.*, 117(13):6032–6037, 2002. [cited at p. 103, 104, 107]

[177] J. E. McGrady and D. M. P. Mingos. The role of transition metal ions in hydrogen bonded networks: a density functional molecular orbital theory study. *J. Chem. Soc., Perkin Trans. 2*, pages 351–358, 1996. [cited at p. 31]

[178] Y. Meng, Z. Zhou, C. Duan, B. Wang, and Q. Zhong. Non-convertional hydrogen bonding interaction of BH_3NH_3 complexes: a comparative theoretical study. *J. Mol. Struct.: THEOCHEM*, 713(1-3):135–144, January 2005. [cited at p. 175, 176]

[179] G. Merino, V. I. Bakhmutov, and A. Vela. Do Cooperative Proton-Hydride Interactions Explain the Gas-Solid Structural Difference of BH_3NH_3? *J. Phys. Chem. A*, 106(37):8491–8494, 2002. [cited at p. 119, 129, 140, 160]

[180] R. E. Mesmer and W. L. Jolly. The Hydrolysis of Aqueous Hydroborate. *Inorg. Chem.*, 1(3):608–612, 1962. [cited at p. 39]

[181] A. Messmer, H. Jacobsen, and H. Berke. Probing Regioselective Intermolecular Hydrogen Bonding to $[Re(CO)H_2(NO)(PR_3)_2]$ Complexes by NMR Titration and Equilibrium NMR Methodologies. *Chem. Eur. J.*, 5:3341–3349, 1999. [cited at p. 29]

[182] David Milstein, Joseph C. Calabrese, and Ian D. Williams. Formation, structures, and reactivity of cis-hydroxy-, cis-methoxy-, and cis-mercaptoiridium hydrides. Oxidative addition of water to Ir(I). *J. Am. Chem. Soc.*, 108(20):6387–6389, 1986. [cited at p. 26]

[183] C. R. Miranda and G. Ceder. Ab initio investigation of ammonia-borane complexes for hydrogen storage. *J. Chem. Phys.*, 126(18):184703, 2007. [cited at p. 41, 158]

[184] T.S. Moore and T.F. Winmill. CLXXVII. The state of amines in aqueous solution. *J. Chem. Soc., Trans.*, 101:1635–1676, 1912. [cited at p. 25]

[185] K. Morokuma. Why do molecules interact? The origin of electron donor-acceptor complexes, hydrogen bonding and proton affinity. *Acc. Chem. Res.*, 10(8):294–300, 1977. [cited at p. 142]

[186] C. A. Morrison and M. M. Siddick. Dihydrogen Bonds in Solid BH_3NH_3. *Angew. Chem. Int. Ed.*, 43(36):4780–4782, 2004. [cited at p. 160, 168, 172]

[187] T. Nagata, O. Takahashi, K. Saito, and S. Iwata. Basis set superposition error free self-consistent field method for molecular interaction in multi-component systems: Projection operator formalism. *J. Chem. Phys.*, 115:3553, 2001. [cited at p. 85]

[188] I. Newton. *Philosophiae Naturalis Principia Mathematica*. Glasguae, 1687. [cited at p. 8]

[189] S. Orimo, Y. Nakamori, J.R. Eliseo, A. Zuttel, and C.M. Jensen. Complex hydrides for hydrogen storage. *Chem. Rev.*, 107(10):4111–4132, 2007. [cited at p. 41, 157]

[190] G. Orlova and S. Scheiner. Intermolecular $H \cdots H$ bonding and proton transfer in semisandwich Re and Ru complexes. *J. Phys. Chem. A*, 102(25):4813–4818, 1998. [cited at p. 37]

[191] G. Orlova and S. Scheiner. Intermolecular $MH \cdots HR$ Bonding in Monohydride Mo and W Complexes. *J. Phys. Chem. A*, 102(1):260–269, 1998. [cited at p. 29, 140]

[192] G. Orlova, S. Scheiner, and T. Kar. Activation and cleavage of $H - R$ bonds through intermolecular $H \cdots H$ bonding upon reaction of proton donors HR with 18-electron transition metal hydrides. *Journal of Physical Chemistry A*, 103(4):514–520, 1999. [cited at p. 37]

[193] L. F. Pacios. Topological Descriptors of the Electron Density and the Electron Localization Function in Hydrogen Bond Dimers at Short Intermonomer Distances. *J. Phys. Chem. A*, 108(7):1177–1188, 2004. [cited at p. 118]

[194] I. R. Padilla-Martínez, M. de J. Rosalez-Hoz, H. Tlahuext, C. Camacho-Camacho, A. Ariza-Castolo, and R. Contreras. Azolylborane adducts. Structural and conformational analysis by x-ray diffraction and NMR. Protic-hydric ($C = H^{\delta+} -^{\delta-} H = B$) and Protic-Fluoride ($C = H^{\delta+} -^{\delta-} F = B$) interactions. *Chem. Ber.*, 129:441–449, 1996. [cited at p. 34]

[195] B. Paizs, P. Salvador, A.G. Csaszar, M. Duran, and S. Suhai. Intermolecular bond lengths: extrapolation to the basis set limit on uncorrected and BSSE-corrected potential energy hypersurfaces. *J. Comput. Chem.*, 22(2):196–207, 2001. [cited at p. 84]

[196] S. Park, A.J. Lough, and R.H. Morris. Iridium(III) Complex Containing a Unique Bifurcated Hydrogen Bond Interaction Involving $Ir - H \cdots H(N) \cdots F - B$atoms. Crystal and Molecular Structure of $[IrH(\eta^1 - SC_5H_4NH)(\eta^2 - SC_5H_4N)(PPh_3)_2](BF_4) \cdot 0.5C_6H_6$. *Inorg. Chem.*, 35(10):3001–3006, 1996. [cited at p. 27]

[197] S. Park, R. Ramachandran, A. J. Lough, and R. H. Morris. A new type of intramolecular $H \cdots H \cdots H$ interaction involving $N - H \cdots H(Ir) \cdots H - N$ atoms. Crystal and molecular structure of $[IrH(\eta^1 - SC_5H_4NH)_2(\eta^2 - SC_5H_4N)(PCy_3)]BF_4 \cdot 0.72CH_2Cl_2$. *J. Chem. Soc., Chem. Commun.*, pages 2201–2202, 1994. [cited at p. 27, 169]

[198] R. G. Parr and W. Yang. *Density-Functional Theory of Atoms and Molecules*. Oxford University Press, New York, 1989. [cited at p. 63, 67]

[199] F. Pascale, S. Tosoni, C. Zicovich-Wilson, P. Ugliengo, R. Orlando, and R. Dovesi. Vibrational spectrum of brucite, $Mg(OH)_2$: a periodic ab initio quantum mechanical calculation including OH anharmonicity. *Chem. Phys. Lett.*, 396(4-6):308–315, October 2004. [cited at p. 162, 177]

[200] B. P. Patel, K. Kavallieratos, and R. H. Crabtree. Effects of dihydrogen bonding on fluxionality in $ReH_5(PPh_3)_2L$. *J. Organomet. Chem.*, 528:205–207, 1997. [cited at p. 28]

[201] B. P. Patel, W. Yao, G. P. A. Yap, A. L. Rheingold, and R. H. Crabtree. $Re - H \cdots H - N$ interactions in the second-coordination sphere of crystalline $[Re(PPh_3)_2(imidazole)]$. *Chem. Commun.*, pages 991–992, 1996. [cited at p. 28]

[202] L. Pauling. *The Nature of the Chemical Bond*, chapter 12. Cornell University Press, Ithaca, 3rd edition, 1960. [cited at p. 19, 20]

[203] L. Pauling and E. B. Wilson Jr. *Introduction to Quantum Mechanics with applications to chemistry*. Dover Publications, New York, 1985. [cited at p. 45]

[204] I. M. Pepperberg, T. A. Halgren, and W. N. Lipscomb. A molecular orbital study of the role of BH_5 in the hydrolysis of tetrahydroborate ion. *J. Am. Chem. Soc.*, 98(12):3442–3451, 1976. [cited at p. 39]

[205] J. P. Perdew. Density-functional approximation for the correlation energy of the inhomogeneous electron gas. *Physical Review B*, 33(12):8822–8824, 1986. [cited at p. 82, 141]

[206] J. P. Perdew, K. Burke, and M. Ernzerhof. Generalized Gradient Approximation Made Simple. *Phys. Rev. Lett.*, 77(18):3865–3868, 1996. [cited at p. 162]

[207] J. P. Perdew and Y. Wang. Accurate and simple analytic representation of the electron-gas correlation energy. *Phys. Rev. B*, 45(23):13244–13249, 1992. [cited at p. 162]

[208] E. Peris, J. C. Lee, J. R. Rambo, O. Eisenstein, and R. H. Crabtree. Factors Affecting the Strength of $N-H\cdots H-Ir$ Hydrogen Bonds. *J. Am. Chem. Soc.*, 117(12):3485–3491, 1995. [cited at p. 26]

[209] E. Peris, J. Wessel, B. P. Patel, and R. H. Crabtree. d^0 and d^2 Polyhydrides as unconventional proton acceptors in lntermolecular hydrogen bonding. *J. Chem. Soc., Chem. Commun.*, 21:2175–2176, 1995. [cited at p. 159]

[210] F. L. Pilar. *Elementary Quantum Chemistry (2nd ed)*. Dover Publications, New York, 2001. [cited at p. 45]

[211] G.C. Pimentel and A.L. McClellan. *The Hydrogen Bond*. WH Freeman & Co Ltd, San Francisco, 1960. [cited at p. 14, 23]

[212] C. Pisani. *Quantum-mechanical ab-initio calculation of the properties of crystalline materials*, volume 67 of *Lectures Notes in Chemistry.* Springer-Verlag Berlin, 1996. [cited at p. 97]

[213] M. Planck. Ueber das Gesetz der Energieverteilung im Normalspectrum. *An. D. Phys.*, 309:553–563, 1901. [cited at p. 46]

[214] J. Poater, X. Fradera, M. Solà, M. Duran, and S. Simon. On the electron-pair nature of the hydrogen bond in the framework of the atoms in molecules theory. *Chem. Phys. Lett.*, 369(1-2):248–255, 2003. [cited at p. 122, 132, 139]

[215] J. Poater, M. Solà, M. Duran, J. Robles, and X. Fradera. Bielectronic densities: analysis and applications in molecular structure and chemical reactivity. In K. D. Sen, editor, *Reviews in modern quantum chemistry: a celebration of the contributions of R.G. Parr*, pages 831–870. World Scientific, 2002. [cited at p. 93]

[216] P. L .A. Popelier. Characterization of a Dihydrogen Bond on the Basis of the Electron Density. *J. Phys. Chem. A*, 102(10):1873–1878, 1998. [cited at p. 34, 118, 126, 135, 159]

[217] P. Pyykkõ and C. Wang. Theoretical study of H_2 splitting and storage by boron-nitrogen-based systems: a bimolecular case and some qualitative aspects. *Phys. Chem. Chem. Phys.*, 12:149–155, 2009. [cited at p. 41]

[218] M. Remko. Thermodynamics of dihydrogen bonds ($A-H\cdots H-B$). *Mol. Phys.*, 94:839–842, 1998. [cited at p. 35, 103, 104, 122]

[219] T. Richardson, S. de Gala, R. H. Crabtree, and P. E. M. Siegbahn. Unconventional Hydrogen Bonds: Intermolecular $B-H\cdots H-N$ Interactions. *J. Am. Chem. Soc.*, 117(51):12875–12876, 1995. [cited at p. 24, 33, 158, 159, 169]

[220] T. B. Richardson, T. F. Koetzle, and R. H. Crabtree. An $M-H\cdots H-C$ hydrogen bonding interaction. *Inorg. Chim. Acta*, 250:69–73, 1996. [cited at p. 30]

[221] K.N. Robertson, O. Knop, and T. S. Cameron. $C-H\cdots H-C$ interactions in organoammonium tetraphenylborates: another look at dihydrogen bonds. *Can. J. Chem.*, 81(6):727–743, 2003. [cited at p. 103, 122]

[222] I. Røeggen and H. R. Skullerud. The interatomic potential for the X^1 Sigma state of $NeLi^+$. *J. Phys. B*, 25(8):1795–1809, 1992. [cited at p. 85]

[223] C. C. J. Roothaan. New Developments in Molecular Orbital Theory. *Rev. Mod. Phys.*, 23(2):69–89, Apr 1951. [cited at p. 74]

[224] I. Rozas, I. Alkorta, and J. Elguero. Field effects on dihydrogen bonded systems. *Chem. Phys. Lett*, 275:423–428, 1997. [cited at p. 39, 103, 106]

[225] E. Rutherford. The Scattering of α and β Particles by Matter and the Structure of the Atom. *Philos. Mag.*, 21:669–588, 1911. [cited at p. 48]

[226] A. J. Sadlej. Exact perturbation treatment of the basis set superposition correction. *The Journal of Chemical Physics*, 95(9):6705–6711, 1991. [cited at p. 85]

[227] A. J. Sadlej. Reply to the Comment on: Exact perturbation treatment of the basis set superposition correction. *The Journal of Chemical Physics*, 97(7):5259–5259, 1992. [cited at p. 85]

[228] S. Sæbø and P. Pulay. Fourth-order Møller–Plessett perturbation theory in the local correlation treatment. I. Method. *J. Chem. Phys.*, 86(2):914–922, 1987. [cited at p. 85]

[229] P. Salvador, M. Duran, and J. J. Dannenberg. Counterpoise Corrected Ion/Molecule Complexes Using Two or Three Fragments. *J. Phys. Chem. A*, 106(29):6883–6889, 2002. [cited at p. 84, 87]

[230] P. Salvador, B. Paizs, M. Duran, and S. Suhai. On the effect of the BSSE on intermolecular potential energy surfaces. Comparison of a priori and a posteriori BSSE correction schemes. *J. Comp. Chem.*, 22:765–786, 2001. [cited at p. 120]

[231] P. Salvador, S. Simon, M. Duran, and J. J. Dannenberg. $C-H\cdots O-H$-bonded complexes: How does basis set superposition error change their potential-energy surfaces? *J. Chem. Phys.*, 113:5666, 2000. [cited at p. 84, 104]

[232] VR Saunders, R. Dovesi, C. Roetti, M. Causà, N.M. Harrison, R. Orlando, and C.M. Zicovich-Wilson. *CRYSTAL 03 user's manual*, 1998. [cited at p. 97]

[233] VR Saunders, R. Dovesi, C. Roetti, M. Causà, N.M. Harrison, R. Orlando, and C.M. Zicovich-Wilson. CRYSTAL03, 2003. [cited at p. 161]

[234] E. Schrödinger. Quantisierung als Eigenwertproblem. *Ann. Phys.*, 384:361–376, 1926. [cited at p. 51]

[235] E. S. Shubina, E. V. Bakhmutova, L. N. Saitkulova, and L. N. Epstein. Intermolecular hydrogen bonds $BH\cdots HX$ in solution. *Mendeleev Commun.*, page 83, 1997. [cited at p. 32, 39]

[236] E. S. Shubina, N. V. Belkova, E. V. Bakhmutova, E. V. Vorontsov, V. I. Bakhmutov, A. V. Ionidis, C. Bianchini, L. Marvelli, M. Peruzzini, and L. M. Epstein. In situ IR and NMR study of the interactions between proton donors and the Re(I) hydride complex $[MeC(CH_2PPh_2)_3Re(CO)_2H]\cdot ReH\cdots H$ bonding and proton-transfer pathways. *Inorg. Chim. Acta*, 280:302–307, 1998. [cited at p. 37, 159]

[237] E. S. Shubina, N. V. Belkova, and L. M. Epstein. Novel types of hydrogen bonding with transition metal π-complexes and hydrides. *J. Organom. Chem.*, 536:17–29, 1997. [cited at p. 31]

[238] E. S. Shubina, N. V. Belkova, A. N. Krylov, E. V. Vorontsov, L. M. Epstein, D. G. Gusev, M. Niedermann, and H. Berke. Spectroscopic Evidence for Intermolecular $M-H\cdots H-OR$ Hydrogen Bonding: Interaction of $WH(CO)_2(NO)L_2$ Hydrides with Acidic Alcohols. *J. Am. Chem. Soc.*, 118(5):1105–1112, 1996. [cited at p. 28, 159]

[239] E.S. Shubina, N.V. Belkova, E.V. Bakhmutova, L.N. Saitkulova, A.V. Ionidis, and L.M. Epstein. Problems of unusual hydrogen bonds between proton donors and transition metal hydrides and borohydrides. *Russ. Chem. Bull.*, 47(5):817–822, 1998. [cited at p. 32, 39]

[240] S. Simon, J. Bertran, and M. Sodupe. Effect of Counterpoise Correction on the Geometries and Vibrational Frequencies of Hydrogen Bonded Systems. *J. Phys. Chem. A*, 105(17):4359–4364, 2001. [cited at p. 110, 111, 120, 122, 132]

[241] S. Simon, M. Duran, and J. J. Dannenberg. How does basis set superposition error change the potential surfaces for hydrogen-bonded dimers? *J. Chem. Phys.*, 105(24):11024–11031, 1996. [cited at p. 87, 104, 111]

[242] S. Simon, M. Duran, and J. J. Dannenberg. Effect of Basis Set Superposition Error on the Water Dimer Surface Calculated at Hartree.Fock, Møller-Plesset, and Density Functional Theory Levels. *J. Phys. Chem. A*, 103(11):1640–1643, 1999. [cited at p. 110, 111]

[243] P. Singh, M. Zottola, S. Q. Huang, B. R. Shaw, and L. G. Pedersen. 2'-deoxycytidine-N(3)-cyanoborane monohydrate. *Acta Cryst. C*, 35:10172–10181, 1996. [cited at p. 34]

[244] J. C. Slater. Atomic Shielding Constants. *Phys. Rev.*, 36(1):57–64, 1930. [cited at p. 82]

[245] J. C. Slater. *Quantum Theory of Molecules and Solids Vol. 4*. McGraw-Hill, New York, 1974. [cited at p. 81, 141]

[246] J. G. Snijders, P. Vernooijs, and E. J. Baerends. Roothaan-Hartree-Fock-Slater atomic wave functions : Single-zeta, double-zeta, and extended Slater-type basis sets for $_{87}\mathrm{Fr} - _{103}\mathrm{Lr}$. *At. Data and Nucl. Data Tables*, 26(6):483–509, 1981. [cited at p. 141]

[247] V. P. Sorokin, B. V. Vesnina, and N. S. Klimova. *Russ. J. Inorg. Chem.*, 8:32, 1963. [cited at p. 158]

[248] A. Staubitz, M. Besora, J. N. Harvey, and I. Manners. Computational Analysis of Amine-Borane Adducts as Potential Hydrogen Storage Materials with Reversible Hydrogen Uptake. *Inorg. Chem.*, 47(13):5910–5918, 2008. [cited at p. 41]

[249] T. Steiner. Inter-anion $\mathrm{O-H\cdots O}$ interactions are classical hydrogen bonds. *Chem. Commun.*, pages 2299–2300, 1999. [cited at p. 32]

[250] F. H. Stephens, R. T. Baker, M. H. Matus, D. J. Grant, and D. A. Dixon. Acid Initiation of Ammonia-Borane Dehydrogenation for Hydrogen Storage. *Angew. Chem. Int. Ed.*, 46(5):746–749, 2007. [cited at p. 41]

[251] R. C. Stevens, R. Bau, D. Milstein, O. Blum, and T. F. Koetzle. Concept of the $\mathrm{H}\,(\delta+)\cdots\mathrm{H}\,(\delta-)$ interaction. A low-temperature neutron diffraction study of $\mathrm{cis-[IrH(OH)(PMe)_4]\,PF_6}$. *J. Chem. Soc., Dalton Trans.*, pages 1429–1432, 1990. [cited at p. 26]

[252] A . J. Stone. Computation of charge-transfer energies by perturbation theory. *Chem. Phys. Lett.*, 211(1):101–109, 1993. [cited at p. 143]

[253] A . J. Stone. The Theory of Intermolecular Forces. In *International Series of Monographs on Chemistry 32*. Oxford University Press, Oxford, 1996. [cited at p. 143]

[254] R. Taylor, O. Kennard, and W. Verichel. Geometry of the nitrogen-hydrogen$\cdots$oxygen-carbon ($\mathrm{N-H\cdots O:C}$) hydrogen bond. 2. Three-center (bifurcated) and four-center (trifurcated) bonds. *J. Am. Chem. Soc.*, 106(1):244–248, 1984. [cited at p. 15]

[255] G. te Velde and E. J. Baerends. Numerical integration for polyatomic systems. *J. Comp. Phys.*, 99(1):84–98, 1992. [cited at p. 141]

[256] G. te Velde, F. M. Bickelhaupt, E. J. Baerends, C. Fonseca Guerra, S. J. A. van Gisbergen, J. G. Snijders, and T. Ziegler. Chemistry with ADF. *J.Comput.Chem.*, 22(9):931–967, 2001. [cited at p. 141, 142]

[257] L. R. Thorne, R. D. Suenram, and F. J. Lovas. Microwave spectrum, torsional barrier, and structure of BH_3NH_3. *J. Chem. Phys.*, 78(1):167–171, 1983. [cited at p. 159, 160]

[258] L. V. Titov, M. D. Makarova, and V. Y. Rosolovskii. *Dokl. Akad. Nauk*, 180:381, 1968. [cited at p. 25]

[259] S. Tosoni, C. Tuma, J. Sauer, B. Civalleri, and P. Ugliengo. A comparison between plane wave and Gaussian-type orbital basis sets for hydrogen bonded systems: Formic acid as a test case. *J. Chem. Phys.*, 127(15):154102, 2007. [cited at p. 162]

[260] C. Tuma, A. D. Boese, and N. C. Handy. Predicting the binding energies of H-bonded complexes: A comparative DFT study. *Phys. Chem. Chem. Phys.*, 1:3939–3947, 1999. [cited at p. 162, 177]

[261] P. Ugliengo, B. Civalleri, R. Dovesi, and C. M. Zicovich-Wilson. Periodic B3LYP calculations on H-Edingtonites, both alone and interacting with acetylene. *Phys. Chem. Chem. Phys.*, 1:545–553, 1999. [cited at p. 162]

[262] P. Ugliengo, F. Pascale, M. Merawa, P. Labeguerie, S. Tosoni, and R. Dovesi. Infrared Spectra of Hydrogen-Bonded Ionic Crystals: Ab Initio Study of $Mg(OH)_2$ and $Be(OH)_2$. *J. Phys. Chem. B*, 108(36):13632–13637, 2004. [cited at p. 162]

[263] H. Umeyama and K. Morokuma. The origin of hydrogen bonding. An energy decomposition study. *J. Am. Chem. Soc.*, 99(5):1316–1332, 1977. [cited at p. 23]

[264] P. Valiron and I. Mayer. Hierarchy of counterpoise corrections for N-body clusters: generalization of the Boys-Bernardi scheme. *Chemical Physics Letters*, 275(1-2):46–55, 1997. [cited at p. 86]

[265] L. Versluis and T. Ziegler. The determination of molecular structures by density functional theory. The evaluation of analytical energy gradients by numerical integration. *J. Chem. Phys.*, 88(1):322–328, 1988. [cited at p. 141]

[266] G. Voronoi. Nouvelles applications des parametres continus a la theorie des formes quadratiques. *J. Reine Angew. Math*, 134:198–287, 1908. [cited at p. 143]

[267] S. H. Vosko, L. Wilk, and M. Nusair. Accurate spin-dependent electron liquid correlation energies for local spin density calculations: a critical analysis. *Can. J. Phys.*, 58(8):1200–1211, 1980. [cited at p. 81, 141]

[268] T. R. Walsh. Exact exchange and Wilson–Levy correlation: a pragmatic device for studying complex weakly-bonded systems. *Phys. Chem. Chem. Phys.*, 7:443–451, 2005. [cited at p. 160]

[269] A. F. Wells. *Structural Inorganic Chemistry*. Clarendon Press, Oxford, 1984. [cited at p. 19, 21]

[270] J. Wessel, J. C. Lee Jr., E. Peris, G. P. A. Yap, J. B. Fortin, J. S. Ricci, G. Sini, A. Albinati, T. F. Koetzle, O. Eisenstein, A. L. Rheingold, and R. H. Crabtree. An Unconventional Intermolecular Three-Center $N - H \cdots H_2Re$ Hydrogen Bond in Crystalline $[ReH_5(PPh_3)_3] \cdot \text{indole} \cdot C_6H_6$. *Angew. Chem. Int. Ed.*, 34:2507–2509, 1995. [cited at p. 28]

[271] P. Wind and J.-L. Heully. Reduction of the basis set superposition error at the correlation level. *Chemical Physics Letters*, 230(1-2):35–40, 1994. [cited at p. 85]

[272] D. J. Wolstenholme and T. S. Cameron. Comparative Study of Weak Interactions in Molecular Crystals: $H \cdots H$ Bonds vs Hydrogen Bonds. *J. Phys. Chem. A*, 110(28):8970–8978, 2006. [cited at p. 119]

[273] X. Wu, M. C. Vargas, S. Nayak, V. Lotrich, and G. Scoles. Towards extending the applicability of density functional theory to weakly bound systems. *The Journal of Chemical Physics*, 115(19):8748–8757, 2001. [cited at p. 160]

[274] X. Xu and W. A. Goddard. The X3LYP extended density functional for accurate descriptions of nonbond interactions, spin states, and thermochemical properties. *Proc. Natl. Acad. Sci. U.S.A.*, 101(9):2673–2677, 2004. [cited at p. 160]

[275] T. Yildirim and S. Ciraci. Titanium-decorated carbon nanotubes as a potential high-capacity hydrogen storage medium. *Phys. Rev. Lett.*, 94(17):175501–175505, 2005. [cited at p. 40, 157]

[276] T. Yokoyama, S. Yokoyama, T. Kamikado, Y. Okuno, and S. Mashiko. Selective assembly on a surface of supramolecular aggregates with controlled size and shape. *Nature*, 413:619–621, 2001. [cited at p. 159, 160]

[277] W. H. Zachariasen and R. C. L. Mooney. The Structure of the Hypophosphite Group as Determined from the Crystal Lattice of Ammonium Hypophosphite. *J. Chem. Phys.*, 2(1):34–37, 1934. [cited at p. 25]

[278] Y. Zhao, Y.H. Kim, AC Dillon, MJ Heben, and SB Zhang. Hydrogen storage in novel organometallic buckyballs. *Phys. Rev. Lett.*, 94(15):155504–155508, 2005. [cited at p. 40, 157]

[279] T. Ziegler and A. Rauk. On the calculation of bonding energies by the Hartree Fock Slater method. *Theor. Chim. Acta*, 46(1):1–10, 1977. [cited at p. 142]

[280] T. Ziegler and A. Rauk. Carbon monoxide, carbon monosulfide, molecular nitrogen, phosphorus trifluoride, and methyl isocyanide as σ donors and π acceptors. A theoretical study by the Hartree-Fock-Slater transition-state method. *Inorg. Chem.*, 18(7):1755–1759, 1979. [cited at p. 142]

[281] M. A. Zottola, P. Pedersen, P. Singh, and B. Ramsay-Shaw. Modeling the Hydrogen Bond. In *ACS Symposium Series*. American Chemical Society, Washington DC, 1994. [cited at p. 34]

Appendices

Appendix **A**

Dirac notation

The Schrödinger wave functions can be regarded as N-dimensional complex vector spaces, and to simplify operations involving terms within the function, the *Dirac notation* is a concise simple notation to do so. The vector $\overrightarrow{a}$ can be written in terms of its N-dimensional basis $\overrightarrow{i}$ in the form of a *ket*, and its complex conjugate as a *bra*, which respectively are written as:

$$|a\rangle = \sum_{i=1}^{N} |i\rangle a_i \qquad \langle a| = \sum_{i=1}^{N} a_i^* \langle i| \tag{A.1}$$

Thus, the scalar product of two wave functions is

$$\int \psi_m^* (x_1, \ldots, z_N)\, \psi_n (x_1, \ldots, z_N)\, d\tau = \langle m|n\rangle \tag{A.2}$$

and when $\psi_m^* (x_1, \ldots, z_N)$ and $\psi_n (x_1, \ldots, z_N)$ are orthonormal, the product can be written as

$$\langle m|n\rangle = \delta_{mn} \tag{A.3}$$

where δ_{mn} is the *Kronecker delta*, a function that is 1 when $n = m$ and 0 otherwise.

If $\hat{A}$ is a linear operator, it can be applied to the function ψ_m to obtain a new function ψ_n. The original function is symbolised by the ket $|m\rangle$ and

applying the $\hat{A}$ operator, the ket $\hat{A}|\psi\rangle$ is obtained and transformed to $|n\rangle$. In the same manner, it can act on a bra from the right hand side $\langle\phi|$ forming $\langle\phi|\hat{A}$. In quantum mechanics it is common to project the eigenfunctions of a function after applying an operator to a different or the same function:

$$\left(\langle\phi|\hat{A}\right)|\psi\rangle = \langle\phi|\left(\hat{A}|\psi\rangle\right) = \langle\phi|\hat{A}|\psi\rangle \tag{A.4}$$

When the *psi* and *phi* wave functions are the same, this expression gives the *expectation value*, also known as *mean value* or *average value*, of the observable A represented by operator $\hat{A}$ for the physical system in the state $|\psi\rangle$.

The notation for two-electron integrals over spin orbitals χ_n can be expressed like this:

$$\langle ij|kl\rangle = \langle\chi_i\chi_j|\chi_k\chi_l\rangle = \int \chi_i^*\left(\vec{x}_1\right)\chi_j^*\left(\vec{x}_2\right)\frac{1}{r_{12}}\chi_i\left(\vec{x}_1\right)\chi_j\left(\vec{x}_2\right)d\vec{x}_1 d\vec{x}_2 \tag{A.5}$$

so the antisymmetrised two-electron integral can be represented as:

$$\langle ij||kl\rangle = \langle ij|kl\rangle - \langle ij|lk\rangle = \int \chi_i^*\left(\vec{x}_1\right)\chi_j^*\left(\vec{x}_2\right)\frac{1}{r_{12}}\left(1-\hat{P}_{12}\right)\chi_i\left(\vec{x}_1\right)\chi_j\left(\vec{x}_2\right)d\vec{x}_1 d\vec{x}_2 \tag{A.6}$$

where $\hat{P}_{12}$ is an operator which interchanges the coordinates of electron one and two.

Appendix **B**

Extra information on the AIM analysis

The following information complements data in Chapter 4.

Table B.1: Equilibrium geometries at the B3LYP and MP2 levels of theory.

	B3LYP/6-31++G(d,p)			MP2/6-31++G(d,p)		
Z	x	y	z	x	y	z
			$NH_3 - HF$			
9	0.000000	0.000000	0.000000	-0.015846	0.000000	0.000000
1	0.971200	0.000000	0.000000	0.947541	0.000000	0.000000
7	2.614900	0.000000	0.000000	2.620625	0.000000	0.000000
1	2.981067	0.000000	-0.949009	2.992327	0.000000	-0.943399
1	2.981067	-0.821866	0.474504	2.992327	-0.817008	0.471700
1	2.981067	0.821866	0.474504	2.992327	0.817008	0.471700

Continues on next page...

Table B.1 – continued from previous page

	B3LYP/6-31++G(d,p)			MP2/6-31++G(d,p)		
Z	x	y	z	x	y	z
			$NH_3 - HCl$			
17	0.673465	0.000000	-0.000033	0.618622	0.000000	-0.000001
1	2.031811	0.000000	0.000042	1.928357	0.000000	0.000000
7	3.715001	0.000000	0.000000	3.745819	0.000000	0.000000
1	4.076440	0.000000	-0.950775	4.118947	0.000000	-0.943062
1	4.076460	-0.823384	0.475383	4.118946	-0.816716	0.471531
1	4.076460	0.823384	0.475383	4.118946	0.816716	0.471531
			$NH_3 - HBr$			
35	0.612264	0.000000	-0.000108	0.549878	0.000000	0.000097
1	2.161126	0.000000	0.000074	2.025983	0.000000	-0.000079
7	3.704578	0.000000	0.000041	3.742833	0.000000	-0.000044
1	4.057089	0.000000	-0.954180	4.110448	0.000000	-0.945442
1	4.057290	-0.826339	0.477086	4.110248	-0.818784	0.472733
1	4.057290	0.826339	0.477086	4.110248	0.818784	0.472733
			$H_2O - HF$			
9	0.000000	0.000000	0.000000	0.010872	0.000000	-0.027755
1	0.000000	0.000000	0.949400	-0.000173	0.000000	0.915730
8	-0.086864	0.000000	2.620544	-0.099581	0.000000	2.628999
1	-0.503154	0.775618	3.018626	-0.502145	0.771566	3.045110
1	-0.503154	-0.775618	3.018626	-0.502145	-0.771566	3.045111
			$H_2CO - HF$			
9	0.000000	0.000000	0.000000	-0.001273	0.000000	-0.041258
1	0.948700	0.000000	0.000000	0.941177	0.000000	0.003107
8	2.615613	0.000000	-0.329617	2.657399	0.000000	-0.303523
6	2.922759	0.000000	-1.506346	2.924262	0.000000	-1.503711
1	3.980384	0.000000	-1.821566	3.963596	0.000000	-1.845591
1	2.154114	0.000000	-2.298254	2.136409	0.000000	-2.264806

Continues on next page...

Table B.1 – continued from previous page

	B3LYP/6-31++G(d,p)			MP2/6-31++G(d,p)		
Z	x	y	z	x	y	z
			$H_2O - HCl$			
17	0.045883	0.001709	-0.390437	0.078343	-0.000013	-0.430277
1	0.013061	-0.001844	0.918092	-0.001013	0.000008	0.851103
8	-0.111560	-0.000318	2.754178	-0.165321	0.000017	2.746947
1	-0.520384	0.774472	3.161545	-0.502648	0.770113	3.219707
1	-0.520171	-0.774019	3.163817	-0.502532	-0.770125	3.219715
			$H_2O - HBr$			
35	0.065664	0.000143	-0.528822	0.095473	-0.000056	-0.569525
1	0.009735	0.000035	0.91117	-0.002718	0.000219	0.849772
8	-0.116855	-0.000048	2.802215	-0.169805	0.000037	2.793879
1	-0.525867	0.773686	3.211338	-0.508133	0.76978	3.266707
1	-0.525848	-0.773817	3.211293	-0.507988	-0.769981	3.266362
			$PH_3 - HF$			
9	0.420823	0.000000	-0.000162	0.405407	0.000000	0.000001
1	1.364540	0.000000	-0.000013	1.343716	0.000000	0.000001
15	3.668339	0.000000	0.000178	3.689371	0.000000	0.000000
1	4.398330	0.000000	-1.214722	4.403714	0.000000	-1.205873
1	4.398803	-1.051978	0.607359	4.403715	-1.044315	0.602935
1	4.398803	1.051978	0.607359	4.403715	1.044315	0.602935
			$H_2S - HF$			
9	-0.056388	-0.000545	0.388807	-0.004575	0.00002	0.320056
1	-0.029909	0.000498	1.331426	-0.031862	0.000017	1.25629
16	-0.075715	0.000051	3.57966	-0.121906	0.000013	3.552056
1	-0.985912	0.979094	3.755002	-0.987796	0.968352	3.840422
1	-0.985924	-0.979098	3.754353	-0.987709	-0.968403	3.840424

Continues on next page...

Table B.1 – continued from previous page

	B3LYP/6-31++G(d,p)			MP2/6-31++G(d,p)		
Z	x	y	z	x	y	z
			$H_2CO - HCl$			
17	-0.242504	0.000000	0.231547	-0.237489	0.000000	0.169067
1	1.059120	0.000000	0.102165	1.046675	0.000000	0.130464
8	2.866618	0.000000	-0.396752	2.915867	0.000000	-0.372427
6	3.102898	0.000000	-1.587970	3.105655	0.000000	-1.585569
1	4.141458	0.000000	-1.963469	4.119817	0.000000	-1.999845
1	2.293980	0.000000	-2.341305	2.271045	0.000000	-2.297474
			$H_2CO - HBr$			
35	-0.290544	0.000000	-0.015377	-0.262061	-0.000007	-0.093234
1	1.142784	0.000000	0.134893	1.141568	0.000007	0.152775
8	3.013699	0.000001	-0.323390	3.063471	-0.000001	-0.298495
6	3.093304	0.000000	-1.535303	3.086342	0.000000	-1.526797
1	4.073011	0.000000	-2.044797	4.033300	-0.000004	-2.077160
1	2.189317	0.000000	-2.171809	2.158950	0.000005	-2.112871
			$HF - HF$			
1	0.164454	0.502847	0.000000	-0.000785	0.000000	-0.031349
9	0.036542	-1.300729	0.000000	-0.013118	0.000000	1.826341
9	0.036542	1.429346	0.000000	-0.181147	0.000000	-0.945752
1	-0.822214	-1.660403	0.000000	-0.829215	0.000000	2.271327
			$HBr - HF$			
1	0.080415	1.732067	0.000000	0.094503	1.775479	0.000000
35	0.029796	-0.714200	0.000000	0.013629	-0.756824	0.000000
9	0.029796	2.666171	0.000000	0.036746	2.704834	0.000000
1	-1.391420	-0.730620	0.000000	-1.396291	-0.770071	0.000000

Continues on next page...

Table B.1 – continued from previous page

	B3LYP/6-31++G(d,p)			MP2/6-31++G(d,p)		
Z	x	y	z	x	y	z
			$PH_3 - HCl$			
17	0.000000	0.000000	0.000000	-0.044726	0.000000	0.000000
1	1.305100	0.000000	0.000000	1.234694	0.000000	0.000000
15	3.780900	0.000000	0.000000	3.820383	0.000000	0.000000
1	4.521212	0.000000	-1.210578	4.546428	0.000000	-1.200952
1	4.521212	-1.048391	0.605289	4.546428	-1.040055	0.600476
1	4.521212	1.048391	0.605289	4.546428	1.040055	0.600476
			$H_2S - HCl$			
17	0.000000	0.000000	0.000000	0.084532	0.000000	-0.107991
1	0.000000	0.000000	1.304500	-0.013712	0.000043	1.166163
16	-0.103377	0.000000	3.722191	-0.169634	0.000141	3.689439
1	-1.015236	0.978553	3.891279	-1.017807	0.966816	4.030762
1	-1.015236	-0.978553	3.891279	-1.017228	-0.967001	4.030875
			$HBr - HCl$			
1	0.054086	1.322083	0.000000	0.073051	1.363271	0.000000
35	0.025752	-1.270262	0.000000	0.011731	-1.302493	0.000000
17	0.025752	2.616589	0.000000	0.023671	2.636313	0.000000
1	-1.393179	-1.344938	0.000000	-1.396043	-1.373618	0.000000
			$HBr - HBr$			
1	0.064351	0.630233	0.000000	0.073600	0.666456	0.000000
35	0.019104	-2.017006	0.000000	0.005108	-2.036629	0.000000
35	0.019104	2.056431	0.000000	0.026586	2.077610	0.000000
1	-1.401600	-2.010106	0.000000	-1.404335	-2.047885	0.000000
			$H_2S - HBr$			
35	-0.039161	-0.000093	0.121181	0.017645	0.000067	0.018957
1	0.028941	0.000143	1.556872	-0.018741	0.000073	1.435195
16	-0.094275	0.000223	4.031492	-0.167314	0.000197	3.990234
1	-1.015061	0.977811	4.149843	-1.015871	0.966483	4.331928
1	-1.014294	-0.978085	4.149861	-1.015119	-0.966732	4.331976

Continues on next page...

Table B.1 – continued from previous page

	B3LYP/6-31++G(d,p)			MP2/6-31++G(d,p)		
Z	x	y	z	x	y	z
			$PH_3 - HBr$			
35	-0.095481	-0.000001	-0.001833	-0.118531	-0.000001	-0.000145
1	1.342373	0.000000	0.000895	1.300117	0.000000	0.000127
15	3.853843	0.000000	0.001376	3.882007	0.000000	0.000000
1	4.593812	0.000000	-1.209962	4.608691	0.000000	-1.200789
1	4.597545	-1.047732	0.604762	4.608676	-1.039920	0.600403
1	4.597545	1.047732	0.604762	4.608676	1.039920	0.600403
			HF − HCl			
1	0.142509	0.042997	0.000000	0.156693	0.009443	0.000000
9	0.024317	2.063053	0.000000	0.003802	2.068957	0.000000
17	0.024317	-1.244066	0.000000	0.027325	-1.257776	0.000000
1	-0.774749	2.538643	0.000000	-0.771426	2.580003	0.000000
			HCl − HF			
1	0.188296	1.212283	0.000000	0.183170	1.239610	0.000000
17	0.040694	-1.130914	0.000000	0.019376	-1.131341	0.000000
9	0.040694	2.134634	0.000000	0.067341	2.162896	0.000000
1	-1.246337	-1.198451	0.000000	-1.246540	-1.253612	0.000000
			HF − HBr			
1	0.116158	0.610567	0.000000	-0.007028	1.168744	0.000000
9	0.014807	2.723507	0.000000	-0.292542	-0.955137	0.000000
35	0.014807	-0.809925	0.000000	0.078403	2.577724	0.000000
1	-0.767660	3.225228	0.000000	-1.066423	-1.467857	0.000000
			HCl − HCl			
1	0.153398	0.687429	0.000000	-0.010851	0.000000	-0.034355
17	0.032060	-1.892334	0.000000	-0.027289	0.000000	2.568303
17	0.032060	1.973778	0.000000	-0.152251	0.000000	-1.299282
1	-1.243452	-2.071972	0.000000	-1.256918	0.000000	2.890631

Continues on next page...

Table B.1 – continued from previous page

	B3LYP/6-31++G(d,p)			MP2/6-31++G(d,p)		
Z	x	y	z	x	y	z
			HCl – HBr			
1	0.15439	0.02922	0.00000	0.138153	0.009927	0.000000
17	0.02120	2.69015	0.00000	-0.003585	2.653995	0.000000
35	0.02120	-1.38885	0.00000	0.053248	-1.398637	0.000000
1	-1.25697	2.84797	0.00000	-1.247990	2.913202	0.000000
			NaH – HBr			
11	0.000000	0.000000	0.000000	0.000000	0.000000	0.000000
1	0.000000	0.000000	1.904723	0.000000	0.000000	2.028719
1	0.000000	0.000000	2.785559	0.898987	0.000000	1.881709
35	0.000000	0.000000	4.617331	2.484085	0.000000	1.847870
			LiH – HBr			
3	0.000000	0.000000	0.000000	0.000000	0.000000	0.000000
1	0.000000	0.000000	1.625594	0.000000	0.000000	1.629306
1	0.000000	0.000000	2.607082	0.000000	0.000000	2.564315
35	0.000000	0.000000	4.299905	0.000000	0.000000	4.285631
			NaH – HF			
11	0.000000	0.000000	0.000000	0.000000	0.000000	0.000000
1	0.000000	0.000000	1.871019	0.000000	0.000000	1.959308
1	0.000000	0.000000	3.198749	1.093136	0.000000	1.692306
9	0.000000	0.000000	4.177426	2.139527	0.000000	1.867717
			NaH – HCl			
11	0.000000	0.000000	0.000000	0.000000	0.000000	0.000000
1	0.000000	0.000000	1.890902	0.000000	0.000000	1.863954
1	0.000000	0.000000	2.854047	0.786377	0.000000	1.710672
17	0.000000	0.000000	4.428599	2.751322	0.000000	1.310419

Continues on next page...

Table B.1 – continued from previous page

	B3LYP/6-31++G(d,p)			MP2/6-31++G(d,p)		
Z	x	y	z	x	y	z
			LiH − HF			
3	0.000000	0.000000	0.000000	0.000000	0.000000	0.000000
1	0.000000	0.000000	1.598739	0.000000	0.000000	1.605196
1	0.000000	0.000000	2.945819	0.000000	0.000000	2.988400
9	0.000000	0.000000	3.918268	0.000000	0.000000	3.952618
			LiH − HCl			
3	0.000000	0.000000	0.000000	0.000000	0.000000	0.000000
1	0.000000	0.000000	1.612590	0.000000	0.000000	1.617388
1	0.000000	0.000000	2.788951	0.000000	0.000000	3.037263
17	0.000000	0.000000	4.209290	0.000000	0.000000	4.363663
			HBeH − HF			
4	0.000000	0.000000	0.000000	0.000000	0.000000	0.000000
1	1.324165	0.000000	-0.015202	1.321540	0.000000	-0.013741
1	-1.335136	0.000000	-0.015328	-1.331749	0.000000	-0.013847
1	-2.399579	0.000000	1.171436	-2.438114	0.000000	1.268709
9	-2.981758	0.000000	1.908112	-2.967626	0.000000	2.037494
			HBeH − HBr			
4	0.000000	0.000000	0.000000	0.000000	0.000000	0.000000
1	1.326854	0.000000	-0.004751	1.324142	0.000000	-0.009444
1	-1.331642	0.000000	-0.004768	-1.328312	0.000000	-0.009474
1	-3.081146	0.000000	0.363224	-3.136584	0.000000	0.753729
35	-4.469857	0.000000	0.704734	-4.405397	0.000000	1.374579
			HBeH − HCl			
4	0.000000	0.000000	0.000000	0.000000	0.000000	0.000000
1	1.326215	0.000000	0.000016	1.323699	0.000000	-0.000394
1	-1.334107	0.000000	0.000016	-1.330019	0.000000	-0.000396
1	-3.119714	0.000000	-0.001318	-3.301205	0.000000	0.103359
17	-4.416520	0.000000	-0.002001	-4.572842	0.000000	0.182798

Continues on next page...

Table B.1 – continued from previous page

	B3LYP/6-31++G(d,p)			MP2/6-31++G(d,p)		
Z	x	y	z	x	y	z
			$H_2BH - HF$			
5	0.000000	0.000000	0.000000	0.000000	0.000000	0.000000
1	1.189094	0.000000	0.000000	1.183276	0.000000	0.000000
1	-0.611732	-1.022199	0.000000	-0.614531	-1.011184	0.000000
1	-0.571915	1.052864	0.000000	-0.582696	1.035989	0.000000
1	-2.410566	0.629705	0.000057	-1.563514	2.779922	-0.000132
9	-3.34146	0.676398	0.000082	-2.018474	3.588876	-0.000213
			$H_2BH - HBr$			
5	0.000000	0.000000	0.000000	0.000000	0.000000	0.000000
1	1.193800	0.000000	0.000000	1.184784	0.000000	0.000000
1	-0.592324	-1.034646	0.000000	-0.604275	-1.016359	0.000000
1	-0.603216	1.029841	0.000000	-0.598715	1.028077	0.000000
1	1.411295	2.344258	0.000007	0.796056	2.517979	0.000025
35	2.141810	3.562406	0.000089	1.266335	3.318613	0.000068
			$H_2BH - HCl$			
5	0.000000	0.000000	0.000000	0.000000	0.000000	0.000000
1	1.190500	0.000000	0.000000	1.184083	0.000000	0.000000
1	-0.606122	-1.026392	0.000000	-0.607183	-1.016554	0.000000
1	-0.583405	1.044171	0.000000	-0.586214	1.032965	0.000000
1	-2.720609	0.732567	-0.000071	-1.641421	2.892363	0.000182
17	-4.003826	0.859707	-0.000120	-2.268999	3.998224	0.000299

Table B.2: Correlations for graphics represented in the AIM section

		Method	Curve fit	R^2
		Figure 4.2		
	● ——	B3LYP	$y = 2.192e^{-2.905x} + 0.004$	0.9998
	○ - - -	MP2	$y = 2.311e^{-2.984x} + 0.004$	0.9992
	▲ ——	B3LYP	$y = 160.15e^{-5.037x} + 0.016$	0.936
	△ - - -	MP2	$y = 62.99e^{-4.458x} + 0.013$	0.870
		Figure 4.4		
λ_3	● ——	B3LYP	$y = 4.342e^{-2.330x} + 0.010$	0.998
	○ - - -	MP2	$y = 2.488e^{-1.850x} - 0.013$	0.992
	▲ ——	B3LYP	$y = 117.845e^{-3.718x} + 0.055$	0.986
	△ - - -	MP2	$y = 304.672e^{-4.232x} + 0.053$	0.982
λ_1	● ——	B3LYP	$y = -20.715e^{-4.208x} - 0.008$	0.9998
	○ - - -	MP2	$y = -24.110e^{-4.399x} - 0.007$	0.9997
	▲ ——	B3LYP	$y = -1271.000e^{-5.832x} - 0.017$	0.971
	△ - - -	MP2	$y = -593.536e^{-5.373x} - 0.013$	0.926
		Figure 4.5		
$G(r_{BCP})$	● ——	B3LYP	$y = 0.124e^{-1.420x} - 0.001$	0.992
	○ - - -	MP2	$y = 0.794e^{-2.855x} + 0.003$	0.988
	▲ ——	B3LYP	$y = 2.948e^{-2.809x} + 0.006$	0.992
	△ - - -	MP2	$y = 7.794e^{-3.337x} + 0.006$	0.992
$V(r_{BCP})$	● ——	B3LYP	$y = -6.272e - 4.205X - 0.005$	0.998
	○ - - -	MP2	$y = -10.030e^{-4.624x} - 0.005$	0.998
	▲ ——	B3LYP	$y = -113.060e^{-4.923x} - 0.008$	0.972
	△ - - -	MP2	$y = -13.754e^{-3.656x} - 0.006$	0.949
		Figure 4.6		
	● ——	B3LYP	$y = -351.254e^{-2.395x} + 1.810$	0.971
	○ - - -	MP2	$y = -630.547e^{-3.091x} + 0.701$	0.949
	▲ ——	B3LYP	$y = -3.206 \cdot 10^3 e^{-3.594x} - 1.986$	0.812
	△ - - -	MP2	$y = -1.161 \cdot 10^5 e^{-5.635x} - 1.967$	0.866
		Figure 4.7		
DHB	● ——	B3LYP	$y = -3.899 \cdot 10^{-3}x + 7.512 \cdot 10^{-3}$	0.955
HB	▲ ——	B3LYP		
DHB	○ - - -	MP2	$y = -3.769 \cdot 10^{-3}x + 6.284 \cdot 10^{-3}$	0.955
HB	△ - - -	MP2		
		Figure 4.8		
	● ——	B3LYP	$y = 1.485e^{-0.002x} - 1.481$	0.882
	○ - - -	MP2		
	▲ ——	B3LYP	$y = -0.212e^{-0.013x} + 0.210$	0.954
	△ - - -	MP2		

Appendix **C**

Extra information on the BH_3NH_3 solid state analysis

In this appendix there is further computational details on how the boraneamine molecule is calculated under the CRYSTAL03 code. All models, molecules, slabs and crystals are computed using the same parameters, except where otherwise stated. All the parameters adopted here are chosen among the values which suited best after making test runs with them.

The unit cell has 16 atoms defined in it with 36 electrons. The basic reciprocal llattice cells of the BH_3NH_3 for crystals and slabs are sampled using a shrinking factor (Monkhorst-Pack and Gilat) of 4, giving a total of 27 k points. The integration grid of points used for the exchange and correlation methods is larger and more adequate than the CRYSTAL03 default grid, using the LGRID command. This grid was made up of 75 radial points, integrated with the Gauss-Legendre algorithm and 5 subintervals for 50, 146, 194, 434 and 184 angular points using Lebedev algorithm, giving 45899 point per unit cell. The tolerance on the desnity matrix is 10^{-8} electrons for geometry calculations and 10^{-11} for frequency calculations.

Tolerances in accuracy controlling Coulomb and HF exchange series are set to 10^{-7} for the overlap and penetration for Coulomb integrals, as well as for the overlap and pseudo-overlap for HF eschange integrals. For the second

pseudo charge, the threshold is to 10^{-14}. The energy threshold parameter for the self consistent field method is set at 10^{-12} a.u. The optimization of the internal coordinate is done using the Berny algorithm. The convergence is tested on the root-mean-square (RMS) and on the absolute value of the largest components of both the gradient and the estimated nuclear displacement. The threshold for the forces has been set to 0.00045 for the maximum and 0.00030 for the RMS, while for the atomic displacement is 0.0018 for the maximum and 0.0012 for the RMS. The evaluation of the gradients are numerical. The mixing of the Fock and Kohn-Sham matrices for the SCF to converge faster was set to 30%.

The BSSE was calculated using the MOLEBSSE key with a maximum number of neighbour atoms of 54 and a maximum explored distance of 100 Å. These parameters were chosen after a series of tests run with different values and chosing the optimal ones for the borazane molecule.

In some anharmonic frequency quirky calculations, a modified Broyden [48] scheme has been used. This scheme follows the method proposed by Johnson [142] and mixes the Fock and KS matrices.

Index